Silicic volcanism of the Tauranga Volcanic Centre and the climactic Waitepariki supereruption at the dawn of the Taupō Volcanic Zone

A thesis

submitted in fulfilment

of the requirements for the degree

of

Doctor of Philosophy in Earth Sciences

at

The University of Waikato

by

Marlena Lee Prentice

THE UNIVERSITY OF
WAIKATO
Te Whare Wānanga o Waikato

2023

Abstract

The Tauranga Volcanic Centre (TgaVC), located in the western Bay of Plenty, Aotearoa New Zealand was active between 2.9–1.9 Ma. Silicic volcanism of this period occurred spatially and temporally between the defined locations of the Taupō Volcanic Zone (TVZ) and its predecessor, the Coromandel Volcanic Zone (CVZ), but despite their prominence, the volcanic origin, eruption dynamics and petrogenetic relationships of the volcanic deposits of this period have not previously been studied in detail. This study combines a comprehensive field study with whole-rock, glass and mineral geochemistry and isotopic (Sr, Nd and O) analysis to interpret the origin, evolution and petrogenetic relations of the volcanic deposits of the TgaVC, with particular emphasis on the deposits of the Waiteariki Ignimbrite.

This thesis provides an enhanced chronology for explosive volcanism of the TgaVC with four locally widespread units named and defined as follows: Welcome Bay and Wharo ignimbrites (together formerly known as Lower Pāpāmoa Ignimbrite); Otawera Ignimbrite; and Arateka Ignimbrite (formerly known as Upper Pāpāmoa Ignimbrite). These eruptives were followed by the eruption of the voluminous (870 ± 87 km^3 DRE) Waiteariki Ignimbrite at 2.1 Ma which has been correlated with the distal Hikuroa Pumice Member in northern Hawke's Bay (150-170 km southeast of TgaVC). The integrated proximal and distal records show that at least eight eruptions occurred in the TgaVC between 2.4 and 1.9 Ma and provide a maximum repose period between explosive eruptions of ca. 50 kyrs.

The magnitude 8 (M8) Waiteariki super-eruption consisted of the eruption of crystal-rich rhyodacite magma from the newly defined Omanawa Caldera, identified here on the basis of ignimbrite thickness variations, textural features and the presence of numerous silicic lava domes in association with a prominent negative gravity anomaly situated at the southern end of an asymmetrical rifted graben underlying the northern Mamaku Plateau. The Waiteariki Ignimbrite is a monotonous intermediate deposit, characterised by crystal-rich (37 %), rhyodacite (ave. 70.7 wt. % SiO_2) magma with a consistent mineralogical assemblage of plagioclase, hornblende, pyroxene, quartz ± biotite; restricted ranges in whole-rock geochemistry and matrix glass compositions; and the complete absence of compositional gradients and a precursory Plinian phase. Phenocrysts, however, record a complex evolutionary history, providing evidence for a highly heterogeneous mush-source zone.

Individual lavas of the Minden Rhyolite Subgroup of the TgaVC can be grouped into either low- and high-$^{87}Sr/^{86}Sr$ magmas exclusively erupted in the west and east, respectively. Juvenile products within the Waiteariki and Welcome Bay ignimbrites are mineralogically, geochemically, and isotopically consistent with the high-$^{87}Sr/^{86}Sr$ Minden Rhyolites, which connects these domes to the magmatic

system underlying the Omanawa Caldera. Nd and Sr isotopic values across the TgaVC are comparable to those of the broader TVZ. Calculated $\delta^{18}O_{melt}$ values for the TgaVC magmas indicate a temporal trend of decreasing $\delta^{18}O$ values in the TVZ through time. Upper crustal differentiation was dominated by fractional crystallisation (i.e western domes) or assimilation-fractional crystallisation followed by mixing of magmas (Omanawa magma body and eastern domes) while segregated melts (e.g. Bowentown, Mt Maunganui, Maungatūtū/Mt Misery) have unique late-stage differentiation histories.

As volcanism associated with the Omanawa Caldera and the broader TgaVC occurred within the defined structural boundaries of the Taupō Rift, volcanism of the TgaVC is regarded here to represent the first silicic system of the TVZ. Geothermobarometry indicate crystallisation and storage occurred within the mid- to shallow crust (c. 3.5 to 6 km depth) between 50-160 MPa and 740-900 °C indicating that magmas have broadly resided under near-identical, shallow conditions over the lifespan of the TVZ (~2.5 Ma). Dominated by high-silica, crystal-poor rhyolitic magmas, the continued eruption of homogenous, crystal-rich magmas throughout the TgaVC is unique within the context of the TVZ and it is inferred that active crustal rifting enabled continual tapping of the crystal-mush reservoir which culminated in a deep-seated failure of the magma reservoir, followed by rapid decompression and large-scale evacuation of the Omanawa magmatic system.

Acknowledgements

This thesis is the culmination of nearly 10 years of continuous study, which have been equally challenging and rewarding. This project would not have been possible without the encouragement, assistance and support that I have received from so many people over the years, and I am grateful for this opportunity to acknowledge and thank them.

Firstly, I am indebted to my supervisors Drs Adrian Pittari, Geoff Kilgour and Professor David Lowe for your guidance, constant support and many hours spent reviewing chapters. The passion you all demonstrate towards volcanology and high quality research has been truly inspirational and I'm extremely grateful for your mentorship over the last five years. Thank you also to Professor Peter Kamp for sharing your extensive knowledge of the stratigraphy of northern Hawkes Bay and for the very memorable days in the field and demonstrating the lengths we must go to for a single sample. To Mike Rosenberg, Matt Sagar, Jenni Hopkins, Kevin Faure and Shane Rooyakkers, thank you for your kindness and the advice you freely gave me with the many varied aspects of this research.

I would like to acknowledge the Department of Conservation (DOC) for granting consent sample collection within the confines of the Kaimai Mamaku Conservation Park, Otawa Scenic Reserve and the Otanewainuku Forest and GNS Science for access to and sampling of drill core. Thank you to Dudley Clemens at J Swap, Barrack from Poplar Lane Quarry, Addline Transport, the Ngamanawa Incorporation, Teacher in the Paddock and to all of the private landowners who allowed me access to their land for sample collection and Willem Alderink for being my guide out in the wild. Thank you to the many people have helped me with field and lab work and data processing. Annette and Kirsty, you are the rock on which the pillars of the Earth Science program at Waikato stands. Thank you so much for all your official technical support, field and lab assistance, laughs and of course cake over the years. I also thank the greater Earth Science team and all the students I have had the pleasure of working and sharing office space with over the years. The endless discussions and procrastination made a stressful time more enjoyable. A special thank you to Oliver McLeod for the endless discussions on all things volcanology, and to Miriam Namaliu and Taya Kinley whose projects have been intricately linked with mine. Thanks for trusting me when I had to work things out on the fly and then repeatedly changed my mind. Your projects and company was a great blessing to me, thank you both for being such an important part of my PhD journey.

Funding was gratefully received from the University of Waikato Doctoral Scholarship, with additional funds provided by a School of Science Trust Fund Research Grant, the Western Australian Skeptics, the Wellman Research Award, Geoscience Society of New Zealand, and DJL whom acknowledges

support from MBIE Endeavour Fund Smart Ideas (grant UOWX1903) and Marsden Fund Te Pūta Rangahau a Marsden (grant UOW1902).

Finally, a very special thank you to my family and friends for all your support over these years which range from childcare to putting up with my endless chatter about rocks. I could not have managed this achievement without the constant support and love of my husband Glen and daughters Evelyn, Felicity and Abigail, to whom I hope I have demonstrated that anything is possible with determination and hard work. May you continually strive to achieve all you dream, live life to the fullest and enjoy this most beautiful, powerful and precious planet on which we are blessed to live.

Table of Contents

List of Figures

CHAPTER 1

CHAPTER 2

CHAPTER 3

CHAPTER 4

List of Tables

CHAPTER 1

CHAPTER 2

CHAPTER 3

CHAPTER 4

Publications arising from this thesis at the time of completion

Journal articles

Prentice, M., Pittari, A., Lowe, D. J., Kilgour, G., Kamp, P. J., & Namaliu, M. (2022). Linking proximal ignimbrites and coeval distal tephra deposits to establish a record of voluminous Early Quaternary (2.4–1.9 Ma) volcanism of the Tauranga Volcanic Centre, New Zealand. *Journal of Volcanology and Geothermal Research*, 429, 107595 – ***This paper is presented in Chapter 2.***

Pittari, A., Prentice, M. L., McLeod, O. E., Yousef Zadeh, E., Vincent, K. A., Kamp, P. J. J., & Danisik, M. (2021). Inception of the modern North Island (New Zealand) volcanic setting: Spatio-temporal patterns of volcanism between 3.0 and 0.9 Ma. *New Zealand Journal of Geology and Geophysics, 64(1-2)*, 250-272 – ***Early findings of this PhD study contributed to this collabrative review paper.***

Conference abstracts

Prentice M.L., Pittari A., Kilgour G., Lowe D.J. Eruption of a large-volume, monotonous intermediate ignimbrite at the dawn of Taupō Volcanic zone activity, New Zealand. *Accepted for presentation at IAVCEI 2023, Rotorua.*

Prentice M.L., Kilgour G., Pittari A., Lowe D.J. (2022) Silicic volcanism at the dawn of the TVZ: Trends in geochemistry, mineralogy and magma storage of the Tauranga Volcanic Centre, New Zealand. *Presented at Geosciences 2022, Palmerston North.* Geoscience Society of New Zealand.

Prentice M., Namaliu, M., Pittari, P., Lowe, D.J., Kamp, P., Kilgour, G. (2021) Advances towards a comprehensive ignimbrite stratigraphy of the Tauranga Volcanic Centre, North Island, New Zealand. In: Zernack A. V., Palmer, J. eds. Geoscience Society of New Zealand Annual Conference 2021: Programme & Abstracts Volume. Geoscience Society of New Zealand Miscellaneous Publication 158. Geoscience Society of New Zealand, Wellington, pp. 123.

Prentice M.L., Pittari A., Kamp P.J.J., Lowe D.J., Kilgour G. (2020). The 2.1 Ma Waiteariki Ignimbrite: Defining a new super-eruption at the onset of TVZ volcanism. In: Bassett K. N., Nichols A. R. L., Fenton C. H. eds. Geosciences 2020: Abstract Volume. Geoscience Society of New Zealand Miscellaneous Publication 157A. Geoscience Society of New Zealand, Wellington, pp. 227.

Prentice M.L., Rosenberg, M.D., Pittari, A., Lowe, D.J., Kilgour, G. (2018). The 2.1 Ma Waiteariki Ignimbrite: Product of a large explosive silicic eruption during the Coromandel-Taupo Transition. In: Sagar M, Prebble J ed. Abstract Volume: Geosciences 2018, Napier, New Zealand. Geoscience Society of New Zealand Miscellaneous Publication 151A. p 212.

CHAPTER 1:

1 Introduction

1.1 Introduction and motivation for research

Subduction-related volcanism within Te Ika-a-Māui/the North Island, Aotearoa New Zealand has migrated southeast since the Late Miocene (Carter *et al.*, 2004). The resulting volcanic deposits and landforms are classified as two broad volcanic zones – the currently active Taupō Volcanic Zone (TVZ) and the older Coromandel Volcanic Zone (CVZ). The transition from the CVZ to the TVZ occurred from 2.9–1.9 Ma (Briggs *et al.*, 2005; Pittari *et al.*, 2021), and is represented by silicic volcanism of the Tauranga Volcanic Centre (TgaVC). Despite its significance, our understanding of volcanism during this period remains limited.

The volcanic deposits of this period are found throughout the Tauranga Basin and adjacent Kaimai Range and are characterised by an eroded andesite to dacite stratovolcano, numerous rhyolitic lava domes and the Waitеariki and Pāpāmoa ignimbrites (Houghton & Cuthbertson, 1989; Briggs *et al.*, 1996). Studies during the 1980s and 90s focused primarily on regional geological mapping, petrography and limited geochemical work entailing a few whole rock XRF analyses and electron microprobe analyses of major mineral phases (Harmsworth, 1983; Morgan, 1986; Hall, 1994; Whitbread-Edwards, 1994; Hollis, 1995). More recently, studies have focused on geochronology via $^{40}Ar/^{39}Ar$ (Briggs *et al.*, 2005) and (U-Th)/He and U-Pb methods (Cook, 2016; Pittari *et al.*, 2021), yet despite the prominence of the various lavas and ignimbrites, their volcanic origin and eruption dynamics and petrogenetic relationships have not been studied.

Sequences of tephra deposits produced by explosive volcanic activity play an important role in helping to construct the eruptive histories of large silicic volcanic fields. In proximal regions, the record of volcanism is often incomplete due to burial or destruction by subsequent volcanic activity and/or, tectonism and by the preferential erosion of unconsolidated pyroclastic deposits rather than resistant welded ignimbrites and lavas. In contrast, medial to distal tephra archives found within lacustrine, marine and ice-cores can provide more detailed records of mainly rhyolitic volcanism which, when combined with proximal records, provide valuable information about eruptive histories of long-lived silicic systems (Carter *et al.*, 2004; Kutterolf *et al.*, 2016; Lukács *et al.*, 2018; Amma-Miyasaka *et al.*, 2020). The Neogene stratigraphic succession in northern Hawke's Bay is positioned to the southeast of Tauranga and several macroscopic tephras and a distal ignimbrite (Hikuroa Pumice Member) have been identified within Mangaheia Group rocks of Nukumaruan (2.4-1.63 Ma) age (Bland *et al.*, 2007). While inferred to have originated from volcanism of the TgaVC (Hopkins & Seward, 2019), their proximal equivalents are yet to be resolved.

This study offers a unique opportunity to synthesise a near-source volcanic reconstruction, distal tephra studies with detailed petrographic and geochemical analysis to establish the extent of volcanism associated with the TgaVC during this important, yet poorly understood part of Aotearoa New Zealand's geological history.

1.2 Research questions

The record of explosive volcanism originating from the TgaVC is poorly constrained. The Waiteariki Ignimbrite is inferred to be the product of large-volume, caldera forming eruption (Briggs *et al.*, 2005), however, the eruption dynamics of this and other prominent ignimbrites found within the region has not been investigated. Limited knowledge also exists regarding magma genesis and the evolution of the magmatic system(s) feeding these pyroclastic units, and how they are linked to each other and the numerous, spatially distinct silicic lavas scattered across the broader region.

This study combines field studies with cutting-edge analytical techniques to interpret the origin, evolution and petrogenetic relations of the volcanic deposits of the Tauranga Volcanic Centre. Key research questions that will be addressed are listed below:

1. What was the frequency and distribution of silicic volcanism within the Tauranga Volcanic Centre?

2. It is hypothesised that the Waiteariki Ignimbrite correlates with the Hikuroa Pumice Member of the Petane Formation in northern Hawke's Bay (P. Kamp, personal communication, 2018). Correlations between the Te Puna and Kidnappers ignimbrites have also been previously inferred (Leonard *et al.*, 2010). Is it possible to confirm these correlations and establish links between the Waiteariki, Te Puna and Pāpāmoa Formation ignimbrites to known terrestrial or marine tephras found in northern Hawke's Bay, Whanganui and the southern Waikato regions?

3. What is the physical (texture, componentry, welding) and chemical (major and trace-element geochemistry and isotopes) characteristics of the Waiteariki Ignimbrite?

4. What is the eruptive volume of the Waiteariki Ignimbrite?

5. Does the eruption of the voluminous Waiteariki Ignimbrite represent caldera forming activity, if so, can the location of the caldera be constrained?

6. What are the eruption mechanisms and magmatic processes associated with the eruption of a crystal-rich magmas of the TgaVC?

7. Is there a geochemical signature for silicic volcanism of the TgaVC?

8. How does volcanism of the Tauranga region sit within the broader context of a migrating continental-arc? Does this period of Aotearoa New Zealand's volcanological history reflect late-stage volcanism associated with the CVZ or onset within the TVZ?

These specific questions are addressed in this thesis as a series of chapters, structured around a common theme of understanding the volcanic evolution of the TgaVC and the underlying magmatic system(s) with particular emphasis on the crystal-rich, dacitic Waitepariki Ignimbrite.

1.3 Thesis aim and objectives

The aim of this research is to reconstruct the frequency and distribution of large-scale silicic volcanism of the TgaVC and, for the first time, physically and chemically characterise eruptive products and determine the pre-eruptive conditions of the underlying magmatic system.

The objectives of this study are:

1. Define a more complete record of Late Pliocene–Early Pleistocene volcanism from the TgaVC through the correlation of distal tephras and ignimbrites in the Hawke's Bay forearc basin, and deep-marine drill cores to proximal ignimbrites of the Tauranga region to refine the stratigraphic framework for the Tauranga area.

2. Reconstruct the eruptive volume, distribution, and emplacement processes of the Waitepariki Ignimbrite and investigate the assembly and evacuation of the associated magmatic system through petrographic, whole-rock and crystal geochemical analysis.

3. Geochemically and isotopically characterise magmas erupted throughout the Tauranga region and explore the nature of upper crustal storage and differentiation processes of a crystal-rich silicic system active spatially and temporally between the Coromandel and Taupō volcanic zones.

This study will address fundamental questions relating to the frequency and distribution of silicic eruptions within the TgaVC and investigate the magma petrogenesis, differentiation and storage processes of the Waitepariki Ignimbrite and those of the broader TgaVC and re-evaluate volcanism of the TgaVC in the context of a migrating continental arc.

1.4 Thesis structure and chapter outlines

The research chapters in this thesis are structured around a common theme of understanding the volcanic evolution and petrogenetic relationships of erupted magmas across the TgaVC using a combination of field and geochemical laboratory studies.

Each chapter is written in manuscript style and are either peer-reviewed published works (Chapter 2: Journal of Volcanology and Geothermal Research) or presented in a style suitable for journal submission (chapters 3 and 4). Although these chapters serve as self-contained studies, each chapter progressively builds on the information from the preceding one forming a single coherent thesis. The presentation of Chapter 2 has been altered from the published version to be consistent in style with the remainder of the thesis, but no scientific content and text modifications have been made to this published work. Supplementary data tables and files linked to the published and prepared manuscripts are available digitally as digital Excel files.

This thesis is organised into five chapters as outlined below.

This chapter ***(Chapter 1)*** has introduced the motivation and contextual reasoning behind this research and outlined key research questions which I wish to address in this thesis. Following this section, I will introduce the geological setting and background of this study by providing an overview of silicic volcanism associated with the Coromandel and Taupō volcanic zones and a detailed review of the current volcanological and geochemical understanding of volcanic deposits associated with the TgaVC. This is followed by a review of magmatic processes and deposits associated with large silicic systems.

Chapter 2 presents a peer-reviewed manuscript published in the Journal of Volcanology and Geothermal Research entitled "Linking proximal ignimbrites and coeval distal tephra deposits to establish a record of voluminous Early Quaternary (2.4–1.9 Ma) volcanism of the TgaVC, New Zealand". This paper is centred around major and trace-element analysis of glass shards and U/Pb dating of zircons to correlate ignimbrites in the Tauranga region with distal pyroclastic deposits in northern Hawke's Bay. I build on the tephrostratigraphic framework established by previous workers (Bland *et al.*, 2007; Stevens, 2010; Hopkins & Seward, 2019) and link these tephras to the TgaVC and advance our knowledge of the regional ignimbrite stratigraphy.

Chapter 3 is a comprehensive field, mineralogical and whole-rock geochemical investigation to understand the volcanological and petrological processes which gave rise to the crystal-rich Waitetariki Ignimbrite. It reconstructs the eruptive volume, distribution, and emplacement processes and re-evaluates volcanism of the TgaVC in the context of the migrating continental-arc. Petrographic

analysis in conjunction with whole-rock and crystal geochemistry is used to understand the assembly and evacuation of the associated magmatic system.

Chapter 4 builds upon on the findings of the previous two chapters by investigating the petrogenetic relationships of magmas erupted throughout the broader Tauranga region and use major and trace element geochemistry in conjunction with radiogenic (Sr and Nd) and stable (O) isotopes to explore the nature of upper crustal storage and differentiation processes of a crystal-rich silicic system active at the dawn of the TVZ.

Chapter 5 summarises the key findings of this research, re-visiting some of the main research questions raised in Chapter 1. This chapter also discusses the remaining gaps in knowledge and identifies opportunities for future research.

1.5 Arc-related silicic volcanism of Aotearoa New Zealand

Arc-related silicic volcanism within Te Ika-a-Māui/North Island of Aotearoa New Zealand currently occurs within the TVZ (**Fig. 1.1**), the southernmost ~300 km continental extension of the ~2800 km long Tonga-Kermadec arc, which results from the oblique, westward subduction of the Pacific Plate beneath the Australian Plate (Wilson & Rowland, 2016). Volcanism of the TVZ coincides with a structurally segmented rift system known as the Taupō rift (Seebeck *et al.*, 2014; Wilson & Rowland, 2016; Villamor *et al.*, 2017) which is the southern continuation of the Havre Trough back-arc basin (Caratori Tontini *et al.*, 2019). This rifted-arc structure is unique globally and the TVZ is renowned for its high caldera density and eruptive frequency and volumes (Hughes & Mahood, 2011; Wilson & Rowland, 2016). Active for c. 2 Myr, the TVZ has a long and complex history, yet it is only the latest manifestation of arc-related silicic volcanism in Aotearoa New Zealand. Rhyolitic volcanism initiated c. 12 Ma in the northern CVZ, and has progressively migrated southeast through time (Adams *et al.*, 1994; Carter *et al.*, 2004). The CVZ and TVZ are generally considered to represent older and younger versions, respectively, of the same, yet continually evolving, arc-related magmatic province (Wilson & Rowland, 2016).

The TgaVC is located in the western Bay of Plenty at the southern end of the Coromandel Peninsula which comprises the eroded remains of the subaerial central and southern sectors of the broader CVZ (**Fig. 1.1**; Adams *et al.,* 1994). The close proximity of volcanic deposits in the Tauranga region to those of the CVZ in the southern Coromandel Peninsula has meant that deposits of the TgaVC have been inferred to represent the final phase of silicic volcanism associated with the CVZ, before activity transferred southeast to the developing TVZ (Carter *et al.*, 2004; Briggs *et al.*, 2005; Booden *et al.*,

2012). Volcanic deposits of the TgaVC overlap temporally and spatially with early TVZ activity, and thus volcanism of the TgaVC represents a significant shift in the volcano-tectonic setting of the volcanic arc (Briggs *et al.*, 2005). Despite its importance as a key transition centre between these two broader volcanic zones, understanding of volcanism during this period remains limited (Briggs *et al.*, 2005; Pittari *et al.*, 2021).

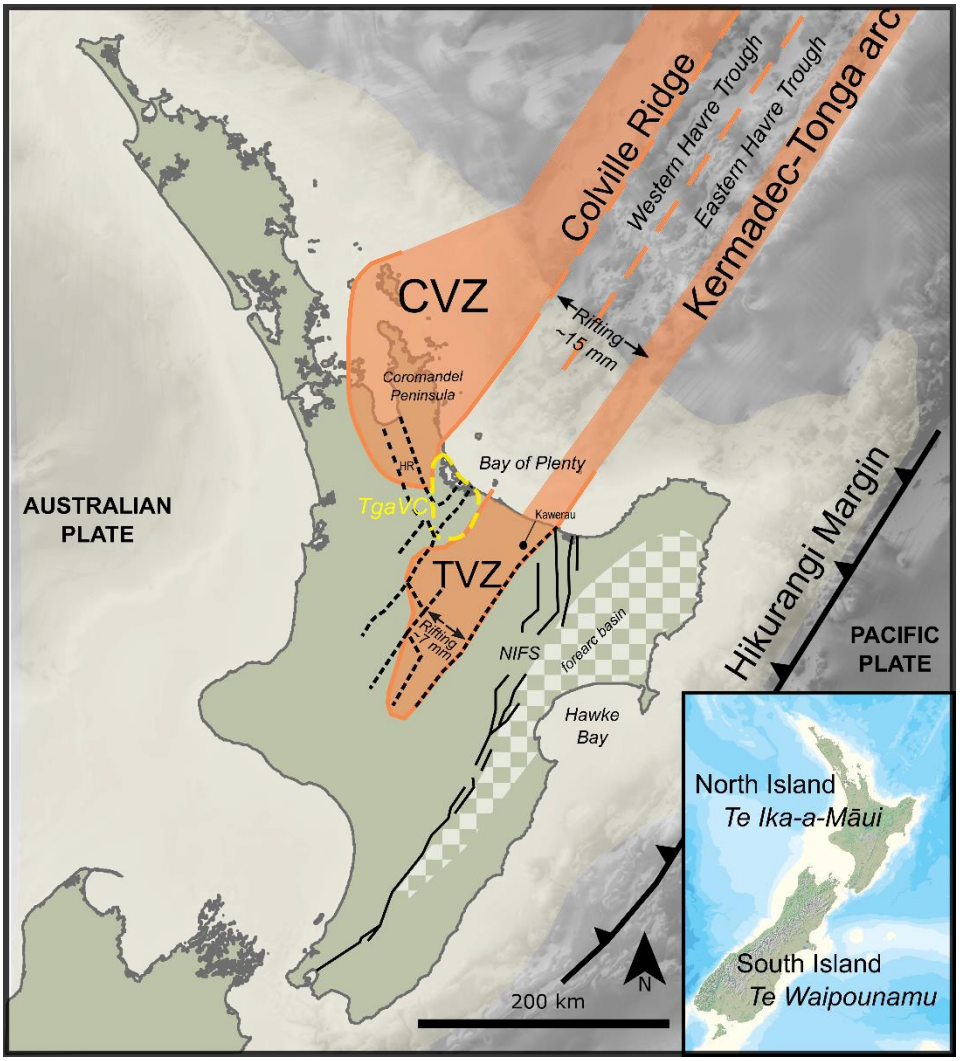

Figure 1.1. Overview map of Te Ika-a-Māui/North Island of Aotearoa New Zealand highlighting the magma-tectonic components: the rifting Havre Trough bound to the northwest and southeast by the Colville and Kermadec ridges (orange) respectively. Remnants of the older volcanic arc - Coromandel Volcanic Zone (CVZ) preserved onshore in the Coromandel Peninsula and west of the Hauraki Rift (HR). Dashed black lines represent main structural faults of the Taupō rift which represents the southern continuation of the Havre Trough back-arc basin and encloses the currently active volcanic arc – Taupō Volcanic Zone (TVZ). Solid black lines represent major faults of the North Island Fault System (NIFS). WB = Whanganui Basin.

1.5.1 Tauranga Volcanic Centre (TgaVC)

The volcanic deposits distributed throughout the western Bay of Plenty region, are dated between 2.95-1.9 Ma and were originally grouped into two distinct silicic centres referred to as the Kaimai and Tauranga volcanic centres (Briggs *et al.*, 2005). The former Kaimai Volcanic Centre (2.87–2.09 Ma) included the voluminous overlapping rhyolite domes of Kaimai and Kakahu (2.86 ± 0.08 Ma and 2.87 ± 0.02 Ma respectively) which lie at the southern-most tip of the Coromandel Range, and the Waiteariki Ignimbrite (2.09 Ma). The remaining silicic lava domes, ranging from 2.69–1.95 Ma and ignimbrites of the Pāpāmoa Formation (2.4-1.9 Ma), comprised the TgaVC. This concept of two discrete volcanic centres suggested by Briggs et al. (2005), has recently been abandoned in favour of a single TgaVC (**Fig. 1.2**) that combines the successions of both former centres and includes all other volcanic deposits in the greater Tauranga region between the age of 2.95–1.9 Ma (Pittari *et al.*, 2021). The combined volcanic succession of the TgaVC now comprises an eroded andesitic stratovolcano (Otawa Formation), a solitary exposure of basalt (Matakana Basalt), several dacite-rhyolite lava domes or dome complexes (Minden Rhyolite Subgroup), and two pyroclastic successions of the Pāpāmoa Formation and the Waiteariki Ignimbrite. A summary of existing radiometric age determinations for the main volcanic units of the TgaVC is presented in **Table 1.1.** In this study I use the preferred U-Pb ages of Pittari *et al.* (2021) as the inferred eruption age as these have been demonstrated to be more statistically robust.

1.5.1.1 Otawa Formation

The andesite to dacite lavas and volcanic breccias of the Otawa Formation represent the eroded remnants of a long-lived stratovolcano which covered an area of c. 35 km^2 on the eastern side of the TgaVC (Briggs *et al.*, 1996). These lavas form the basis of the modern day Pāpāmoa Range and are onlapped by numerous NNE-aligned dacitic to rhyolitic lava domes of the Minden Rhyolite subgroup (**Fig. 1.2**). Lavas of the Otawa Formation are blue-grey in colour, fine to medium grained and porphyritic. Plagioclase is the dominant phenocryst with subordinate orthopyroxene, Fe-Ti oxides, ± hornblende, clinopyroxene and quartz within an intergranular to hyalopilitic groundmass. Accessory minerals include chlorite, apatite, zircon and iron oxides and sulphides. Two K-Ar ages obtained from andesite lavas indicate activity occurred between 2.95 and 2.54 Ma (**Table 1.1**; Stipp, 1968), and thus comprise the earliest known volcanic activity associated with the TgaVC.

1.5.1.2 Matakana Basalt

The Matakana Basalt is a solitary outcrop of basalt with pseudo-pillow structures that form a small island 30 m offshore of Matakana Island, K-Ar dated at 2.7 ± 0.1 Ma (**Fig. 1.2**; Hollis, 1995). This is the only known occurrence of basaltic magma within the TgaVC, however, a high gravity anomaly (c. -15

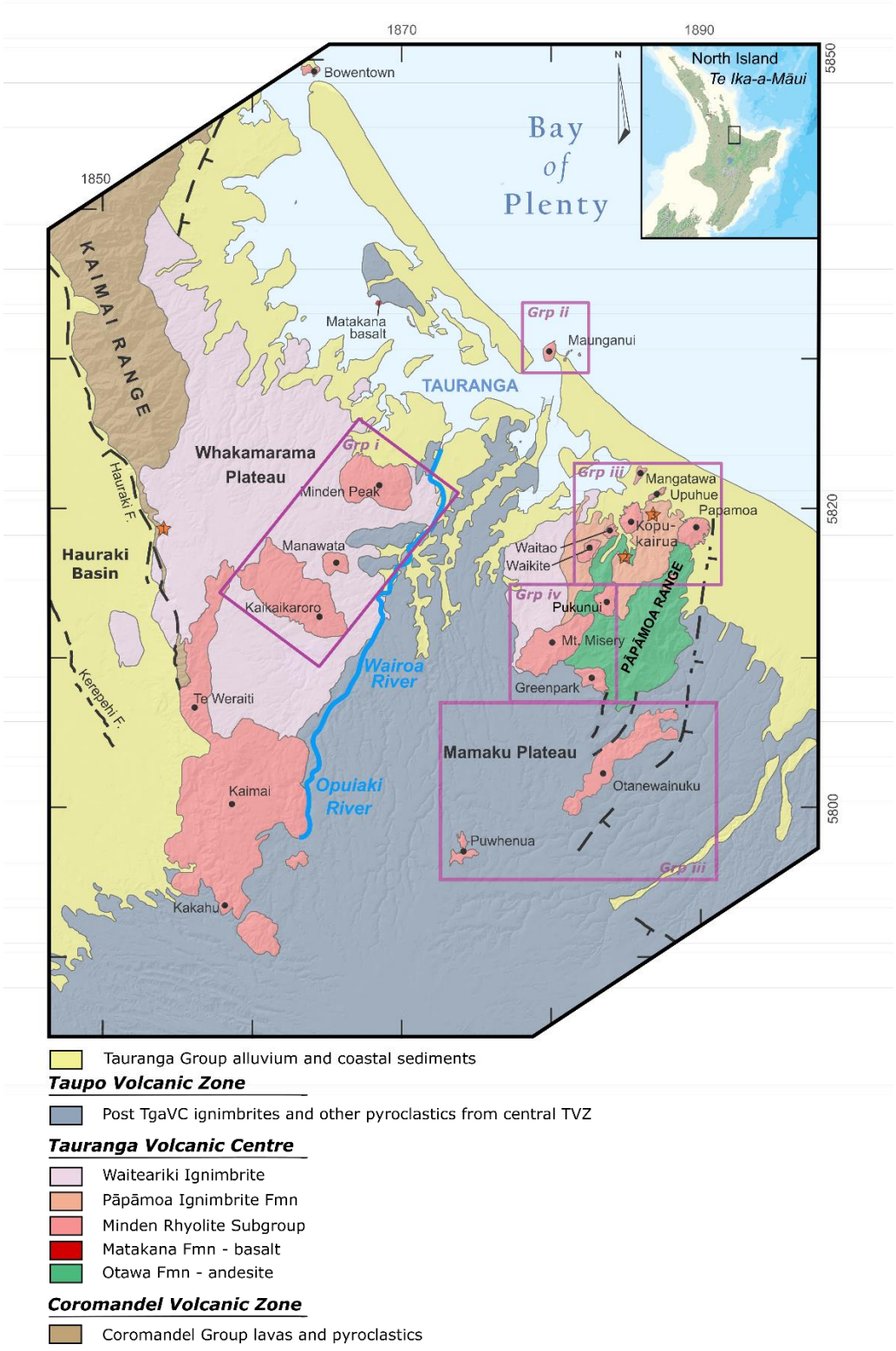

Figure 1.2. Simplified geological map of the Tauranga Volcanic Centre (TgaVC) as redefined by Pittari *et al.* (2021) highlighting volcanic units and areas covered by younger pyroclastic and sedimentary deposits. Mineral-geochemical dome groupings of Briggs *et al.* (2005) are (i) Minden Peak group, (ii) Maunganui dome complex, (iii) Mangatawa group, and (iv) Mount Misery group. Redrawn from Pittari *et al.* (2021). Orange stars represent type-localities of ignimbrite units: 1. Te Ariki Falls, Waitearikí Ignimbrite; 2. Upper Pāpāmoa and 3. Lower Pāpāmoa ignimbrite.

Table 1.1. Volcanic stratigraphy and summary of published geochronological data for the Tauranga Volcanic Centre (TgaVC)

Geological Map Unit[1]	Eruption Deposit(s)	K-Ar age[2] (Ma)	$^{40}Ar/^{39}Ar$ age[6] (Ma)	U-Pb zircon age[7] (Ma)	(U-Th)/He zircon age[7] (Ma)
Waitearikiki Fm	Waitearikiki Ignimbrite	2.18 ± 0.15 w 2.13 ± 0.17 p	*2.09 ± 0.03**		2.25 ± 0.26
Papamoa Fm	Papamoa ignimbrites	-	2.40 ± 0.02 L 1.90 ± 0.10 U	2.21 ± 0.13	-
Minden Rhyolite Subgroup	Bowentown Dome	2.51 ± 0.25 (wr) 2.77 ± 0.31 (p) 2.89 ± 0.07[3]	-	2.83 ± 0.16 2.09 ± 0.39[8]	2.55 ± 0.59
	Minden Peak Dome	1.52 ± 0.23 (wr)	2.16 ± 0.03	2.135 ± 0.066*	2.04 ± 0.18
	Kaikaikaroro Dome	-	2.39 ± 0.06	-	-
	Maunganui Dome	-	2.35 ± 0.06	-	-
	Mangatawa Dome	2.36 ± 0.08 (wr) 2.28 ± 0.15 (p)	2.39 ± 0.13	2.31 ± 0.18*	2.45 ± 0.31
	Upuhue Dome	-	2.69 ± 0.04	2.530 ± 0.089*	2.84 ± 0.17
	Papamoa Dome	-	2.50 ± 0.03	2.25 ± 0.16*	2.88 ± 0.20
	Kopukairua Dome	-	*2.20*	2.53 ± 0.14*	2.69 ± 0.13
	Waitao Dome	-	-	2.64 ± 0.15	2.71 ± 0.14
	Waikite Dome	-	-	2.25 ± 0.10	2.37 ± 0.12
	Otanewainuku Dome	-	1.95 ± 0.02	-	-
	Puwhenua Dome	-	2.14 ± 0.04	-	-
	Mount Misery Dome	-	2.69 ± 0.03	-	-
	Kaimai Dome	-	2.86 ± 0.08	2.236 ± 0.038*	2.20 ± 0.49
	Kakahu Dome	-	2.87 ± 0.02	-	-
Matakana Fm	Basalt lava	2.7 ± 0.1[4]	-	-	-
Otawa Fm	Andesitic volcano	2.95 ± 0.30[5] 2.54 ± 0.05[5]	-	-	-

[1]Stratigraphic nomenclature as defined by Institute of Geological and Nuclear Sciences 1:250 000 Geological Map Series (Leonard et al., 2010), after Briggs et al. (1996).
[2]Except where specified, K-Ar ages are from Takagi (1995); wr, whole rock; p, plagioclase
[3]Brathwaite and Christie (1996)
[4]Hollis (1995)
[5]Stipp (1968)
[6]Briggs et al. (2005); $^{40}Ar/^{39}Ar$ ages on feldspar separates are isochron ages, except italicised plateau ages (± 1σ); ages for the Lower (L) and Upper (U) Papamoa ignimbrites as defined by Hughes (1993) and Briggs et al. (1996)
[7]Pittari *et al.,* 2021; U-Pb weighted average, corrected for common Pb (95% CI); (U-Th)/He weighted average (± 2σ)
[8]Cook (2016)
*preferred approximation of eruption age when the various dating methods are discordant (Pittari *et al.,* 2021)

mGal) underlies Matakana Island and therefore may represent a lava flow associated with a larger yet buried structure or an isolated lava with underlying near-surface basement rocks (Stagpoole *et al.*, 2021). The Matakana Basalt is porphyritic containing medium-grained (1-5 mm) phenocrysts of plagioclase, olivine (altered to iddingsite), orthopyroxene and Fe-Ti oxides which are set within an intergranular groundmass (Briggs *et al.*, 1996).

1.5.1.3 Minden Rhyolite Subgroup

The Minden Rhyolite Subgroup includes all orthopyroxene-, hornblende- and biotite-bearing and flow banded rhyolites located within the Coromandel and Bay of Plenty regions, north of the TVZ (Houghton & Cuthbertson, 1989; Leonard et al., 2010). Within the TgaVC, there are c. 16 individual rhyolite-rhyodacite lava domes or dome complexes (**Fig. 1.2**). Lavas are typically crystal-rich (up to 40 % phenocrysts), with the notable exceptions of crystal-poor lavas at Mt Maunganui and Bowentown, and have a consistent mineral assemblage of plagioclase ± quartz ± orthopyroxene ± hornblende and biotite (Hughes, 1993; Hall, 1994; Whitbread-Edwards, 1994; Hollis, 1995; Cook, 2016; Kinley, 2022). All lavas are pervasively devitrified. The NNE alignment of many of the domes has been inferred to represent northeast-trending basement faults (Healy *et al.*, 1964; Briggs *et al.*, 1996), however no faults are currently recognised.

Briggs *et al.* (2005) divided the Minden rhyolite domes of the TgaVC into four groups (**Fig. 1.2**) based on their spatial, mineralogical, and geochemical characteristics.

(i) The Minden Peak group consist of the crystal-rich hornblende rhyolite domes of Minden Peak, Manawata and Kaikaikaroro which lie northwest of the Wairoa River and are characterised by high SiO_2, K_2O and intermediate Zr concentrations (132–193 ppm) (**Fig. 1.2**).

(ii) The crystal-poor Mt Maunganui group lavas are found at the northern end of the Minden Peak group lineament (**Fig. 1.2**) and includes the prominent dome of Mt Maunganui along with the remains of associated lava flows at Mt Drury, Moturiki and Motuotau Islands. These rocks are the most evolved of the TgaVC rhyolites and have the highest SiO_2 (> 76 wt. %) and K_2O, yet the lowest concentrations of Zr (90–110 ppm).

(iii) The Mangatawa group is the largest group and includes the rhyolite and dacite domes of Mangatawa, Upuhue, Papamoa, Kopukairua, Waitao, Waikite, Otanewainuku, and Puwhenua. They are characterised by low SiO_2, (< 73 wt. %), high K_2O and have intermediate Zr (100–190 ppm) abundances which distinguishes them from group iv lavas below.

(iv) The Mount Misery group includes the large dome of Maungatūtū/Mt Misery along with Greenpark and Pukunui. While these domes occur in the same geographical location and have geochemical affinities with Mangatawa Group lavas, they have been differentiated by their Zr concentrations which exceed 200 ppm.

The Bowentown dome has geochemical and mineralogical similarities to both the Minden Peak and Mt Maunganui domes (Hall, 1994; Whitbread-Edwards, 1994; Cook, 2016), however is spatially removed from the other domes and is not currently linked with any dome group. Multiple dating methods have been applied to the Bowentown Rhyolite which have provided a wide range of age estimates from c. 2.9–2.1 Ma (**Table 1.1**). In many cases the age estimates are concordant, with the exception of a young U-Pb zircon age of 2.09 ± 0.39 Ma (Cook, 2016). In this case, I adopt a nominal age for the Bowentown Rhyolite of 2.7 Ma, which is the average of all concordant age estimates. While the Bowentown Rhyolite occurs spatially and temporally within the defined boundaries of the TgaVC, its inclusion in the TgaVC, along with the Matakana Basalt, is tentative (Pittari *et al.*, 2021).

No detailed descriptions or characterisation of the rhyolite lavas comprising the Kaimai-Kakahu-Te Weraiti dome complex has been found within the existing literature.

In general, the rhyolites and dacites of the TgaVC form spatially associated groups of similar mineralogical and geochemical composition. These clusters may represent genetically related silicic magmas that were either independently or broadly synchronously derived (Briggs *et al.*, 2005), however no detailed geochemical study of silicic magmas of the TgaVC has been undertaken to date.

1.5.1.4 Pāpāmoa Formation

The Pāpāmoa Formation is a northward-dipping succession of dacite to rhyolite ignimbrites and interbedded fall deposits which overlie lavas of the Otawa Formation in central and northern parts of the Pāpāmoa Range on the eastern side of the TgaVC (**Fig. 1.2**) (Briggs *et al.*, 1996; Leonard *et al.*, 2010). Hughes (1993) differentiated the formation into a lower and upper unit on the basis of juvenile clast compositions.

The Lower Pāpāmoa Ignimbrite is complex and contains large (up to 190 mm) juvenile clasts with a diversity of compositions ranging from andesite to rhyolite (c. 55–71 wt. %; **Table 1.2**; Hughes, 1993). The ignimbrite is pumice- (15–30 %) and crystal-rich (15–20 %) with a matrix mineral assembledge consisting of plagioclase, quartz, hornblende, orthopyroxene, Fe-Ti oxides, and in some juvenile clasts, rare biotite. Lithics consist of clasts of andesite and rhyolite which are ocassionally concentrated into lithic-rich zones (up to c. 10 %), but predominately the matrix is lithic-poor. The

Table 1.2. Comparison of colour, geochemistry, classification and petrography of pumice types in the lower Papamoa Ignimbrite from Hughes (1993). Mineral abbreviations: qtz = quartz, pl = plagioclase, hbl = hornblende, opx = orthopyroxene, bt = biotite.

Juvenile Type	Colour	Composition	Mineralology
Type 1	White	Dacitic-rhyolite	Qtz, pl, Large hbl, ± opx
Type 2	Whitish grey with orange rims	Dacitic	Qtz, pl, hbl, ± opx
Type 3	Brown-grey	Dacitic	Qtz, pl, opx, ± bt ± hbl
Type 4	Dark grey-brown	Basaltic andesite	Qtz, pl, hbl, ± bt
Type 5	Dark grey to black	Andesitic	Qtz, pl, bt, ± hbl
Scoria	Dark brown to black	Andesitic	Qtz, pl, hbl, bt

type section of the Lower Pāpāmoa Ignimbrite is found at NZ Topo50 map reference BD37 871 189 (location 3; **Fig. 1.2**) where the unit forms a northward-dipping fan in the northern foothills of the Pāpāmoa Range. In contrast, the Upper Pāpāmoa Ignimbrite contains only juvenile clasts of rhyodacite composition with the same mineral assembledge as found in the Lower Pāpāmoa Ignimbrite (Briggs *et al.*, 1996). The type section of the Upper Pāpāmoa Ignimbrite is found at NZ Topo50 map reference BD37 845 168 where it crops out as promient bluffs (location 2; **Fig. 1.2**).

Briggs *et al.* (2005) obtained bracketing age dates of 2.4 ± 0.02 and 1.9 ± 0.1 Ma for the lower and upper units respectively. A more recent U-Pb zircon age of 2.21 ± 0.13 Ma (Pittari *et al.*, 2021) is consistent with the formation-level ages of Briggs et al. (2005) which overlaps with those obtained for many of the domes of the Mangatawa group. The source of the Pāpāmoa ignimbrites is uncertain, however their restricted distribution and geochemical, spatial and temporal affinities with Mangatawa group domes suggests a source in the eastern TgaVC (Briggs *et al.*, 2005).

1.5.1.5 Waiteariki Formation

The widespread Waiteariki Ignimbrite has been described by numerous authors throughout the Tauranga and Kaimai regions (Healy, 1967; Harmsworth, 1983; Morgan, 1986; Houghton & Cuthbertson, 1989; Hughes, 1993; Hall, 1994; Whitbread-Edwards, 1994; Hollis, 1995; Briggs *et al.*, 1996). It is exposed throughout the eastern foothills of the Kaimai Range and underlies the gently sloping upper surface of the Whakamarama Plateau where it dips eastward beneath younger sediments of the Tauranga Basin (**Fig. 1.2**). Exposures are also found along the western margin of the Pāpāmoa Range (Briggs *et al.*, 1996). Throughout central and southern areas, the Waiteariki

Ignimbrite is buried by younger TVZ-derived deposits where it is encountered in drill holes at a depth of 50–150 m (Houghton & Cuthbertson, 1989; Briggs *et al.*, 1996). As such, the Waiteariki Ignimbrite is considered to form the local basement throughout the region where it is encountered in drill holes 50-150 m below the surface (Harmsworth, 1983). It is down-faulted to the west by the Hauraki and Okauia faults (**Figs. 1.2, 1.3**) and is believed to underlie much of the southern Hauraki plains (Davidge, 1982; Houghton & Cuthbertson, 1989). The widespread distribution of the Waiteariki Ignimbrite suggests that it is the product of a voluminous dacitic eruption that was likely to have been associated with a caldera-collapse (Houghton & Cuthbertson, 1989), however this unit has not yet been attributed to any known caldera. Houghton and Cuthbertson (1989) suggested that, given the predominance of rhyolitic lithic ejecta, the Waiteariki Ignimbrite originated from a source in the northern TVZ. In contrast, Morgan (1986) suggested a source in the southern Kaimai Ranges close to its type locality at Te Ariki Falls (NZ Topo50 map reference BD36 541 181; Location 1; **Fig. 1.2**). The evidence for both locations, however, is conflicting and the source location remains unresolved.

Multiple age determinations have been undertaken for the Waiteariki Ignimbrite (**Table 1.1**) and provide an early Pleistocene age of between 2.25 and 2.09 Ma. This age is supported by field evidence where it has flowed around and thinned over the Minden Rhyolite domes of Kaikaikaroro, Manawata and Minden Peak (Harmsworth, 1983; Whitbread-Edwards, 1994).

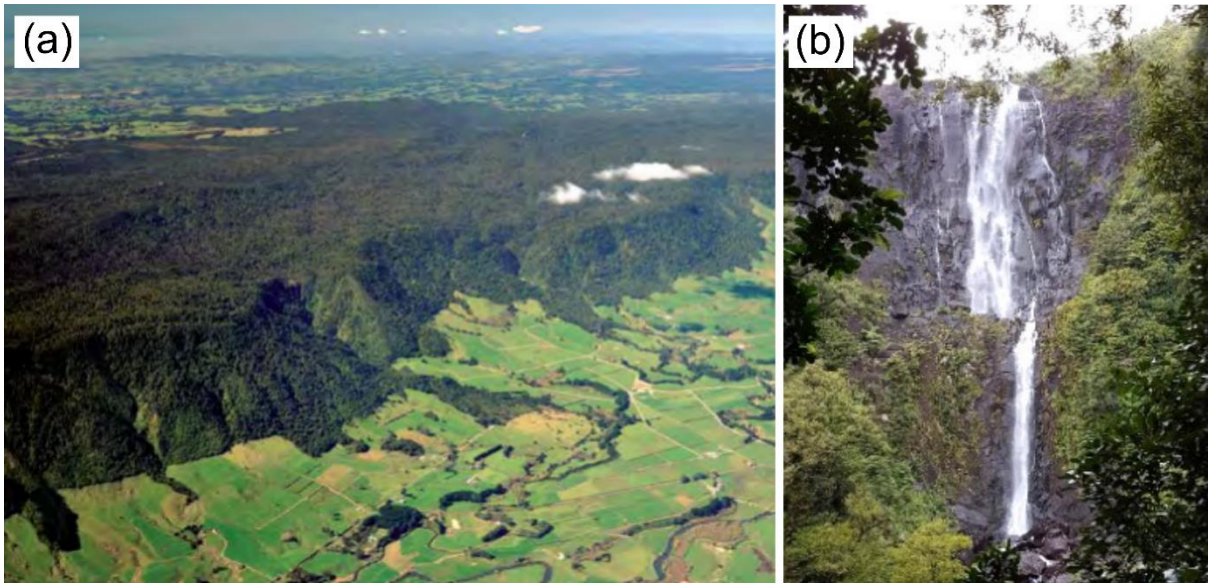

Figure 1.3 (a) The southern Kaimai Range constituting the dissected Whakamarama plateau viewed southeast across the Hauraki-Okauia fault scarp. Photo credit: D.B. Townsend, Leonard *et al.,* 2010. **(b)** Densely welded Waiteariki Ignimbrite at Wairere Falls (NZ Topo 50 map reference BD36 538 198). The falls drop 153 metres over the steep Hauraki-Okauia escarpment.

The majority of lithological and thickness data for the Waiteariki Ignimbrite has been obtained by exploratory drilling during the preliminary geologic investigations prior to the drilling of the Kaimai Rail Tunnel (Healy, 1967; Hegan, 1972, 1973). Of the numerous cores drilled, ES112 contains up to 157 m of Waiteariki Ignimbrite and is currently in storage at GNS Science.

Thickness of the Waiteariki Ignimbrite is variable due to considerable underlying relief but maximum thicknesses of up to 220 m are documented (Healy, 1967). Healy (1967) considered it to consist of numerous flow units and subdivided it into four lithological units: upper non-welded pumiceous breccia, two welded ignimbrite units, and a basal unit consisting of pumiceous breccia and tuff. Subsequent authors (Hegan, 1972; Morgan, 1986; Houghton & Cuthbertson, 1989), have combined the two welded ignimbrite units to define a total of three distinct units:

1) an upper soft, non-welded to welded zone between 50–70 m thick, with extensive vapour phase alteration of pumice to cristobalite and alkali feldspar;
2) a middle zone up to 150 m thick of welded ignimbrite containing alternating moderately welded and densely welded lenticular zones; and
3) a 3–5 m thick non-welded basal zone consisting of pumiceous tuff breccia and ash.

Much of the upper unit has been eroded so most surface exposures consist of the middle-welded unit. Isolated field exposures of basal Waiteariki Ignimbrite have been described in the Ngamuwahine (NZ Topo50 map reference BD36 638 112) and Mangakarengorengo rivers (NZ Topo50 map reference BD36 658 100; Morgan, 1986).

Lithology and Petrography

The Waiteariki Ignimbrite is a crystal- (up to 30 %) and pumice- (20 %) rich, eutaxitic and dacitic ignimbrite (Briggs *et al.*, 1996). Phenocrysts consist of plagioclase and subordinate amounts of quartz, hornblende, orthopyroxene and in the upper unit, biotite (Houghton & Cuthbertson, 1989), however, Morgan (1986) also identified biotite within the basal unit.

Pumice clasts are crystal-rich and are commonly deformed into dark grey to black elongate fiamme. In less welded zones, pumices are less flattened and the matrix is vitriclastic, with platy, cuspate and Y-shaped glass shards which are variably devitrified and may have undergone extensive vapour phase alteration (Briggs *et al.*, 1996).

Lithic fragments within the Waiteariki Ignimbrite are rare (< 4 %) and comprise dense dacite and flow-banded or spherulitic rhyolite (Houghton & Cuthbertson, 1989; Whitbread-Edwards, 1994), andesite and rhyolite (Harmsworth, 1983) and densely welded Waiteariki Ignimbrite (Morgan, 1986). Clasts of

andesite and rhyolite are predominately small (10–20 cm) while blocks of Waitearikiignimbrite reach sizes of 300–500 mm in diameter. The presence of welded Waitearikiignimbrite lithic fragments within the ignimbrite itself is atypical and implies that the deposition of this unit resulted from at least two discrete pyroclastic flows which were interceded by a period of time, allowing the initial unit(s) to harden prior to the eruption of subsequent units.

Geochemistry

Geochemical analysis of the Waitearikiignimbrite is restricted to a few whole-rock analyses using X-ray fluorescence spectrometry (XRF), and electron microprobe analyses (EPMA) of mineral separates of plagioclase, amphibole, orthopyroxene, biotite and Fe-oxides obtained by Master of Science students during the mid-1990s (Hall, 1994; Whitbread-Edwards, 1994; Hollis, 1995). Available major and trace element data is presented in **Table 1.3** with phenocryst compositions presented on their respective classification diagrams (**Fig. 1.4**).

The composition of the Waitearikiignimbrite ranges from dacitic (67.54–70.15 % SiO_2) to low-SiO_2 rhyolite (71.6 % SiO_2). Major element composition is consistent across all analyses with the exception of sample Wt116 (Hollis, 1995). This sample appears to be significantly weathered (~10 % LOI; **Table 1.3**), resulting in elevated normalised major element concentrations (e.g. Al_2O_3 = 22.13 wt. %, all other samples Al_2O_3 = c. 17 wt. %) and thus should be excluded from geochemical interpretations. Trace element abundances are typically quite variable (e.g. Sr = 151–232 ppm, Ba = 680–800 ppm) yet some elements show very tight compositional ranges (e.g. Zr = 169–179).

Phenocrysts are anhedral to euhedral and highly fragmented. Plagioclase phenocrysts are defined as oligoclase to labradorite ($An_{28–70}$), of which most fall within the range of andesine ($An_{30–50}$). Microprobe analysis of two phenocryst cores and rims indicates the crystals have normal compositional zoning (Whitbread-Edwards, 1994), although limited, this data does not exclude oscillatory or reverse zoning which is frequently described in large plagioclase crystals as a regular decrease in An content rarely dominates for the full crystallisation period (Coote & Shane, 2016). Orthopyroxenes range in composition from $En_{45–62}$ and calcic amphiboles are classed as magnesio- to tschermakitic-hornblende based on the classification of Leake *et al.* (1997). The amphibole crystals analysed in Hollis (1995) plot apart from those in Hall (1994) and Whitbread-Edwards (1994) with lower Mg, classifying them as ferro-hornblende.

Table 1.3. Existing whole-rock XRF geochemical analyses for the Waiteariki Ignimbrite.

Sample Name	**Wai 62**	**Wt 116**	**Wt 120**	**Wtr GH16**	**Wtr GH33**
Sample Location	McLaren Falls	Hopping's farm	Ruahihi	E of Oropi Rd	?
Source	*Whitbread-Edwards (1994)*	*Hollis (1995)*	*Hollis (1995)*	*Hall (1994)*	*Hall (1994)*
Major elements (XRF, wt. %)					
(Normalized to 100 % on LOI, volatile free; LOI and Totals are original values)					
SiO_2	67.54	69.33	71.60	69.88	70.15
Al_2O_3	16.84	22.16	16.3	17.17	17.8
TiO_2	0.54	0.60	0.39	0.44	0.43
MnO	0.01	0.07	0.02	0.07	0.12
Fe_2O_3	0.95	1.05	0.65	0.78	0.74
FeO	3.41	3.78	2.33	2.79	2.66
Na_2O	3.91	0.72	3.35	3.36	2.69
MgO	0.67	0.09	0.19	0.25	0.37
K_2O	2.15	1.98	2.95	2.59	2.79
CaO	3.76	0.19	2.2	2.64	2.23
P_2O_5	0.02	0.03	0.02	0.02	0.02
LOI (%)	2.28	9.54	2.92	3.14	4.1
Sum (%)	100	100.22	99.53	99.54	99.83
Trace elements (XRF, ppm)					
F	-	-	-	-	-
S	-	-	-	-	-
Cl	-	-	-	-	-
Sc	14	9	9	10	10
V	55	47	35	43	38
Cr	8	5	8	6	4
Co	-	-	-	-	-
Ni	5	3	4	3	4
Cu	8	7	8	7	8
Zn	62	43	48	66	57
Ga	17	21	17	18	17
As	3	1	6	1	2
Rb	73	70	104	87	96
Sr	232	24	156	176	151
Y	56	6	19	21	23
Zr	170	203	169	179	176
Nb	7	6	4	7	7
Mo	-	-	-	-	-
Sn	-	-	-	-	-
Sb	-	-	-	-	-
Cs	-	-	-	-	-
Ba	680	466	725	726	800
La	30	8	19	20	20
Ce	48	35	36	41	43
Nd	-	-	-	-	-
Tl	-	-	-	-	-
Pb	12	15	13	11	15
Th	8	11	10	9	9
U	2	3	2	2	2

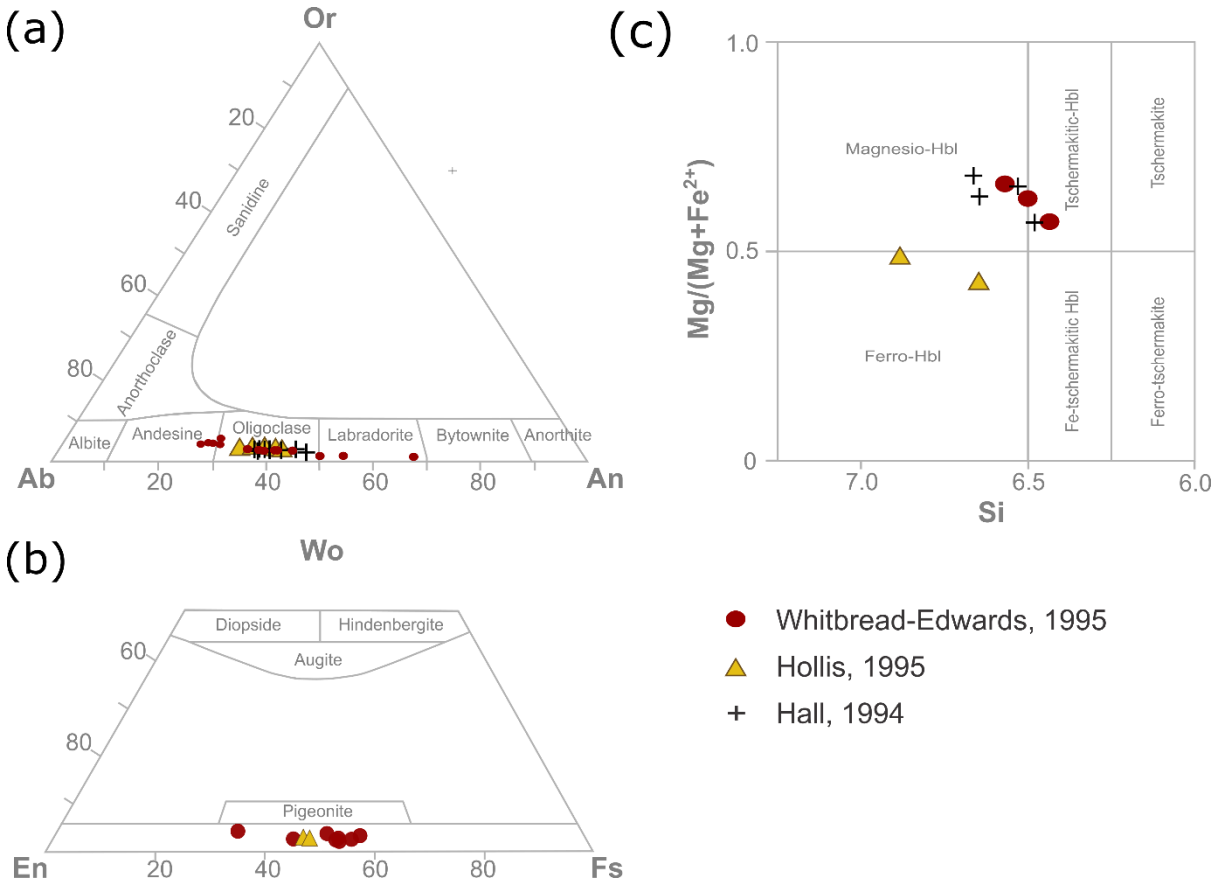

Figure 1.4. Plagioclase **(a)**, pyroxene **(b)** and hornblende **(c)** classification diagrams of phenocrysts in the Waitеariki Ignimbrite. Redrawn with data from Hall (1994); Hollis (1995) and Whitbread-Edwards (1994).

1.5.2 Post-TgaVC volcanic and volcaniclastic deposits

Intercalated with the volcanic units of the TgaVC are the deposits of the Matua Subgroup. Originally defined by Harmsworth (1983) and refined by Briggs *et al.* (2006), the Matua Subgroup includes fluvial pumiceous and rhyolitic silts, sands and gravels, diatomaceous lacustrine and estuarine muds, peats and sediments derived from reworked ignimbrites, lava domes and flows from the Tauranga region and distal TVZ. Nomenclature used here follows that of Leonard *et al.* (2010) and alternative names used in published papers and non-published student theses are shown in italics as parentheses. Distinguishing characteristics of all TgaVC- and TVZ-derived ignimbrites found in the broader Tauranga region are summarised in **Table 1.4**.

1.5.2.1 Ongatiti Ignimbrite

Isolated outcrops of the Ongatiti Ignimbrite are found in the Tauranga region north of the Wairoa River between Manawata and Minden Peak domes (**Fig. 1.2**). The voluminous Ongatiti Ignimbrite

Table 1.4. Distinguishing characteristics of ignimbrite units found within the Tauranga region (Healy, 1967; Harmsworth, 1983; Morgan, 1986; Hughes, 1993; Hall, 1994; Whitbread-Edwards, 1994; Hollis, 1995; Briggs *et al.*, 1996). Ignimbrite names in bold are derived from the TgaVC. Italicised names in parentheses, represent ignimbrites defined by Briggs *et al.* (1996). Fmn = Formation

Ignimbrite:	**Waiteariki**	**Papamoa**	Ongatiti	*Te Puna*	Chimp Fmn *(Te Ranga)*	Pokai Fmn *(Waimakariri)*	Mamaku
Outcrop characterisation	Forms bluffs and cascading waterfalls. Widely spaced columnar jointing	Bluff forming, valley infilling	Columar jointed cliffs	Exposed in coastal cliffs and road cuttings	Steep sided interfluves and flat-topped ridges	Bluff forming	Bluff forming. Columnar jointed where welded
Colour:							
Matrix	Light grey brown, varying to cream or grey	Cream grey upper and brown grey-buff brown lower unit	Buff brown	Buff brown	Cream	Cream to brown to grey	Pink to purple grey
Pumice	Dark grey fiamme or lenticulites	White-black	Whitish cream	White-grey	Cream	Cream to orange	
Welding degree	Non-welded to strongly welded	Variable	Non to strongly welded	Non- to partially-welded	Non-welded, partially consolidated	Non-welded base with welded upper	Highly variable
Juvenile material:							
Clast type	Pumice (crystal-rich up to 20%)	Pumice and scoria	Pumice (up to 20%)	Pumice (15-20%)	Pumice (5-25%)	Pumice (15-20%)	Pumice (7-20%)
Size	up to 400 mm	Upper: <25 mm; Lower: max 190 mm	50 mm	?	?	30-80 mm	
Crystal %	~30%	Upper: ? Lower: 15-20%	25%	25%	7-12%	10-20%	~10%
Mineral phases	Pl (Oligoclase-labradorite)	Pl	Pl	Pl	Pl	Pl (glomerocrystic)	Pl
	Qtz	Qtz	Qtz	Qtz	Opx	Subordinate qtz	Qtz
	Hbl	Hbl	Opx	Opx	Qtz	Opx	Opx
	Opx	Opx	Hbl		Hbl	Hbl (trace)	Cpx, Hbl (trace)
	Bt (upper & lower units only)	Bt			Cpx	Bt (rare)	Bt (rare)
Lithics							
% and size	Variable (up to 300-500 mm)	25-55 mm	Variable	Lithic poor (1-2%)	Lithic poor (1-5%)	<1-8%	<20 %
Type	Andesite-rhyolite, welded Waiteariki Ignimbrite	Grey to pink rhyolite and black to dark grey andesite	Andesite to rhyolite	Rhyolite	Obsidian and rhyolite	Rhyolite. Rare greywacke	Argilite, rhyolite and ignimbrite

(~500 km^3 DRE) was erupted at c. 1.3 Ma (Pittari *et al.*, 2021) from the Mangakino volcanic centre, which lies southwest of Tauranga within the TVZ. Within Tauranga, the ignimbrite is welded with white dense fibrous pumice (up to 20 % and 50 mm in size) set in a buff-brown matrix with a distinctive coarsely vitriclastic texture (Briggs *et al.*, 1996). It is crystal-rich (up to 25 %) and contains phenocrysts of plagioclase, quartz, hornblende, orthopyroxene, with accessory Fe-Ti oxides and zircon.

1.5.2.2 Undifferentiated Pakaumanu Group Ignimbrites (Te Puna Ignimbrite)

The Pakaumanu Group consists of voluminous and widespread ignimbrites and phreatomagmatic fall deposits derived from the Mangakino caldera, on the western limits of the TVZ (Leonard *et al.*, 2010). Eroded remnants of the Ongatiti Ignimbrite and, the informally named, Te Puna Ignimbrite crop out within central and coastal areas of the Tauranga region.

The name Te Puna Ignimbrite was first used by Harmsworth (1983) to describe a non-welded, light grey-yellow, lapilli ash tuff breccia which cropped out in cliff sections along the Wairoa River, Omokoroa, Pahoia Point and Matakana Island. The Te Puna Ignimbrite was further described by Whitbread-Edwards (1994), and consists of a non-welded, buff brown ignimbrite containing white to grey fibrous pumice (15–20 %) with a mineral assemblage of plagioclase, quartz, hornblende, orthopyroxene, Fe-Ti oxides and biotite which has weathered to a distinct golden colour. Lithics include variable coloured rhyolites, occasional charcoal and obsidian along with fragments of Ongatiti Ignimbrite. Single pumice clasts are rhyolite (72–76 wt. %).

Known exposures are confined to the vicinity of the Tauranga Harbour and hence, the Te Puna Ignimbrite has been considered in the past to represent a small volume ignimbrite derived from a local Tauranga source (Briggs *et al.*, 1996). However, $^{40}Ar/^{39}Ar$ dating provided a much younger age (0.929 ± 0.012 Ma; Briggs *et al.*, 2005) than all other TgaVC eruptives and it is now considered to be a distal ignimbrite originating within the TVZ. Similarities in lithology and age suggest the Te Puna Ignimbrite may represent distal Kidnappers or Rocky Hill ignimbrites of the Raepahu Formation (Leonard *et al.*, 2010), but unpublished paleomagnetic data cited by Briggs *et al.* (2005) prevents a direct correlation. As such this unit is currently referred to as undifferentiated Pakaumanu Group deposits.

1.5.2.3 Young TVZ-derived ignimbrites

The Chimp (*Te Ranga Ignimbrite*), Pokai (*Waimakariri Ignimbrite*) and Mamaku Plateau (*Mamaku Ignimbrite*) formations underlie the surface of the Mamaku Plateau and crop out within central areas of the Tauranga region between the Wairoa River and Pāpāmoa Range (**Fig. 1.2**). These ignimbrites

were erupted during a significant ignimbrite flare-up event which occurred between ~350 and 280 ka (Gravley *et al.*, 2016).

Within the Tauranga region, the Chimp Formation (*Te Ranga Ignimbrite*) consists of a non-welded, poorly-consolidated ignimbrite with rare (< 10 %) almost aphyric pumice clasts (Leonard *et al.*, 2010). No radiometric age determination has been undertaken for the Chimp Formation, however, its age is constrained by the underlying Whakamaru Group ignimbrites (340 ka; Downs et al., 2014) and that of the overlying Pokai (*Waimakariri Ignimbrite*) Formation (c. 300 ka; Downs *et al.,* 2014). The Pokai (*Waimakariri*) Ignimbrite varies in texture from non-welded with cream coloured at its base to welded with columnar jointing with a distinctive dark grey matrix with orange pumice clasts (Karhunen, 1993). Pumice clasts typically contain glomerocrysts or crystal clots of plagioclase and quartz up to 5 mm in size. Orthopyroxene and hornblende are generally only present in trace amounts (Briggs *et al.*, 1996). The ignimbrites of the Chimp and Pokai Formations are inferred to have originated from the Kapenga caldeara located to the south of the Tauranga region (Karhunen, 1993; Briggs *et al.*, 2005).

The Mamaku Plateau Formation Ignimbrite (hereafter referred to as simply the Mamaku Ignimbrite) is the youngest major, landscape-forming volcanic unit within the Tauranga region (Briggs *et al.*, 2005). Dated at c. 290 ka (Downs *et al.*, 2014), this ignimbrite is inferred to have been associated with the formation of the Rotorua Caldera (Milner *et al.*, 2003). The Mamaku Ignimbrite extends north, into the southern Tauranga region where the texture is highly variable, ranging from weakly welded to densely welded where the ignimbrite is thick. It has a moderate crystal abundance (c. 10 %) of quartz, plagioclase, orthopyroxene and hornblende and pumice clasts are usually powdery due to extensive vapour phase alteration, which also imparts a distinctive pink-purple hue (Briggs *et al.*, 1996). The plateau surface is deeply dissected by rivers, many of which cut down into the underlying Pokai, or Waiteariki ignimbrite (Harmsworth, 1983).

1.5.3 Postulated caldera structures within the Tauranga Volcanic Centre

Caldera structures of the CVZ and TVZ have been recognised from the location of lava dome complexes, Bouguer gravity anomalies, distribution and thickness of ignimbrites, location of lithic lag breccia facies and structural evidence of collapse (Malengreau et al., 2000; Wilson et al., 1995a). The rhyolitic lava dome complexes of the TVZ predominately lie within, on or just outside the rims of calderas. The rhyolitic domes of the TgaVC also occur in spatially associated groups and three locations have been postulated in literature as a possible caldera(s). The first described by Briggs et al. (2005) is situated in the north-western area of the Tauranga Basin between Katikati and Matakana Island which is marked by a strongly negative Bouguer gravity anomaly (Stagpoole *et al.*, 2021). Alternatively, a large area of low residual gravity located under the northern Mamaku Plateau may

also indicate a potential caldera source and origin for the Waiteariki Ignimbrite (Wilson *et al.,* 1995a). Finally, laucustrine diatomaceous siltstones and extensive lag breccia facies were attributed by Morgan (1998) to represent a broadly elongate north-south striking caldera structure located within the southern Kaimai Range which is bounded to the northeast and west by the lava domes of Kaikaikaroro, Kaimai and Te Weraiti. The above evidence, however, is inconclusive. The position of the gravity anomalies does not coincide with the distribution of the rhyolite domes (Briggs *et al.*, 2005), and no anomaly has been identified in the area of laucustrine sediments and lag breccia facies documented in the southern Kaimai Range. Circular depressions created as a result of structural collapse are also not observed within the Tauranga-Kaimai area which may result from infill and burial by younger volcanic and/or sedimentary deposits, or the ignimbrites were not voluminous enough to initiate collapse and caldera formation (Briggs *et al.*, 2005). Without evidence of a caldera structure, Briggs et al. (2005) designated the silicic domes, and ignimbrites of Tauranga as a volcanic centre, however, the boundaries and size of the TgaVC were poorly defined.

1.6 Possible correlatives of TgaVC eruptives

The Neogene stratigraphic succession in northern Hawke's Bay is positioned downwind to the southeast where several macroscopic tephras and a distal ignimbrite have been identified within Mangaheia Group rocks of Nukumaruan age (2.4-1.63 Ma; Bland et al., 2007; Hopkins & Seward, 2019).

The Esk Mudstone is laterally extensive, cropping out between the Ohara depression in the southwest to Putorino (**Fig. 1.5**) in the northeast. It consists of a blue-grey, non-cemented, non- to slightly fossiliferous sandy siltstone frequently punctuated by bioturbated tephra beds of lower Nukumaruan (up to 2.4 Ma) age (Bland *et al.*, 2007). Tephra beds are particularly well exposed in Waikoau and Mangaone rivers (locations c,d respectively, **Fig. 1.5**). The Esk Mudstone grades into the overlying Tutira Member of the lower Petane formation, which consists of alternating cyclotherm sequences of mudstone, sandstone to conglomerate or limestone in lower and upper parts respectively, attributed to glacio-eustatic sea level changes (Haywick *et al.*, 1991). The Tutira Member comprises a coarsening-upwards package of sandstone to greywacke conglomerate facies representing nearshore to shoreface and non-marine braid-plain depositional environments (Bland *et al.*, 2007). Sharply overlying the Tutira Member is the Hikuroa Pumice Member, a distal ignimbrite overlain by reworked pumiceous ash and lapilli.

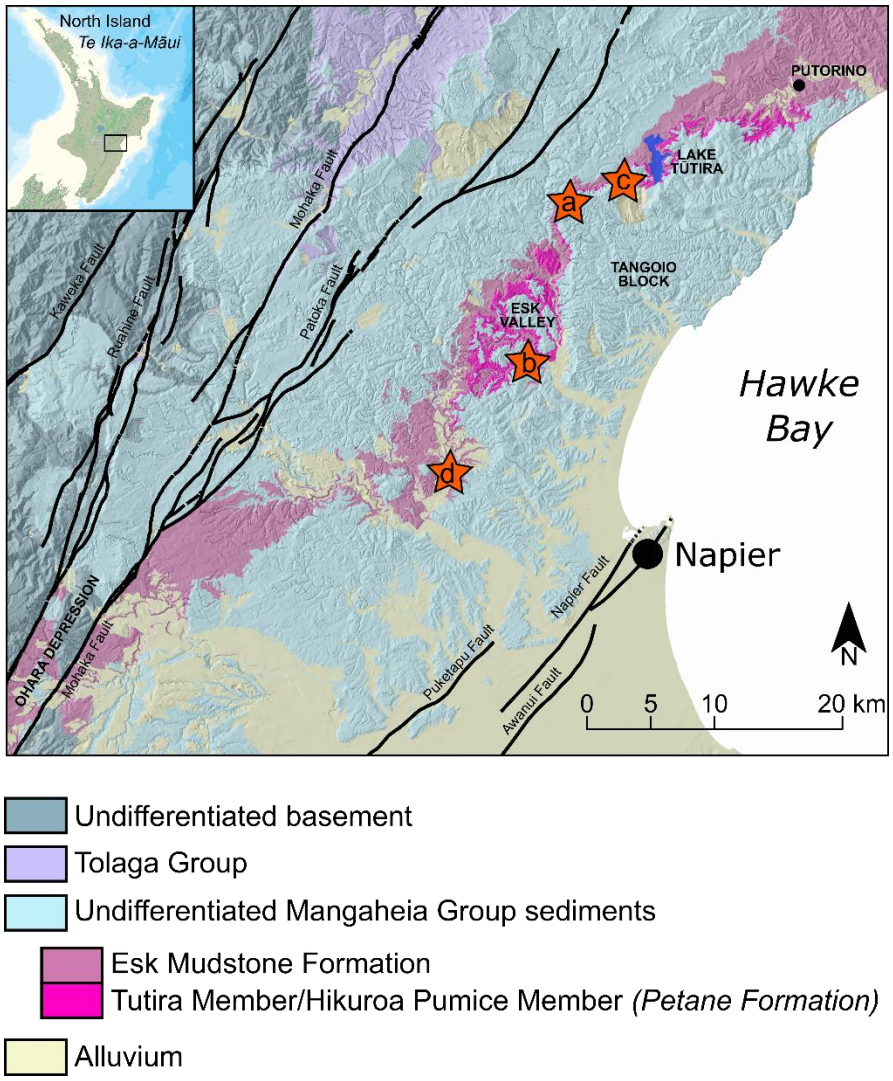

Figure 1.5. Simplified geological map of the northern Hawke's Bay region highlighting the distribution of Nukumaruan aged (2.4-1.63 Ma) sedimentary units (Hikuroa Pumice Member, Esk Mudstone Formation) which contain macroscopic tephra which are inferred to originate from the TgaVC. Orange stars represent outcrop locations referred to in the text: a, Darkys Spur; b, Beattie Road; c, Waikoau river; d, Mangaone river, Rissington.

The Hikuroa Pumice Member is the most conspicuous unit and provides an important marker bed within the lower Petane Formation throughout the Tangoio, Tūtira and Esk Valley regions (**Fig. 1.5**). The type locality is located along Darkys Spur Road (NZ Topo50 map reference BJ39 230 491, Location a, **Fig. 1.5**) with well exposed reference sections also found and near Beattie Road (NZ Topo50 map reference BJ39 263 350; Location b, **Fig. 1.5**) where it is between 8-15 m thick (Bland *et al.*, 2007). The Hikuroa Pumice Member has previously been correlated to an offshore tephra deposit in core OPD 1124C (Bland et al., 2007) which corresponds to tephra AT-313 of Carter et al. (2004). Hopkins and Seward (2019) presented zircon fission-track ages for the Hikuroa Pumice Member at Darkys Spur of 2.0 ± 0.6 and 1.9 ± 0.4 Ma, which overlap within error with the paleomagnetic (2.165 Ma) and biostratigraphic (2.1496 Ma) ages of Stevens (2010). The Hikuroa Pumice and the tephras contained

within the Esk Mudstone are therefore chronologically equivalent to volcanic deposits of the TgaVC and have correlative potential.

Ignimbrites of the Rotoroa Formation identified within geothermal drill cores at Kawerau (**Fig. 1.2**) also have correlative potential with TgaVC deposits. Two thin pyroclastic units (< 15 m) were identified in cores KA25 (−796 m relative to seal level (mRL)) and KA34 (−707 mRL) and zircons were U-Pb dated at 2.17 ± 0.05 Ma and 2.38 ± 0.05 Ma, respectively (Milicich *et al.*, 2013a). KA25 consists of eutaxitic tuff with crystals of embayed quartz, plagioclase, ferromagnesian minerals and biotite and minor lithics of rhyolite lava (some spherulitic) and greywacke. The pumice-bearing ignimbrite in KA34 also contains plagioclase, quartz and minor biotite, and minor lithics of rhyolite and andesite lava, tuff and greywacke. Both units are inferred to be distal ignimbrites sourced from the wider Tauranga region on the basis of radiometric age (Milicich et al., 2013a).

1.7 Overview of silicic magma systems and the products of voluminous eruptions

Silicic magmas of evolved dacite to rhyolite composition (> 63 % SiO_2) typically result from the fractional crystallisation of a less evolved magma composition, accompanied by assimilation of crustal material through partial melting or the physical mixing of two or more discrete magmas (Hildreth, 1981; de Silva *et al.*, 2006; Bachmann & Bergantz, 2008; Grove & Brown, 2018). These processes were traditionally viewed as occurring within a large, melt-dominant body where crystallising phases were progressively removed through gravitational settling (**Fig. 1.6 a**), however, modern concepts of silicic magmatic systems revolve around the crystal mush model (**Fig. 1.6 b**; Hildreth, 2004; Bachmann & Huber, 2016; Jackson *et al.,* 2018; Wilson *et al.,* 2021). Crystal mushes consist of viscous mixtures of crystals and interstitial melt which are stored within sill-like structures in mid to upper crustal subvolcanic reservoirs that differentiate over tens to hundreds of thousands of years (Cashman & Giordano, 2014). At low crystallinities, convection leads to the dynamic stirring of crystals and melt which stops when rheological lock-up occurs at c. 50–60 vol % crystals.

The mush model is evoked for many large silicic systems where both crystal-rich and crystal-poor magmas have been erupted through time (e.g Lindsay *et al.,* 2001; Kay *et al.,* 2011; Cooper *et al.,* 2014). Mechanisms proposed to segregate the rhyolitic interstitial melt to form eruptible melt-rich caps or pockets include hindered settling, micro-settling and viscous compaction (cf. Bachmann and Bergantz, 2004) and invoke internal buoyancy forces. However, Holness (2018) cast doubts on the

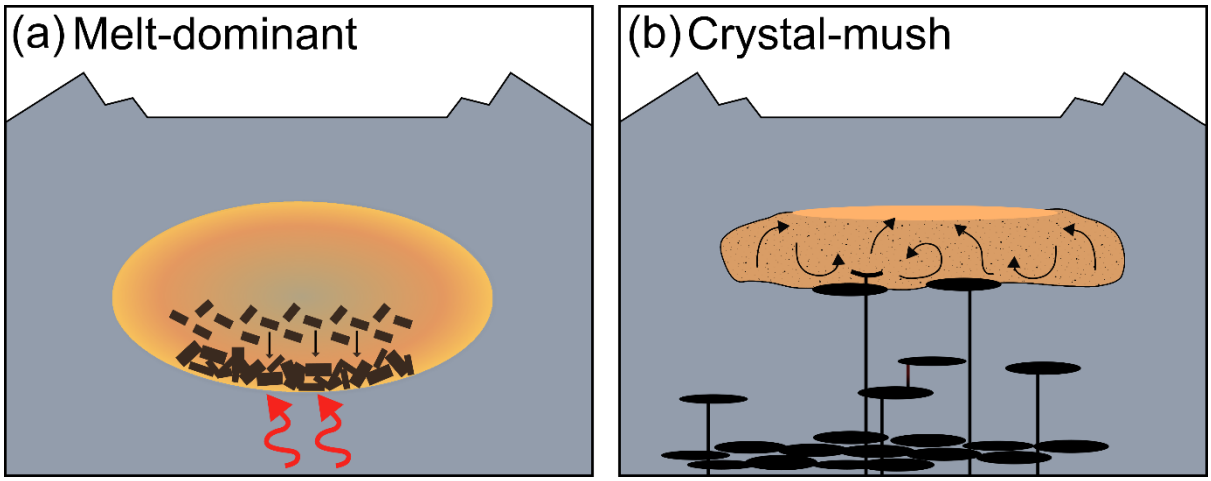

Figure 1.6. Models for subvolcanic magma reservoirs. **(a)** Traditional model consisting of large, melt-dominant body where crystallising phases were progressively removed through gravitational settling and, **(b)** trans-crustal crystal mush model where viscous mixtures of crystals and interstitial melt are stored within sill-like structures in mid to upper crustal subvolcanic reservoirs.

applicability of these mechanisms for silicic mushes as hindered settling requires very low particle concentrations and there remains a lack of textural evidence which demonstrates the crystal deformation expected during gravitationally driven viscous compaction. Instead Holness (2018) propose that other factors are more likely and include the thermal rejuvenation and mobilization of interstitial liquid within the mush (Bergantz *et al.,* 2015; Sliwinski *et al.,* 2017), gas filter-pressing of H_2O-rich magmas within in the shallow crust (Anderson *et al.,* 1984; Sisson & Bacon, 1999), or an externally-imposed stress field (Hildreth, 2004; Allan *et al.,* 2017; Schaen *et al.,* 2017).

The crystal cargos of mushes attest to these reservoirs as being trans-crustal features, where multiple, variably evolved reservoirs are distributed throughout the crust, of which, some or all are tapped during eruptions (Wilson *et al.*, 2021). The formation of crystal mush zones has been proposed as the driving mechanism behind large long-lived silicic systems. Overall, such systems are dominated by the sporadic eruption of small volumes of magma, however, numerous large volume (≥ 100 km^3 DRE) silicic ignimbrites are also documented (e.g Taupō Caldera; Barker et al., 2021). These large, caldera-forming eruptions can be classified according to dominant whole-rock magma type as either crystal-rich (≥ 35 %) dacites, often referred to as monotonous intermediates (MIs), or crystal-poor (≤ 15 %) rhyolites (CPR) (Cashman & Giordano, 2014). The volumetrically largest eruptions (e.g. Fish Canyon Tuff; Bachmann *et al.*, 2002) almost always involve MI magma, which have mostly homogenous whole-rock compositions and consistent mineral assemblages (Hildreth, 1981; Christiansen, E. H., 2005), although exceptions are known (e.g. Lund Tuff; Maughan *et al.*, 2002) and are interpreted to represent the evacuation of significant volumes of partially remobilised crystal mushes (Bachmann *et al.*, 2002;

Maughan *et al.*, 2002a; Folkes *et al.*, 2011; Willcock *et al.*, 2013; Yamamoto, 2021). Such eruptions are inferred to be triggered by external forces such as tectonism (Gregg *et al.,* 2015), which initiate with sustained pyroclastic density currents along bounding ring faults following catastrophic decompression of the underlying magmatic system during regional extension events (cf. Gottsmann *et al.*, 2009). The resulting deposits are typified by voluminous and thick ignimbrite sheets with vesicle-poor juvenile clasts, low lithic content, syn-eruption of co-magmatic plutonic lithics and a high proportion of crystal fragments due to explosive expansion of phenocryst-hosted melt inclusions.

In contrast, eruptions involving CPR initiate with widespread and voluminous pyroclastic fall deposits of high-SiO_2 rhyolitic magmas which are followed by pyroclastic flows only after caldera collapse occurs. Yet, despite their distinct differences, overlap in glass compositions attests that these endmember-type ignimbrites have similar origins and likely represent separate parts of complex magma-mush storage reservoirs (Hildreth, 1981; Lindsay *et al.,* 2001; Christiansen, 2005; Huber *et al.*, 2012; Cashman & Giordano, 2014).

CHAPTER 2:

2 Linking proximal ignimbrites and coeval distal tephra deposits to establish a record of voluminous Early Quaternary (2.4-1.9 Ma) volcanism of the Tauranga Volcanic Centre, New Zealand

Marlena Prentice[a*], Adrian Pittari[a], David J. Lowe[a], Geoff Kilgour[b], Peter J.J. Kamp[a], Miriam Namaliu[a]

[a]*School of Science-Te Aka Mātuatua, University of Waikato, Hamilton, New Zealand*

[b]*GNS Science, Wairakei*

*Corresponding author

Email: prenticelm@gmail.com

Abstract

The Tauranga Volcanic Centre (TgaVC) of the North Island, New Zealand, was active from 2.95 to 1.9 Ma. It lies temporally and spatially between the currently active Taupō Volcanic Zone, one of the most productive regions of Quaternary silicic volcanism globally, and its predecessor, the Coromandel Volcanic Zone. This study provides an enhanced chronology for pyroclastic volcanism of the TgaVC with four locally widespread units named and defined as follows: Welcome Bay and Wharo ignimbrites (together formerly known as Lower Pāpāmoa Ignimbrite); Otawera Ignimbrite; and Arateka Ignimbrite (formerly known as Upper Pāpāmoa Ignimbrite). These eruptives were followed by the eruption of the large-volume Waiteariki Ignimbrite at 2.1 Ma. In northern Hawke's Bay (150-170 km southeast of TgaVC), several distal tephra-fall horizons and an ignimbrite (Hikuroa Pumice Member) are preserved in marine-hosted sediments and are stratigraphically equivalent to the five ignimbrites of the TgaVC. Using new major- and trace-element data on glass in conjunction with new zircon-derived U-Pb ages, a correlation between the Hawke's Bay tephras and the TgaVC ignimbrites is established and the Hikuroa Pumice Member is confirmed as the distal deposit of the Waiteariki Ignimbrite. The integrated proximal and distal records show that at least eight eruptions occurred in the TgaVC between 2.4 and 1.9 Ma and provide a maximum repose period between explosive eruptions of ca. 50 kyrs.

Keywords

Taupō Volcanic Zone; Coromandel Volcanic Zone; Tauranga Volcanic Centre; Tephrochronology; U-Pb zircon geochronology; Geochemistry

2.1 Introduction

Sequences of tephra deposits produced by explosive volcanic activity play an important role in helping to construct the eruptive histories of large silicic volcanic fields. In proximal regions, the record of volcanism is often incomplete due to burial or destruction by subsequent volcanic activity and/or, tectonism and by the preferential erosion of unconsolidated pyroclastic deposits rather than resistant welded ignimbrites and lavas. In contrast, medial to distal tephra archives found within lacustrine, marine and ice-cores can provide more detailed records of mainly rhyolitic volcanism which, when combined with proximal records, provide valuable information about eruptive histories of long-lived silicic systems (Carter *et al.*, 2004; Kutterolf *et al.*, 2016; Lukács *et al.*, 2018; Amma-Miyasaka *et al.*, 2020). The use of tephrostratigraphy underpins such records and, together with stratigraphic superpositioning, is focused on the mineralogical and geochemical correlation and dating of key tephra units (Lowe, 2011).

The correlation of widespread distal tephras to proximal deposits originating from single eruption episodes provides an understanding of the eruptive histories, eruption volumes and recurrence intervals (Ponomareva *et al.*, 2015) and provide robust intra- and inter-regional isochronous marker beds which can then be used within a wide range of fields (Hopkins *et al.,* 2021a). These correlations then form the basis to determine distributions to reliably estimate and/or re-evaluate eruptive volumes and magnitudes of significant volcanic events (Kutterolf *et al.*, 2016; Ponomareva *et al.*, 2018; Silleni *et al.*, 2020). Additionally, geochemical analysis of the tephras (primarily glass shard constituents) can led to identification of source volcanoes (Kutterolf *et al.*, 2016) and magmatic evolution (Bryant *et al.*, 2003; Straub *et al.*, 2015; Pearce *et al.*, 2020).

Within Te Ika-a-Māui/North Island of Aotearoa New Zealand, the modern loci of arc-related volcanism occurs within the Taupō Volcanic Zone (TVZ) (**Fig. 2.1**). Active for c. 2 Myr, the TVZ has a long and complex history, yet it is only the latest manifestation of volcanism in Aotearoa New Zealand. Prior to activity within the TVZ, rhyolitic volcanism migrated southeast through the Coromandel Volcanic Zone (CVZ; 12-3.5 Ma). Combined, the CVZ and TVZ have created an extensive rhyolitic tephra record dating back over 12 Myr (Carter *et al.*, 2004). Yet despite this comprehensive record, very few correlations have been established between tephra-fall deposits and known proximal deposits because the chronological and geochemical record defining the history of volcanism in many source locations and their products remains poorly defined (Hopkins *et al.*, 2021b).

The silicic Tauranga Volcanic Centre (TgaVC), located in the Bay of Plenty region of North Island (**Fig. 2.1**), was active from 2.95 to 1.90 Ma (Pittari *et al.*, 2021). Volcanism of the TgaVC lies temporally and spatially between the defined locations and time frames of activity in TVZ and CVZ. Despite its

importance as a key transition centre between these two broader volcanic zones, understanding of volcanism during this period remains limited (Briggs *et al.*, 2005; Pittari *et al.*, 2021).

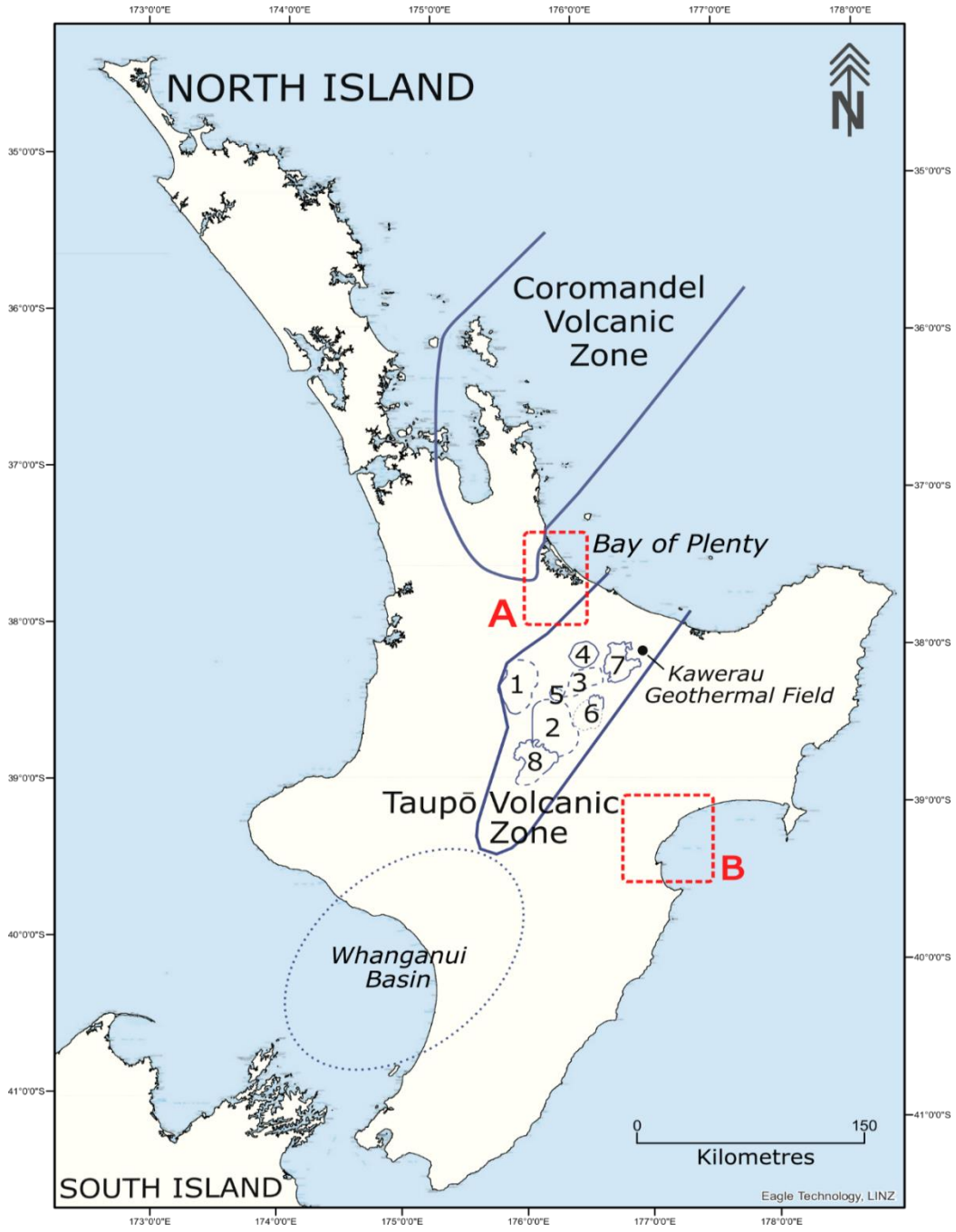

Figure 2.1. Map showing main centres of rhyolitic volcanism active in Te Ika-a-Māui/North Island since c. 3 Ma: the Coromandel Volcanic Zone (CVZ) (active c. 12–3.5 Ma (Carter *et al.*, 2004; Pittari *et al.*, 2021) and Taupō Volcanic Zone (TVZ) (active since c. 2 Ma) (Wilson & Rowland, 2016), and the locations of the Whanganui Basin and the Bay of Plenty **(A)** and Hawke's Bay **(B)** regions depicted in Figure 2.2. TVZ calderas are numbered as follows: 1, Mangakino; 2, Whakamaru; 3, Kapenga; 4, Rotorua; 5, Ohakuri; 6, Reporoa; 7, Okataina; 8, Taupō (after Leonard et al., 2010).

This study provides an enhanced chronology for volcanism of the TgaVC and we undertake new analyses of both ignimbrites in the TgaVC and stratigraphically-equivalent tephra horizons in northern Hawke's Bay which is located 150-170 km southeast of Tauranga (**Fig. 2.1**). Using major- and trace-element analyses of glass in conjunction with new zircon-derived U-Pb ages, we examine and test the previous assumption that tephra deposits preserved within northern Hawke's Bay marine sediments (2.4–1.63 Ma) were sourced from a vent region located in the TgaVC, primarily due to the similar ages of proximal deposits in the Tauranga region (**Fig. 2.2 a**) (Hopkins & Seward, 2019). These correlatives are linked in turn to other previously identified horizons, both onshore and offshore. The main focus of this paper is to demonstrate the multi-faceted approach required to confidently correlate proximal and distal pyroclastic deposits from the Early Quaternary period in order to establish a comprehensive eruptive history for the TgaVC. The petrogenesis of the magmas is not investigated here, but will be presented in subsequent chapters. We follow the definition in Lowe (2011) where the term "tephra" (*sensu lato*) refers to all unconsolidated pyroclastic products of volcanic eruptions including both fall deposits and those arising from (non-welded) pyroclastic density currents (pyroclastic flows or surges). For additional clarity, specific pyroclastic deposits are referred to as either tephra-fall, or distal or proximal ignimbrites.

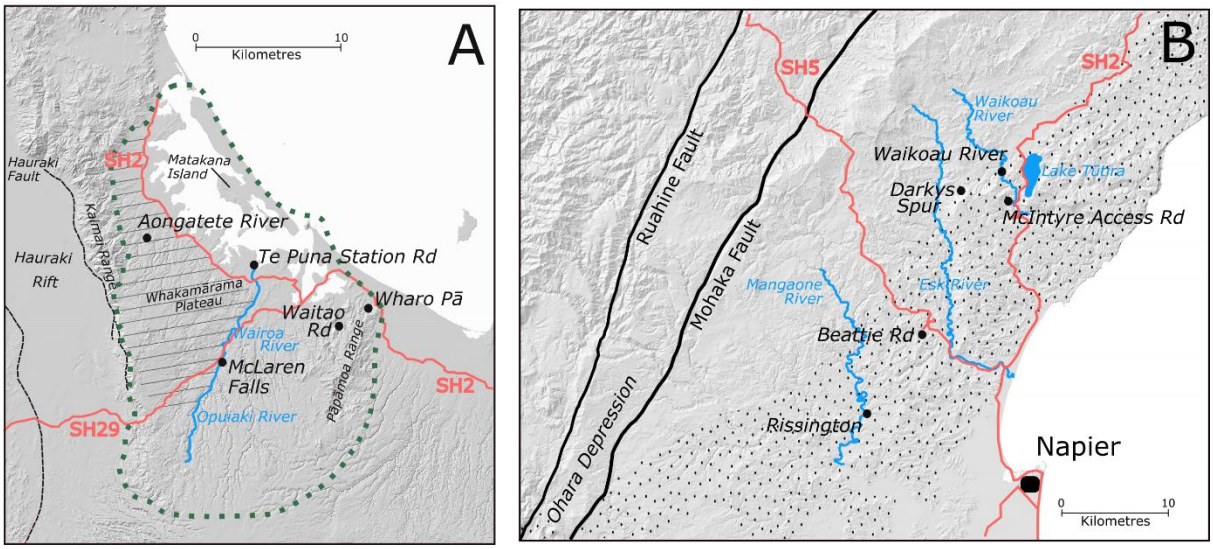

Figure 2.2 **(a)** Tauranga region with sample locations and features mentioned in the text with the extent of the Tauranga Volcanic Centre (TgaVC) outlined in green dots. **(b)** Northern Hawke's Bay with sample location sites and names referred to in the text. Stippled area shows regional extent of 2.4–1.63 Ma marine sedimentary deposits (known as the Esk and Petane formations) in which distal tephras have been preserved. State highways (SH) in red.

2.1 Stratigraphy and properties of ignimbrites in Tauranga Volcanic Center and Early Quaternary tephrostratigraphy of northern Hawke's Bay

2.1.1 Tauranga Volcanic Centre (TgaVC)

Deposits of the TgaVC (**Fig. 2.2 a**) consist of an eroded andesitic stratovolcano (Otawa Formation), numerous rhyolite-dacite lava dome or dome complexes (Minden Rhyolite Subgroup), a single emergent exposure of basalt found off the coast of Matakana Island within the Tauranga Harbour, and several ignimbrites within the Waitekariki and Pāpāmoa formations. Although the source(s) of these ignimbrites is yet to be formally defined, they are inferred to be of local (i.e. TgaVC) origin (Briggs *et al.*, 2005; Pittari *et al.*, 2021). Radiometric age determinations of deposits of the TgaVC have been undertaken using K-Ar (Takagi, 1995), $^{40}Ar/^{39}Ar$ (Briggs *et al.*, 2005), and U-Pb and (U-Th)/He (Pittari *et al.*, 2021) methods on whole-rock and crystal separates. Together, these dates have provided understanding of the volcanic stratigraphy of major geological units (**Fig. 2.3**) within the region and insight into the evolution of the TgaVC. Prominent ignimbrite units selected for analysis in this study are described below.

2.1.1.1 Waitekariki Ignimbrite

The welded Waitekariki Ignimbrite is the most prominent and voluminous pyroclastic unit of the TgaVC. It is exposed throughout the eastern foothills of the Kaimai Range and underlies the gently sloping upper surface of the Whakamārama Plateau (**Fig. 2.2 a**) (Houghton & Cuthbertson, 1989; Briggs *et al.*, 1996). Exposures are also found along the western margin of the Pāpāmoa Range. Throughout central and southern areas, the Waitekariki Ignimbrite is buried by younger TVZ-derived deposits where it is encountered in drill holes at a depth of 50–150 m with thicknesses exceeding 200 m in some localities (Houghton & Cuthbertson, 1989; Briggs *et al.*, 1996). This ignimbrite unit is a crystal- and pumice-rich, lithic-poor ignimbrite which is extensively welded and has pronounced eutaxitic texture (**Fig. 2.4 a**). The predominant mineral assemblage comprises is plagioclase, hornblende, pyroxene, and quartz with minor amounts of biotite with rare lithic clasts (< 2 %), predominantly derived from rhyolite lava (Briggs *et al.*, 1996). In outcrop, the Waitekariki Ignimbrite is pervasively devitrified making the groundmass glass unsuitable for geochemical analysis. However, during the 1970s, a series of cores were drilled across the eastern side of the southern Kaimai Range as part of geological investigations for the Kaimai Rail Tunnel (Healy, 1967; Hegan, 1972). Located near the eastern portal above the Aongatete River (**Fig. 2.2 a**), one such core, ES112, intersected 157 m of Waitekariki Ignimbrite with

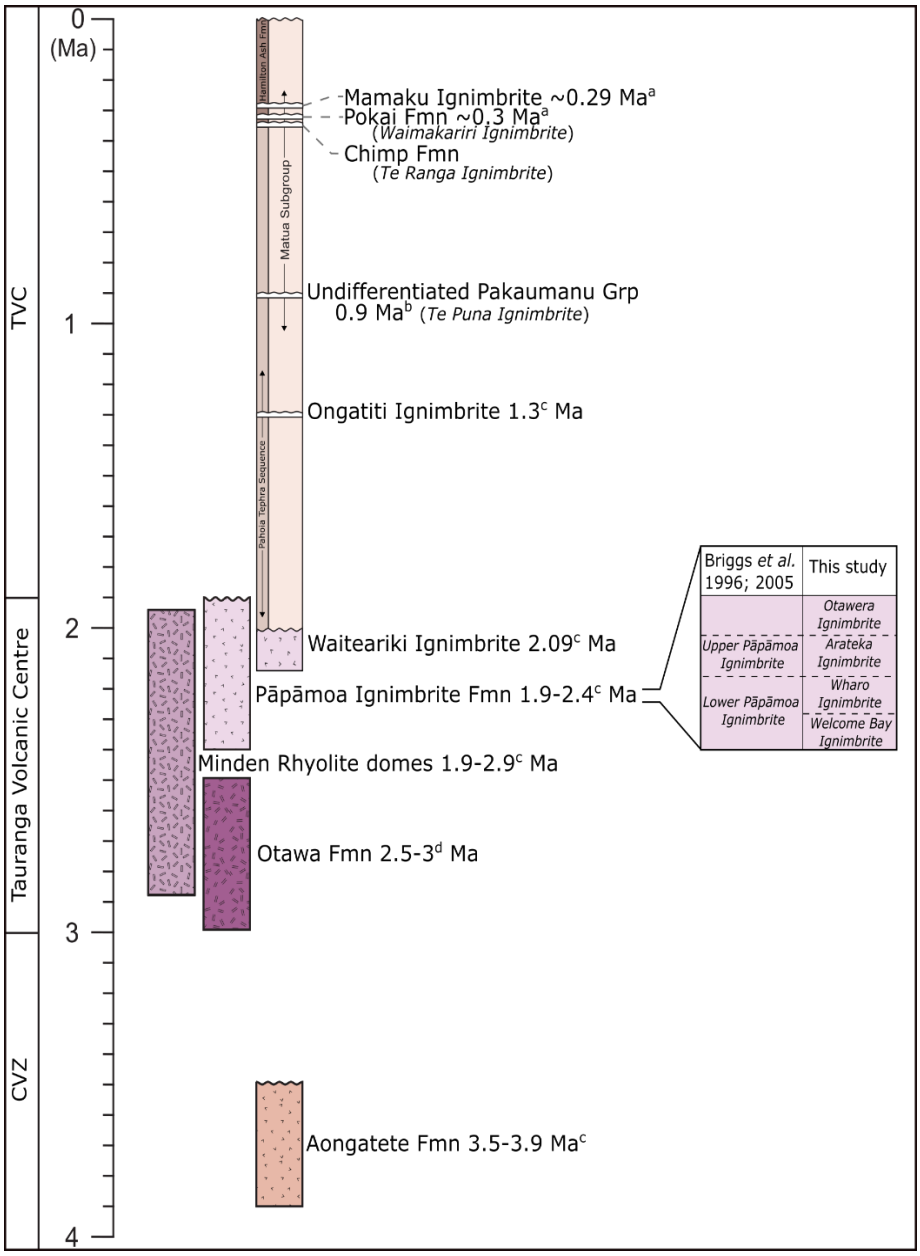

Figure 2.3. Generalised stratigraphy of the Tauranga region including deposits associated with TgaVC. Italicised names in parentheses, represent ignimbrites defined by Briggs *et al.* (1996). Ages obtained from Downs *et al.* (2014)[a]; Briggs *et al.* (2005)[b]; Pittari *et al.* (2021)[c]; Stipp (1968)[d]. Fmn, Formation; Grp, Group. Note that in this study we refer to four newly-named ignimbrite units within the Pāpāmoa Formation, amended from Briggs *et al.* (1996; 2005). See text for details.

light-brown perlitic glass preserved in the lower 10 m, a phenomenon documented in some other highly welded ignimbrites (e.g. Fish Canyon Tuff; Bachmann *et al.* 2002), and this basal glass provided material for geochemical analysis (see **Section 2.5** for discussion).

Zircon crystals for dating were obtained from a bulk sample collected from the Aongatete River. A second sample collected from an outcrop at McLaren Falls, 20 km to the southwest (**Fig. 2.2 a**), was unsuitable for glass analysis because of extensive devitrification, but zircons were extracted for dating.

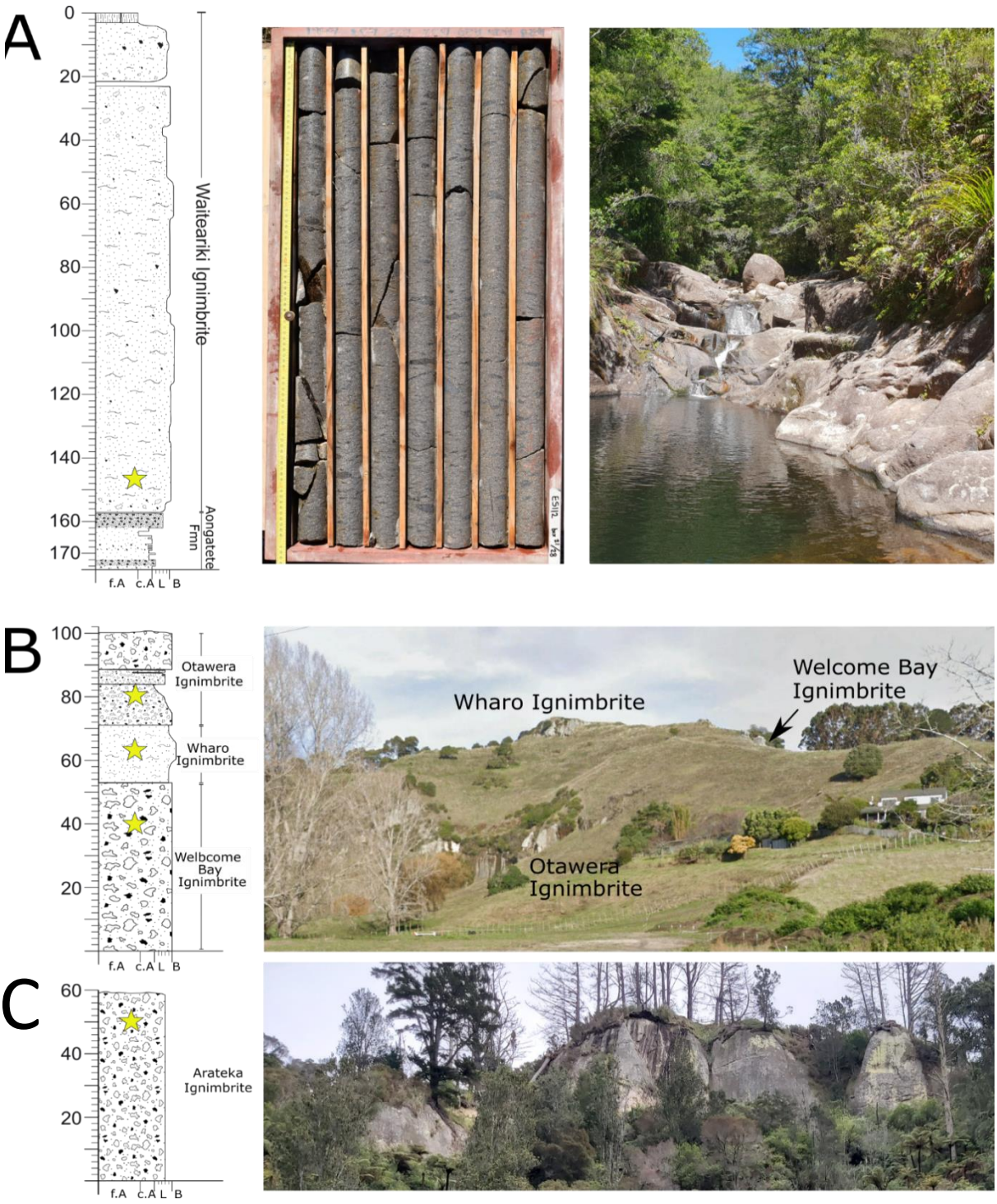

Figure 2.4. Simplified stratigraphic log and a photograph of pyroclastic deposits of the TgaVC. **(a)** Section of core ES112 through the Waiteariki Ignimbrite (left; see text); photo (right) shows a typical outcrop for the Waiteariki Ignimbrite (Aongatete River). **(b)** Outcrop photographs demonstrating the stratigraphic relationships of the newly named ignimbrite unit of the Pāpāmoa Formation: (top) Welcome Bay, Wharo and Otawera ignimbrite succession at Wharo Pā; (bottom) bluffs of Arateka Ignimbrite near Waitao Road. Note the inversion of relief. Yellow stars in stratigraphic columns indicate approximate sampling positions. Grain size abbreviations in columns **(b)** and **(c)** follow nomenclature defined by White and Houghton (2006): f.A, fine ash (< 1 mm); c.A, coarse ash (0.5–1 mm); L, lapilli (2–64 mm); B, blocks/bombs (> 64 mm).

2.1.1.2 Ignimbrites of the Pāpāmoa Formation

The Pāpāmoa Formation is a complex package of pyroclastic flows (**Fig. 2.4 b**) and interbedded fall deposits confined to the northern and western foothills of the Pāpāmoa Range where it overlies andesite and dacite lavas of the Otawa Formation (Briggs *et al.*, 2005). Briggs *et al.* (1996) divided the formation into the upper and lower ignimbrite units which are dated at 1.9 ± 0.1 Ma and 2.4 ± 0.02 Ma, respectively (Briggs *et al.*, 2005). A recent review of the internal stratigraphy of the Pāpāmoa Formation demonstrated that the formation is comprised of the deposits from several discrete eruptive events including the Arateka, Welcome Bay and Wharo ignimbrites (previously referred to as the Upper and Lower Pāpāmoa ignimbrites, respectively, (Briggs *et al.*, 1996), and the newly recognised Otawera ignimbrite and are described below.

Welcome Bay Ignimbrite

The Welcome Bay Ignimbrite is up to 115 m thick and is the major ridge-forming rock of the northern Pāpāmoa Range (**Fig. 2.2 a**). They type section is found at NZ Topo50 BD37 869 194 where the ignimbrite consists of a 1.2-m-thick, well sorted, massive, medium lapilli, pumiceous fall deposit overlain by 115 m of creamy grey-beige, massive, pumice- and lithic-rich (30 and 15 %, respectively), moderately-welded ignimbrite. This ignimbrite was previously named the Lower Pāpāmoa Ignimbrite by Briggs *et al.* (1996), but is re-named here with the recognition of a second ignimbrite unit (Wharo Ignimbrite, see below) lying stratigraphically above it. Welding increases slightly towards the top of the ignimbrite which produces irregular bluffs 6–10 m high that can be traced across the valleys (**Fig. 2.5 a**).

The Welcome Bay Ignimbrite is distinctive with two distinct juvenile clast compositions. The dominant clast type is a white-coloured dacitic pumice (~67 wt. % SiO_2; Namaliu, 2021) with a mineral assemblage comprising plagioclase, hornblende, and pyroxene. Subordinate clasts of dark-grey coloured andesitic pumices (~61 wt. % SiO_2) are less common and contain plagioclase and pyroxene but lack hornblende. Magma mingling between these two end-members is evident in flow-banded clasts. Pumice clast size is typically med-coarse lapilli (32–64 mm). Lithics are dominantly black to dark-grey andesite with subordinate clasts of pink rhyolite.

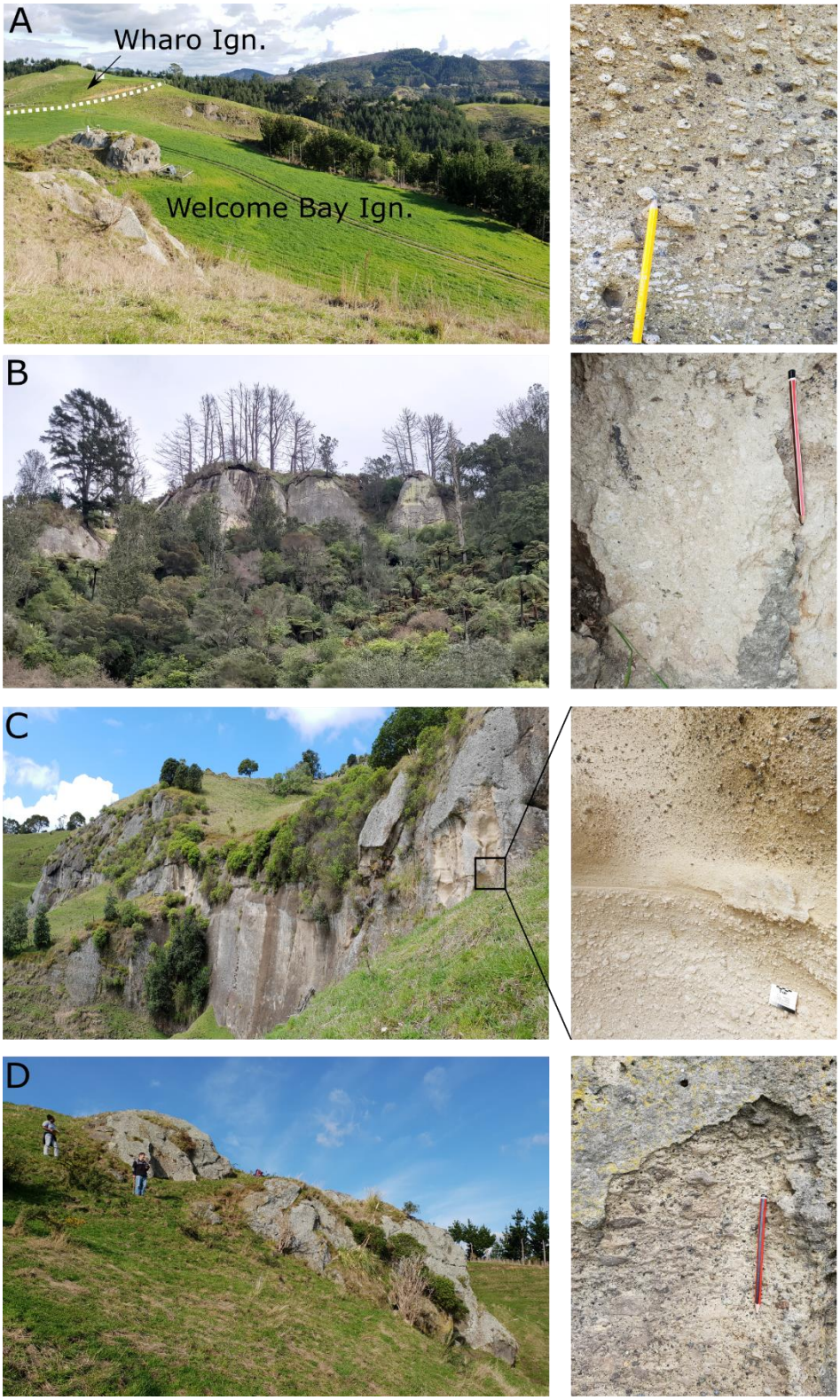

Figure 2.5. Photographs demonstrating typical outcrop features and textures of ignimbrites of the Pāpāmoa Formation. **(a)** Welcome Bay Ignimbrite in type region. Note bluffs on opposite (far) side of the valley, dark-grey pumice clasts (photo at right), and the overlying Wharo Ignimbrite. Contact lies at the base of the farm track. **(b)** Bluffs of Arateka Ignimbrite and (at right) white pumice clasts. **(c)** Otawera Ignimbrite and the contact between flow units 1 and 2. **(d)** Outlier bluffs of Wharo Ignimbrite. Note the distinct dark coloured fiamme and casehardening.

Wharo Ignimbrite

Overlying the Welcome Bay Ignimbrite is the Wharo Ignimbrite, a dark-grey, eutaxitic ignimbrite that infills paleo-valleys and forms caps on the top of some ridges. The type section is at the same location as the Welcome Bay Ignimbrite (i.e. NZ Topo50 BD37 869 194). The Wharo Ignimbrite was previously included as an upper unit within the Lower Pāpāmoa Ignimbrite, but has been renamed here on the basis of stratigraphic relationships, texture, and geochemical composition (Namaliu, 2021). Bluffs are commonly case hardened, forming outliers up to 10 m high in the upper portions of valleys formed within the Welcome Bay ignimbrite (**Fig. 2.5 d**). Fiamme are dominated by plagioclase ± quartz, hornblende, pyroxene, and rare biotite.

Arateka Ignimbrite

The Arateka Ignimbrite is a cream-grey, massive, pumice-rich (20 %), moderately-welded ignimbrite (**Fig. 2.5 b**) and is equivalent to the Upper Pāpāmoa Ignimbrite of Briggs *et al.* (1996) that was dated at 1.9 ± 0.1 Ma (Briggs *et al.*, 2005). The type locality has previously been identified at NZ Topo50 BD37 944 777 (Hughes, 1993) where bluffs c. 60 m high crop out along Waitoa Road (**Fig. 2.2 a**). Pumice clasts are typically small to med-lapilli in size with phenocrysts of plagioclase, hornblende, and resorbed pyroxene. Highly resorbed fragments of quartz are also present in vitroclastic matrix.

Otawera Ignimbrite

The non-welded Otawera Ignimbrite is composed of multiple flow units and is found forming a 30 m high outlier bluff in the valley below Wharo Pā (**Figs. 2.2 a, 2.5 c**). The type location is at NZ Topo50 BD37 881 197. It is also found cropping out in a similar manner at several locations throughout the central and western Pāpāmoa Range. It is radiometrically dated at 2.21 ± 0.13 Ma (Pittari *et al.*, 2021). This ignimbrite is generally fine grained (fine-mid lapilli), with lithic concentration zones at the base of flow units 1 and 2 which are dominated by andesite and flow-banded rhyolite lavas. Phenocrysts constitute plagioclase and orthopyroxene with subordinate hornblende, rare quartz and juvenile clasts are set in a crystal-rich vitroclastic matrix.

Bulk samples for glass and zircon analysis were collected from the Welcome Bay, Wharo and Otawera ignimbrites (glass only) in the vicinity of Wharo Pā. Prominent bluffs of the Arateka Ignimbrite are visible along Waitao Road and were sampled from an outcrop near the top of the ridge (**Fig. 2.2 a**).

2.1.1.3 Te Puna Ignimbrite

The Te Puna Ignimbrite, formally defined by Briggs *et al.* (1996), is a non-welded, crystal-rich ignimbrite found in coastal sections around western areas of the Tauranga Harbour and the harbour side of Matakana Island. The thickest exposures are found at the type section along Te Puna Station

Road (NZ Topo50 BD36 725 239) where the ignimbrite forms a terrace > 16 m thick (**Fig. 2.2 a**). Glass and zircons were separated from a bulk ignimbrite sample collected from a road cutting near the base of the ignimbrite forming this terrace. Phenocrysts include plagioclase, quartz, hornblende, orthopyroxene and biotite which has a distinctive golden colour. The Te Puna Ignimbrite has an $^{40}Ar/^{39}Ar$ age of 0.929 ± 0.012 Ma and is inferred to be a distal ignimbrite which flowed into the Tauranga region from Mangakino Volcanic Centre (MVC) (**Fig. 2.1**) (Briggs *et al.*, 2005; Leonard *et al.*, 2010; Cunningham *et al.*, 2016).

2.2 Early Quaternary tephrostratigraphy of northern Hawke's Bay

Numerous tephra beds are preserved in terrestrial, marginal-marine to marine rocks of the 2.4 to 1.63 Ma-aged Esk and lower Petane formations of northern Hawke's Bay, which crop out extensively within the valleys of the Mangaone, Esk, and Waikoau rivers, and in the Lake Tūtira area (**Fig. 2.2 b**) (Bland *et al.*, 2007). The regional stratigraphy is summarised in **Figure 2.6**. The Esk Mudstone Formation is punctuated by numerous tephra beds and is conformably overlain by sandstone to greywacke conglomerates of the lower Petane Formation. Sharply overlying the conglomerates is the Hikuroa Pumice Member. The Hikuroa Pumice Member has previously been correlated to an offshore tephra deposit in core OPD 1124C (Bland *et al.*, 2007) which corresponds to tephra AT-313 of Carter *et al.* (2004). Hopkins and Seward (2019) presented zircon fission-track ages for the Hikuroa Pumice Member at Darkys Spur of 2.0 ± 0.6 and 1.9 ± 0.4 Ma, which overlap within error with the paleomagnetic (2.165 Ma) and biostratigraphic (2.1496 Ma) ages of Stevens (2010). The Hikuroa Pumice Member within the Petane Formation (**Fig. 2.6 b**), and the two tephras Esk Mst-T1 and Esk Mst-T2 contained within the Esk Mudstone Formation (**Fig. 2.6 c**), are therefore chronologically equivalent to eruptive deposits of the Tauranga Volcanic Centre. More detailed descriptions of the Hikuroa Pumice Member, and Esk Mudstone tephras, Esk Mst-T1 and -T2, and sampling, are given below.

2.2.1 Hikuroa Pumice Member

The Hikuroa Pumice Member is a prominent non-welded, basal primary ignimbrite overlain by reworked pumiceous ash and lapilli, and capped by a highly fossiliferous shell and pebble bed. Exposures can be found along Darkys Spur, Beattie Road and MacIntyre Access Road (**Figs. 2.2 b, 2.6 b**).

The deposit is best exposed at Darkys Spur where the unit is over 9 m thick (**Fig. 2.7**). A basal, normally-graded, laterally continuous, crystal-rich coarse ash underlies the lower 1.6 m of ignimbrite with

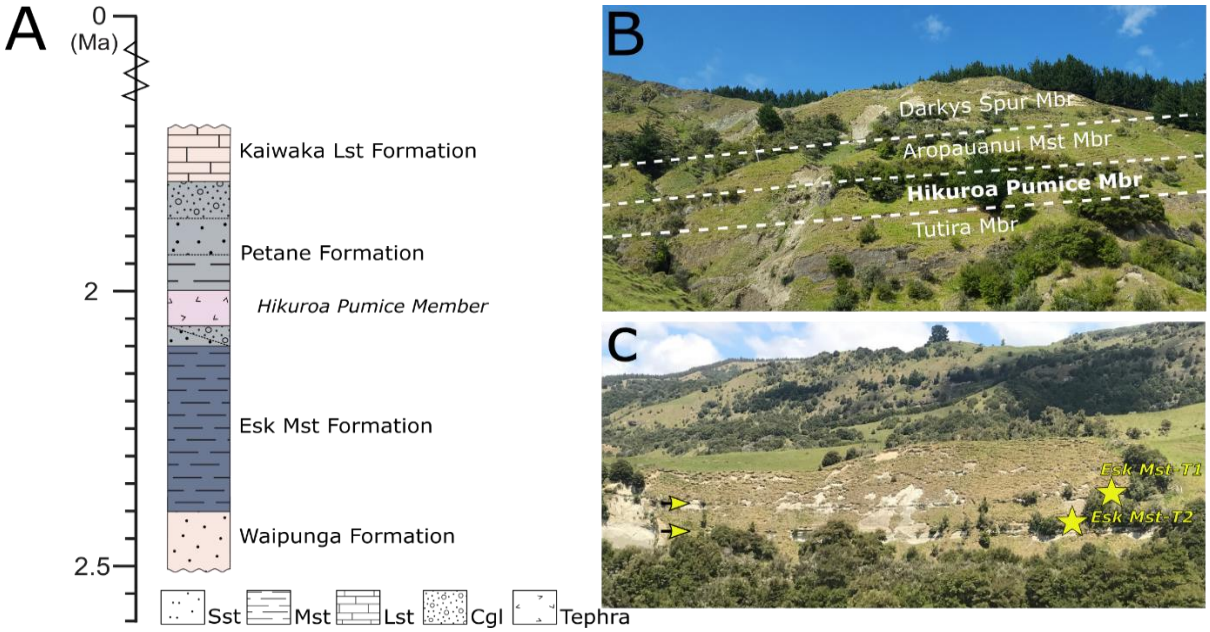

Figure 2.6. (a) Simplified stratigraphy and lithofacies of Early Quaternary marine sedimentary deposits in northern Hawke's Bay in the Lake Tūtira, Darkys Spur and Waikoau River areas (**Fig. 2.2 b**). Lithofacies of the Petane Formation are simplified to key lithologies of the repeating sequences (see Bland *et al.*, 2007, for full details). Lithological abbreviations are as follows: Sst, sandstone; Mst, mudstone; Lst, limestone; Cgl, conglomerate. **(b)** Annotated photo of outcrop at Darkys Spur. Mbr, Member. **(c)** Tephra-fall units Esk Mst-T1 and Esk Mst-T2 (yellow arrows) in the Esk Mudstone Formation, Waikoau River section. Approximate sampling positions indicated by yellow stars.

centimetre-scale horizontal stratification or low-angle (~10°) cross-stratification of very fine and coarse fine ash with occasional very fine to fine pumice lapilli layers. Primary depositional structures are overprinted by secondary deformation structures which present as convolute laminations where individual laminae can be traced through multiple folds and load casts. The upper 5.5 m consists of massive or centi- to decimetre-stratified, very-poorly to poorly sorted, fine-grained matrix-supported (fine-coarse ash to medium-fine ash) ignimbrite. This upper unit is overlain by a further 2.5 m of reworked volcaniclastic sediment dominated by fine ash and up to medium-lapilli-sized pumice clasts and carbonaceous fragments. An upper shell bed with rounded greywacke pebbles and cobbles, and disarticulated and broken bivalve and cockle shells overlies the Hikuroa Pumice Member.

The exposures at Beattie and MacIntyre Access roads were 1.75 m and ~7 m thick, respectively. Both outcrops show the same depositional and post-depositional structures in the lower 1.6 m below massive or stratified ignimbrite, reworked volcaniclastic sediments, and the capping shell bed. Charcoal fragments were prominent at the McIntyre Access Road outcrop and were found both in the overlying reworked volcaniclastic sediments and within the basal primary ignimbrite.

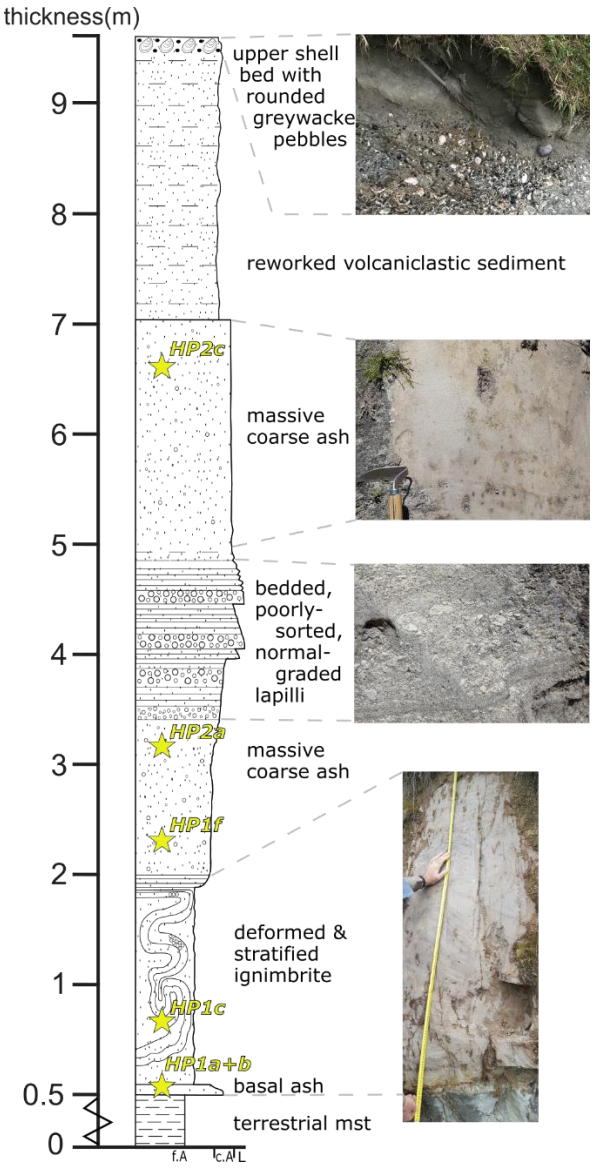

Figure 2.7. Stratigraphic log and outcrop photographs of Hikuroa Pumice Member at Darkys Spur, Hawke's Bay. Grain size abbreviations as in **Figure 2.4**. Samples collected for glass and/or zircon analysis are highlighted by yellow stars.

Glass samples were collected from multiple stratigraphic heights throughout deposits of this distal-ignimbrite at all three locations. Zircons for dating were collected from the basal crystal-rich coarse ash at Darkys Spur.

2.2.2 Esk Mudstone tephras

The Esk Mudstone Formation is exposed within the cliffs of the Waikoau River from approximately 3 km downstream from Waikoau Road to MacIntyre Access Road, off SH2, south of Lake Tūtira (**Fig. 2.1 c**). The Waikoau River has extensively cut into the soft Esk Mudstone creating steep-sided cliffs up to

70 m high. The upstream section is located on the eastern cliff face of a large meander bend (**Fig. 2.6 c**) where the base of the Esk Mudstone sits sharply above sandstone comprising the Waipunga Formation a few metres above the present river level. In the upper parts of the section, the blue-grey siltstone is punctuated by the two prominent tephra-fall beds, Esk Mst-T1 and T2, spaced 8 m vertically apart. The lower tephra (Esk Mst-T2) is 40 cm thick and consists of light-grey, coarse-ash. In contrast the upper tephra (Esk Mst-T1) consists of very fine, white-coloured ash and is 19 cm thick. Both tephra units have sharp, planar, basal contacts with the underlying siltstone, and are normally graded and bioturbated in upper parts. Bulk samples for glass and zircon analysis were collected from the lower 10–15 cm of each unit to minimise the presence of detrital glass shards or zircon which may have been introduced into the tuffs by bioturbation after deposition.

2.3 U-Pb dating and characterisation of glass shards

2.3.1 U-Pb zircon dating

Zircons were concentrated from seven tephra-fall and ignimbrite samples for U-Pb geochronology. Separation methods included standard rock crushing (to 250 µm) with heavy minerals concentrated using a Gemini table and heavy liquid (sodium polytungstate, ρ = 2.8–3.0 g cm^{-3}) followed by magnetic separation using a Frantz isodynamic magnetic separator (10° incline, 15° forward tilt, 0.5 A). Individual crystals for analysis were hand-picked using a binocular microscope from the non-magnetic fraction, mounted in epoxy blocks, ground and polished to reveal internal sections. U-Pb ages were determined by laser ablation, inductively coupled, plasma mass spectrometry (LA-ICP-MS) at the School of Science facility, University of Waikato, Hamilton, using an Agilent 8900 Triple Quadrupole ICP-MS coupled with a Laurin Technic S155 SE ablation cell and a RESOlution 1963 nm ArF excimer laser. Atomic masses ^{29}Si, ^{48}Ti, ^{89}Y, ^{91}Zr, ^{177}Hf, ^{204}Pb, ^{206}Pb, ^{207}Pb, ^{208}Pb, ^{232}Th, ^{235}U, and ^{238}U were measured using a spot size of 30 µm with total ablation time of 45 s with a gas blank/background measurement of 15 s. The primary reference material GJ-1 and secondary reference zircon Temora-2 were analysed twice, both at the beginning and end of each run with two additional analyses of GJ every 10 unknowns. Data processing was performed using Iolite™ (V3) software package (Paton *et al.*, 2011) using the VizualAge data reduction scheme (Petrus & Kamber, 2012). Individual grain age determinations provided in the **supplementary data table SM2.8** are ^{206}Pb/^{238}U dates that have been corrected for common Pb using the ^{207}Pb method (Williams, 1998) and Pb isotope evolution model of Stacey and Kramers (1975). Uranium decay constants and the ^{238}U/^{235}U ratio used are those recommended by Steiger and Jäger (1977). Correction for initial ^{230}Th-disequilibrium follows the method of Schärer (1984), using a Th/U magma ratio of 3 ± 1 (Sagar *et al.*, 2019), and a ^{230}Th decay

constant of 9.1705 ± 0.0138 (Cheng *et al.*, 2013). Error-weighted mean ages and mean square weighted deviations (MSWD) were calculated using IsoplotR (Vermeesch, 2018) where discordia ages on Terra-Wasserburg plots were corrected using an anchored projection from a mean $^{207}Pb/^{206}Pb_c$ (0.836), and for initial ^{230}Th disequilibrium using a mean $f = (Th/U_{zircon})/(Th/U_{magma})$. Older zircon grains were excluded until MSDW values fell within acceptable limits relative to *N,* determined using the formula $1 + 2\sqrt{2/(n-1)}$ (Spencer *et al.*, 2016).

2.3.2 Glass composition

Glass-shard separates from the unconsolidated tephra-fall deposits and non-welded proximal and distal ignimbrites were obtained through disaggregation, sieving and magnetic separation before being mounted in epoxy resin and polished. Glass analysis of welded proximal ignimbrites were conducted using polished thin sections because the separation of individual juvenile clasts for analysis was not possible. Matrix glass was analysed to enable consistent comparison between both proximal and distal deposits.

In situ major element analyses by electron probe microanalysis (EPMA) was undertaken on individual glass shards using a JEOL JXA 8230 Superprobe at Victoria University of Wellington. A beam diameter of 10 µm at 8 nA and 15 kV accelerating voltage, was used to analyse major elements as oxides (SiO_2, TiO_2, Al_2O_3, $FeO_{(t)}$, MgO, MnO, CaO, Na_2O, and K_2O), along with Cl. During analysis, stage co-ordinates and back-scattered electron images of the shards were taken to allow the relocation of the analysis spots for subsequent LA-ICP-MS analysis. The matrix-matched standard VG-568 was used as a bracketing standard and run twice every 25 to 30 unknowns to monitor and correct for instrumental drift. Analytical totals for unknown glasses were between 92 and 99 %, with deviations from 100 % attributed to the omission of volatiles (predominately water) and non-analysed minor or trace elements (Lowe *et al.*, 2017). Major elements are normalised by recalculating to 100 % on a volatile-free basis. Accuracy of the analyses are within 3 % of the recommended values for VG-568, with the exception of MnO, TiO_2, and Cl, which had offsets of 8.4 %, 10 %, and 8.24 %, respectively. Analytical precision (2σ) is 1.30–1.43 wt % for SiO_2 and Na_2O and < 0.3 wt. % for all other major elements.

In-situ trace elements were analysed by the same LA-ICP-MS set up as described above. Data was acquired using a static spot method with spot sizes of 15 µm, and an ablation time of 40 s at 5 Hz. The standards ATHO-G and NIST-612 were run twice at the beginning and end of each session and every 10 unknowns. All data were reduced off-line on Iolite(TM) (V3), using ^{29}Si as the internal standard with NIST-612 as the calibration standard and ATHO-G as an independent secondary standard. Data was corrected for elemental fractionation as described by Pearce *et al.* (2011). Analytical precision (2σ) of analyses of ATHO-G is < 5 with the exceptions of Cu, Rb, Sr, Y, Ce and Nd (2σ = 6–10 ppm), Ni (2σ = 20

ppm) and Zn, Zr and Ba (2σ = 35–92 ppm). The accuracy for all elements is < 3 %. Refer to **supplementary data tables SM2.2-2.5** for the full dataset and standard comparisons.

2.4 Results

2.4.1 Zircon U-Pb ages

New zircon U-Pb ages for the two Esk Mudstone tephras, Esk Mst-T1 and -T2, and the Hikuroa Pumice Member (from northern Hawke's Bay), and for six samples derived from the five ignimbrites in Tauranga, are presented in **Table 2.1** and **Figure 2.8**. Average U-Pb ages are crystallisation ages of the youngest zircon phenocryst population and provide a maximum eruption age for the eruptive deposits.

MSWD values indirectly assess the degree to which the weighted average and associated uncertainty represents a single population. If MSWD is > 1, it is typically assumed that the data do not represent a single population, or if < 1, the associated uncertainty may not fully represent the variation in the

Table 2.1. Summary of weighted average U-Pb zircon ages of five ignimbrites in TgaVC and of the Esk-Mudstone tephras T1 and T2, and Hikuroa Pumice Member, northern Hawke's Bay.

Geological formation/group	Pyroclastic unit (sample number)[1]	Age (Ma)	2σ error	N[2]	MSWD[3]
Pakaumanu Group	Te Puna Ignimbrite (TePu)	1.11	0.046	32	0.1
Petane Formation	Hikuroa Pumice Member (HP1&2)	2.13	0.029	48	1.0
Waiteariki Formation	Waiteariki Ignimbrite: McLaren's Falls (Wai#2)	2.09	0.029	49	1.2
	Waiteariki Ignimbrite: Aongatete River (Wai22)	2.18	0.031	54	1.1
Pāpāmoa Formation	Otawera Ignimbrite[4]	2.21	0.13	na	na
Esk Mudstone Formation	Esk Mst-tephra (Esk Mst-T1)	2.22	0.088	47	0.8
	Esk Mst-tephra (Esk Mst-T2)	2.23	0.026	45	1.2
Pāpāmoa Formation	Arateka Ignimbrite (Pap4)	2.25	0.044	36	1.1
	Wharo Ignimbrite (Pap1)	2.26	0.046	41	1.0
	Welcome Bay Ignimbrite (Pap2)	2.31	0.046	31	0.84

[1]Sample location information provided in **supplementary data table SM2.1**

[2]*N* = number of individual zircon grains contributing to the weighted average age

[3]MSWD = mean square weighted deviation. Acceptable limits relative to *N* were determined using the formula outlined in section 2.4.1. Individual grain age determinations are provided in **supplementary data table SM2.8**

[4]Age reported in Pittari et al. (2021)

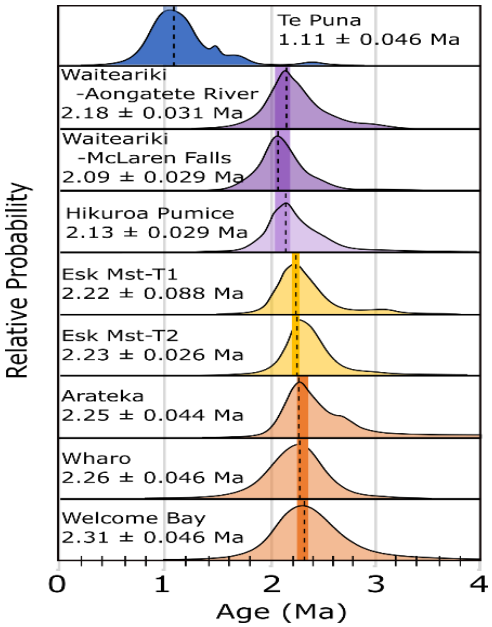

Figure 2.8. Probability density function plots of U-Pb zircon ages for four ignimbrite deposits in Tauranga, and of Hikuroa Pumice Formation and Esk Mst-Ti and -t2 tephras in Hawke's Bay, as dated in this study. Preferred average youngest-population zircon crystallisation ages are represented by the dashed lines (see also **Table 2.1**). Shaded bars represent the determined age for the each of the formations. Note the overlapping age bars for Esk Mudstone tephras and for Welcome Bay, Wharo, and Arateka ignimbrites (see text for discussion).

data set (Spencer *et al.*, 2016). Most of the age determinations for our study produced MSWD values of around 1 and thus are within the calculated range that indicates a single population at the 95 % confidence level.

The ignimbrites erupted from the TgaVC range in age from 2.31 ± 0.046 Ma (Welcome Bay Ignimbrite) to 2.09 ± 0.029 Ma (Waiteariki Ignimbrite at McLaren Falls). The newly-defined ignimbrites of the Pāpāmoa Formation have ages of 2.31 ± 0.046 Ma (Welcome Bay Ignimbrite), 2.26 ± 0.046 Ma (Wharo Ignimbrite) and 2.25 ± 0.044 Ma (Arateka Ignimbrite). These ages are consistent with previous age determinations for the formation of 2.4 ± 0.02–1.9 ± 0.1 Ma (Lower and Upper Pāpāmoa ignimbrites respectively, Briggs *et al.*, 2005) and 2.21 ± 0.13 for the Otawera Ignimbrite (Pittari *et al.*, 2021). However, the previously determined age for the (former) Upper Pāpāmoa Ignimbrite (1.9 ± 0.1 Ma) is younger than the date obtained for the newly-defined, equivalent Arateka Ignimbrite in our study of 2.25 ± 0.044 Ma. Two age determinations for the Waiteariki Ignimbrite were 2.18 ± 0.031 Ma (Aongatete River) and 2.09 ± 0.029 Ma (McLaren Falls), which overlap within error of each other and provide an average maximum age for this eruption of 2.1 Ma. The Te Puna Ignimbrite is dated at 1.1 ± 0.046 Ma, which is outside the age range for known volcanic activity of TgaVC and consistent with the inference that it is a distal ignimbrite derived from MVC (85 km SW of Tauranga) rather than a TgaVC origin (Briggs *et al.*, 2005).

The Esk Mudstone tephras have ages of 2.23 ± 0.026 Ma (Esk Mst-T2) and 2.22 ± 0.088 Ma (Esk Mst-T1) which overlap within error and cannot be distinguished on the basis of radiometric age alone. The two tephras, however, are separated stratigraphically by 8 m of blue-grey siltstone which means that Esk Mst-T1 is younger than Esk Mst-T2 and, therefore, that a period of time elapsed between the two eruptions. The Hikuroa Pumice Member stratigraphically overlies the Esk Mudstone and the sandstone to greywacke conglomerates of the lower Petane Formation. The Hikuroa Pumice Member is dated here at 2.13 ± 0.029 Ma an age that is consistent with a biostratigraphic age of 2.14 Ma (Stevens, 2010), and two previously-published (but less precise) zircon fission-track ages of 1.9 ± 0.4 Ma and 2.0 ± 0.6 Ma (Hopkins & Seward, 2019).

2.4.2 Glass composition

Representative major and trace element compositions of glass shards from ignimbrite and tephra-fall units are presented in **Table 2.2**, with the full dataset available as **supplementary data table SM2.5**.

All samples analysed have SiO_2 contents of between 69.4 and 77.4 wt. % (normalised on an anhydrous basis) with K_2O values between 2.2–5.4 wt. %, thus classifying them as medium to high-K calc-alkaline rhyolites (Le Maitre *et al.*, 2002). Values for SiO_2/K_2O and Na_2O+K_2O are between 14.4–25.2 and 6.8–8.2, respectively, a characteristic shared with other magmas erupted from pre- and early TVZ sources (Hopkins *et al.*, 2021b). Individual tephra horizons can often be distinguished from one another using a number of major element oxide bivariate plots, for example FeO_t vs. CaO or K_2O and SiO_2 vs. K_2O or Al_2O_3. For additional fingerprinting, trace element compositions (e.g. Zr vs Y, Rb and Sr) and trace element ratios were used (e.g. Zr/Y vs. Ba/Sr; or Rb/Sr and Zr/Nb vs Rb/Sr).

The Wharo, Otawera, Waiteariki and Te Puna ignimbrites, the Hikuroa Pumice Member and the Esk Mst-T2 tephra, all show homogenous major element glass compositions, typically within < ± 1 wt. % (**Figs. 2.9-2.11**). In contrast, glass shards from the Esk Mst-T1 tephra, and the Arateka and Welcome Bay ignimbrites show bimodal major element populations, as depicted by relatively 'low' vs 'high' SiO_2 contents of 73.0–74.1 and 75.7–77.8 wt. %, respectively (**Fig. 2.9**). Consistent groupings can also be distinguished in CaO, FeO_t, K_2O, Al_2O_3 and MgO along with bivariate plots of trace-element ratios where the low SiO_2 population has higher abundances of CaO (+ 1.0 wt. %), FeO_t (+ 1.5 wt. %), K_2O (+ 1.0 wt. %) but lower Ba/Sr and higher Zr/Y ratios (- 4 and + 1–3, respectively). Zr/Y vs Ba/Sr trace element ratios also suggest heterogeneity within the Hikuroa Pumice Member (**Fig. 2.9**). Mixed-shard

Table 2.2. Major and trace-element analyses of glass shards in tephra-fall and ignimbrite deposits from Hawke's Bay and TgaVC. Major-element oxide values in wt % (± 2σ for *n* analyses) are normalised to 100% volatile free; trace-element values are in ppm (± 2σ for *n* analyses); *n* = number of individual glass shards analysed for major/minor elements (EPMA) and trace elements (LA-ICP-MS). See **supplementary data table SM2.5** for full dataset.

Sample no.	Esk Mst-T1				Esk Mst-T2		HP1 & 2		HP3		HP4		WAI22	
Formation	Esk Mudstone				Esk Mudstone		Hikuroa Pumice – Darkys Spur		Hikuroa Pumice – MacIntyre Access Rd		Hikuroa Pumice – Beattie Rd		Waiteariki Ignimbrite[2] Core ES112	
Major elements as oxides (wt %) (2σ errors)														
	Population1		*Population2*											
SiO_2	73.93	(0.20)	77.14	*(0.44)*	75.60	*(0.34)*	77.33	*(0.37)*	77.28	*(0.32)*	77.34	*(0.39)*	77.53	*(0.39)*
Al_2O_3	13.67	(0.55)	12.82	*(0.21)*	13.40	*(0.16)*	12.46	*(0.16)*	12.45	*(0.17)*	12.46	*(0.19)*	12.55	*(0.28)*
MgO	0.29	(0.05)	0.12	*(0.02)*	0.06	*(0.02)*	0.06	*(0.03)*	0.06	*(0.06)*	0.06	*(0.03)*	0.10	*(0.05)*
CaO	1.94	(0.09	1.17	*(0.07)*	1.28	*(0.03)*	0.89	*(0.11)*	0.92	*(0.17)*	0.89	*(0.12)*	1.01	*(0.18)*
TiO_2	0.26	(0.10)	0.08	*(0.02)*	0.10	*(0.04)*	0.08	*(0.03)*	0.09	*(0.04)*	0.08	*(0.02)*	0.09	*(0.04)*
MnO	0.03	(0.03)	0.03	*(0.03)*	0.04	*(0.03)*	0.04	*(0.04)*	0.04	*(0.04)*	0.04	*(0.05)*	0.03	*(0.03)*
FeO_t[3]	2.69	(0.51)	1.30	*(0.21)*	1.78	*(0.19)*	1.45	*(0.28)*	1.46	*(0.25)*	1.43	*(0.28)*	1.16	*(0.29)*
Na_2O	3.93	(0.16)	3.56	*(0.30)*	3.81	*(0.46)*	3.87	*(0.35)*	3.83	*(0.35)*	3.86	*(0.38)*	3.36	*(0.33)*
K_2O	3.13	(0.17)	3.65	*(0.38)*	3.86	*(0.44)*	3.69	*(0.41)*	3.73	*(0.44)*	3.70	*(0.54)*	4.06	*(0.38)*
Cl	0.17	(0.01)	0.18	*(0.02)*	0.10	*(0.01)*	0.19	*(0.02)*	0.20	*(0.02)*	0.20	*(0.02)*	0.17	*(0.05)*
Total	95.27	(0.60)	94.86	*(0.84)*	95.98	*(1.76)*	96.14	*(2.21)*	95.60	*(1.81)*	96.09	*(2.49)*	97.08	*(1.42)*
n	5		*7*		15		63		34		29		25	
Trace elements (ppm)[1] (2σ errors)														
Sc	7.27	*(4.87)*	2.42	*(1.02)*	8.40	*(4.98)*	5.78	*(1.98)*	5.19	(1.65)	5.55	*(1.67)*	3.30	*(1.45)*
V	15.30	*(8.88)*	2.80	*(1.52)*	3.57	*(1.40)*	2.60	*(6.38)*	1.97	(4.50)	3.83	*(9.07)*	2.72	*(1.68)*
Co	4.81	*(5.42)*	1.14	*(0.50)*	0.72	*(0.71)*	0.64	*(0.54)*	0.65	(0.50)	0.87	*(1.35)*	0.90	*(0.66)*
Cu	13.68	*(21.10)*	3.82	*(1.84)*	6.00	*(3.63)*	7.93	*(16.28)*	5.80	(15.03)	6.76	*(15.49)*	5.20	*(7.79)*
Zn	48.24	*(38.09)*	37.93	*(7.46)*	78.44	*(32.01)*	43.19	*(17.18)*	38.56	(20.12)	36.41	*(17.20)*	31.90	*(16.81))*
Ga	18.95	*(4.07)*	16.62	*(2.25)*	23.66	*(8.20)*	17.14	*(3.55)*	16.23	(3.15)	17.30	*(2.94)*	14.03	*(4.01)*
Rb	121.80	*(16.93)*	134.09	*(14.27)*	130.01	*(11.87)*	130.21	*(18.32)*	127.09	(17.23)	134.50	*(15.17)*	128.10	*(31.06)*
Sr	102.17	*(25.87)*	80.81	*(12.35)*	88.83	*(16.47)*	54.69	*(24.36)*	51.78	(21.35)	52.93	*(14.38)*	69.25	*(32.59)*
Y	16.48	*(15.47)*	14.90	*(4.15)*	29.11	*(6.58)*	24.56	*(8.92)*	21.19	(8.84)	23.58	*(7.93)*	17.63	*(5.73)*
Zr	153.45	*(99.03)*	85.88	*(18.56)*	145.77	*(21.38)*	113.05	*(39.75)*	101.63	(39.40)	108.21	*(34.10)*	89.22	*(29.21)*
Nb	5.83	*(2.87)*	5.56	*(0.70)*	7.58	*(0.92)*	8.00	*(0.99)*	7.29	(1.39)	7.83	*(1.48)*	5.38	*(1.78)*
Cs	5.45	*(0.89)*	6.43	*(0.65)*	6.70	*(0.95)*	6.08	*(0.96)*	5.79	(0.93)	6.19	*(1.05)*	5.95	*(1.73)*
Ba	614.80	*(144.91)*	786.97	*(94.94)*	759.03	*(128.86)*	817.68	*(136.57)*	770.53	(140.56)	801.73	*(155.62)*	813.16	*(228.45)*
La	16.50	*(7.28)*	20.51	*(4.58)*	24.13	*(4.10)*	22.81	*(5.64)*	21.11	(5.64)	22.80	*(5.04)*	22.30	*(6.21)*
Ce	40.87	*(11.79)*	42.49	*(5.63)*	55.80	*(10.60)*	49.43	*(10.55)*	45.44	(9.92)	49.51	*(9.87)*	44.25	*(11.72)*
Pr	4.18	*(2.12)*	4.10	*(0.98)*	6.21	*(1.52)*	5.34	*(1.28)*	4.89	(1.36)	5.25	*(1.33)*	4.64	*(1.33)*
Nd	18.82	*(9.06)*	14.84	*(2.46)*	24.90	*(6.27)*	20.16	*(5.57)*	17.79	(5.40)	19.83	*(5.76)*	16.48	*(5.24)*
Sm	2.86	*(2.23)*	2.48	*(0.97)*	4.91	*(1.91)*	4.31	*(1.54)*	3.64	(1.41)	3.97	*(1.47)*	3.01	*(1.25)*
Eu	0.49	*(0.73)*	0.41	*(0.24)*	0.58	*(0.33)*	0.53	*(0.31)*	0.48	(0.30)	0.53	*(0.28)*	0.41	*(0.19)*
Gd	2.89	*(3.52)*	2.40	*(1.14)*	5.07	*(2.02)*	4.05	*(1.75)*	3.39	(1.86)	3.72	*(1.63)*	2.81	*(1.19)*
Tb	0.47	*(0.28)*	0.36	*(0.16)*	0.77	*(0.30)*	0.63	*(0.28)*	0.58	(0.28)	0.59	*(0.32)*	0.46	*(0.17)*
Dy	2.76	*(2.86)*	2.11	*(0.76)*	5.35	*(1.54)*	4.22	*(1.51)*	3.61	(1.59)	3.76	*(1.46)*	2.83	*(1.10)*
Ho	0.55	*(0.65)*	0.44	*(0.16)*	1.04	*(0.33)*	0.82	*(0.37)*	0.76	(0.38)	0.82	*(0.31)*	0.60	*(0.24)*
Er	1.79	*(2.17)*	1.54	*(0.76)*	2.98	*(0.97)*	2.58	*(1.12)*	2.25	(1.35)	2.46	*(1.07)*	1.82	*(0.72)*
Tm	0.24	*(0.33)*	0.24	*(0.10)*	0.40	*(0.18)*	0.37	*(0.20)*	0.34	(0.19)	0.35	*(0.17)*	0.27	*(0.10)*
Yb	1.40	*(2.31)*	1.68	*(0.87)*	3.23	*(1.50)*	2.79	*(1.19)*	2.37	(1.39)	2.55	*(1.40)*	2.08	*(0.73)*
Lu	0.27	*(0.34)*	0.26	*(0.17)*	0.42	*(0.22)*	0.39	*(0.24)*	0.35	(0.22)	0.41	*(0.23)*	0.33	*(0.12)*
Hf	3.54	*(3.09)*	2.74	*(0.90)*	4.22	*(1.20)*	3.57	*(1.43)*	3.25	(1.40)	3.43	*(1.30)*	3.08	*(1.05)*
Ta	0.27	*(0.24)*	0.41	*(0.18)*	0.53	*(0.16)*	0.60	*(0.24)*	0.54	(0.22)	0.58	*(0.24)*	0.52	*(0.17)*
W	1.37	*(0.97)*	1.56	*(0.35)*	2.00	*(0.45)*	1.53	*(0.38)*	1.49	(0.45)	1.56	*(0.42)*	1.54	*(0.49)*
Pb	30.92	*(6.39)*	27.19	*(4.60)*	41.45	*(13.37)*	31.68	*(23.49)*	30.43	(16.62)	30.73	*(12.77)*	22.09	*(7.54)*
Th	5.98	*(5.40)*	10.47	*(3.31)*	10.50	*(2.39)*	10.41	*(4.19)*	9.22	(4.35)	10.08	*(3.57)*	11.75	*(3.50)*
U	1.90	*(0.69)*	2.89	*(0.72)*	2.76	*(0.64)*	2.83	*(0.75)*	2.56	(0.70)	2.77	*(0.74)*	2.89	*(0.84)*
N	*5*		*7*		15		63		34		29		22	

[1]Ni & Cr removed because of inconsistent analytical results

[2]McLaren Falls sample was not analysed for major and trace elements because of the lack of suitable glass. [3]Total iron expressed as FeO_t

Table 2.2. Continued

Sample no.	Te Pu		L11				L5		L12		L2WP/L4		L2BP/L7	
Formation	Te Puna Ignimbrite		Arateka Ignimbrite				Wharo Ignimbrite		Otawera Ignimbrite		Welcome Bay Ignimbrite			
Major elements as oxides (wt %) (2σ errors)														
			Population1		*Population2*									
SiO_2	76.94	*(0.37)*	73.57	(0.71)	77.02	*(0.08)*	71.51	*(0.91)*	76.09	*(0.36)*	77.02	*(1.13)*	74.72	*(2.78)*
Al_2O_3	12.37	*(0.13)*	13.74	(1.18)	12.47	*(0.20)*	14.42	*(0.60)*	12.66	*(0.18)*	12.72	*(0.54)*	13.10	*(0.82)*
MgO	0.09	*(0.05)*	0.30	(0.04)	0.11	*(0.01)*	0.41	*(0.16)*	0.05	*(0.03)*	0.08	*(0.06)*	0.20	*(0.19)*
CaO	0.81	*(0.20)*	1.93	(0.06)	1.16	*(0.00)*	2.49	*(0.34)*	0.89	*(0.10)*	1.23	*(0.21)*	1.71	*(0.62)*
TiO_2	0.09	*(0.05)*	0.33	(0.02)	0.09	*(0.01)*	0.38	*(0.04)*	0.11	*(0.03)*	0.09	*(0.03)*	0.25	*(0.23)*
MnO	0.03	*(0.03)*	0.07	(0.01)	0.02	*(0.02)*	0.08	*(0.03)*	0.03	*(0.03)*	0.02	*(0.03)*	0.04	*(0.03)*
FeO_t[3]	1.11	*(0.23)*	2.71	(0.13)	1.23	*(0.11)*	3.08	*(0.87)*	1.57	*(0.15)*	0.82	*(0.64)*	2.17	*(1.29)*
Na_2O	3.83	*(0.25)*	3.81	(0.44)	3.86	*(0.14)*	4.22	*(0.32)*	4.61	*(0.29)*	4.11	*(0.34)*	4.25	*(0.37)*
K_2O	4.05	*(0.19)*	3.36	(0.21)	3.84	*(0.15)*	3.29	*(0.34)*	3.80	*(0.17)*	3.75	*(0.23)*	3.40	*(0.32)*
ClO	0.26	*(0.03)*	0.17	(0.05)	0.19	*(0.01)*	0.13	*(0.03)*	0.18	*(0.02)*	0.14	*(0.09)*	0.16	*(0.05)*
Total	98.97	*(0.54)*	94.99	(4.35)	95.99	*(1.32)*	94.31	*(2.34)*	96.08	*(1.22)*	95.01	*(2.79)*	95.62	*(2.96)*
n	20		4		*2*		9		50		24		6	
Trace elements (ppm)[1,4] (2σ errors)														
Zn	39.29	*(9.33)*	168.43	*(123.34)*	52.51	*(7.12)*	86.70	*(104.04)*	58.97	*(27.22)*	40.50	*(37.88)*	58.21	*(39.67)*
Ga	15.13	*(4.65)*	33.06	*(18.91)*	19.09	*(0.00)*	32.91	*(53.87)*	19.59	*(9.65)*	18.87	*(6.59)*	22.26	*(5.28)*
Rb	153.76	*(17.33)*	110.53	*(33.47)*	131.68	*(24.81)*	121.56	*(21.50)*	140.89	*(21.70)*	142.05	*(24.84)*	120.44	*(22.06)*
Sr	53.19	*(19.14)*	76.90	*(25.29)*	66.29	*(30.60)*	158.91	*(31.77)*	57.54	*(15.70)*	83.66	*(35.04)*	92.81	*(50.01)*
Y	23.93	*(5.44)*	19.79	*(7.64)*	12.83	*(6.36)*	22.39	*(10.39)*	30.27	*(8.96)*	14.90	*(6.03)*	20.67	*(17.16)*
Zr	93.89	*(26.55)*	151.40	*(51.41)*	76.10	*(31.25)*	190.19	*(62.21)*	165.42	*(48.32)*	88.02	*(41.54)*	157.34	*(147.76)*
Nb	8.33	*(1.44)*	4.66	*(1.95)*	4.62	*(1.57)*	7.94	*(1.35)*	8.65	*(1.16)*	5.22	*(1.28)*	6.57	*(3.24)*
Cs	4.44	*(1.06)*	4.86	*(3.14)*	4.15	*(0.29)*	4.41	*(4.00)*	4.21	*(1.58)*	4.46	*(1.87)*	3.77	*(0.72)*
Ba	883.59	*(104.11)*	501.38	*(143.10)*	703.10	*(371.51)*	608.63	*(152.15)*	822.02	*(200.95)*	784.78	*(133.14)*	712.79	*(201.78)*
La	27.24	*(5.35)*	14.85	*(4.93)*	17.29	*(11.31)*	18.74	*(7.03)*	25.57	*(6.52)*	20.33	*(5.69)*	19.17	*(6.75)*
Ce	55.76	*(11.96)*	30.55	*(10.14)*	32.92	*(17.29)*	38.70	*(21.40)*	54.12	*(15.28)*	40.68	*(9.28)*	40.36	*(16.49)*
Pr	5.79	*(1.14)*	3.73	*(1.52)*	3.59	*(1.98)*	4.97	*(2.16)*	6.00	*(1.51)*	4.11	*(1.13)*	4.39	*(2.14)*
Nd	23.25	*(7.28)*	15.35	*(4.92)*	11.16	*(7.73)*	18.33	*(7.14)*	23.23	*(7.61)*	13.81	*(6.36)*	18.81	*(13.28)*
Sm	4.15	*(1.81)*	3.11	*(1.93)*	4.50	*(2.65)*	3.95	*(2.04)*	5.16	*(2.75)*	2.41	*(1.91)*	3.75	*(2.80)*
Eu	0.59	*(0.37)*	0.75	*(0.57)*	0.36	*(0.16)*	0.92	*(0.57)*	0.68	*(0.51)*	0.43	*(0.39)*	0.83	*(0.80)*
Gd	3.84	*(1.36)*	3.16	*(2.64)*	2.03	*(2.71)*	2.93	*(2.85)*	5.29	*(2.25)*	2.36	*(1.36)*	3.95	*(2.62)*
Tb	0.59	*(0.19)*	0.44	*(0.29)*	0.20	*(0.39)*	0.71	*(0.35)*	0.81	*(0.35)*	0.35	*(0.32)*	0.59	*(0.63)*
Dy	3.75	*(1.33)*	3.38	*(2.17)*	1.91	*(1.97)*	4.06	*(1.16)*	5.27	*(1.59)*	2.10	*(1.65)*	3.11	*(3.21)*
Ho	0.85	*(0.27)*	0.70	*(0.39)*	0.37	*(0.15)*	0.78	*(0.48)*	1.01	*(0.49)*	0.52	*(0.42)*	0.90	*(0.44)*
Er	2.52	*(1.25)*	2.05	*(1.09)*	1.32	*(0.76)*	2.58	*(1.62)*	3.13	*(1.28)*	1.58	*(1.32)*	2.01	*(1.74)*
Tm	0.39	*(0.24)*	0.19	*(0.25)*	0.39	*(0.00)*	0.39	*(0.24)*	0.44	*(0.28)*	0.24	*(0.21)*	0.34	*(0.38)*
Yb	2.87	*(1.51)*	2.45	*(0.60)*	1.66	*(0.62)*	2.85	*(1.80)*	3.35	*(1.62)*	2.19	*(1.67)*	3.01	*(2.07)*
Lu	0.48	*(0.27)*	0.40	*(0.21)*	0.24	*(0.00)*	0.39	*(0.21)*	0.50	*(0.30)*	0.35	*(0.30)*	0.53	*(0.28)*
Hf	3.39	*(0.65)*	3.47	*(1.55)*	2.04	*(1.58)*	4.54	*(2.81)*	5.01	*(1.38)*	2.65	*(1.42)*	4.29	*(3.26)*
Ta	0.87	*(0.45)*	0.32	*(0.26)*	0.42	*(0.28)*	0.61	*(0.49)*	0.65	*(0.25)*	0.47	*(0.31)*	0.40	*(0.41)*
W	5.07	*(26.98)*	1.50	*(0.94)*	2.10	*(1.18)*	1.91	*(1.56)*	2.10	*(2.27)*	1.60	*(0.80)*	1.66	*(0.69)*
Pb	27.25	*(4.99)*	28.28	*(12.05)*	21.06	*(8.91)*	37.67	*(40.87)*	30.07	*(8.69)*	29.95	*(11.80)*	22.12	*(10.46)*
Th	14.85	*(4.73)*	5.55	*(1.39)*	7.80	*(5.06)*	8.06	*(5.39)*	12.28	*(3.99)*	10.21	*(4.10)*	8.48	*(2.92)*
U	3.60	*(0.96)*	1.98	*(0.85)*	2.39	*(0.56)*	2.07	*(0.90)*	3.00	*(0.95)*	2.56	*(0.91)*	2.25	*(0.40)*
n	20		4		2		*8*		48		22		5	

[1]Ni & Cr removed because of inconsistent analytical results
[2]McLaren Falls sample was not analysed for major and trace elements because of the lack of suitable glass
[3]Total iron expressed as FeO_t
[4]Sc, V, Co, and Cu not analysed

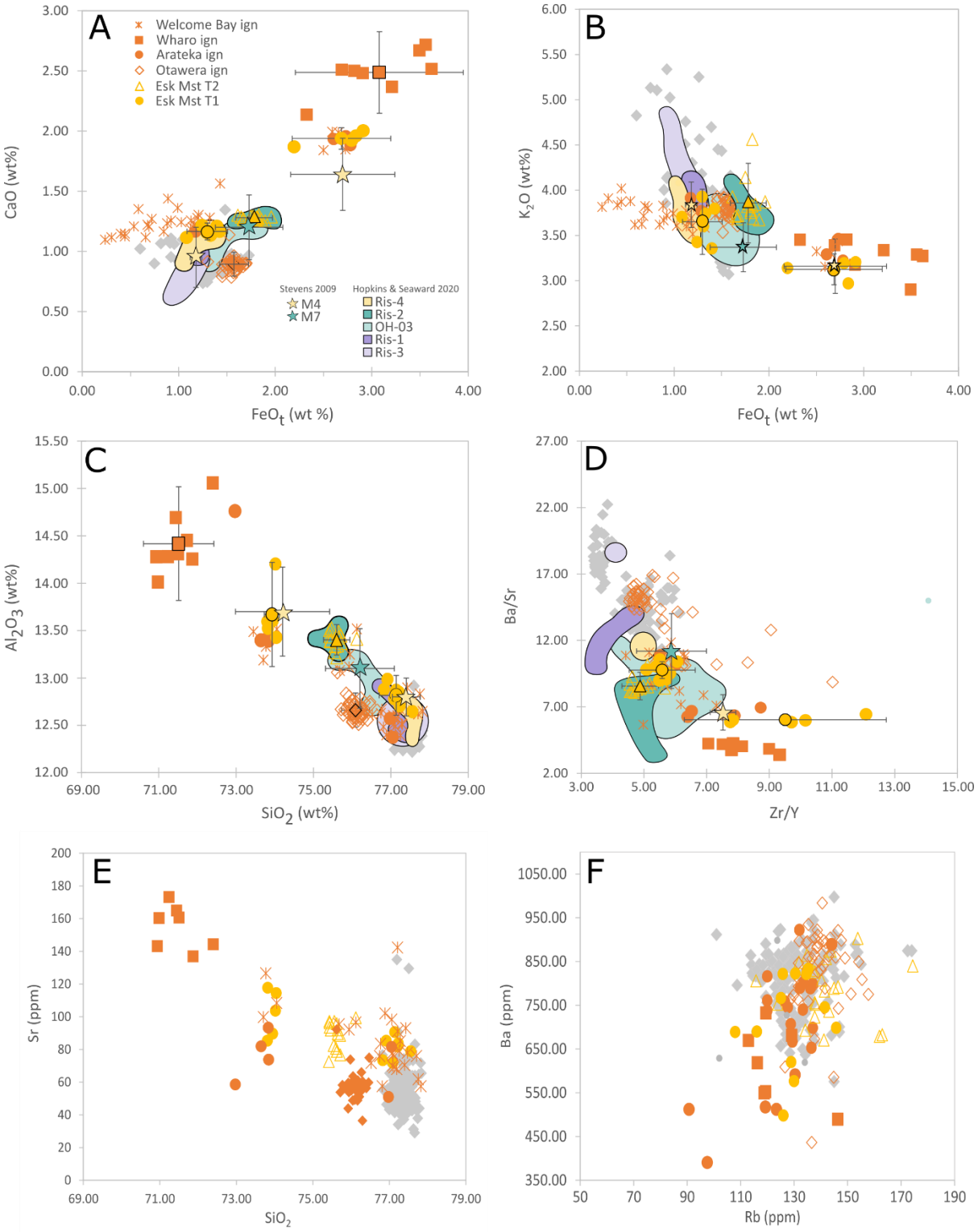

Figure 2.9. Representative bivariate plots of analyses including means (± 2σ error bars) of selected major elements (as oxides, normalised to 100% volatile free) and trace element ratios of glass from four proximal ignimbrites in TgaVC (Arateka, Welcome Bay, Wharo, and Otawera) and from the Esk-Mudstone tephras T1 and T2. Distal correlatives are shown as coloured polygons, representing so-called Rissington tephras (Ris, OH) of Hopkins and Seward (2019), and ODP 1124 tephra horizons of Stevens (2010) as stars (see **Section 2.6**). Grey diamonds represent Waitea riki Ignimbrite and Hikuroa Pumice glass analyses (see **Fig. 2.10** for details).

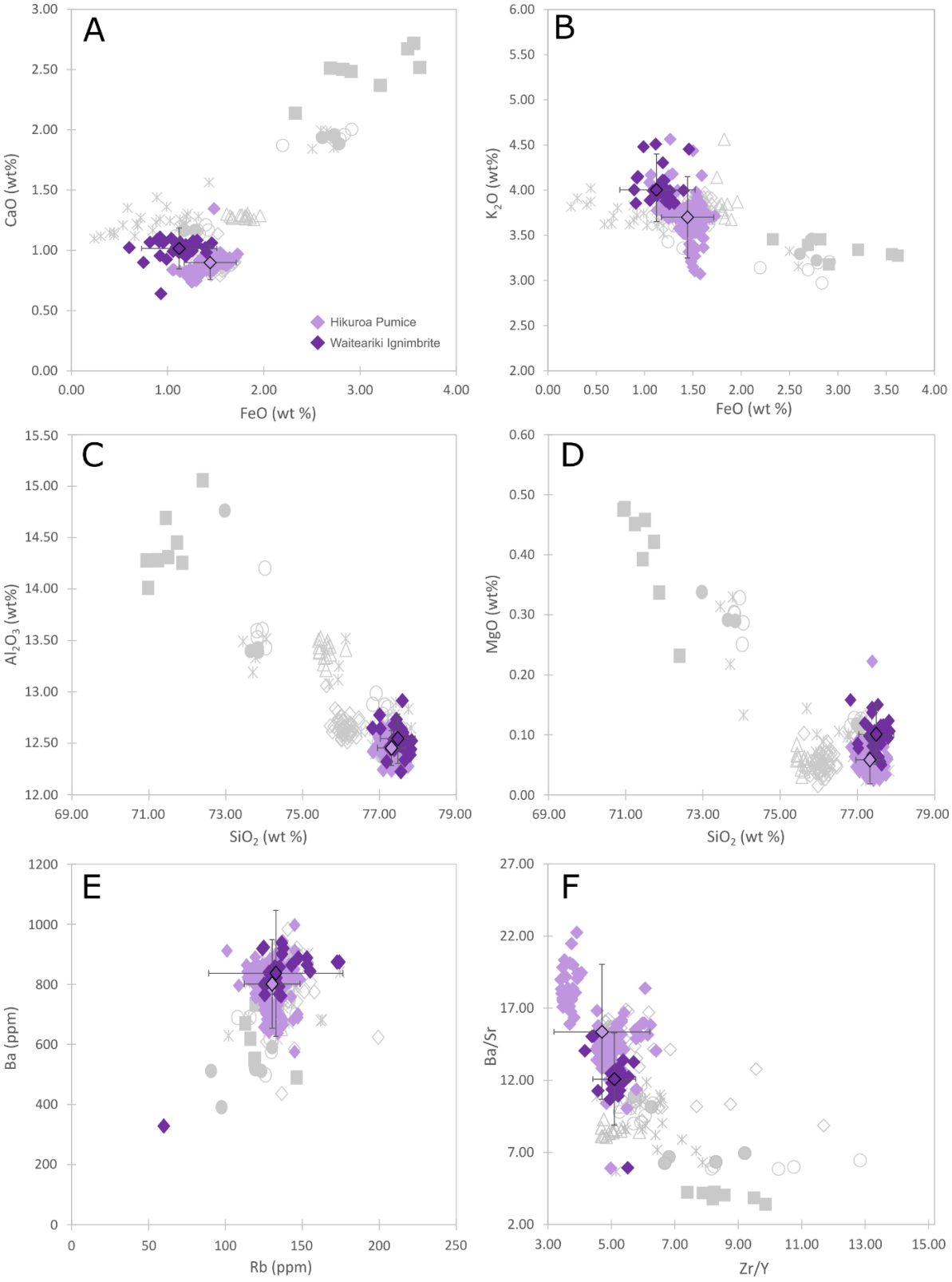

Figure 2.10. Representative bivariate plots of analyses including means (black outline with ± 2σ error bars) of selected major elements (as oxides, normalised to 100% volatile free), trace elements and trace element ratios, of glass from the Waiteariki Ignimbrite and Hikuroa Pumice Member. Other proximal ignimbrites in the TgaVC (Arateka, Welcome Bay, Wharo, and Otawera) and the Esk-Mudstone tephras, Esk Mst-T1 and -T2 are shown in grey (as per **Fig. 2.9**).

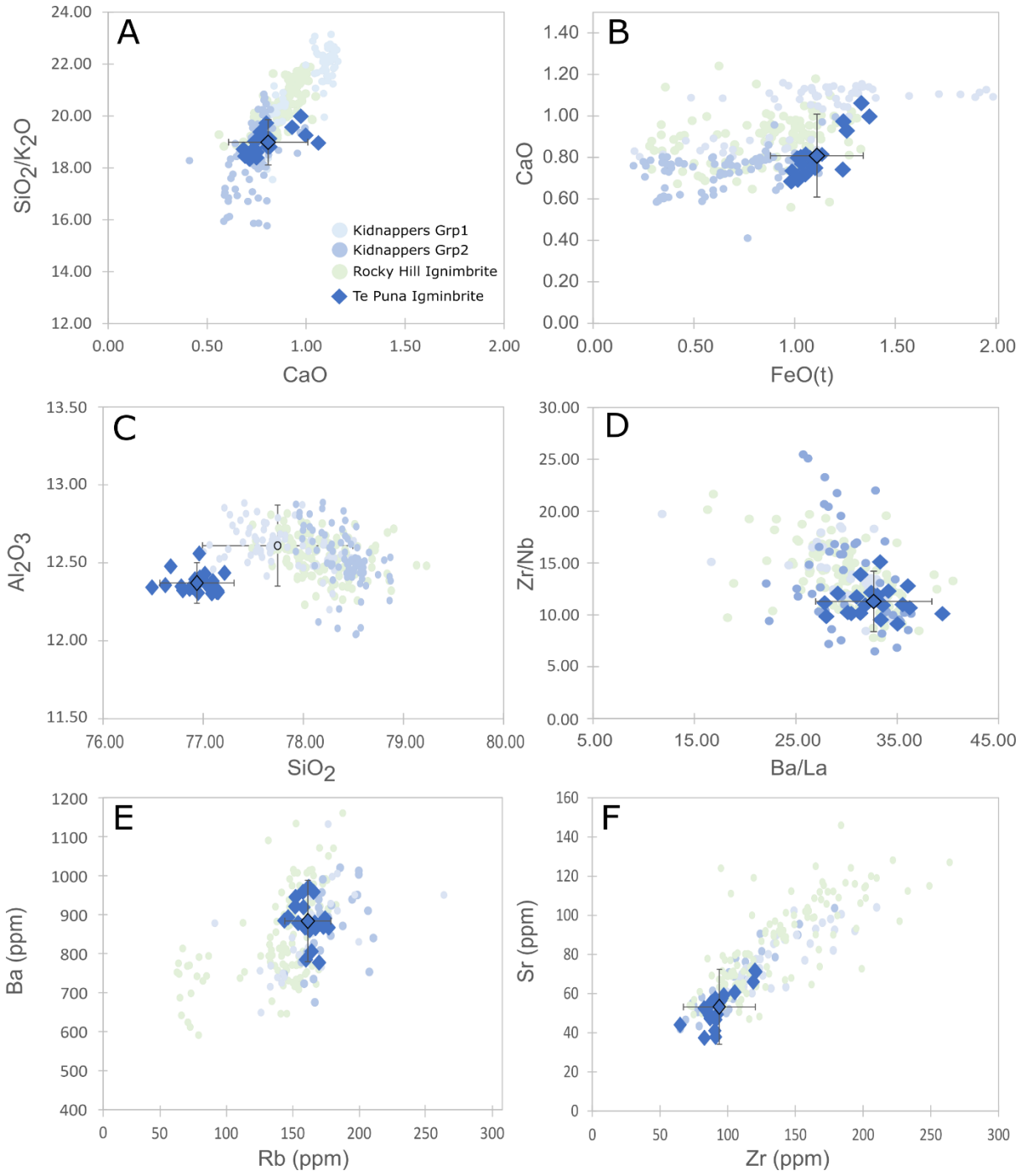

Figure 2.11. Bivariate plots of analyses including mean (± 2σ error bars) of glass of Te Puna ignimbrite (this study) compared with analyses of Kidnappers and Rocky Hill ignimbrites (data from Cooper *et al.* 2016). Major elemental data (as oxides) all on normalised basis.

populations may result from variations in magma composition (Naish *et al.*, 1996; Kilgour & Smith, 2008; Cooper *et al.*, 2012), or post- or syn-depositional reworking (Schneider *et al.*, 2001; Lowe *et al.*, 2017), and possible causes for mixed populations are discussed further below.

2.5 Discussion

2.5.1 Correlations

Using the new U-Pb zircon ages and glass compositional data, together with stratigraphic considerations, correlations between the TgaVC-derived ignimbrites and the Hikuroa Pumice Member and Esk-Mudstone tephras T1 and T2 , and the MVC-derived Te Puna Ignimbrite, are made with other previously identified horizons both onshore and offshore (**Table 2.3**).

2.5.2 Proximal ignimbrites from TgaVC and Esk-Mudstone tephras T1 and T2

The U-Pb zircon ages of the Arateka and Wharo ignimbrites overlap with those of the Esk-Mudstone tephras T1 and T2 (**Fig. 2.8; Table 2.1**), and of the Otawera Ignimbrite, meaning all three are potential correlatives for the two Esk-Mudstone tephras on the basis of their similar age. Stratigraphic field relationships and an older zircon crystallisation age of 2.31 ± 0.046 Ma for the Welcome Bay Ignimbrite indicates it is unlikely to be a correlative of Esk-Mudstone tephras T1 and T2. The Otawera Ignimbrite (2.21 Ma) cannot be separated from the Aretaka, Welcome Bay, and Wharo ignimbrites on age alone, but stratigraphically it is younger than the Welcome Bay and Wharo ignimbrites (**Figs. 2.3, and 2.5 b**).

Table 2.3. Summary of proximal ignimbrites and distal tephra correlatives and sources proposed in this study for the Tauranga ignimbrites and Hawke's Bay tephra deposits.

Unit names (this study)			**Correlatives**	
Proximal	***Distal***	***Source****	***Onshore***	***Offshore***
	Te Puna Ignimbrite	MVC	Kidnappers Ignimbrite; OH-16-01[1,2]	-
Waiteariki Ignimbrite	Hikuroa Pumice Member	TgaVC	KATY824 (?)[3]	M2[4]
Otawera Ignimbrite	-	TgaVC	-	-
Arateka Ignimbrite[5]	Esk Mst-T1	TgaVC	RIS-16-04[2]	M4[4]
-	-	TgaVC (?)	Ris-16-03[2]	M5
-	-	TgaVC (?)	Ris-16-01[2]	M6
-	Esk Mst-T2	TgaVC	OH-16-03; RIS-16-02; Ohingaiti 1[6]	M7[4]
Wharo Ignimbrite[7]	-	TgaVC	-	-
Welcome Bay Ignimbrite[7]	-	TgaVC	SA470 (?)[3]	-

*MCV, Mangakino Volcanic Centre; TgaVC, Tauranga Volcanic Centre

[1]Cooper *et al.* (2012)
[2]Hopkins and Seward (2019)
[3](?) = probable correlation, Milicich *et al.* (2013b)
[4]Stevens (2010)
[5]Previously known as Upper Pāpāmoa Ignimbrite (Briggs *et al.*, 2005)
[6]Naish *et al.* (1996)
[7]Previously known as Lower Pāpāmoa Ignimbrite (Briggs *et al.*, 2005)

The Arateka, Welcome Bay, Wharo, and Otawera ignimbrites, although having broadly similar rhyolitic glass compositions, can nevertheless be discriminated on bivariate plots (**Fig. 2.9**). The Welcome Bay and Arateka ignimbrites show bimodal geochemical populations, with the second population comprising glass with elevated contents of FeO_t, CaO and Al_2O_3, lower SiO_2 and K_2O contents, and higher ratios of incompatible trace elements, such as Zr/Y. This bimodality was not unexpected for the Welcome Bay Ignimbrite, because field specimens have both white and dark juvenile clasts of two distinct compositions and textual evidence for magma mixing (Namaliu, 2021). The Arateka Ignimbrite, however, contains only white pumice and no physical evidence for magma mixing was observed, yet the same two geochemical populations can be discerned in the glass compositions. The glass analyses of the Otawera and Wharo ignimbrites show distinct groupings separate from those of the Welcome Bay and Arateka ignimbrites. The Wharo Ignimbrite is the least evolved of these four ignimbrites but lies along the mixing line of the two magma compositions identified in the Welcome Bay and Arateka ignimbrites, and hence may represent a (relatively) mafic end-member from this system. The glass analyses of Otawera Ignimbrite are distinct from those of the other three ignimbrites: it has lower Al_2O_3, CaO, and Sr, and high abundances of Na_2O, K_2O, Rb, Ba, Y and higher Ba/Sr and Rb/Sr trace-element ratios.

Glass analyses of the Esk-Mudstone tephras T1 and T2 are compared with those of the four proximal TgaVC ignimbrites (Arateka, Welcome Bay, Wharo, and Otawera) in **Figure 2.9**. The analyses of the Esk-Mst-T1 tephra show bimodal populations overlapping with those for the Arateka and Welcome Bay ignimbrites. Since the Welcome Bay Ignimbrite is older than either Esk Mst-T1 or -T2, it is likely therefore that Esk-Mst-T1 and the Arateka Ignimbrite represent the same eruptive event (**Table 2.3**). In contrast, the glass composition of Esk-Mst-T2 excludes any correlation to the proximal Pāpāmoa ignimbrites (Arateka, Welcome Bay, Wharo, and Otawera) analysed in this study. However, an undefined source within the TgaVC remains likely because of the broad similarities in age.

Hopkins and Seward (2019) identified a sequence of five tephras within a mudstone at Rissington and within the Ohara Depression in Hawke's Bay (**Fig. 2.2 b**). Their tephras OH-16-03 and RIS-16-02 were identified as correlatives, providing a tie point between the sequences at the two locations. Kamp *et al.* (2007) identified deposits at these locations as part of the Esk Mudstone Formation, and so we have compared the glass compositions of tephras RIS-16-01 to RIS-16-04, and OH-16-03 (of Hopkins and Seward, 2019), with those of Esk-Mst-T1 and T2 to see if any are correlatives (**Fig. 2.9**). Glass analyses of Esk-Mst-T2 and RIS-16-02/OH-16-03 are essentially identical with regard to both major and trace elements and, along with stratigraphic positioning, meaning that these deposits are very likely to be correlatives.

Although strong similarities within the glass major elements are evident for Esk-Mst-T1 and RIS-16-01, RIS-16-03, and RIS-16-04, these units can be distinguished as separate eruptive deposits on the basis of glass trace-element abundances and ratios (**Fig. 2.9**). RIS-16-04 glass has a composition which strongly represents that of the high-SiO_2 population of Esk-Mst T1/Arateka Ignimbrite, and both these tephra-fall units represent the youngest deposit in each respective location, with RIS-16-01 and RIS-16-03 stratigraphically older, but above RIS-16-02/OH-16-03/Esk Mst-T2 (**Table 2.3**)**.** Strong chemical similarities are also evident in glass analyses from offshore deposits ODP 1124C 7H-4 (M4-1 and M4-2) and ODP 1124C 7H-6 (M7) (Stevens, 2010). The glass composition of tephra M7 consistently overlaps with that of Esk Mst-T2, and RIS-16-02/OH-16-03 and M4 show the same two chemical populations found within Esk Mst-T1. In addition, the stratigraphic relationships of the tephras are consistent both onshore and offshore, and hence the deposits can be identified as correlatives (**Table 2.3**). Therefore, it is likely that the middle two tephras in the Rissington sequence of Hopkins and Seward (2019), RIS-16-01 and RIS-16-03, either were not deposited or were not preserved in the Waikoau River area (**Fig. 2.2 b**).

2.5.3 Waitеariki Ignimbrite and Hikuroa Pumice Member

The U-Pb zircon ages for the Waitеariki Ignimbrite provide an average maximum eruptive age of 2.1 Ma (**Table 2.1**). This age is consistent with previous K-Ar age determinations of 2.18 ± 0.15 Ma (whole-rock) and 2.13 ± 0.17 Ma (plagioclase) (Takagi, 1995), an $^{40}Ar/^{39}Ar$ age of 2.09 ± 0.03 Ma (Briggs *et al.*, 2005) and a (U/Th)/He zircon age of 2.25 ± 0.26 Ma (Pittari *et al.*, 2021).

Milicich *et al.* (2013b) described two ignimbrites, KATY824 and SA470, found within drill cores from the Kawerau Geothermal Field (**Fig. 2.1**) and suggested that these deposits may be correlatives of the Waitеariki and Welcome Bay ignimbrites on the basis of similar U-Pb zircon ages of 2.17 ± 0.05 Ma (KATY824) and 2.38 ± 0.05 Ma (SA470), respectively. In addition to similar ages for the Waitеariki Ignimbrite, KATY824 and SA470 have mineral assemblages of plagioclase, quartz, altered ferromagnesian minerals, biotite, minor lithics of rhyolitic lava and, in KATY824, a eutaxitic texture (Milicich *et al.*, 2013a). These mineralogical characteristics are consistent with those of the Waitеariki and Welcome Bay ignimbrites, and hence (together with the age data) support a probable correlation between these deposits. Because of the intense alteration, comparison of glass composition between KATY824 and SA470, and that of TgaVC ignimbrites is not feasible.

The brown-coloured glass in the lower Waitеariki Ignimbrite was examined using a scanning electron microscope prior to analysis. This investigation demonstrated that microlite development from devitrificaton is not widespread at this stratigraphic level although a degree of post-depositional hydration is a certainty due to the formation of perilitic cracking within the fiamme (Denton *et al.*,

2009). However, the relatively high analytical totals and consistent geochemical composition (**Table 2.2**) obtained in our study indicate that the brown Waitearikiglass remains a fair approximation of melt composition. Comparison of glass composition of the Hikuroa Pumice Member with that of Waitearikiignimbrite is shown in **Figure 2.10.** The two ignimbrites have extremely similar major and trace element abundances and trace-element ratios, although **Figure 2.10 a** shows a systematic offset in the FeO_t (-0.35 wt %) and CaO (+0.11 wt %), which may be linked to the 'browning' of the Waitearikiglass. Based on major and trace element geochemistry, corresponding stratigraphic positions and ages, we conclude that the Waitearikiignimbrite and Hikuroa Pumice Member are correlatives.

Glass-analysis-derived bivariate plots of FeO_t vs CaO, and plots of trace-element ratios of large ion lithophile (LIL) elements (e.g. Ba and Rb vs Sr) against Zr/Y (**Fig. 2.10 e,f**), show a bimodal composition for the Hikuroa Pumice Member where lower FeO_t, CaO and Zr/Y ratios along with higher LIL ratios, define a distinct sub-group (e.g. **Fig. 2.10 f**). This sub-group, however, is not observed in the equivalent glass analyses from the proximal Waitearikiignimbrite which may reflect the limited stratigraphic interval sampled because of the predominance of unsuitable glass, or geochemical zonation within the proximal deposit. Glass from deposits at the three distal sites (Darkys Spur, Beattie Road and McIntyre Access Road) show this sub-group but no link with stratigraphic position within the deposit nor SiO_2 content can be discerned. Therefore, it remains unclear if this bimodality reflects the eruption of a magma source with systematic zonation with subsequent mixing of shards during transportation of > 150 km from the source region, tapping of discrete magma batches, or both.

Previous studies have correlated the Hikuroa Pumice Member to the offshore deposit ODP 1124C 7H 3W (M2) (Bland *et al.*, 2007; Stevens, 2010; Hopkins & Seward, 2019). Hopkins and Seward (2019) investigated a potential link between the Hikuroa Pumice Member and known tephra deposits of similar age in the Whanganui Basin (**Fig. 2.1**), but no correlatives have yet been identified.

2.5.4 Te Puna Ignimbrite

This study dates the Te Puna Ignimbrite at 1.11 ± 0.046 Ma, a little older than the previously determined $^{40}Ar/^{39}Ar$ age of 0.929 ± 0.012 Ma (Briggs *et al.*, 2005). The Rocky Hill and Kidnappers ignimbrites were erupted from the MVC around this time, the former being separated from the Kidnappers Ignimbrite by an erosional surface which represents a period of only years to decades (possibly ~10–20 years) (Cooper *et al.*, 2017). The two ignimbrites share the same magmatic system, and the very close time span between the two eruptions means the eruptive glasses have extremely similar major and trace element compositions (**Fig. 2.11**). The Rocky Hill Ignimbrite, however, was a much smaller eruption volumetrically (although still substantial, c. 200 km^3 DRE) with deposits

restricted to the west and north of the Mangakino Caldera (**Fig. 2.1**). Juvenile clasts have a distinct texture which includes large (up to 5 mm), euhedral amphibole crystals and only minor biotite which allows the unit to be distinguished from Kidnappers Ignimbrite. Three geochemical populations have been identified within the Kidnappers ignimbrite, with Groups 1 and 2 being more volumetrically significant (Cooper *et al.*, 2012). **Figure 2.11** demonstrates that the glass composition of the Te Puna Ignimbrite is highly consistent with that of the Kidnappers Ignimbrite and contains shards of both Group 1 and 2 glass compositions. The offset in SiO_2 in **Figure 2.11 c** is likely to be an artefact of data normalization, where SiO_2 values can vary upwards of 5 wt. % when analytical totals are low (e.g. 91.7–99%, average 95.86 %: Cooper *et al.* 2016); 98.45–99.44 %, average 98.97 %, our study). Despite this, SiO_2 averages for Kidnappers Group 1 and Te Puna glass still overlap within error. Bivariate plots of trace-element and trace-element-ratio data (**Fig. 2.11 d-f**) also show consistent overlap in geochemical composition and augment the correlation suggested from the major element glass compositions.

Our new data (equivalent age, identical glass composition, mineralogy, similar textures) suggest that the Te Puna and Kidnappers ignimbrites are correlatives. However, Briggs *et al.* (2005) refers to unpublished paleomagnetic data which states the Te Puna Ignimbrite is reversely magnetised. This orientation, however, conflicts with a normal polarity (Jaramillo subchron) reported for the Kidnappers Ignimbrite (Cooper *et al.*, 2012), which would exclude such a correlation. Notwithstanding, we propose that based on the numerous lines of evidence presented here, the Te Puna Ignimbrite is highly likely to be a correlative of the Kidnappers Ignimbrite. The magnetic polarity of these units should be re-examined to authenticate the unpublished palaeomagnetic data before the correlation proposed here can be excluded.

2.6 Implications of correlations

We have correlated a number of the TgaVC-derived proximal ignimbrite deposits of the Tauranga region, and the MVC-derived Te Puna Ignimbrite, with deposits in northern Hawke's Bay and elsewhere as summarised in **Table 2.3**. These correlations show that deposits from explosive rhyolitic volcanism of the TgaVC are more extensive than previously recognised.

Five separate ignimbrite-forming eruptions are currently recognised as occurring in the TgaVC, namely Arateka, Welcome Bay, Wharo, Otawera ignimbrites (previously undifferentiated deposits of the Pāpāmoa Formation of Briggs *et al.*, 1996, 2005), and Waiteariki ignimbrite. These five eruptives are likely a minimum because our knowledge of the proximal stratigraphy of the Pāpāmoa Range remains incomplete. Local investigations are hampered by limited outcrop exposures due to subsequent burial by younger TVZ-derived deposits and pervasive devitrification and/or welding of deposits.

Additionally, the sample of Upper Pāpāmoa Ignimbrite dated by Briggs *et al.*, (2005) was not collected from the type locality for this unit. Instead, it appears to be a sample derived from an unrecognised ignimbrite that was erupted after the Waiteariki Ignimbrite.

The identification of distal correlative deposits of the Waiteariki Ignimbrite located throughout northern Hawke's Bay suggests the eruption of the Waiteariki Ignimbrite was a significant large-scale silicic event. Large-volume silicic eruptions have been common throughout the history of the TVZ with 25 inferred caldera-forming eruptions taking place in the last 1.6 Ma ranging in volume from 30 to 1500 km^3 (Wilson *et al.*, 2009). The largest four eruptions are classed as supereruptions, and include the Ongatiti (> 500 km^3 DRE; Yousef Zadeh, 2020) and Kidnappers ignimbrites (1200 km^3 DRE; Cooper *et al*., 2012) from the Mangakino Volcanic Centre, the Whakamaru Group ignimbrites (2200 km^3 DRE; Gravely *et al.*, 2016), Whakamaru Caldera and the Oruanui Ignimbrite (> 530 km^3 DRE; Barker *et al.*, 2021) from the Taupō caldera. While the runout distances of ignimbrites can vary considerably, such distances are directly related to increasing mass flow rates feeding the pyroclastic currents and bulk volumes (Giordano & Cas, 2021). Of the Aotearoa New Zealand supereruptions, the runouts vary from c. 75 km for the Whakamaru ignimbrites, to 90, 140 and 180 km for the Oruanui, Ongatiti, and Kidnappers ignimbrites, respectively (Wilson *et al.*, 1995b; Alloway *et al.*, 2004; Barker *et al.*, 2021). The runout distance for the Waiteariki Ignimbrite is ambiguous as the eruptive source is still to be determined precisely. However, it is assumed to be within the TgaVC (Briggs *et al.*, 2005) and so the location of distal deposits ~150 km south-east of TgaVC, implies that the Waiteariki Ignimbrite is almost certainly the product of a caldera-forming eruption which has the potential to be one of the largest eruptive events in New Zealand's geological record. The source caldera of the Waiteariki, and possibly other ignimbrites within the TgaVC is yet to be formally defined (Prentice *et al.*, 2020; Pittari *et al.*, 2021) and the link between these and the numerous rhyolite domes found throughout the region is yet to be investigated, but both would likely share a common magmatic system with any local caldera.

The Esk Mudstone tephra-T1, a correlative of Rissington RIS-16-04 (Hopkins & Seward, 2019), was able to be positively matched to the proximal Arateka Ignimbrite. The new U-Pb zircon ages for the Esk Mudstone tephras T1 and T2 provide the first radiometric age constraints for the lower Esk Mudstone Formation of c. 2.2 Ma and significantly extends the known extent of these tephra-fall deposits. The ages on the Esk Mudstone tephras, together with those of the five TgaVC-derived ignimbrites, and other deposits of the TgaVC (Briggs *et al.*, 2005; Pittari *et al.*, 2021), indicate that the period from c. 2.4 to 2.0 Ma was a period of frequent rhyolitic activity in northern New Zealand, which culminated with the eruption of the large-volume Waiteariki Ignimbrite. From the combined proximal and distal records, we identify eight rhyolitic events over this period, giving an average repose period for the

TgaVC of c. 50 kyrs. We stress that this is a maximum value as local dome eruptions have been excluded due to uncertain links between them and known tephra deposits. As previously noted, it is also likely that there are further ignimbrites to be defined in the southern Pāpāmoa Range.

In comparison, a repose period for late CVZ activity (c. 7–3.5 Ma) was determined to be c. 75 kyrs (Stevens, 2010). It is worth noting, that older records, such as those for the TgaVC and CVZ, are likely to be biased towards larger (more voluminous) events that would tend to have greater preservation potential in both proximal and distal locations. The TVZ is known to be one of the most prolific silicic eruption centres on Earth, with voluminous ignimbrites occurring every c. 50 kyrs over the past 1.6 Myrs (Wilson *et al.*, 2009; Gravley *et al.*, 2016). However, this average repose period disguises several clusters of activity which occurred at 1.2, 1.0, 0.35, and 0.06 Ma, referred to as short ignimbrite flare-up events (Gravley *et al.*, 2016). The largest of these flare-up events occurred from ~350 to ~280 ka, where at least eight large ignimbrite eruptions occurred in > 100 kyrs. The frequency of silicic volcanism from the TgaVC is similar to that of the TVZ, with voluminous ignimbrite eruptions occurring on average every 50 kyrs, but, as with the TVZ, many of these events occurred clustered in time. For example, the four ignimbrite eruptions in TgaVC of Welcome Bay, Wharo, Otawera, and Arateka ignimbrites, occurred within c. 90 kyrs between 2.3 and 2.2 Ma, and therefore may represent an early ignimbrite flare-up event, similar to those described for the TVZ.

Borehole geological data from TVZ geothermal wells implies continuing rhyolitic volcanism between c. 2 and 1.6 Ma (Chambefort *et al.*, 2014; Milicich *et al.*, 2020). This period covers suspected caldera volcanism of late TgaVC activity and the onset of volcanism at MVC, but it is not known whether these deposits are related in any way to volcanism originating from either centre, or an additional unrecognised silicic system (or caldera) with an overlapping eruptive timespan, a phenomenon well recognised within young and modern TVZ periods (Charlier *et al.*, 2003; Gravley *et al*., 2007, 2016). Originating from the Mangakino Caldera, the Kidnappers Ignimbrite is exceptionally widespread ignimbrite with a known distribution stretching from Auckland to Hawke's Bay (Wilson *et al.*, 1995b; Cooper *et al.*, 2012). The confirmed correlation between the Te Puna and Kidnappers ignimbrites formally extends the known distribution of this eruptive into the Tauranga region.

2.7 Conclusions

The TgaVC, active from 2.95 to 1.9 Ma, lies temporally and spatially between the defined locations and time frames of activity in the CVZ and the currently active TVZ, one of the most productive regions of Quaternary silicic volcanism on Earth. New U-Pb zircon ages and major and trace element glass compositional analyses of five prominent proximal ignimbrites from the TgaVC confirm previously postulated links between these units and age-equivalent tephra deposits in northern Hawke's Bay.

The Arateka ignimbrite (correlative Esk Mst-T1) and Esk Mst-T2 tephra provide the first radiometric age constraints (2.2 Ma) for the lower Esk Mudstone Formation, and a robust isochronous tie point for the wider region. The Hikuroa Pumice Member in Hawke's Bay is a distal ignimbrite found 150-170 km southeast from the southern-most exposures of its proximal (coeval) equivalent, the Waitearikí Ignimbrite. Hence these eruptive products are distributed more extensively than previously recognised. Volcanic activity in the TgaVC documented here, and the record of tephra deposits elsewhere, indicates that rhyolitic activity in New Zealand between 2.4 and 2 Ma was frequent: at least eight eruptions occurred within TgaVC, culminating with the eruption of the very large-volume Waitearikí Ignimbrite at 2.1 Ma. This record provides a maximum mean repose period for the TgaVC of ca. 50 kyrs. Our study demonstrates the importance of combining proximal and distal records in reconstructing the early eruptive histories of active volcanic regions, and the newly-established correlation between the Hikuroa Pumice Member and Waitearikí Ignimbrite will form the basis for further investigations to define the distribution, volume and source caldera for the Waitearikí Ignimbrite. Our findings also allow the transition of volcanic activity from the previously active CVZ to the TVZ to be reassessed and have implications for our understanding of the onset of large-volume rhyolitic activity during the Early Quaternary at the dawn of the TVZ.

2.8 Acknowledgments

This research was funded by a University of Waikato Doctoral Scholarship and a School of Science Trust Fund Research Grant. MLP thanks Jenni Hopkins for discussions on tephrostratigraphy of Hawke's Bay and Whanganui Basin; Matt Sagar for advice on common Pb corrections and calculation of U-Pb ages; and field and laboratory assistance from Rochelle Hansen, Edie Fisher, Kirsty Vincent and Annette Rodgers. We would also like to thank two anonymous reviewers for helpful comments that helped clarify and improve this manuscript. This paper is an output of the Commission on Tephrochronology (COT) of the International Association of Volcanism and Chemistry of the Earth's Interior (IAVCEI).

CHAPTER 3:

3 Eruption of a large-volume, monotonous intermediate ignimbrite at the dawn of the TVZ: 2.1 Ma Waitea riki Ignimbrite, Tauranga Volcanic Centre, New Zealand

3.1 Introduction

The products of large-volume (≥ 100 km^3 DRE) dacitic to rhyolitic supereruptions are commonly placed into two categories: crystal-rich, dacitic monotonous intermediates (MIs) (e.g. Fish Canyon Tuff, La Garita, Colarado USA Bachmann *et al*., 2002; Lund Tuff, White Rock, Great Basin USA, Maughan *et al*., 2002; Cerro Galan, South America , Folkes *et al*., 2011; Hotokezawa Ignimbrite, Aizu, Japan, Yamamoto, 2021) and the crystal-poor rhyolites (CPR) (e.g. Oruanui supereruption, Taupō, New Zealand, Barker *et al*., 2021; Peach Springs Tuff, Silver Creek, Arizona, Pamukcu *et al*., 2013; Bishop Tuff, Long Valley, California, Chamberlain *et al*., 2015). Despite their distinct differences, overlap of glass compositions suggests the two categories have similar origins and represent separate parts of complex magma storage reservoirs (Hildreth, 1981; Huber *et al.*, 2012; Cashman & Giordano, 2014). Monotonous intermediates are interpreted to represent the evacuation of significant volumes of partially remobilised crystal mushes that produce voluminous pyroclastic flows that are typically crystal-rich (≥ 35 %), pumice- and lithic-poor, have homogenous whole-rock compositions, consistent mineral assemblages and commonly lack early-phase Plinian eruption deposits. Despite this apparent homogeneity at hand-specimen scale, MIs typically have highly heterogenous crystal populations, reflective of complex storage and evolutionary histories (cf. Bachmann *et al*., 2002; Kay *et al*., 2011; Grocke *et al*., 2017; Maughan *et al*., 2002). Crystal-poor rhyolites, however, represent a segregated, fractionated melt-dominant body which accumulated in upper parts of the magma reservoir and may or may not be compositionally zoned. In contrast to MIs, CPR eruptions typically initiate with the eruption of high-SiO_2, crystal-poor (< 15 %) magma to produce widespread and voluminous pyroclastic-fall deposits that underlie ignimbrites that may vary stratigraphically in both crystallinity and bulk composition (Chamberlain *et al.*, 2015; Allan *et al.*, 2017).

Large volume silicic volcanism within New Zealand has been a prominent feature during the c. 2 Ma history of the Taupō Volcanic Zone (TVZ; Wilson *et al.,* 1995a). During this time, the vast majority of eruptions involved crystal-poor (< c. 10 %) rhyolites that are compositionally variable, but often not systematically zoned (Briggs *et al.*, 1993; Deering *et al.*, 2011a; Cooper *et al.*, 2012; Bégué *et al.*, 2014; Allan *et al.*, 2017). The eruption of voluminous crystal-rich (> c. 20 %) ignimbrites is rare, and limited

to the Rotoiti (c. 55-45 ka, Okataina Volcanic Complex; Schmitz & Smith, 2004; Hopkins *et al*., 2021a), Whakamaru (349 ± 4 ka, Whakamaru Caldera; Brown *et al*., 1998a; Downs et al., 2014) and Ongatiti (1.21 Ma; Mangakino Caldera; Cooper & Wilson, 2014; Yousef Zadeh, 2020) ignimbrites, but these eruptives don't conform with typical MIs, and are instead inferred to reflect the syn- or sequential eruption of two or more magma bodies, which may include at least the partial remobilisation of the mush-source zone. Here we examine the Waiteariki Ignimbrite, which is an outlier from the typical TVZ ignimbrite endmembers described above. This voluminous, crystal-rich, dacitic ignimbrite erupted from the Tauranga Volcanic Centre (TgaVC) (Pittari *et al.*, 2021; Prentice *et al.*, 2022). It has been studied in limited detail until now and in this paper, we present comprehensive field, mineralogical and whole-rock data. We then seek to characterise this ignimbrite as either a crystal-rich rhyodacite ignimbrite (cf. Ongatiti Ignimbrite, Cooper & Wilson, 2014; Whakamaru Ignimbrite, Brown *et al*., 1998a) or that of a typical monotonous intermediate. Monotonous intermediates are common offshore, but never before documented within the New Zealand geological record. Furthermore, we re-evaluate volcanism of the TgaVC in the context of the migrating continental-arc.

3.2 Regional geologic setting

Arc-related silicic volcanism within Te Ika-a-Māui/North Island of Aotearoa New Zealand currently occurs within the TVZ, the southernmost ~300 km continental extension of the ~2800 km long Tonga-Kermadec arc, resulting from the oblique, westward subduction of the Pacific Plate beneath the Australian Plate (Wilson & Rowland, 2016). Consisting of a rifting arc, rather than a conventional arc-back arc system (Wilson & Rowland, 2016; Villamor *et al.*, 2017), the TVZ is globally known for its high caldera density and eruptive volumes (Hughes & Mahood, 2011). Volcanism of the TgaVC (2.95–1.90 Ma; Briggs *et al*., 2005) lies spatially between the defined locations of the TVZ and its predecessor, the Coromandel Volcanic Zone (CVZ; 12–3.5 Ma) (**Fig. 3.1**). Temporally, early andesitic TVZ volcanism overlaps with waning silicic volcanism of the TgaVC, thus the TgaVC has been seen as an important transition zone between the two broader volcanic zones.

Volcanism of the TgaVC began c. 3 Ma with the eruption of andesitic lavas on the eastern side of the field forming the Otawa stratovolcano, the eroded remnants of which form the Pāpāmoa Range. This was rapidly followed by the onset of rhyolitic volcanism from c. 2.8 Ma with the eruption of numerous lava domes, which continued over the entire age range of the TgaVC (Stipp, 1968; Briggs *et al.*, 2005; Pittari *et al.*, 2021; Prentice *et al.*, 2022). A heightened period of explosive volcanism occurred between c. 2.4 and 2.0 Ma where extensive ignimbrites were deposited throughout the Tauranga region. Pyroclastic activity culminated with the eruption of the Waiteariki Ignimbrite at 2.1 Ma (Prentice *et al.*, 2022). The Waiteariki Ignimbrite is crystal- and pumice-rich, lithic-poor and is extensively welded with a pronounced eutaxitic texture. The predominant mineral assemblage

comprises plagioclase, hornblende, pyroxene and quartz with minor amounts of biotite. Prentice *et al.* (2022) identified the distal deposits of the Waiteariki Ignimbrite throughout northern Hawke's Bay and suggested that this eruption was a significant large-scale silicic event. In this contribution, we seek to estimate the eruption volume and the identification of the probable source for the Waiteariki Ignimbrite.

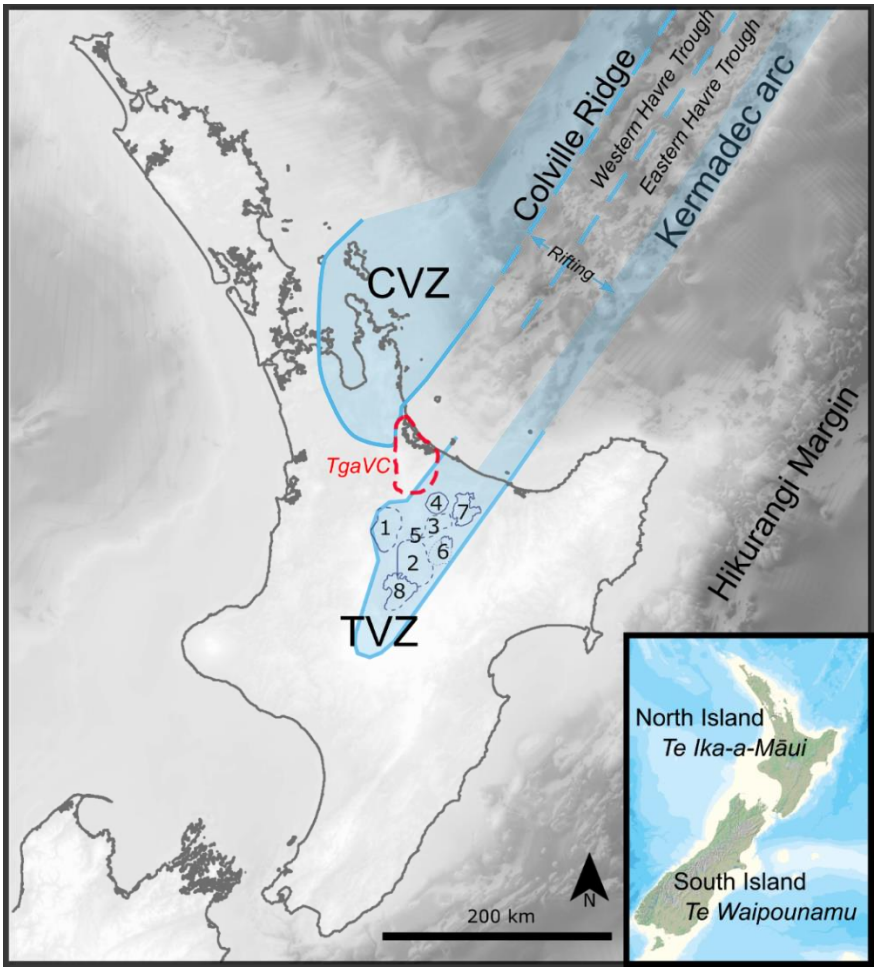

Figure 3.1. Overview map showing the main zones of rhyolitic volcanism within Te Ika-a-Māui/North Island of Aotearoa New Zealand: CVZ (Coromandel Volcanic Zone), the TgaVC (Tauranga Volcanic Centre), and the presently active TVZ (Taupō Volcanic Zone). TVZ calderas are numbered as follows: 1, Mangakino; 2, Whakamaru; 3, Kapenga; 4, Rotorua; 5, Ohakuri; 6, Reporoa; 7, Okataina; 8, Taupō (after Leonard et al., 2010).

3.3 Methodology

Samples of the Waiteariki Ignimbrite were collected from ~ 30 outcrops throughout the Tauranga region. At each site, detailed observations of lithofacies and textural characteristics were made in addition to stratigraphic logging of (mostly) vertically restricted sections to enable interpretation of large-scale eruption and pyroclastic flow processes. During the 1970s, a series of cores were drilled across the eastern side of the southern Kaimai Range as part of geological investigations for the Kaimai

Rail Tunnel (Healy, 1967; Hegan, 1972). Located near the eastern portal above the Aongatete River, one such core, ES112, intersected 157 m of Waiteariki Ignimbrite. This core covers the full thickness of the Waiteariki Ignimbrite and was sampled at 15 stratigraphic intervals (**Supplementary data table SM3.1**).

Due to the degree of welding and devitrification of proximal Waiteariki Ignimbrite deposits, geochemical analysis was restricted at many sites to bulk analysis. Wherever possible, large fiamme were also sampled from the same stratigraphic level for comparative whole-rock analysis between bulk-ignimbrite and juvenile clasts. This is often the situation when studying large, welded ignimbrites (ie. Fish Canyon Tuff, Bachmann *et al*., 2002; Ora Ignimbrite, Willcock et al. 2013) and introduces several complexities to be considered when interpreting magmatic chemistry which include:

1) mixing and mingling of distinct magma chemistries immediately prior to and/or during eruption (e.g. Allan et al., 2017);

2) physical fractionation processes, such as elutriation causing crystal enrichment (Bachmann *et al.*, 2002);

3) acquisition of xenolithic material from the conduit or pre-existing surface deposits;

4) variable degrees of welding that affect petrographic estimations of magmatic crystallinity and mineralogy; and

5) post-deposition devitrification and vapor phase alteration (Heled *et al.*, 2022).

While these complexities are unavoidable, we have, however, done everything in our capacity to avoid, mitigate, or assess the potential impact of these processes on our findings.

Whole-rock major and trace-element analysis were undertaken at the School of Science, University of Waikato (New Zealand). Thirty-five bulk-ignimbrite or fiamme samples were lightly crushed, and fresh rock chips were handpicked and powdered in a tungsten-carbide mill (**Supplementary data table SM3.6**). Loss-on-ignition (LOI) was measured by the weight loss of ~2 g of sample after heating for an hour at 1100 °C. Homogeneous glass disks were made using 0.8 g of dried sample powder mixed with 8 g of Li-metaborate 12-22 flux and fusing at 1050 °C for 20 minutes in a platinum crucible. Analysis was conducted using a Bruker S8 Tiger X-ray fluorescence (XRF) spectrometer. LOI values are typically < 2.5 % with four samples returning LOI values between 2.65–2.88 %. Major element abundances cited in the text and shown on diagrams were recalculated to total 100 wt. % on an anhydrous basis. Analytical precision was assessed using repeat analyses of the international standard GSP-2. Mean values are within 1.5 % of the recommended values with the exception of MnO for GSP-2 (3.6 %

offset). Analytical precision (2σ) is < 0.3 wt. % for all elements except SiO_2 (0.56 wt. %). Trace elements were determined by laser ablation inductively coupled plasma mass spectrometry (LA-ICP-MS) using an Agilent 8900 Triple Quadrupole ICP-MS coupled with a Laurin Technic S155 SE ablation cell and a RESOlution 1963 nm ArF excimer laser. The analytical method follows that outlined by Eggins (2003) which utilises the fused glass disks following XRF analysis. Individual disks were stacked vertically and set in epoxy, sectioned and polished prior to analysis. NIST612 glass standard was used as the calibration standard with repeat analyses of Atho-G used as an independent secondary standard. Replicate analyses of Atho-G are accurate to within 10 % (usually < 5 %) of published values, excluding Nb (< 12 %), Ta (< 15 %) and Pb (< 20 %). Precision (2σ) is better than 2 %, except Zr and Ba at < 16 ppm and < 9 ppm respectively. Details on LA-ICP-MS set up and data for individual analyses of standard reference materials used to assess analytical precision and accuracy are available in **Supplementary data tables SM3.4** and **SM3.5**.

Loose crystals of plagioclase, pyroxene, and amphibole from distal Waitearikiri samples were handpicked under a binocular microscope embedded in epoxy blocks and polished. This was augmented by crystals from welded proximal samples using polished thin-sections from various stratigraphic levels to capture any chemical variability and ensure representative spatial sampling. Mineral compositional data was obtained for pyroxene, plagioclase and biotite crystals using a scanning electron microscope coupled with energy dispersive spectroscopy (SEM-EDS) at the Otago Micro and Nanoscale Imaging Centre at the University of Otago, Dunedin. Grain mounts and thin sections were coated with approximately 10 nm of carbon in a Quorum Q150T E turbo-pumped carbon coater and then analysed in a Zeiss Sigma variable-pressure SEM, equipped with an Oxford X-Max EDS detector. EDS analysis was performed with Aztec version 4.1 using factory standardization. Data was filtered to exclude those with totals that deviated from 100% by > 2.5 %. Amphibole crystals were analysed in two separate analytical sessions. The first session was conducted at Victoria University of Wellington using a JEOL JXA 8230 Superprobe with an accelerating voltage of 15 kV with a beam current and diameter of 12 nA and 10 µm respectively. Amphibole crystals were randomly selected from matrix and fiamme within polished thin-sections. Additional crystals were analysed using a JEOL 8530F field emission electron probe microanalyser at the University of Auckland equipped with a time-dependant intensity correction (TDI) system using an accelerating voltage of 15 kV with a beam current and diameter of 20 nA and 1 µm respectively. Precision and accuracy were monitored using standards NMNH 122142 (Kakanui augite), USNM746 (Hypersthene), NMNH137041 (Anorthite), and Engels and Kakanui Hornblende (NMNH143965). Replicate analyses give an indication of precision and accuracy (see **Supplementary data tables SM3.7, SM3.8 and SM3.9**). Obtained mean values are mostly within 5 % of published values, although offset is greater on elements with abundances of < 1 wt. %.

3.4 Field relations, distribution and volume estimates

Waitеariki Ignimbrite outcrops are commonly preserved west of the Wairoa River throughout the eastern foothills of the Kaimai Range (**Fig. 3.2**). The ignimbrite forms the upper surface of the gently sloping Whakamarama Plateau where it onlaps the lower flanks of the Minden Rhyolite domes of Minden Peak (2.135 ± 0.066; Pittari *et al*., 2021), Manawata, Kaikaikaroro (2.39 ± 0.06 Ma; Briggs *et al.,* 2005) and the Kaimai-Kakahu-Te Weraiti dome complex (c. 2.8 Ma; Briggs *et al.,* 2005). West of the Kaimai Range, it is down-faulted by the Hauraki and Okauia faults (not shown) and is believed to

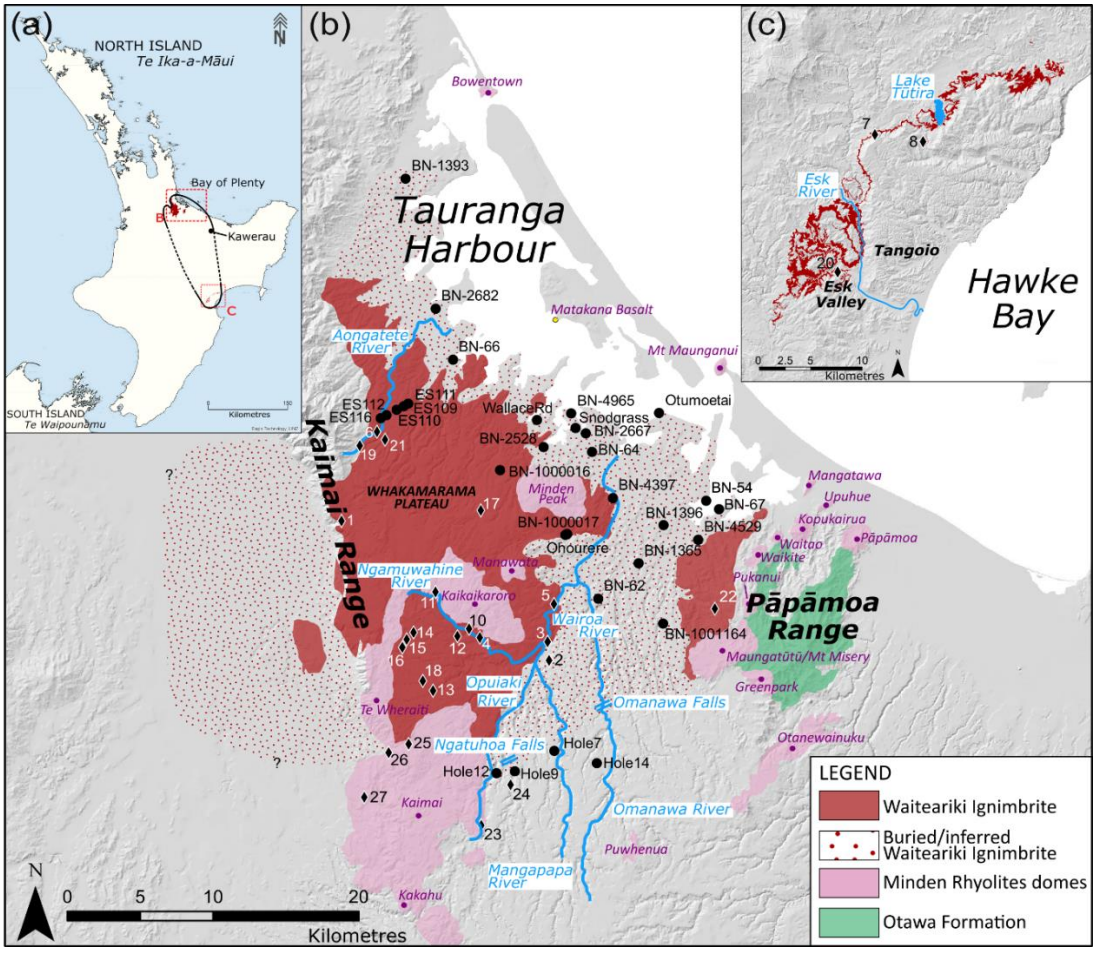

Figure 3.2. (a) Minimum extent of Te Ika-a-Māui/North Island likely inundated by the pyroclastic density current and location of Tauranga and Hawke's Bay study sites. **(b)** Outcrop map highlighting the distribution of surface exposures of Waitеariki Ignimbrite (solid colour) and known and inferred buried (stippled) deposits, along with key topographic features and major rivers in Tauranga, and **(c)** northern Hawke's Bay. Dots and diamonds represent bore hole locations and field sample sites respectively. See **Supplementary data table SM3.1** and **SM3.2** for location details.

underlie much of the southern Hauraki plains (Davidge, 1982; Houghton & Cuthbertson, 1989). Exposures are also found in eastern parts of the Tauranga Basin along the western margin of the Pāpāmoa Range. Throughout central and southern areas, the Waitеariki Ignimbrite is encountered in drill holes at depths of 50–150 m buried by deposits from younger TVZ ignimbrites (Chimp, Pokai and

Mamaku ignimbrites), volcaniclastic and estuarine sedimentation (Matua Subgroup) and tephra-fall deposition (Pahioa tephras and Hamilton Ash Formation) (Leonard *et al.*, 2010). The thickness of the Waiteariki Ignimbrite obtained from bore hole data is highly variable, ranging from a few 10s m to thicknesses exceeding 200 m (**Supplementary data table SM3.2**). Maximum thicknesses (100–> 200 m) are found in boreholes within the central areas of the Tauranga region along with outcrops exposed along the Hauraki Fault in the southern-most Kaimai Range. In general, the Waiteariki Ignimbrite thins towards the north-west with isolated thinning observed in boreholes located behind topographic highs (e.g. Minden Peak rhyolite dome), and paleo-ridgelines. The southern-most field exposures within the Tauranga region occur in stream beds at the Omanawa and Ngatuhoa Falls and Opuiaki River dam.

Distal deposits correlated to the Waiteariki Ignimbrite are found in northern Hawke's Bay (**Fig. 3.2 c**; **Chapter 2** - Prentice *et al*., 2022) and consists of a prominent non-welded ignimbrite overlain by reworked pumiceous ash and lapilli referred to as the Hikuroa Pumice Member of the Petane Formation (Lee *et al.*, 2011). The thickness of this unit ranges from c. 2-15 m (Haywick *et al.*, 1991; Prentice *et al.*, 2022) and clearly crops out in the hills and rivers around Lake Tūtira, Tangoio and Esk Valley areas. The Hikuroa Pumice Member is also correlated with a 9 cm thick tephra-fall deposit in the OPD core 1124C 7H 3W – M2 (Bland *et al.*, 2007). Additionally, an ignimbrite found in drill cores at Kawerau (KATY824; Milicich *et al*., 2013b) has been identified as a probable correlative on the basis of U-Pb zircon ages, texture and mineral assemblage (Milicich *et al.*, 2013a; **Chapter 2** - Prentice *et al.*, 2022).

Deposits of Waiteariki Ignimbrite between those in the Tauranga, Kawerau and Hawkes Bay regions are not currently recognised despite extensive drilling associated with local geothermal fields, some penetrating basement greywacke (e.g. Ōhaaki, Wairakei, Rotokawa and Ngatamariki, Chambefort *et al.,* 2014; Milicich *et al.,* 2020). Within the Ngatamariki and Rotokawa geothermal fields, an ignimbrite within the Tahorakuri Formation has been dated at c. 1.9 Ma (Chambefort *et al.*, 2014; Milicich *et al.*, 2020). This formation is up to 1.7 km thick at Ngatamariki (Chambefort *et al.,* 2014), and it is plausible that there are underlying older ignimbrite units that have not yet been drilled. Additionally, the extreme degree of hydrothermal alteration masks primary rock textures and makes the correlation of units highly challenging. This is compounded by the thickness required (> 5 m) to minimise mixing and loss of return while drilling, regional faulting and subsequent greywacke extension, and post-depositional erosion which may have all contributed to hindering the recognition of Waiteariki Ignimbrite deposits through central TVZ regions.

The estimated minimum distribution of the Waiteariki Ignimbrite is focussed along a narrow zone, oriented NNW-SSE, extending > 200 km from Katikati (NW Bay of Plenty) to northern Hawke's Bay

(**Fig. 3.2 a**). This encompasses all known and presumed deposits for the Waitearikі Ignimbrite and delimits the areal extent likely inundated by the pyroclastic density current, equating to an area of c. 18 000 km^2. Using 60 thickness values from boreholes, outcrops, and geological sections (**Supplementary data table SM3.2**), an isopach map (**Fig. 3.3**) has been created to provide the first volume estimate for the Waitearikі Ignimbrite. Throughout the Tauranga region, the Waitearikі Ignimbrite mostly consists entirely of welded faces (cf. **Section 3.5**) and textural evidence indicates this extends at least 50–60 km eastward to Kawerau (Milicich *et al.*, 2013b), thus, we restrict welded faces to thickness > 20 m with those < 20 m considered non-welded. The complete lack of thickness data points across the central TVZ creates significant uncertainty. However, the overall geometry of deposits indicates significant flow toward the SE and therefore it is likely that the Waitearikі Ignimbrite formerly covered most or all of the area between proximal and distal outcrops in Tauranga and Hawke's Bay. The intervening isopach contours are constrained only by known minimum thickness in northern Hawke's Bay (**Fig. 3.1 c, Supplementary data table SM3.2**) and it is acknowledged that the paleotopography would have been extremely varied with localised thickening and thinning. To minimise overestimation, we adopt a conservative approach where isopach contours > 50 m are restricted to 20 km south of the inferred caldera source (cf. **Section 3.8**) with all remaining areas north of the axial ranges appointed a nominal thickness of 20 m. Within the Tauranga region, areas for pre-Waitearikі Ignimbrite volcanic edifices and the source caldera were calculated and removed from volume calculations (**Supplementary data table SM3.3**), but no further allowance for pre-Waitearikі Ignimbrite topography has been made. Post-depositional extension within the Taupō Rift is incorporated using current estimates of 15 mm/yr (Villamor & Berryman, 2001; Wilson & Rowland, 2016) for the Bay of Plenty coastline.

This gives an estimated volume of 490–502 km^3 for the Waitearikі Ignimbrite out-flow deposit and we adopt a minimum error ± 50 km^3, which is consistent with those assessed by Silleni *et al.* (2020) and Brown *et al.* (2014) for the Campanian Ignimbrite and similar sized eruptions within the Large Magnitude Explosive Volcanic Eruptions (LaMEVE) database respectively and reflective of the high uncertainty associated with of our calculated volume. Generalized models suggest an approximate 1:1:1 relationship for the relative volumes of intra- versus extra-caldera material and co-ignimbrite ash (cf. Mason *et al.,* 2004; Croswellеr *et al*., 2012; Silleni *et al.,* 2020). However, Cook *et al.* (2016) demonstrated that the use of this general model may not be applicable for every ignimbrite especially those where the distribution of the various components are well defined. Despite this, Cook *et al.* (2016) states that for caldera forming eruptions, the 1:1:1 assumption holds to better than an order-of-magnitude basis and as such is therefore adopted here to provide a first order estimate for the Waitearki Ignimbrite of c. 1500 ± 150 km^3, classifying it as a super caldera-forming ignimbrite (Giordano & Cas, 2021).

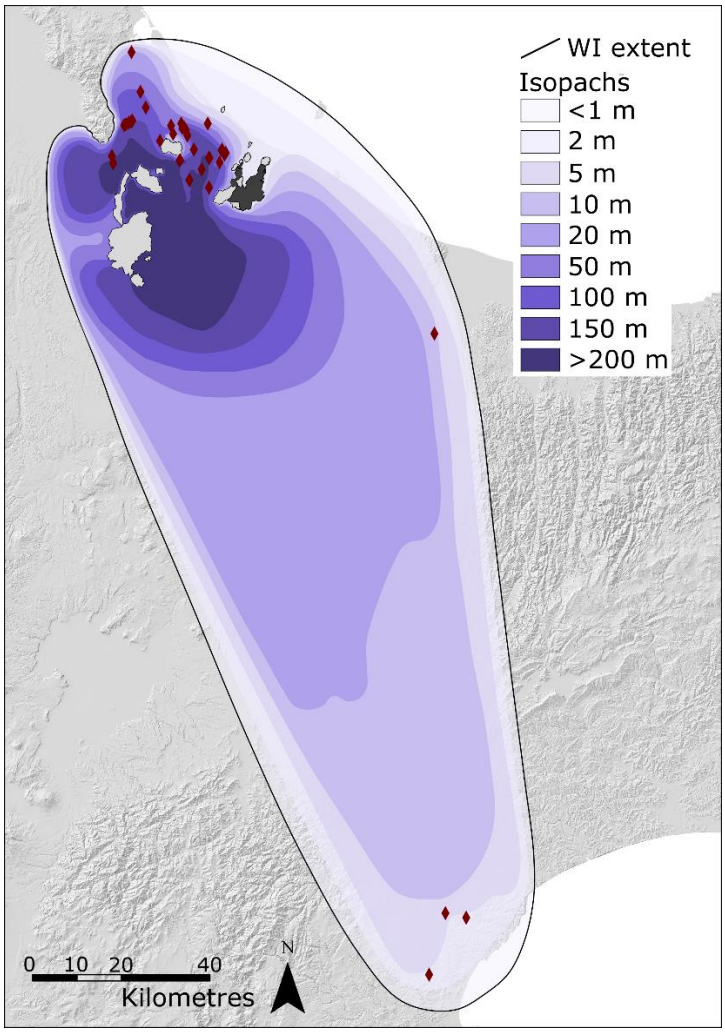

Figure 3.3. Isopach map of the preserved and presumed deposits of the Waitearikí Ignimbrite. This map refers to pyroclastic density current deposits only and excludes the co-ignimbrite ash. Red diamonds represent location and distribution of thickness values (**Supplementary data table SM3.2)**. Refer to text for discussion of uncertainties, associated volumes and source.

Proximal exposures of the Waitearikí Ignimbrite are dominated by densely welded facies. This was confirmed by eleven density measurements obtained from samples from varying stratigraphic heights throughout the outflow sheet which range from 1230–2110 kg/m^3, with a weighted average of 1700 kg/m^3 (see **Supplementary data table SM3.3** for individual measurements). The density of non-welded facies is assumed to be 1000 kg/m^3 (Crosweller *et al.*, 2012). Dense rock equivalent (DRE) volumes and magnitude were calculated using the methods outlined in Crosweller *et al.* (2012) to give a minimum DRE volume of 317 ± 30 km^3 for out-flow deposits, 348 ± 35 km^3 for intra-caldera fill and 205 ± 20 km^3 of co-ignimbrite ash to give a total DRE bulk-deposit volume of 870 ± 87 km^3 which equates to a magnitude (*M*) of 8.3.

3.5 Internal stratigraphy of the Waitearikí Ignimbrite

Complete exposures of the vertical thickness of the Waitearikí Ignimbrite are limited but occur in the southern Kaimai Range where uplift along the Hauraki Fault has dissected the full ignimbrite sheet at Te Ariki (220 m) and Wairere (153 m; location 1, **Fig. 3.2 b**) falls. Currently, the only complete accessible record of the Waitearikí Ignimbrite is found in drill core ES112 (NZ Topo50 BD36 5696 2694), drilled as part of geological investigations for the Kaimai Rail Tunnel (**Fig. 3.2 a**; Healy, 1967; Hegan, 1972). This is augmented by partial exposures found in streams on the eastern side of the southern Kaimai Range, in particular, the nearby Aongatete River, where subsequently lower stratigraphic sections are exposed with increasing elevation. Only surficial stream outcrops are found east and south of the Wairoa River.

We revise the nomenclature of previous workers (i.e. Hegan, 1972; Houghton & Cuthbertson, 1989), and subdivide the Waitearikí Ignimbrite into earlier (Eu I) and later (Eu II) eruptive units (**Fig. 3.4**). Eu I is further subdivided into 3 broad facies:

Facies 1: a thin non-welded basal zone consisting of pumiceous tuff breccia and ash,

Facies 2: multiple flow packages of welded to densely welded ignimbrite with a strong eutaxitic texture up to 150 m thick;

Facies 3: an upper non-welded to welded unit, with zones of extensive vapour phase alteration of pumice to cristobalite and alkali feldspar.

Eu II can be distinguished from Eu I by the presence of large lithic clasts of recycled Waitearikí Ignimbrite and the general presence of trace amounts of biotite in juvenile clasts (see **Sections 3.5.2** and **3.5.3** below). A stratigraphic log showing the internal stratigraphy and key stratigraphic variations of the Waitearikí Ignimbrite is presented in **Figure 3.4**. The majority of surface exposures throughout the Tauranga region consists of the middle-welded facies of Eu I due to extensive erosion and down-cutting of streams (**Fig. 3.5 b,c**). Underlying pumiceous fall deposits indicative of a precursory Plinian phase are not observed in drill cores, nor have they been found in outcrop where the basal Waitearikí Ignimbrite has been found in the field (**Fig. 3.2**, location 19, bore hole ES112).

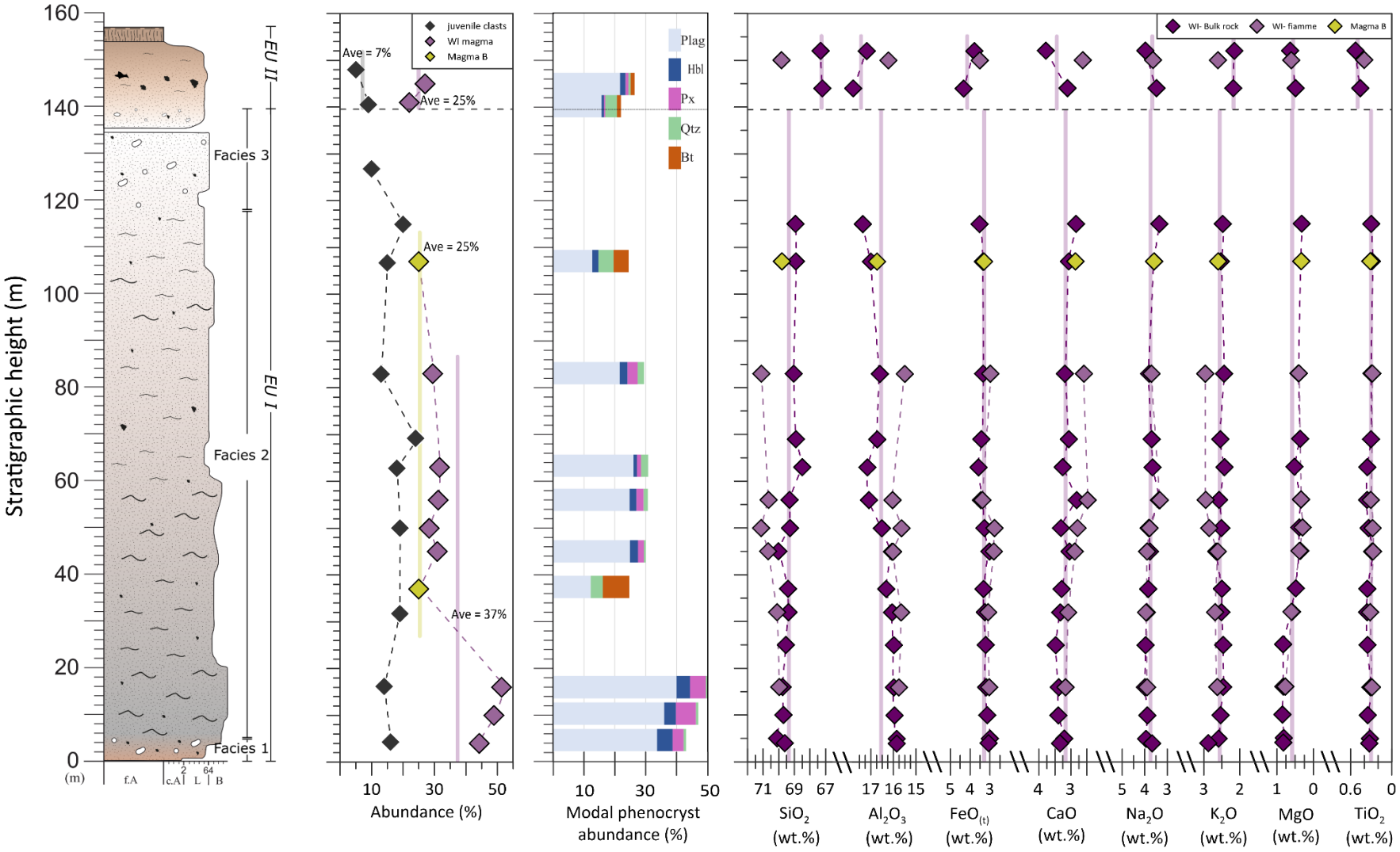

Figure 3.4. Stratigraphic log and key textural, mineralogical, and geochemical variations throughout the Waitearíki Ignimbrite in drill core ES112. The ignimbrite is divided into two eruptive units, Eu I and Eu II. Eu I is further divided into 3 textural facies. See text for details on eruptive units, magma types and geochemistry.

3.5.1 Juvenile clasts

Juvenile clast textures vary greatly throughout the Waitеariki Ignimbrite from dense fiamme to poorly vesicular sub-rounded, fibrous pumices. The abundance of juvenile clasts ranges from 5–24 % (average 15 %) and are variable with stratigraphic height, peaking in the middle and top of facies 2 (**Fig. 3.4**). Facies 3 contains below average abundance (c. 10 %) of juvenile clasts. Juvenile clast abundance for EU II is 5-10 %. Clast sizes are typically up to medium-coarse lapilli (c. 32–64 mm) with maximum juvenile clast sizes exceeding 300 mm in outcrops (**Fig. 3.5 a**) denoting the upper parts of individual flow units.

The total crystal content of juvenile clasts is high, ranging from 22–51 % crystallinity (**Table 3.1; Fig. 3.4**). The crystallinity is highest throughout Eu I, with an average of 37 %, but this increases significantly within the lower 30 m of facies 2 to 44–51 %. Crystallinity of Eu II deposits is lower but remains crystal-rich at 22–27 %.

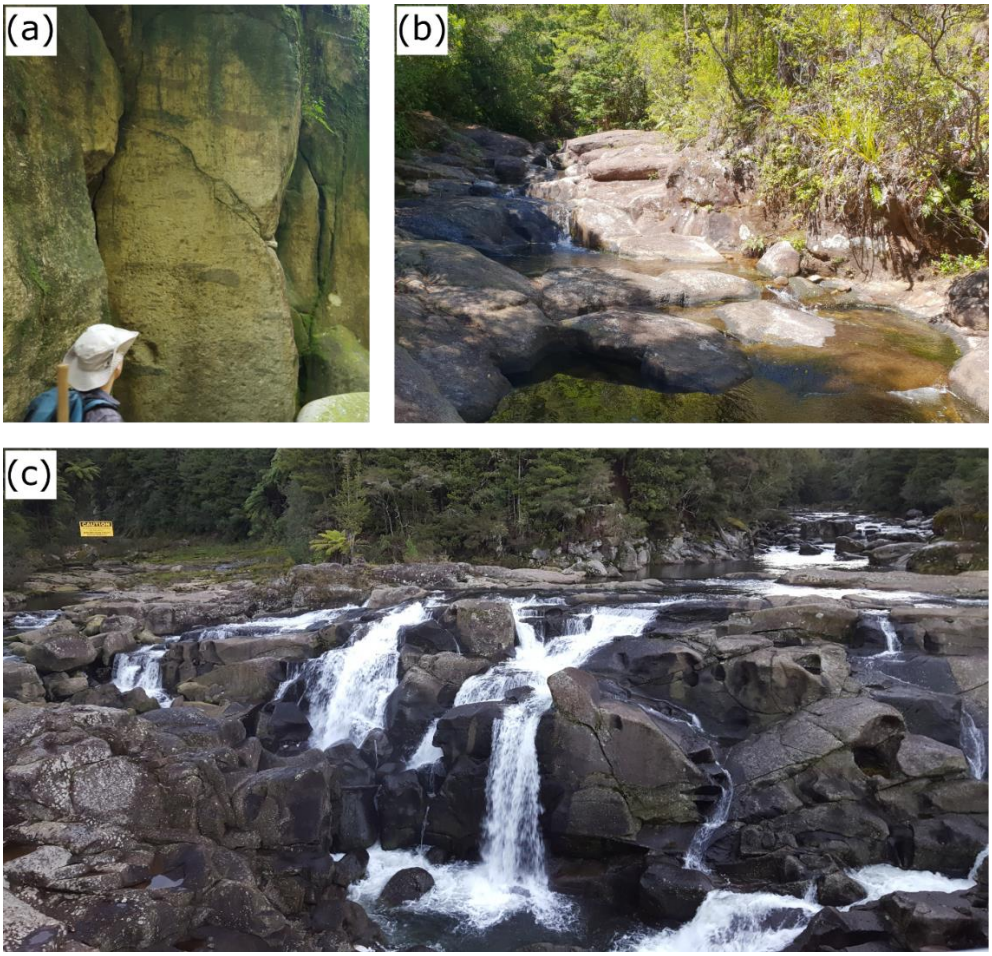

Figure 3.5. Waitеariki Ignimbrite outcrop photographs. **(a)** Small bluffs of densely welded ignimbrite with very large juvenile clasts (Facies 2, Eu I), Aongatete River, Bay of Plenty. **(b)** Typical river outcrop consisting of wide, mostly flat bedrock intersected by occasional small, cascading waterfalls. **(c)** Waitеariki Ignimbrite at McLaren Falls, Tauranga.

Table 3.1. Representative modal data (normalized void-free) of thin sections[1] from various stratigraphic intervals throughout the Waiteariki Ignimbrite.

Sample[2]	Stratigraphic height (m)[3]	Plagioclase %	Quartz %	Hornblende %	Pyroxene %	Biotite %	Fe-Oxides %	% crystals	Matrix %
ES112-501'	4	33.9	1.0	5.8	6.3	0.2	0.8	48.0	52.0
ES112-501'p	4	33.7	0.8	5.0	3.6	0.0	1.1	44.2	55.8
ES112-498'	5	31.0	2.1	4.5	6.3	0.0	1.4	45.3	53.8
ES112-483'	10	37.1	2.0	3.8	5.8	0.1	1.0	49.8	50.2
ES112-483'p		36.0	0.8	3.8	6.5	0.0	1.8	48.9	51.1
ES112-462'p	16	39.4	0.5	4.2	5.8	0.1	0.8	50.8	48.7
ES112-462'		34.4	2.9	3.1	5.0	0.0	1.4	46.8	51.3
ES112-432'	25	34.0	0.9	2.7	5.0	0.0	0.9	43.5	56.2
ES112-411'	32	36.0	1.1	3.8	3.7	0.3	1.2	46.1	53.9
ES112-393'	37	35.6	1.9	3.4	1.5	0.1	1.5	44.0	56.0
ES112-393'p*		12.2	3.9	0.0	0.0	8.6	0.3	25.0	75.1
ES112-366'*	45	37.2	2.0	3.1	1.3	0.2	1.1	44.9	55.2
ES112-366'p		24.9	0.6	2.6	1.9	0.0	0.9	30.9	69.1
ES112-351'	50	32.7	2.7	4.1	2.2	0.1	0.4	42.2	57.8
ES112-351'p		21.9	2.4	2.7	1.1	0.0	0.2	28.3	71.7
ES112-330'	56	30.3	1.0	3.0	4.0	0.0	1.1	39.4	60.6
ES112-330'p		24.8	1.4	2.2	2.3	0.0	0.5	31.2	68.8
ES112-309'	63	28.5	1.4	3.6	2.6	0.0	0.6	36.7	63.3
ES112-309'p		26.0	2.3	1.2	1.3	0.0	0.8	31.6	68.4
ES112-288'	69	30.2	1.2	2.2	1.2	0.0	0.5	35.3	64.7
ES112-243'	83	28.9	2.4	2.4	3.6	0.0	0.5	37.8	62.2
ES112-243'p		21.6	1.4	2.5	3.3	0.0	0.6	29.4	70.6
ES112-165'	107	28.3	2.5	5.0	2.1	0.6	0.6	39.1	60.9
ES112-165'p*		12.7	4.9	2.0	0.0	4.9	0.2	24.7	75.4
ES112-138'	115	26.9	2.4	3.1	2.1	0.7	0.4	35.6	64.3
ES112-126'	119	28.6	3.4	1.7	2.3	1.0	0.7	37.7	62.3
ES112-99'	127	24.2	0.9	3.2	1.6	1.3	0.0	31.2	68.0
ES112-69'	136	25.4	3.3	3.2	2.2	1.2	0.3	35.6	64.4
ES112-54'p*	141	15.7	3.8	0.8	0.4	1.3	0.2	22.2	77.9
ES112-54'		27.4	1.8	4.6	1.5	0.9	0.7	36.9	63.1
ES112-39'	145	29.6	4.5	3.7	1.7	1.3	0.6	41.4	58.5
ES112-39'p*		21.7	0.7	1.8	0.9	1.3	0.0	26.4	73.5

[1] 1000 points per section were analysed using a 0.5x0.5 mm grid unless marked with an *, where the number of points was limited by clast size.

[2] Samples taken from drill core ES112 (refer to **Supplementary data table SM3.2** for location details). Sample names ending in p indicate juvenile clasts.

[3] Height in metres above Waiteariki base as inferred from core ES112.

Juvenile clasts throughout the Waitеariki Ignimbrite have a consistent mineral assemblage of plagioclase, hornblende, pyroxene, quartz ± biotite with accessory Fe-oxides, zircon and apatite. There is no systematic variation in mineralogy with stratigraphic height (**Fig. 3.4**), however, substantial variations are observed in modal abundance, plagioclase (12–40 %), hornblende (0–6 %), pyroxene (0–6.5 %), and quartz (< 1–5 %), are recognised. Biotite only occurs as phenocrysts in juvenile clasts at two stratigraphic intervals (37 and 107 m) within Eu I deposits. In contrast, within Eu II, it is commonly found in trace amounts (< 2 %). Biotite-bearing fiamme typically have a lower total crystallinity (20–25 %) and significantly lower proportions of plagioclase, pyroxene and hornblende crystals than deposits from Eu I and higher quartz (c. 5 %).

Juvenile clast groundmass glass textures are dominated by fiamme where the fibrous texture has been compacted during welding to form foliations highlighted by brown glass which has been moulded around individual crystals. The glass has varying degrees of crystallite and microlite development depending on the overall degree of devitrification. Fully-devitrified clasts have pervasive spherulitic or felsitic microlite development. Post-depositional hydration is evident by the formation of perilitic cracking within the fiamme (Denton *et al.*, 2009).

3.5.2 Ignimbrite matrix crystal population and glass textures

The matrix of the Waitеariki Ignimbrite has a crystal assemblage identical to that found within juvenile clasts (plagioclase, hornblende, pyroxene, quartz, Fe-oxides ± biotite). Crystal fracturing is common, limiting individual crystal fragment size to typically less than 1.5 mm. Large whole crystals (> 2.5 mm) are rare and dominated by resorbed quartz and subordinate plagioclase. Many crystals display in situ crystal fragmentation with jigsaw-fit textures, commonly centred around melt inclusions.

The modal abundance of phenocryst phases within the matrix is high, with crystal contents of 35–50 %. Crystallinity of juvenile clasts at the bottom of unit 2 (44–50 %) is similar to that found within juvenile clasts, but higher at other stratigraphic levels due to winnowing during ignimbrite emplacement. Total modal proportions of plagioclase, hornblende and pyroxene show almost identical ranges and averages to that of the juvenile clasts with ranges of 67–86 %, average 76 %, 4–13 %, average 8 % and 2–14 %, average 7 % respectively.

Throughout most of the ignimbrite, pervasive devitrification of felsitic microlites obscure primary textures, however often crystallised pseudo shards can be recognised. Where evident, matrix glass has a vitriclastic texture dominated by platy and cuspate shards, in addition to poorly-developed lunate and y-shaped shards which are typically < 0.2 mm in size.

3.5.3 Lithic clasts

Lithic clasts in the Waiteariki Ignimbrite are rare (< 2–5 %) and typically small (< 10–20 mm). Throughout Eu I deposits, lithic compositions are dominated by spherulitic rhyolite and dacite clasts. In the upper reaches of the Aongatete River, facies 1 deposits include a zone of abundant (10–15 %) sub-rounded grey andesitic lithics < 50 mm in size. These lithics are not present within core ES112 and are likely accidental lithic clasts derived from the underlying substrate within a paleo-valley.

Larger lithic clasts are found within Eu II deposits in the vicinity of the Ngamuwahine River (**Fig. 3.2 a**) and along the eastern margin of the Whakamarama Plateau which include abundant clasts of recycled Waiteariki ignimbrite and subordinate rhyolite lava. The largest clasts (up to 36 cm in size) are matrix supported and exclusively found in the Ngamuwahine River and upper parts of its associated catchment. Clast size decreases to the north where they are typically between 5–10 cm and < 5 cm in core ES112.

3.6 Petrography and mineral chemistry

Here, we follow the size classification scheme of Zellmer (2021) where phenocrysts (*stricto sensu*) are defined as any crystal (or crystal fragment) larger than the groundmass (> 0.3 mm), without implying any connotations regarding its petrological origins. Phenocrysts in the Waiteraiki Ignimbrite are typically macrocrysts (0.5–10 mm in size) and where genetic interpretations of the crystal cargo are made, phenocrysts may be described as autocrysts (grown from carrier melt), antecrysts (grown from same magmatic system and picked up by carrier melt), or xenocrysts (foreign to the magmatic system).

The Waiteariki Ignimbrite is characterised by a crystal-rich (25–51 %), low-variance mineral assemblage of up to five silicate mineral phases (plagioclase, hornblende, pyroxene, quartz, ± biotite, described below) and three accessory phases (Fe-oxides, zircon and apatite). All phenocryst phases are found throughout the ignimbrite matrix in relative abundances similar to those found in the juvenile clasts.

3.6.1 Plagioclase

Plagioclase is the dominant phenocryst phase throughout the Waiteariki Ignimbrite (**Table 3.1**). Crystals occur as euhedral, subhedral to anhedral, medium-grained macrocrysts (typically 1.5–2.5 mm) which can be divided into three texturally and compositionally distinct populations. Groups 1 and 2 are dominant and occur in relatively equal proportions with subordinate Group 3 plagioclases. Group 1 plagioclases are dominantly euhedral to subhedral that exhibit broad to fine oscillatory zoning (**Fig. 3.6 a,b**). Group 2 plagioclases are similar in appearance to Group 1, but have cores that display

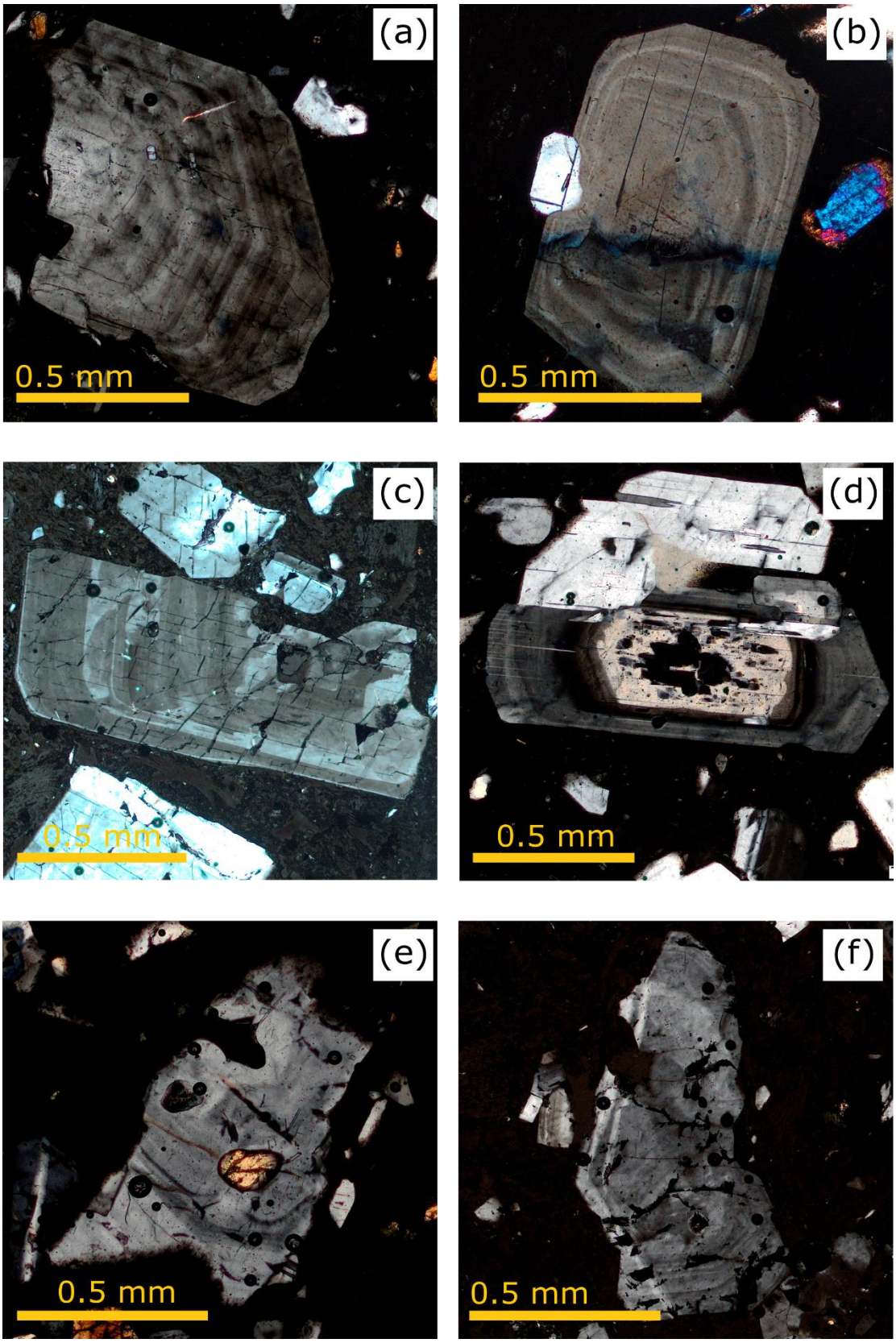

Figure 3.6. Crossed-polarised light photomicrographs of typical plagioclase crystals in the Waiteariki Ignimbrite. **(a)** Fractured and **(b)** whole Group 1 crystals dominated by euhedral crystal shapes and oscillatory zoning; **(c-d)** Group 2 crystals with cores displaying prominent disequilibrium textures; and **(e-f)** anhedral Group 3 crystals.

strong disequilibrium textures such as either skeletal textures representing up to half the surface area of the crystal, or sieve textures along specific growth zones, and highly rounded or irregular resorbed cores. Cores are typically surrounded by prominent rims consisting of texturally simple or complex growth bands (**Fig. 3.6 c,d**). Group 3 plagioclases are less common and consist of highly resorbed, anhedral grains, which may or may not exhibit disequilibrium textured cores and oscillatory zoning. Plagioclases in Group 3 may also display a mild to strong poikilitic texture (**Fig. 3.6 e,f**). While the textural groups documented here are most common, a greater diversity of subordinate types may be present as crystals are commonly fragmented, and/or not optimally orientated for the optical observation of zoning patterns.

Plagioclase crystals within the WI have a broad compositional range, extending from oligoclase to bytownite ($An_{22–78}$, $An_{\#}$= Ca/(Ca+Na+K); **Fig. 3.7, Supplementary data table SM3.7**), with no clear compositional clustering. Cores show the most compositional diversity and can be subdivided relative

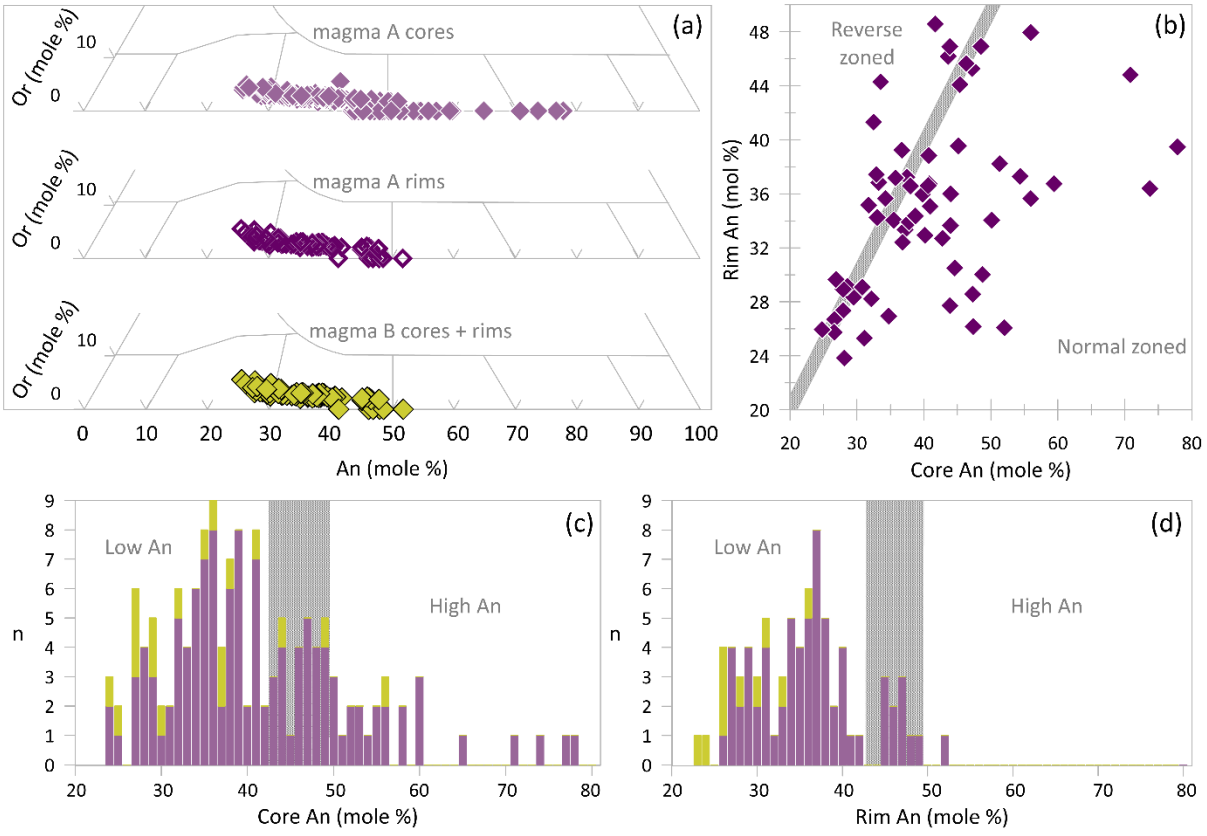

Figure 3.7. Plots of plagioclase compositions determined by SEM-EDS. **(a)** An-Ab-Or classification diagram displaying the broad diversity of core and rim compositions for Waiteariki plagioclase crystals; **(b)** Magma A plagioclase rim verses core anorthite content. Shaded bar represents crystals with ± < 1 mol % An; **(c-d)** Histograms of plagioclase cores **(c)** and rims **(d)** divided into low ($An_{20–42}$), mid ($An_{43–49}$) and high ($An_{>50}$) An groups. Grey bar represents mid-An range. Refer to **section 3.10.2** for discussion on magma types.

to the An content. Low-An cores have a compositional range of $An_{23–42}$ (oligoclase-andesine) and exclusively contain crystals with Group 1 textures. Mid-An cores have a restricted compositional range of $An_{43–49}$ (andesine) and are dominated by Group 1 textures with subordinate Group 2 crystals. High-An cores range from $An_{50–78}$ (labradorite-bytownite) and all crystals display strong resorption textures with subsequent oscillatory growth rims. Calcic cores ($An_{60–78}$) are typical within the highly resorbed Group 3 crystals, along with plagioclase crystals within crystal clots (see **Section 3.6.2**).

Rim compositions show significant diversity, ranging from $An_{23–51}$ (oligoclase-andesine). However, **Figure 3.7 a** demonstrates that the majority of crystal rims fall between $An_{23–41}$ with only a small proportion having more calcic andesine compositions between $An_{44–51,}$ which overlap with mid- and high-An core compositions.

Irrespective of crystal texture, ~ 70 % of all plagioclase crystals display normal-zoned rims. Group 2 crystals exhibit significant variations between core and rim compositions, with An content decreasing rim-ward by > 15 mol % An. This contrasts with Group 1 crystals which exhibit a < 10 mol % An reduction. A subordinate number of crystals (~10 % of total crystals) are homogeneous with < 1 mol % change in An compositions. These crystals predominantly have core and rim compositions between $An_{26–29}$, with occasional crystals found to have more calcic core and rim compositions between An_{37} and An_{46}. The remaining crystals are reversely-zoned and have low-mid An core compositions. No systematic variation with stratigraphic height has been identified.

3.6.2 Pyroxene

Orthopyroxene is the dominant pyroxene throughout the Waitearikiri Ignimbrite and they occur as euhedral, subhedral and anhedral crystals with weak pleochroism from pale pink to green. Macrocrysts are typically c. 1 mm in size, but individual large crystals reach up to 1.8 mm and poikilitic texture with Fe-oxide, plagioclase and apatite inclusions are common (**Fig. 3.8**).

The major element composition of orthopyroxene crystals covers an extremely broad range from $En_{28–79}$ ($En_{\#}$=Mg/(Mg+Fe+Ca)) and $Wo_{1–4}$ ($Wo_{\#}$=Ca/(Ca+Mg+Fe); **Fig. 3.9**) with magnesium numbers from $Mg\#_{28–82}$ (Mg#= 100x(Mg/(Mg+Fe)). Two prominent compositional peaks occurring at $Mg\#_{44–47}$ and $Mg\#_{57–59}$ with smaller peaks between $Mg\#_{28–33}$ and $Mg\#_{67–68}$ (**Fig. 3.9 b**). Similarly to plagioclase, no stratigraphic trends have been identified, however orthopyroxene crystals become progressively more altered with increasing stratigraphic height to become complete pseudomorphs at the top of the ignimbrite which may mask any compositional trends.

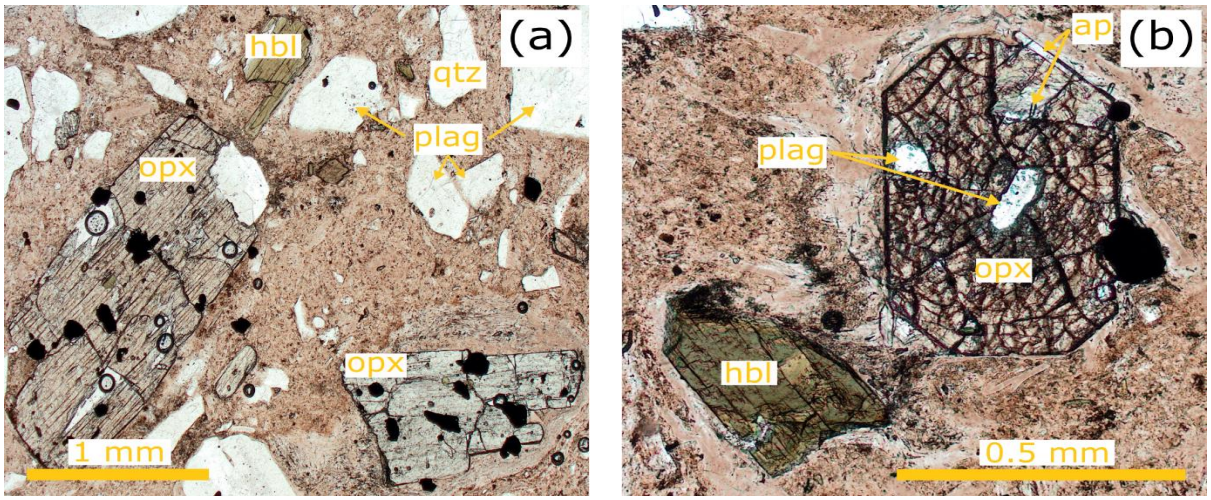

Figure 3.8. Plane-polarised light photomicrographs of typical orthopyroxene (opx) crystals in the Waitearikí Ignimbrite. **(a)** Large, pleochroic crystals with poikilitic Fe-oxides, surrounded by crystal fragments of plagioclase (plag), hornblende (hbl) and quartz (qtz). Note the fiamme enclosing the crystal in the lower right; **(b)** Euhedral crystal with poikolitic plagioclase and apatite (ap).

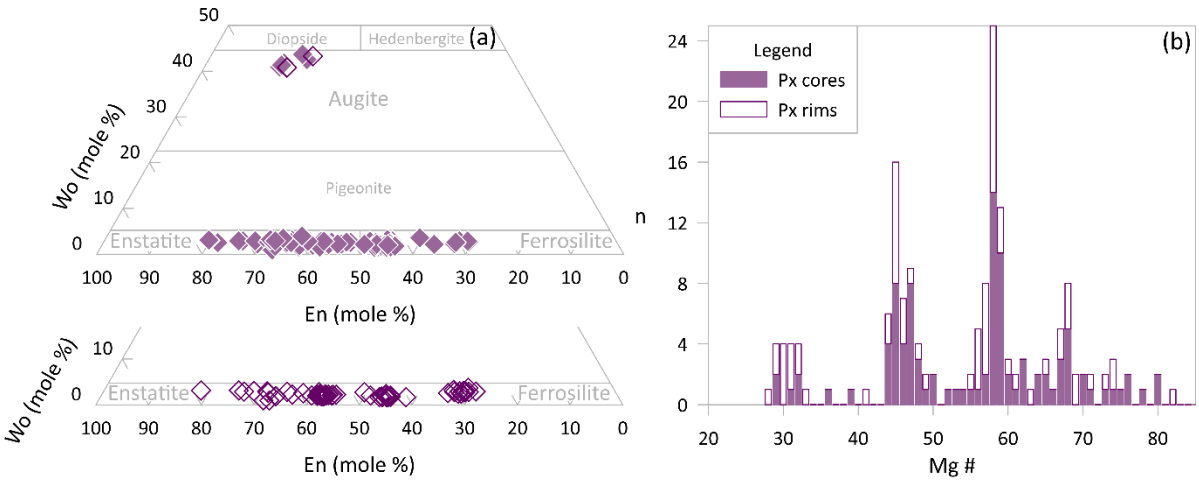

Figure 3.9. Plots of orthopyroxene and clinopyroxene compositions determined by SEM-EDS. Ternary diagram **(a)** and histogram **(b)** showing the main compositional fields of Waitearikí Ignimbrite pyroxene crystals.

Individual crystals are generally homogeneous or have only slight normal zonation trends evident by core to rim compositional changes of between 1 and 9 mol % En. Rare crystals have greater core-rim variations of between 10–20 mol % En. Reverse-zoning occurs in c. 10 % of crystals with core-rim reductions between 1–6 mol % En.

Clinopyroxene crystals are rare and have compositions of $En_{38–45}$ and $Wo_{40–45}$ classifying them as augite (**Fig. 3.9 a**). Macrocrysts are typically small (< 0.5 – 1 mm), subhedral to anhedral grains which are rounded edges and embayments. Poikilitic textures with Fe-oxide, plagioclase inclusions are common (**Fig. 3.10**).

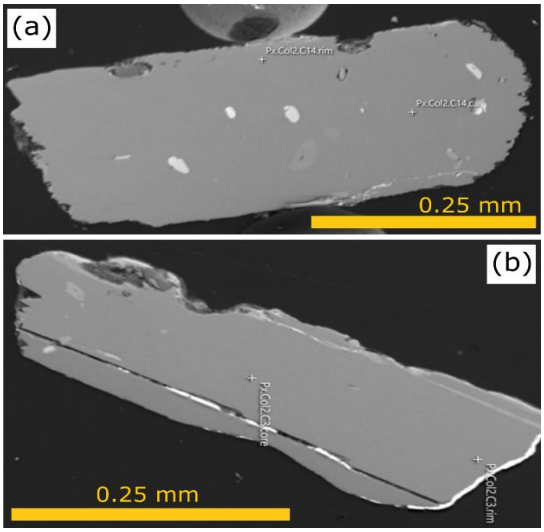

Figure 3.10. Scanning electron microscope (SEM) backscattered images of selected augite crystals within the Waitеariki Ignimbrite. **(a)** subhedral augite with multiple mineral inclusions. **(b)** anhedral augite crystal due to resorption of all crystal faces.

3.6.3 Amphibole

Amphibole typically occurs as subhedral tabular macrocrysts mostly c. 1 mm in size with rarer crystals found up to 2 mm in length. Amphibole crystals display strong yellow-green to brown pleochroism and are optically non-zoned. There is no evidence of reaction rims, however, resorption textures are often observed with crystals showing varied characteristics ranging from rounded to irregular anhedral crystal forms to prominent embayments (**Fig. 3.11**). Inclusions of Fe-Ti oxides, apatite, plagioclase are common.

Electron microprobe analyses of 97 crystals from juvenile clasts and ignimbrite bulk-rock samples were normalised based on 24 anions, using the Excel spreadsheet of Locock (2014). The greatest compositional variation is observed for Mg (2.08–3.18 apfu) and $Fe_{(t)}$ (1.47–2.75 apfu) which is reflected in the wide range in Mg# ($Mg\#_{43–68}$; **Fig. 3.12**; **Supplementary data table SM3.9**). Moderate major elemental compositional diversity in Si (6.28–6.99 atoms per formula unit, apfu), $Al_{(t)}$ (1.15–2.11 apfu) and K (0.04–0.11 apfu) while Ca (1.51–1.76 apfu), Ti (0.10–0.34 apfu) and Na (0.37–0.65 apfu) are relatively invariant (**Fig. 3.13**). When Mg# is plotted against $Al_{(t)}$ (**Fig. 3.12**), the composition of

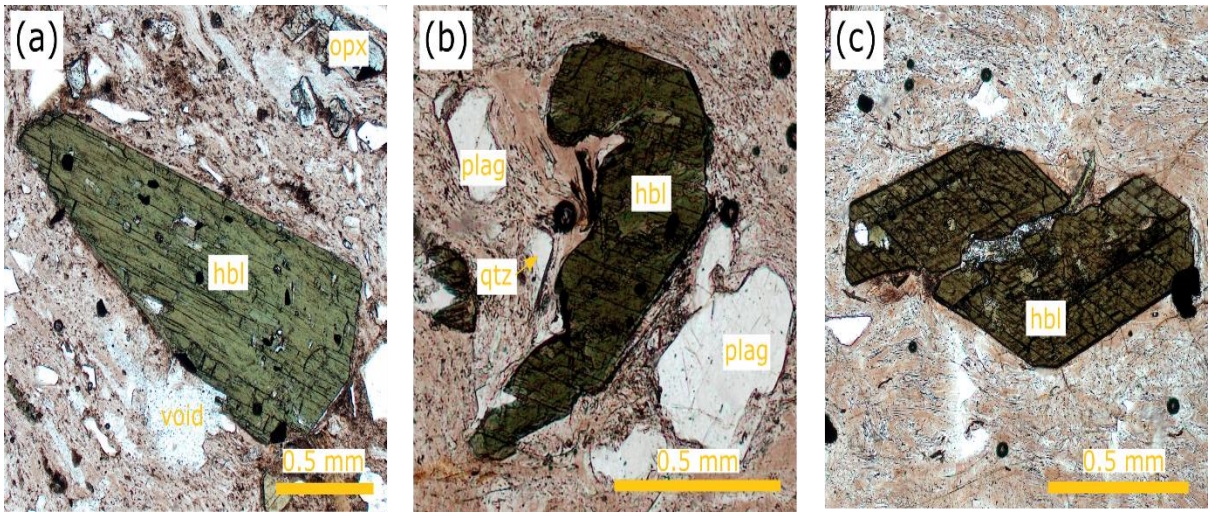

Figure 3.11. Representative photomicrographs of typical amphibole crystals in the Waiteariki Ignimbrite. **(a)** Large euhedral single crystal of hornblende (hbl); **(b)** Highly resorbed, anhedral crystal and **(c)** jigsaw-fit, fractured, euhedral crystal.

amphibole crystals form three visually discrete clusters, here termed groups 1, 2 and 3. Group 1 crystals have relatively low Mg# ($Mg\#_{43–68}$, average $Mg\#_{49}$) and $Al_{(t)}$ (1.15–1.70 apfu, average 1.40 apfu) compared to Group 2 which has high Mg# ($Mg\#_{58–68}$, average $Mg\#_{64}$) and $Al_{(t)}$ (1.22–2.02 apfu, average 1.65 apfu). Group 3 appears to be intermediate between Groups 1 and 2 with Mg# ($Mg\#_{48–60}$, average $Mg\#_{55}$) and $Al_{(t)}$ (1.22–2.21 apfu, average 1.54 apfu). These broad groupings are also observed in Ti and K (**Fig. 3.13 e,g**), although there is significant overlap as with many of the major elements.

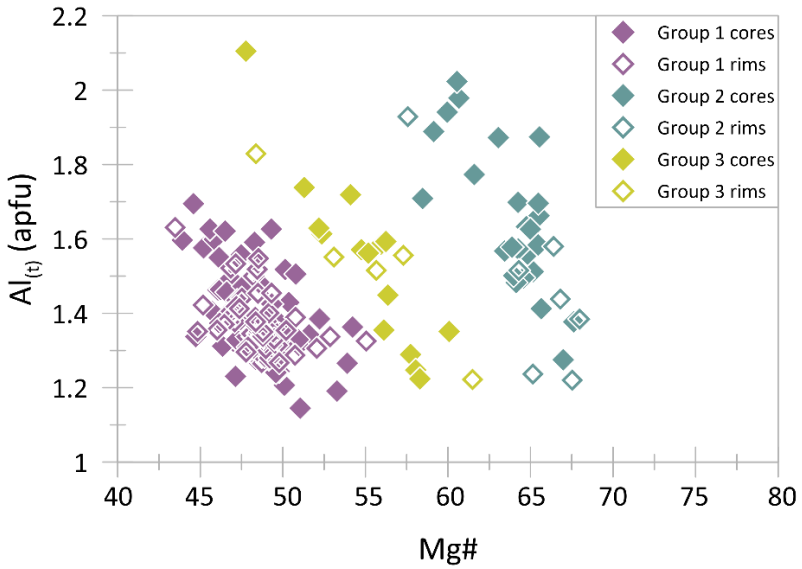

Figure 3.12. Amphibole crystal Mg# verses total aluminium ($Al_{(t)}$). Crystals are subdivided into discrete groups. Group 1 (low Mg#, $Al_{(t)}$), Group 2 (high Mg#, $Al_{(t)}$), and intermediate Group 3 crystals.

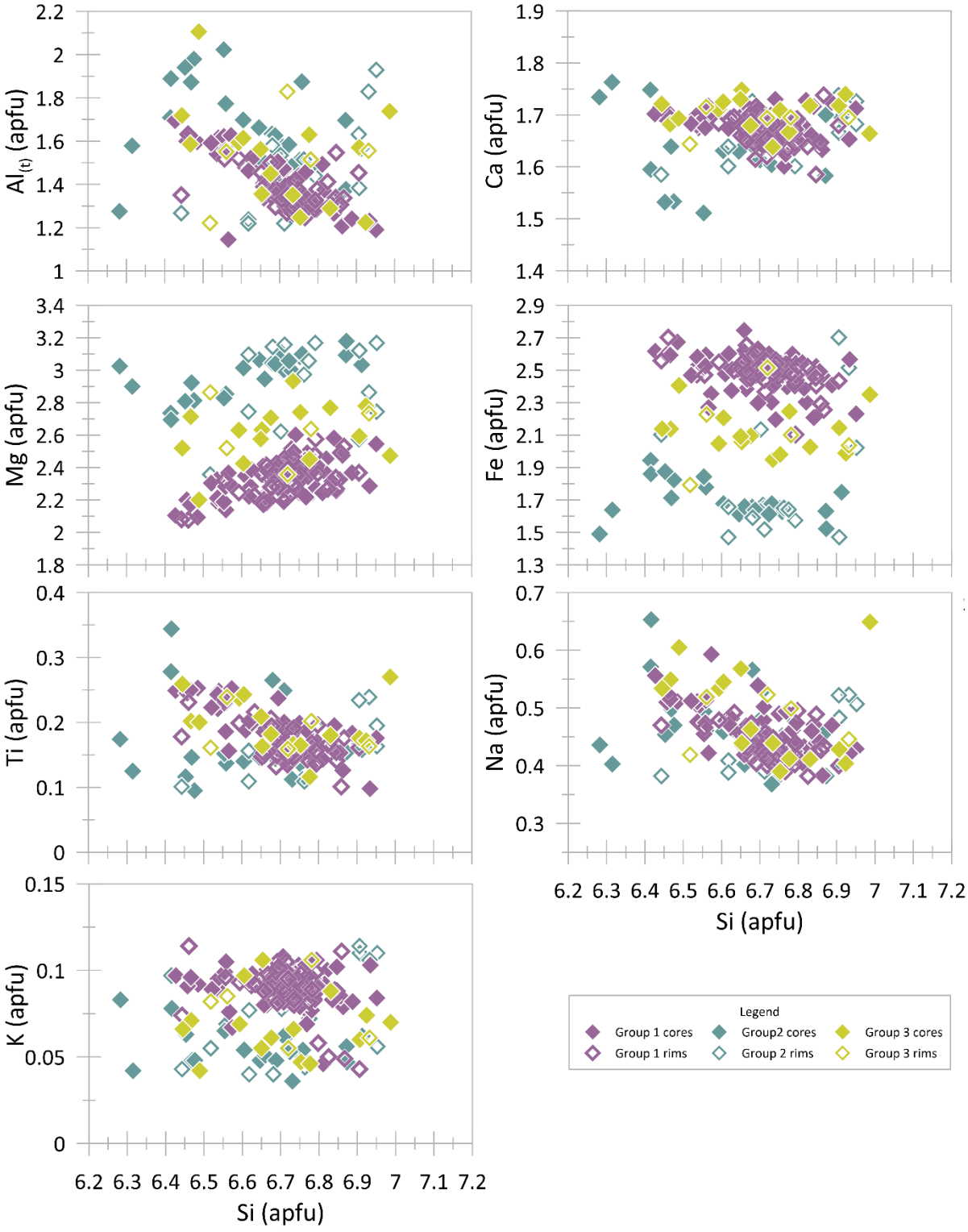

Figure 3.133. Cation variation diagrams for amphibole crystals in the Waiteariki Ignimbrite. Note that distinct populations visible in Mg, Fe and K. Crystals are grouped on the basis of $Al_{(t)}$ and Mg# (see text for details).

Core-rim analyses reveal that Group 1 is the dominant rim composition (**Figs. 3.12, 3.13**), with only < 10 % and 7 % having Group 2 and Group 3 compositions respectively. Of these crystals there is no systematic rim-ward change with corresponding core compositions and cover all three geochemical groupings reflective of highly variable crystallisation histories.

Amphibole nomenclature is assigned according to the International Mineralogical Association (IMA) classification scheme by Hawthorne *et al.* (2012). The vast majority of crystal cores and rims classify as magnesio-ferri-hornblende with ^{A}(Na + K + 2Ca) apfu < 0.5 and ^{C}(Al + Fe^{3+} +2Ti) apfu between 0.5 and 1 (**Fig. 3.14**). A few Na_2O-rich crystal cores classify as magnesio-hastingsite and two rims falling into the range of tschermakite.

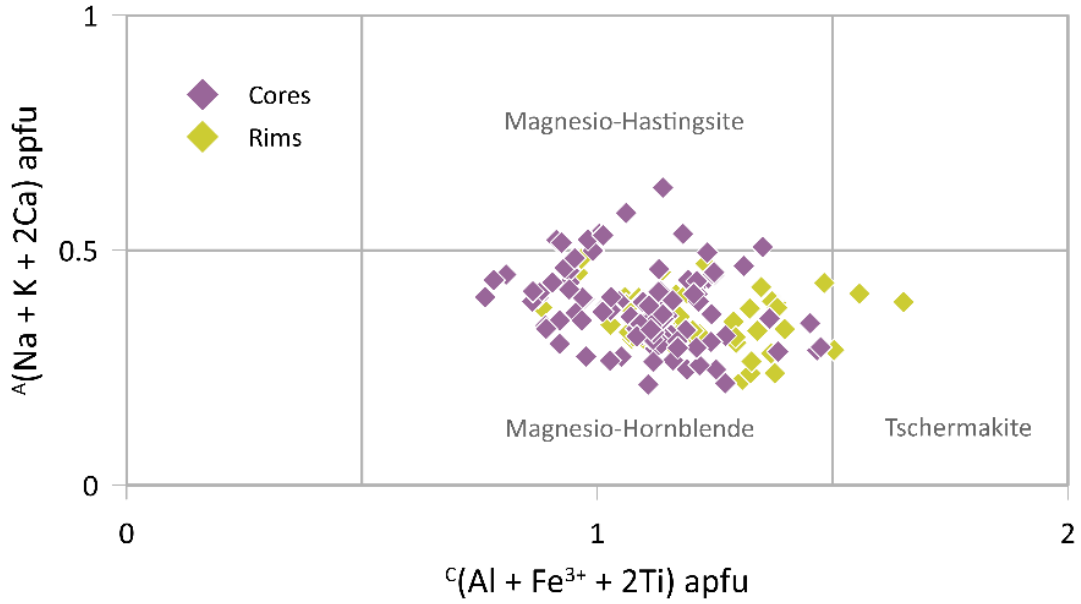

Figure 3.14. Waitearikí amphibole compositions (cations in structural formula) plotted on a classification diagram of Hawthorne *et al.* (2012).

3.6.4 Quartz

Quartz is a minor component of the Waitearikí Ignimbrite with modal abundances typically < 4 % (**Table 3.1**). Macrocrysts range in size from 0.8–2.5 mm, typically 1–1.5 mm with rare large crystals of up to 3 mm. They typically have subhedral forms with common disequilibrium textures consisting of prominent embayments and resorption surfaces. Quartz crystals also host numerous melt inclusions (**Fig. 3.15**), many of which show evidence of crystallisation or devitrification.

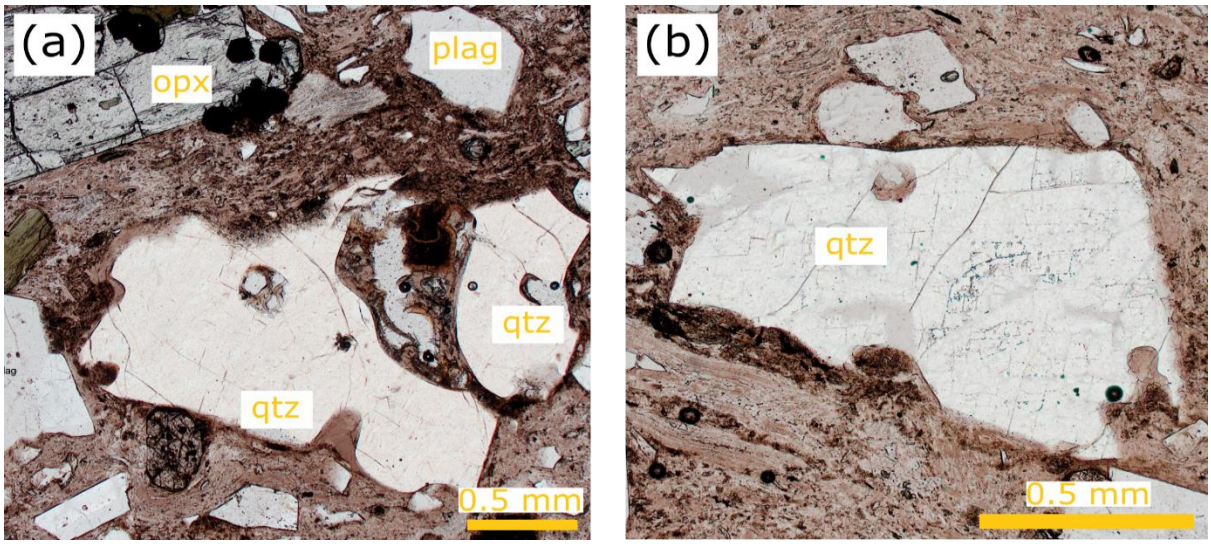

Figure 3.15. Representative photomicrographs of quartz (qtz) crystals in the Waitearikí Ignimbrite. **(a)** Anhedral, fractured, resorbed and embayed crystal with large, crystallised melt inclusion; and **(b)** subhedral crystal with embayments.

3.6.5 Biotite

Biotite abundance is typically very low throughout the Waitearikí Ignimbrite, except at two stratigraphic intervals in core ES112 (**Table 3.1,** 37 and 107 m, samples ES112-393 and ES112-165 respectively; **Fig. 3.4**) where it is the dominant ferromagnesian mineral found in the juvenile clasts with modal abundances of 4.9 and 8.6 % respectively. Above 107 m in Eu I and throughout Eu II deposits, biotite is found as a rare mineral phase in both bulk-rock and fiamme samples. When present, biotite crystals appear as reddish-brown euhedral to subhedral, lath-like, microphenocrysts between 0.5–0.8 mm in length with several crystals displaying flame-like kinks (**Fig. 3.16**).

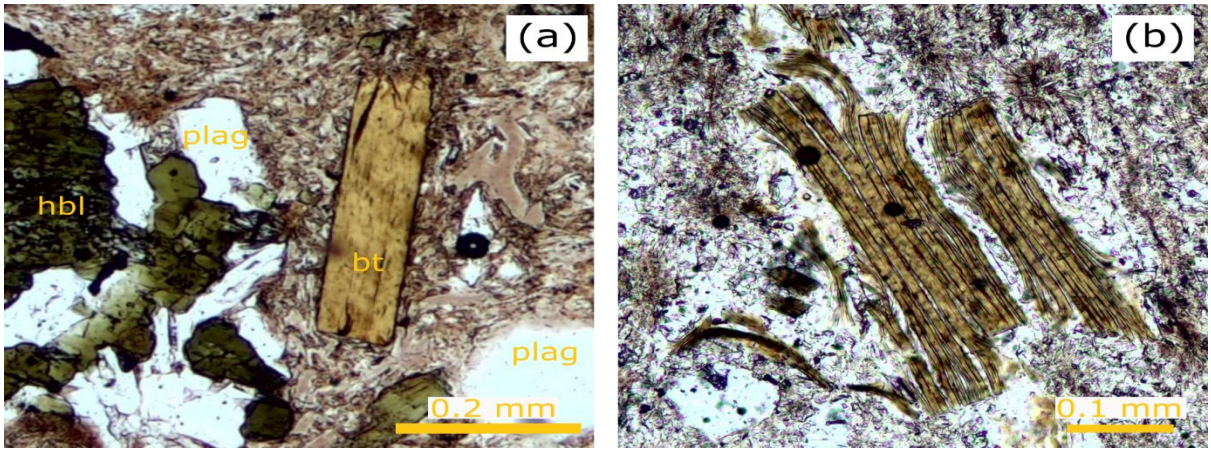

Figure 3.16. Representative plane polarised light photomicrographs of biotite crystals in the Waitearikí Ignimbrite. **(a)** Euhedral, lath shaped crystal within ignimbrite matrix; and **(b)** fractured crystal with flame-like kinks in devitrified fiamme groundmass glass.

3.6.6 Microcrystalline clots

Crystal clots of plagioclase ± orthopyroxene ± hornblende are often found throughout the matrix of the Waiteariki Ignimbrite. The clots are hypocrystalline and medium grained (1–4 mm), with equigranular and hypidiomorphic textures (**Fig. 3.17**). The clots vary from a few adjoined minerals of plagioclase and orthopyroxene (**Fig. 3.17 d**) to larger clots, comprising of plagioclase, orthopyroxene ± subordinate hornblende and Fe-oxides crystals (**Fig. 3.17 b**). The same mineral assemblage described here is identical to that found within juvenile clasts and bulk-ignimbrite samples.

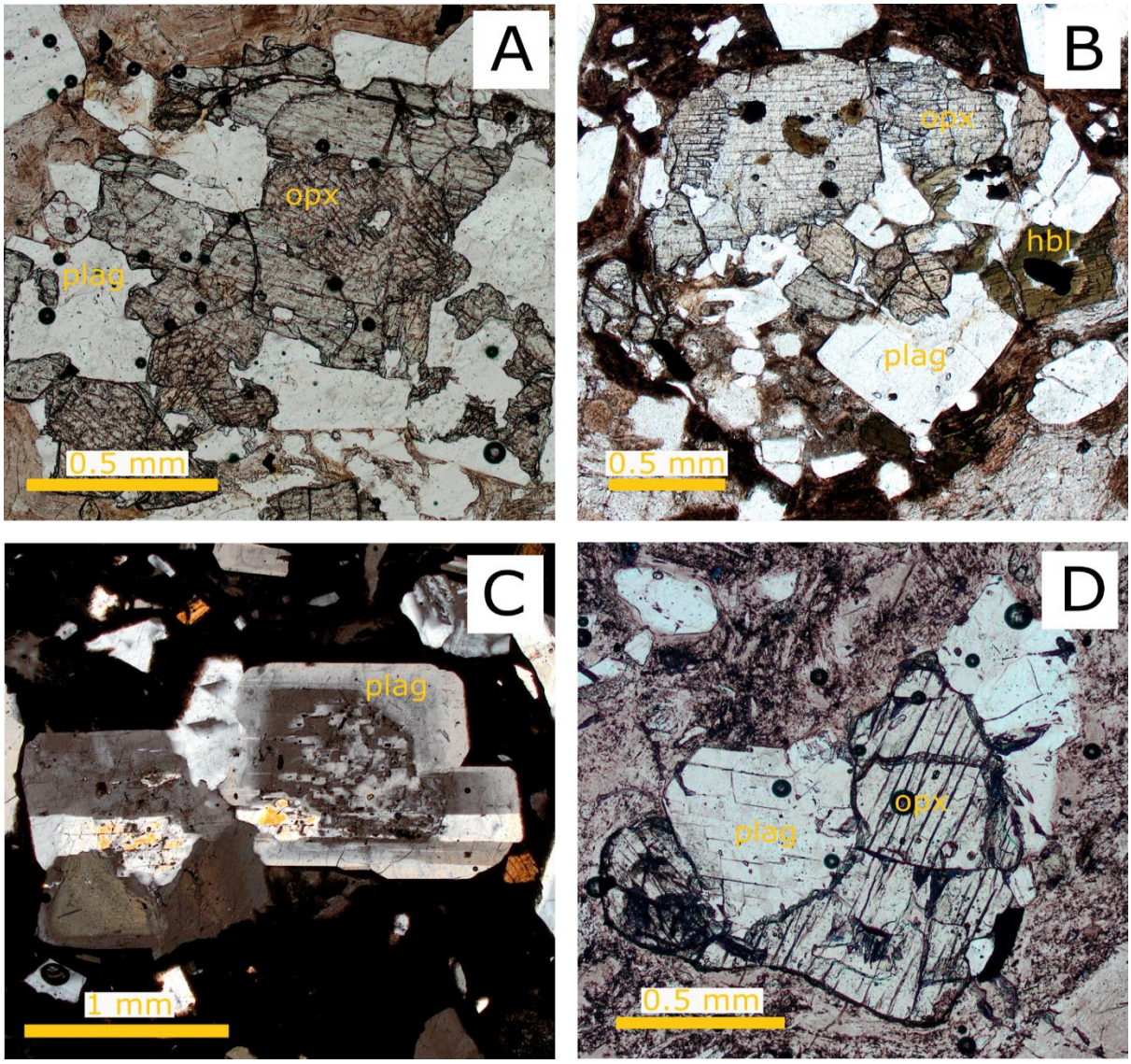

Figure 3.17. Photomicrographs of plutonic crystal clots found throughout the Waiteariki Ignimbrite. **(a)** Large (2–3 mm), medium-grained, equigranular, hypidiomorphic orthopyroxene and plagioclase, and **(b)** orthopyroxene, plagioclase, hornblende and Fe-oxide crystal clots. **(c)** Plagioclase glomerocryst with prominent disequilibrium textured cores; and **(d)** small (< 2 mm) crystal clot of plagioclase and orthopyroxene.

3.7 Geochemical characterisation of bulk-rock, fiamme and matrix glass

New whole-rock compositions of juvenile clast and bulk-ignimbrite samples from the Waiteariki Ignimbrite were analysed for major and trace elements using XRF and LA-ICP-MS techniques described in section 2.3 and are presented below. Major elements have been normalised to 100% volatile free and the entire dataset is available in **supplementary data table SM3.6.** These new analyses are combined with matrix glass data presented in **Chapter 2** (Prentice *et al.*, 2022) to cover the full stratigraphic variation (both vertical and lateral) to geochemically characterise the Waiteariki Ignimbrite.

3.7.1 Bulk-rock chemistry

Waiteariki Ignimbrite bulk-rock and fiamme clasts are calc-alkaline, medium-K dacite to rhyolite with SiO_2 contents of 67.27–71.13 wt. % following the classification of Le Maitre *et al.* (2002) (**Fig. 3.18**). In general, fiamme analyses sit on the boundary between dacite and rhyolite. As these samples are most representative of bulk magma compositions, we refer to the Waiteariki magma as rhyodacite in composition. The observed major element geochemical trends in Waiteariki Ignimbrite bulk-rock and fiamme samples show limited compositional diversity (**Fig. 3.19**), with fiamme that have narrowly restricted SiO_2 compositions (69.79–71.13, average 70.48 wt. %) and all other major oxides have geochemical variance of < 1 wt. % but not entirely homogeneous within the limits of analytical precision.

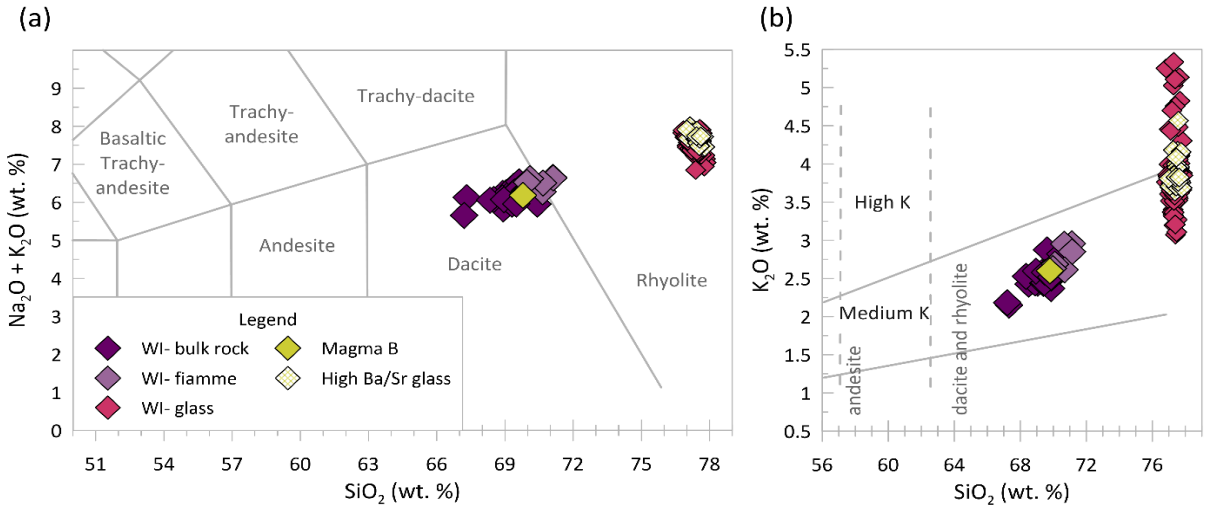

Figure 3.18. Classification diagrams for Waiteariki Ignimbrite bulk-rock, juvenile clast (fiamme) and glass analyses. **(a)** Total alkali verses silica (TAS) diagram, after Le Maitre *et al.* (2002). **(b)** Subdivision of calc-alkaline rocks using K_2O verses SiO_2. Subdivision lines after Le Maitre *et al.* (2002). Refer to **section 3.10.2** for descriptions and discussion on magma types. 2σ analytical error calculated from repeat analyses of the GSP-2 standard is smaller than symbol size.

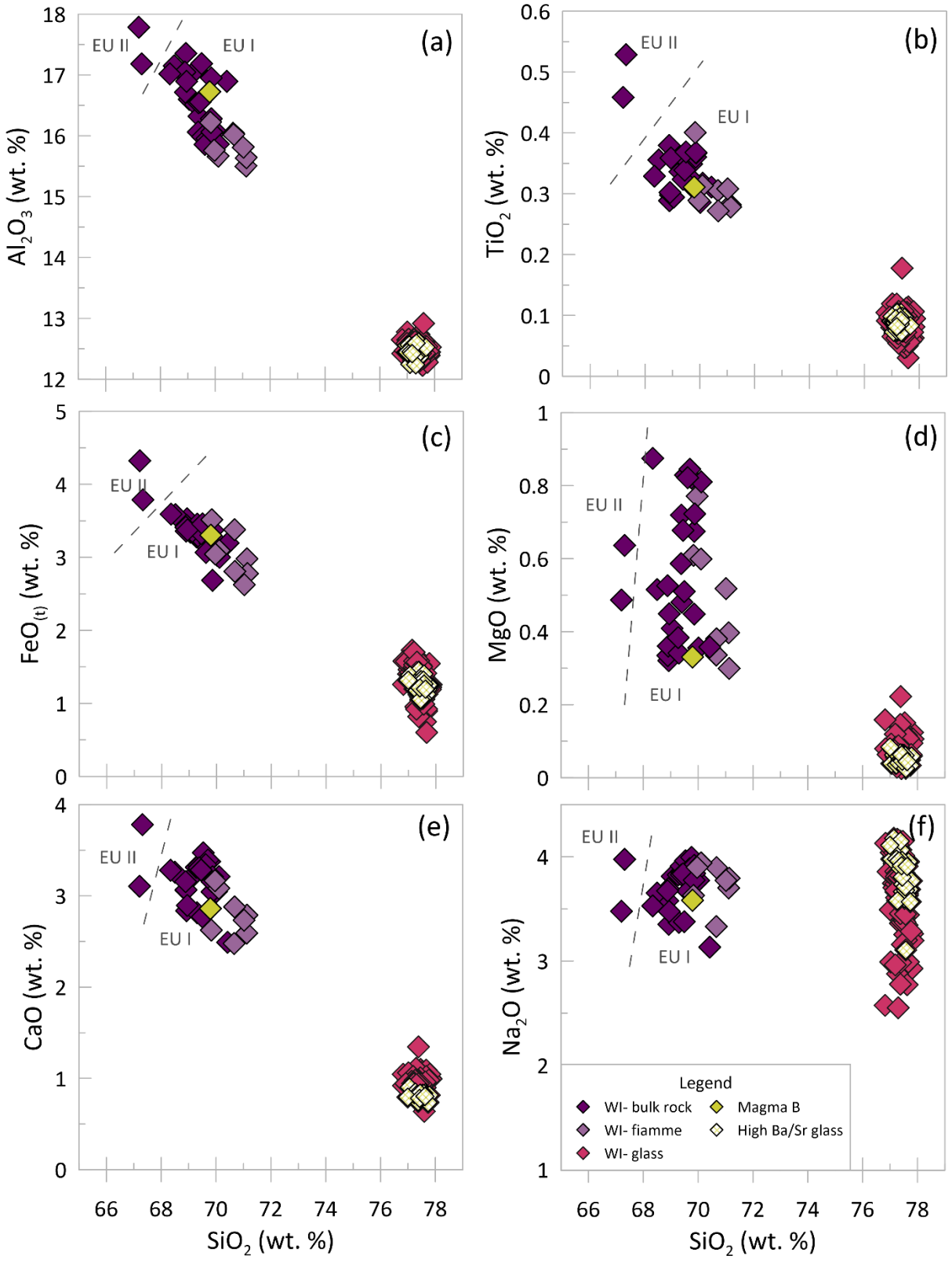

Figure 3.19. Bivariate plots of major element compositions (normalised to 100 % volatile free) verses SiO_2 for bulk-rock, fiamme (this study), and matrix glass data from **Chapter 2** (Prentice *et al.,* 2022). Analytical error (2σ) calculated from repeat analyses of the GSP-2 standard is smaller than symbol size. Eu I and II refer to eruption units 1 and 2 respectively. Refer to text for descriptions on eruptive units (**Section 3.5**) and discussion of magma types (**Section 3.10.2**).

Bulk-rock analyses overlap with fiamme compositions but extend the geochemical range towards more dacitic compositions. Analyses from bulk-rock and fiamme samples from the same stratigraphic interval and sampling sites vary by 0.2-2.07 wt.% SiO_2, < 0.1-1.1 wt. % Al_2O_3 and all other oxides by < 0.5 wt. % with no changes in slope or inflection points demonstrating that geochemical variance is related to the abundance of glass rather than contamination from lithic clasts. Most major elements show strong linear correlations with decreasing Al_2O_3, $FeO_{(t)}$, MgO, MnO (not shown), CaO and TiO_2, and increasing Na_2O and K_2O concentrations that can be extrapolated to matrix glass compositions.

The chemical composition of the bulk-ignimbrite and fiamme samples show only minor variation throughout 157 m of vertical thickness of core ES112 with slight variation being most pronounced in SiO_2, Al_2O_3 and CaO between 56 and 83 m (**Fig. 3.4**)**.** Bulk-ignimbrite samples from Eu II (Wai55 and Wai6a) are consistently the least evolved, with lower values for SiO_2, MgO, Na_2O and K_2O and higher in Al_2O_3, $FeO_{(t)}$, CaO and TiO_2, and cluster separately in all bivariate plots of major elements (**Fig. 3.19**).

Bulk-rock trace element concentrations also demonstrate a relatively restricted composition (e.g., ~ 174–222 ppm Sr, ~160–185 ppm Zr, ~661–890 ppm Ba, ~62–88 ppm Rb, ~18–28 ppm La). Fiamme compositions typically overlap with bulk-rock values and extend towards matrix glass compositions (**Fig. 3.20**). Primitive mantle normalised rare earth element (REE) patterns (**Fig. 3.21 a**) show LREE enrichment, moderately steep LREE-MREE trends and flat MREE-HREE trends with a subdued negative Eu anomaly (La_N/Yb_N = 4.87–8.99 and 6.35–6.95; La_N/Sm_N = 3.28–4.54 and 3.68–4.36; Dy_N/Lu_N = 0.92–1.11 and 0.95–1.07; and Eu/Eu* = 0.7–0.96 and 0.68–0.82 for bulk-rock and fiamme respectively). Trace element patterns (**Fig. 3.21 b**) of bulk-rock and fiamme samples are also indistinguishable with prominent negative Nb, Ta, La, Ce and P and positive Pb and Zr anomalies.

3.7.2 Matrix glass chemistry

In proximal outcrops, the Waitеariki Ignimbrite is pervasively devitrified with the exception of the lower 10 m where light-brown perlitic glass is preserved. In Chapter 2, it was determined that this glass is a reasonable approximation of the original melt composition based on the high analytical totals and consistent geochemical composition (Prentice *et al.*, 2022), although outliers of anomalously low or high concentrations of Na_2O and K_2O are evident relative to rapidly quenched distal matrix glasses (**Figs. 3.18 b, 3.19 f**).

Matrix glass is calc-alkaline, medium- to high-K rhyolite with SiO_2 contents of 76.82–77.84 wt. % (normalised anhydrous; **Fig. 3.18**), with limited geochemical variance in most major and trace element compositions (**Figs. 3.19, 3.20**). A notable exception is observed in **Figure 3.20 a** where a distinct subgroup is observed that has high and low Ba/Sr and Zr/Y ratios respectively. This subgroup typically

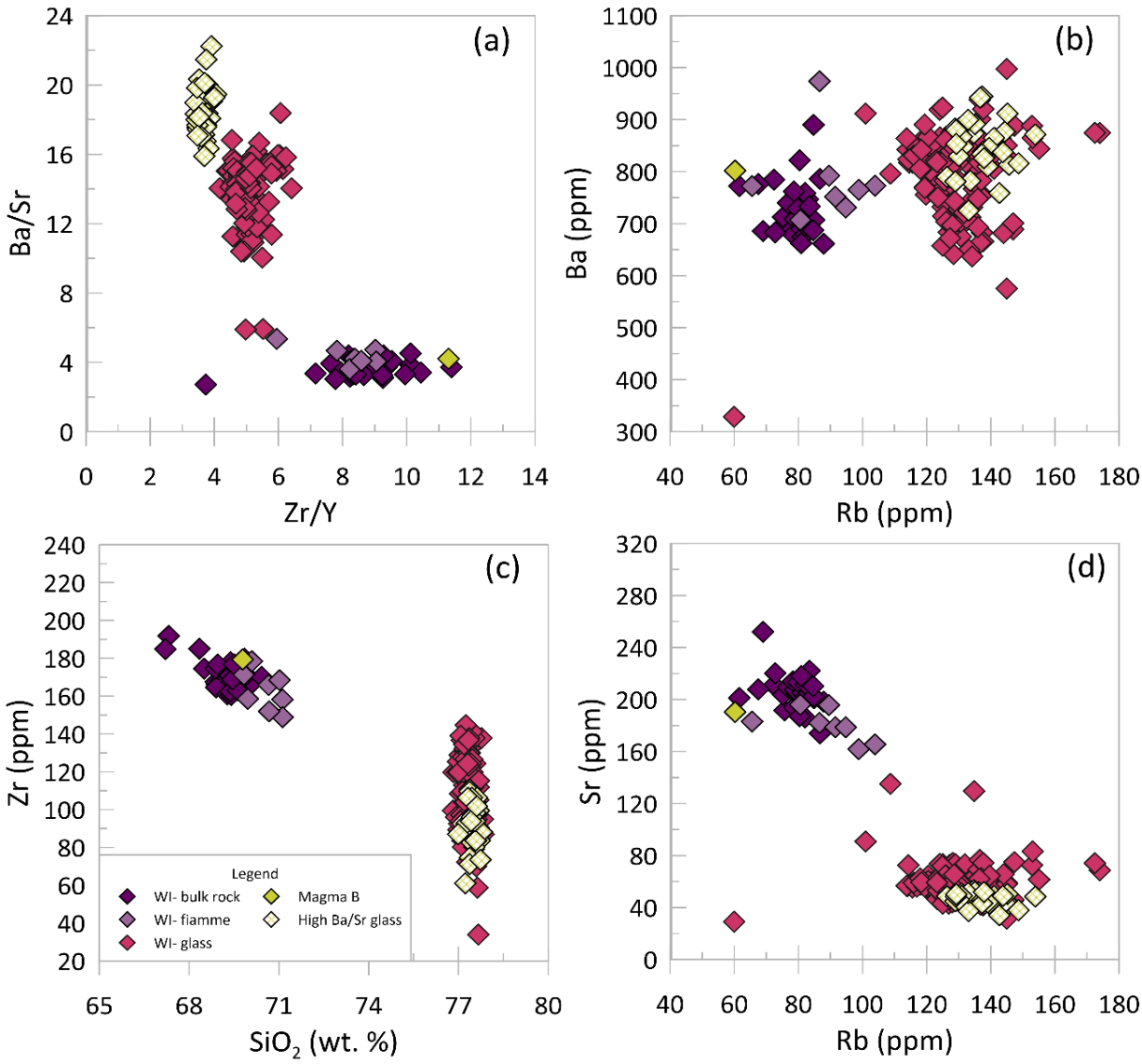

Figure 3.20. Selected bivariate plots of bulk-rock, fiamme and matrix glass trace element compositions and ratios. Analytical error (2σ) determined by repeat analyses of the standard Atho-G are comparable to or smaller than symbol size.

overlaps with Waitearikiki Ignimbrite glass data but tends to have concentrations on the higher or lower extremes (**Figs. 3.19, 3.20**).

Primitive mantle normalised multi-element plot patterns of matrix glasses show identical patterns to bulk-ignimbrite and fiamme samples (**Fig. 3.21**) with a stronger negative Eu anomaly (Eu/Eu* = 0.44) and wider range of values across the HREE. The high Ba/Sr subgroup multi-element pattern is generally very similar to Waitearikiki glass, but with a more moderate negative Eu anomaly (Eu/Eu* = 0.35), a prominent negative Sr anomaly and lower values for Cs, Rb and the mid-heavy REEs.

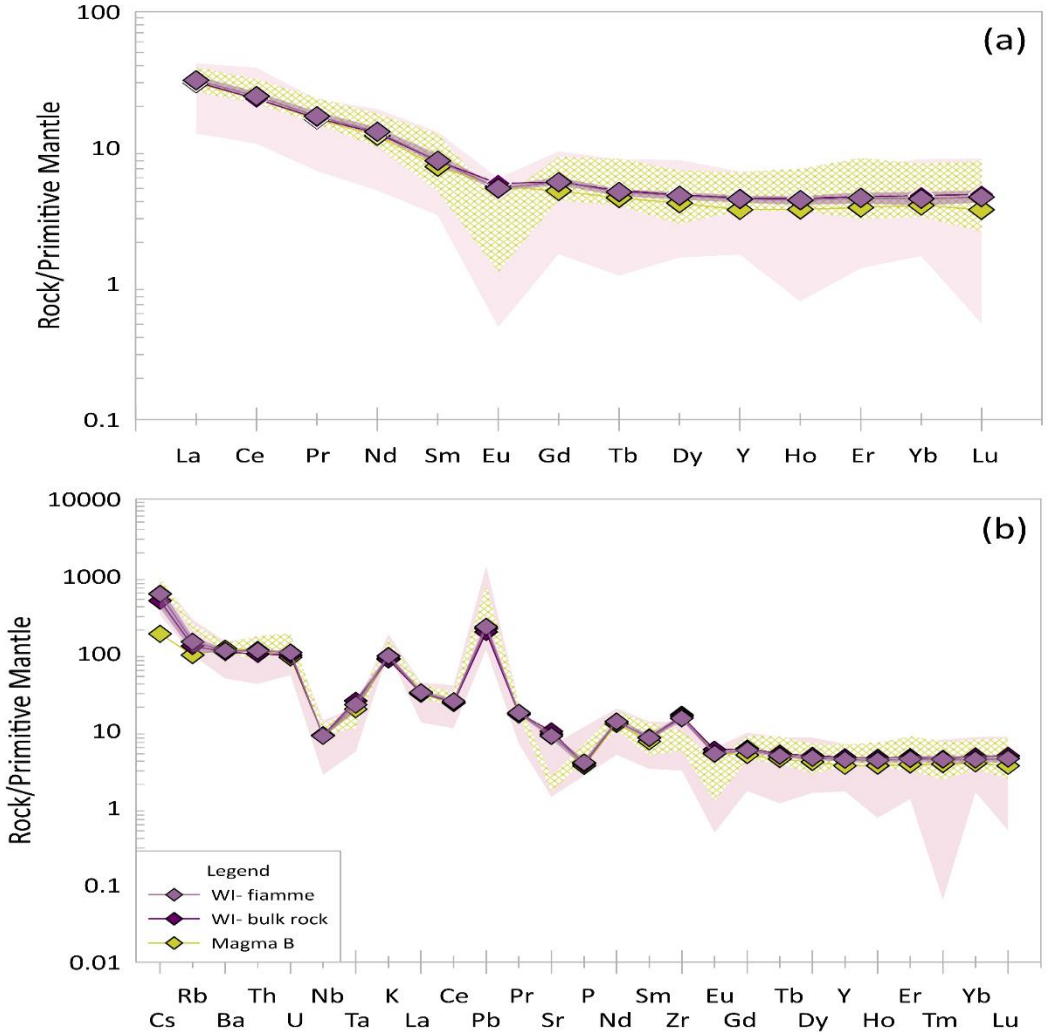

Figure 3.21. Trace element plots normalised to primitive mantle values of Sun and McDonough (1989). Average values are shown with shaded areas representing the range of data for Waiteariki fiamme (purple), Waiteariki matrix glass (pale red) and high Ba/Sr glass (yellow checkered).

3.8 Reinterpretation of Tauranga regional geology, evolution and caldera source

The correlation between the Waiteariki Ignimbrite with the distal Hikuroa Pumice Member throughout northern Hawke's Bay led Prentice *et al.* (2022) to suggest that the eruption of the Waiteariki Ignimbrite must represent a significant large-scale silicic event and as such, a reliable volume estimate is essential to calculate eruption magnitude. However, obtaining accurate volume estimates for voluminous ignimbrites are generally problematic due to a lack of knowledge of paleo-topography, post-depositional erosion, and subsequent burial and rifting of deposits (Silleni *et al.*, 2020; Giordano & Cas, 2021; de Silva & Self, 2022). This study estimates the eruptive volume of the Waiteariki Ignimbrite between c. 1500 km^3 (870 ± 87 km^3 DRE). The higher density of thickness data

points from borehole logs within the Tauranga region is reflected by an increased level of complexity in isopach shapes in proximal regions which represents variation between valley-fill and veneer deposits and shadowing effects caused by topographic barriers (i.e. pre-existing lava domes) blocking the passage of the pyroclastic flow (**Fig. 3.3**). In contrast, the complete lack of outcrops in medial regions and a limited distribution in distal areas results in simplified oblate shapes and generalised thickness isopachs. Overall, there is relatively high density of raw thickness data points, especially throughout proximal regions providing a reliable estimate of eruption volume (Crosweller *et al.*, 2012; Engwell *et al.*, 2015). With an eruption volume of c. 1500 km^3, the Waiteariki Ignimbrite is classified as a super-caldera-forming ignimbrite (Giordano & Cas, 2021), but is not currently associated with any known caldera. Calderas within the CVZ and TVZ are recognised predominantly by negative Bouguer gravity anomalies in association with silicic vents, the distribution, thicknesses and lag breccia facies of proximal ignimbrites and structural evidence for collapse (Wilson, 1986; Nairn *et al.*, 1994; Krippner, 2000; Smith *et al.*, 2006; Ashwell *et al.*, 2013; Cole *et al.*, 2014; Rosenberg, 2017). The stratigraphic relationships, clast sizes and thickness variations throughout Tauranga strongly suggest that the Waiteariki Ignimbrite likely erupted from a volcanic vent(s) located to the south and flowed northwest into the region. Underlying the Mamaku Plateau (**Fig. 3.22**) is a large negative Bouguer anomaly (-34 to -46 mGal) which may be partly related to a thick, elevated succession of pyroclastic deposits (Stagpoole *et al.*, 2021) or a buried caldera structure (Wilson et al., 1995a). While there is no direct surficial evidence for a caldera, we favour the later interpretation due to several lines of evidence consistent with the presence of a caldera in this location which we name the Omanawa Caldera (**Fig. 3.22**).

Contours defining the Mamaku Plateau gravity anomaly are predominantly concentric except in the southeast where they merge with the gravity anomaly defining the Rotorua Caldera. The most negative values (-42 to -46 mGal) form two conjoined elliptical lobes and may suggest the regions of greatest collapse related either to the largest eruption or the cumulative effect of several caldera forming eruptive events (Stagpoole et al., 2021). Between these two low points, is the silicic dome of Puwhenua (Fig. 3.22) which may represent an intra-caldera dome partially buried by the overlying Mamaku Ignimbrite. Topographical evidence for the caldera is ambiguous and no lag breccia lithofacies are currently recognised due to extensive burial of the Waiteariki Ignimbrite and TgaVC dome lavas by younger TVZ pyroclastic deposits. However, Healy et al. (1964) and Lloyd (1965) identified northeast-trending faults that displace the Waiteariki Ignimbrite within the upper reaches of the Opuiaki and Mangapapa rivers (**Fig. 3.2**). These faults coincide with both the southern extent of stream outcrops of the Waiteariki Ignimbrite and the northern extent of the gravity anomaly as defined by Stagpoole et al. (2021), and thus are interpreted here to represent the northern topographic boundary for the caldera (**Fig. 3.22**). Historic drilling in this region intersected pumiceous

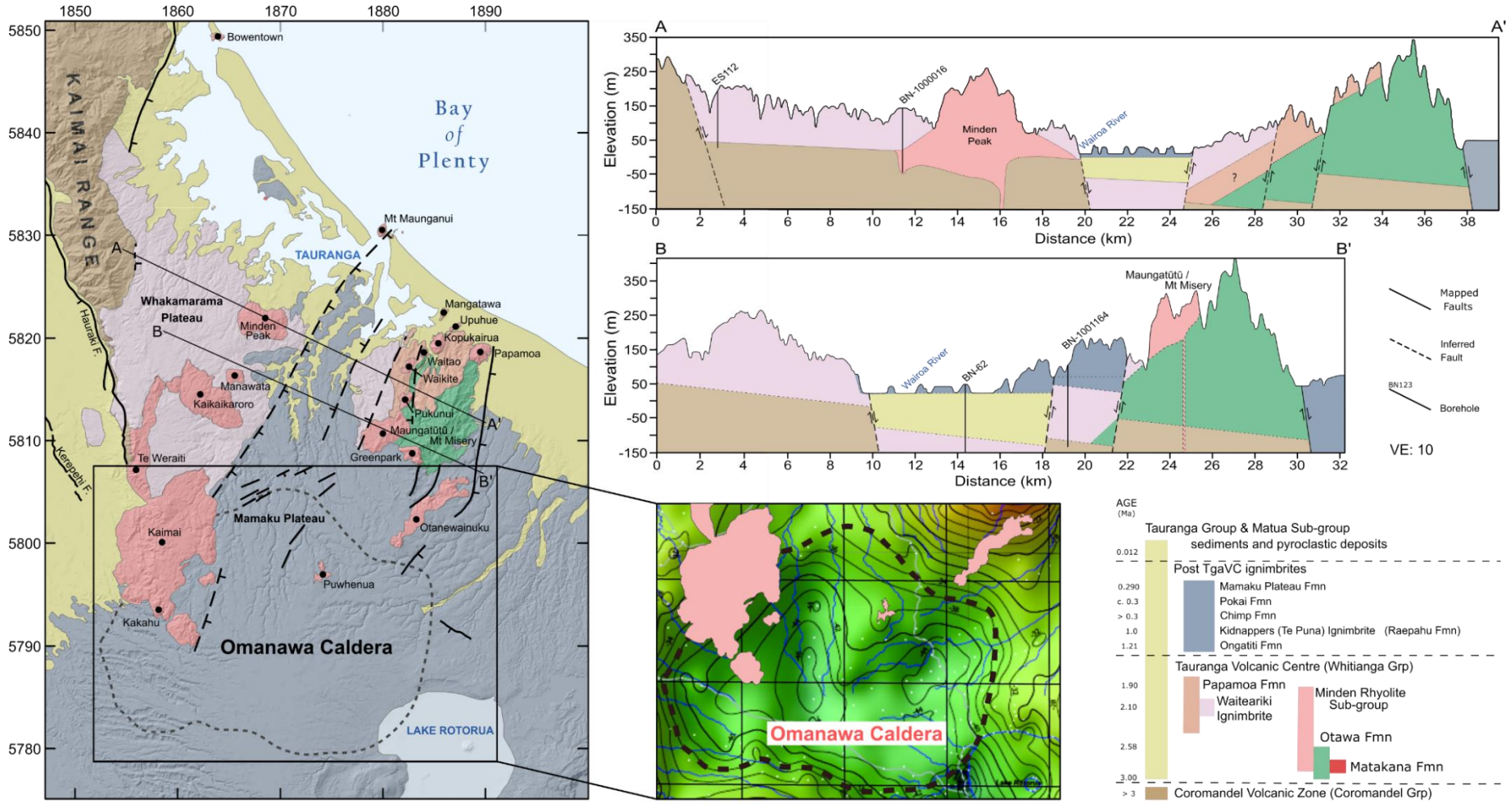

Figure 3.22. Simplified geological map and cross sections of the Tauranga Volcanic Centre highlighting volcanic units and confirmed or inferred structural features. Map unit distributions have been modified from Pittari *et al.* (2021), Edbrooke (2001), Briggs *et al.* (1996), and Leonard *et al.* (2010). Insert of gravity data from Stagpoole *et al.* (2021) highlights the extent of the Omanawa caldera based on gravity contours and its spatial relationship to silicic lava domes as described in the text.

silts and sands which were inferred to be of lacustrine origin (**Fig. 3.2**, Holes 7, 9 and 14; Lloyd 1965) and lie stratigraphically between the Waiteariki and Pokai ignimbrites. The northwest margin is obscured by the large dome complex of Kaimai-Kakahu-Te Weraiti. The SE flank of this dome complex consists of an elevated ignimbrite plateau surface of Pokai Ignimbrite that has been uplifted against the rest of the Mamaku Plateau surface. The southwest, east and southern topographic margins are completely obscured and are defined solely on the basis of the gravity data. The Otanewainuku dome is situated near the inferred northeast caldera margin and extends northeast parallel to the major fault delineating the eastern margin of the TgaVC (**Fig. 3.22**).

The geological map presented in **Fig. 3.22** has been redrawn as a result of new field-mapping and the interpretation of geomorphology for volcanic units using LiDAR. Geological cross-sections made in conjunction with borehore logs confirm that the northeast alignment of domes throughout the TgaVC are fault-related (cf. Healy *et al.,* 1964; Briggs *et al.,* 1996). The major western fault forms the eastern boundary of the Whakamarama Plateau and follows the Wairoa/Opuiaki rivers (**Fig. 3.2**) where borehole logs indicate up to 90 m of displacement on the Waiteariki Ignimbrite. To the east, the western flanks of the Pāpāmoa Range consists of a series of down-faulted blocks, which in conjunction with the Wairoa/Opuiaki river fault form an asymmetrical rifted graben. The proposed Omanawa Caldera is situated at the southern end of this graben structure which has acted to channel younger pyroclastic density currents entering the Tauranga Region from the modern TVZ. The strong spatial association between the newly recognised faults, silicic domes and the Omanawa caldera structure suggests that dome growth throughout the region is likely to have occurred in close association with faulting (cf. Villamor *et al.,* 2022).

3.9 Revised geological history of the TgaVC

Volcanism throughout the region was frequent yet episodic with two key periods of activity occurring between 2.5-2.3 and 2.2-2.1 Ma (**Fig. 3.23**; Pittari *et al.*, 2021; **Chapter 2**, Prentice *et al.,* 2022). Volcanic activity began c. 3 Ma with the eruption of pyroxene and hornblende basaltic andesite to dacite lavas and breccias of the Otawa Formation (Stipp, 1968) which represent the remains of an eroded stratovolcano complex that forms the basis of the modern day Pāpāmoa Range (Stage 1, **Figs. 3.23; Fig. 3.2 a**).

Rhyolitic volcanism followed rapidly in central areas of the TgaVC with the eruption of early lavas of the Kaimai-Kakahu dome complex (c. 2.8 Ma; Briggs *et al.,* 2005), Maungatūtū/Mt Misery (c. 2.7 Ma; Briggs *et al.,* 2005) and Waitao (c. 2.6 Ma, Pittari *et al.*, 2021) and the onset of rifting (Stage 2, **Fig.**

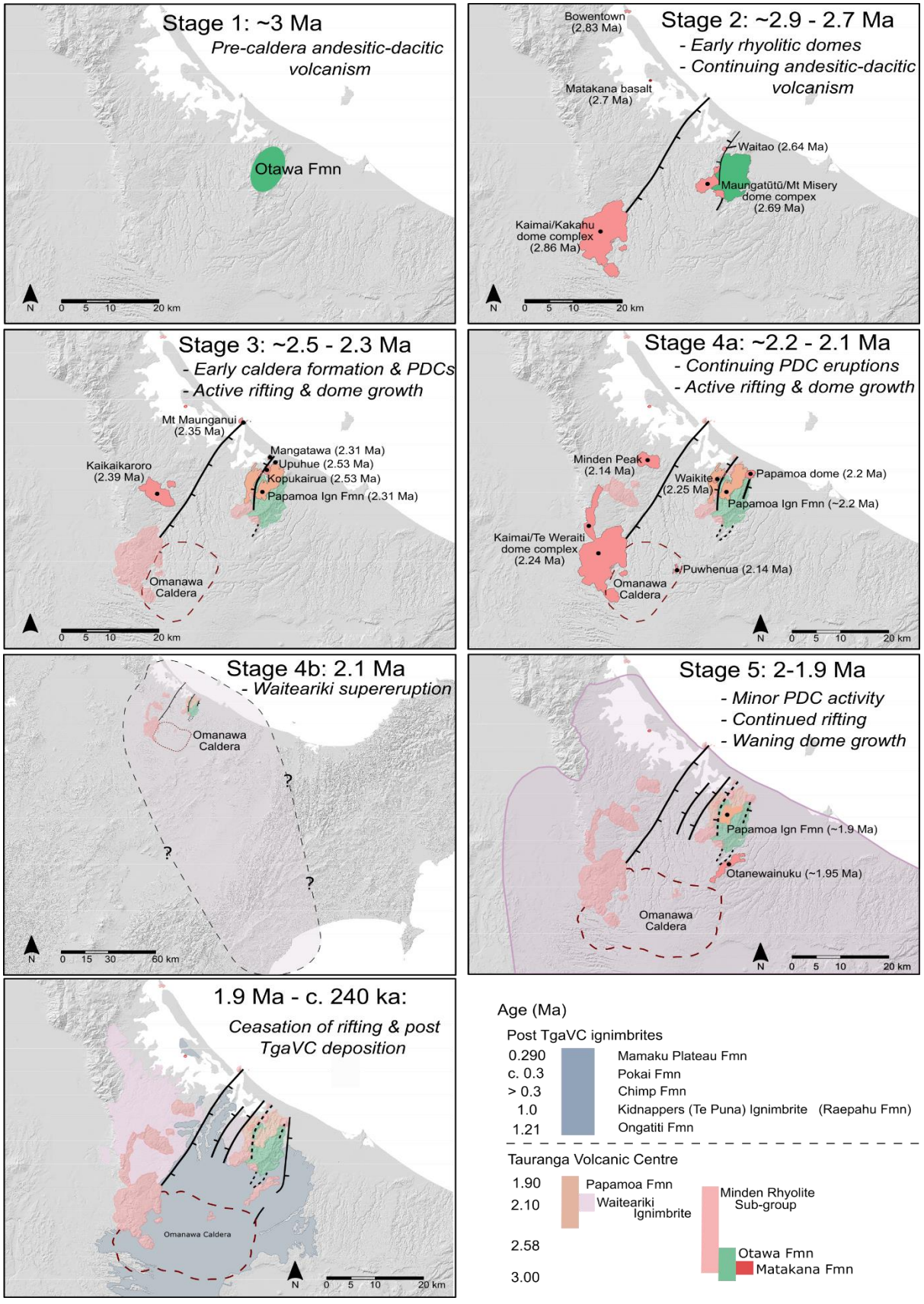

Figure 3.23. Structural and volcanic evolution of the Tauranga Volcanic Centre (TgaVC), western Bay of Plenty. Age data is taken from **Chapter 2** (Prentice *et al.*, 2022), Stipp (1968), Briggs *et al.* (2005), and Pittari *et al.* (2021) and highlights the clustering of dome activity in time along inferred faults.

3.23). The western (Wairoa/Opuiaki river) and eastern rift-bounding faults are inferred to have been active during stage 2 and acted as a pathway for magmas to propagate to the surface. These faults are parallel with those of the old Taupō Rift as defined by Villamor *et al.* (2017) and Stagpoole *et al.* (2021). This period also marks the eruption of the Matakana Basalt and Bowentown Rhyolite whose inclusion within the TgaVC remains tentative.

Stages 3 and 4 mark a period of frequent silicic activity throughout the TgaVC. Stage 3 includes the eruption of Upuhue and early Kopukairua lavas c. 2.5 Ma (Pittari *et al.*, 2021), followed by those at Mangatawa (c. 2.3 Ma; Briggs *et al.,* 2005; Pittari *et al.*, 2021) along the inferred eastern rift-boundary and Kaikaikaroro, Manawata and Mt Maunganui (2.4–2.3 Ma; Briggs *et al.,* 2005) in the west. The onset of moderate-volume pyroclastic volcanism is represented by the Welcome Bay Ignimbrite of the Pāpāmoa Formation, which is the first of four ignimbrites erupted during an ignimbrite flare-up event between c. 2.3–2.2 Ma (**Chapter 2**, Prentice *et al.*, 2022). Pyroclastic activity continued into Stage 4 with renewed activity at Kaimai-Kakahu-Te Weraiti dome complex along with coeval volcanism at Pāpāmoa and Waikite domes at the northern end of the Tauranga graben (c. 2.2 Ma, Briggs *et al.,* 2005; Pittari *et al.*, 2021) and further dome growth at Minden Peak (2.16 Ma, Briggs *et al.,* 2005; Pittari *et al.*, 2021) and Puwhenua (2.14 Ma; Briggs *et al.,* 2005) domes in the north and south respectively. Activity during this time culminated with the Waitearikiupereruption at 2.1 Ma (**Chapter 2,** Prentice *et al.*, 2022).

Stage 5 is characterised by continued rifting, waning dome growth and minor pyroclastic activity. Post-depositional displacement of the Waitearikiignimbrite indicates normal faulting continued for a period along the Wairoa/Opuiaki river fault and the eastern side of the graben structure, but the extensive c. 300–240 ka old ignimbrite surface is not displaced by these faults. Post-WI deposits are limited to the growth of the Otanewainuku dome (1.95 Ma; Briggs *et al.,* 2005) which is oriented along known faults at the eastern margins of the TgaVC. An ignimbrite in central parts of the Pāpāmoa Range is dated at 1.9 Ma (Briggs *et al.*, 2005) but it remains unknown if caldera activity continued after 2 Ma or if this deposit is related to minor activity associated with one of the nearby silicic domes.

3.10 Origin of textural and chemical signatures in the Waitearikiignimbrite

To a first order, the Waitearikiignimbrite is homogenous throughout up to 220 m of thickness with a consistent mineralogical assemblage of plagioclase, hornblende, pyroxene, quartz ± biotite (**Table 3.1**) and accessory Fe-oxides, zircon and apatite; restricted ranges in whole-rock geochemistry and matrix

glass compositions; and absence of compositional gradients (**Fig. 3.4**). As expected, there is a larger range in compositions for bulk-rock samples than for juvenile clasts and associated high-SiO_2 matrix glass, which extend towards more dacitic compositions due to crystal-rich nature of the ignimbrite. The strong linear arrays defined by the Waitepariki bulk-ignimbrite, fiamme and glass in **Figures 3.18-3.20** demonstrate that most of the compositional variability is the result of elutriation during pyroclastic flow transportation, rather than systematic pre-eruptive compositional zonation (cf. Fish Canyon Tuff; Bachmann *et al*., 2002). The range in whole-rock compositions of individual fiamme reflect differences in the crystal assemblage and crystallinity.

3.10.1 Magma assembly and evolution as recorded in phenocrysts

In contrast to this large-scale homogeneity, textural and chemical variations within individual crystals of plagioclase, orthopyroxene and amphibole, suggest a complex and dynamic magmatic system. Plagioclase crystals exhibit a very broad compositional range, extending from $An_{22–78}$ which form distinct textural and compositional populations. Group 1 and 2 plagioclases are predominately euhedral to subhedral grains with non-descript or strongly resorbed, skeletal core textures respectively with low- ($An_{23–42}$) to mid- ($An_{43–49}$) An core compositions. Group 3 crystals are less common and consist of highly resorbed, anhedral grains with high-An cores ranging from $An_{50–78}$ which are relatively high anorthite contents for a high-SiO_2 rhyolitic glass. If fractional crystallisation is the dominant evolutionary process in the Waitepariki magmatic system, we would expect mineral cores and rims to be dominated by primitive and more evolved compositions respectively. However, both primitive and evolved compositions are present in crystal cores and rims (**Fig. 3.7**) implying that recharge and magma mixing played a substantial role in assembling the crystal cargo of the Waitepariki Ignimbrite. This is supported by a number of reversely zoned crystals that have low-mid An core compositions with more calcic-An rims (**Fig. 3.7 b**). Autocrystic plagioclase are represented by a subordinate number of crystals (~ 10 % of total crystals) that are homogeneous with < 1 mol % change in An compositions. These crystals predominantly have core and rim compositions between An_{26} and An_{29} and are considered to have grown in-situ within the upper mush zone of the magma system. Rarer crystals were found to have more calcic core and rim compositions between An_{37} and An_{46} and these are inferred to have grown within a less evolved melt in deeper parts of the crystal mush zone. The rare, very calcic plagioclase cores ($An_{71–78}$) are xenocrystic, relicts from a deeper-sourced primitive magma that hosted clinopyroxene and was intruded at shallower levels. Resorption of these crystals is likely to have occurred during ascent.

Orthopyroxene crystals are generally homogenous with core and rim compositions dominated by primitive compositions ($Mg\#_{> 50}$), with strong compositional peaks from $Mg\#_{44–47}$ ($En_{42–46}$) and $Mg\#_{57–}$

$_{59}$ ($En_{54–59}$) (**Fig. 3.9**). Slight to moderate normal zoning is also common, but like plagioclase, several crystals show reversed core-rim compositional trends. A subordinate number of crystals have cores and rim compositions between $Mg\#_{28–33}$ and are inferred to have grown alongside autocrystic plagioclase within the upper mush zone.

Amphibole crystals display a large range in major and trace element chemistries that are subdivided into two end-member groups based on Al content and Mg# (Group 1: $Mg\#_{43–55}$, $Al_{(t)}$ 1.15–1.70 apfu; Group 2: $Mg\#_{58–68}$, $Al_{(t)}$ 1.22–2.02 apfu) (**Fig. 3.13)**. The strong correlation between amphibole Si, Al and Mg with temperature (Putirka, 2016) indicates Group 2 crystals likely formed in a more mafic melt. Mixing of melts is evidenced by intermediate compositions (Group 3 crystals) and Group 2 cores having rims of Group 1 composition.

The microcrystalline clots and glomerocrysts within the Waitearikí Ignimbrite display strong plutonic textures and may represent crystallised portions of the crystal mush, cumulate residues from crystal fractionation, or xenoliths from fragments of genetically unrelated igneous rock (Cooper *et al.*, 2019). The identical mineral assemblage along with relatively primitive plagioclase and orthopyroxene compositions indicate that these clasts are likely cognate in origin and are interpreted here as fragments of antecrystic cumulate mush from the lower regions of the Waitearikí magma body.

The diversity in composition of multiple phenocryst phases and incorporation of co-magmatic cumulates indicate complex and contrasting early growth histories along with open-system processes. Many crystals were then mixed or assimilated into a final common mush-zone in which they experienced further rim growth before eruption. The partial resorption of quartz macrocrysts and xenocrystic clinopyroxene documents heating and partial melting of the upper mush zone (Bachmann *et al.*, 2002) due to a mafic recharge event just prior to eruption. The common presence of more primitive plagioclase, orthopyroxene and hornblende compositions suggest the simultaneous tapping and disaggregation of different levels of a complex magma reservoir that were entrained into the overlying mush body, probably during eruption as the lower regions of the chamber were disturbed by decompression and magma withdrawal (Neave *et al.*, 2017).

3.10.2 Magma types and eruption processes

The dominant magma erupted during the Waitearikí supereruption is a crystal-rich (37 %) rhyodacite (ave. 70.7 wt. % SiO_2) with a mineral assemblage that consists of plagioclase, hornblende, orthopyroxene and quartz (Type-A). Within core ES112, however, prominent biotite bearing fiamme at 37 and 107 m (**Table 3.1**), provide evidence of mixing with a volumetrically minor, yet genetically distinct second magma. Magma mixing is defined here as the physical interaction of magmas that

have different chemical composition and mineral assemblages without implying total homogenization of the two magmas. We refer to this contrasting, biotite-rich magma as Type-B. Both Type-A and B magmas are med-K, rhyodacites with broadly similar bulk compositions, but with variations in some major and trace element abundances and normalised multi-element patterns (**Figures 3.18–3.21**). Plagioclase core and rim compositions (**Fig. 3.7**), demonstrate, however, that the two magmas are chemically distinct. Typically found in trace amounts in many of the lavas erupted throughout the TgaVC, biotite is a minor phenocrystic phase except in lavas found in the north of the centre where it features more prominently. These lavas include those erupted at Mt Maunganui, Waikite, and Mangatawa (Hughes, 1993; Hall, 1994) which have a mineral assemblage identical to that of Type-B fiamme found in the Waitеariki Ignimbrite. Lavas from Mt Maunganui and Waikite are rare examples of crystal-poor magma within the TgaVC and have compositions that overlap with the high Ba/Sr matrix-glass subgroup (cf. **Chapter 4**). We infer that syn-eruptive rifting processes caused the southerly propagation of this northern dome biotite-rich magma, to intercept and mix with Waitеariki rhyodacite magma in the conduit. This scenario accounts for the overlap in plagioclase compositions between the two magma types evident in **Figure 3.7**.

Precursory activity leading to the eruption of the Waitеariki Ignimbrite is ambiguous. The Minden Peak rhyolite (**Fig. 3.22**) has an identical mineral assemblage to the Type-B magma identified in this study (Whitbread-Edwards, 1994) and was erupted c. 2.1 Ma (Pittari *et al.*, 2021). Basal deposits of the Waitеariki Ignimbrite lie directly above Aongatete Formation ignimbrites and consist of c. 30 cm of coarse ash which grades rapidly from fine-lapilli pumiceous tuff to a densely welded, eutaxitic ignimbrite highlighting the lack of an underlying Plinian fallout deposit (**Fig. 3.4**). Plinian deposits are typical for large-volume, predominately crystal-poor ignimbrites and indicate a sustained single vent phase (or phases) prior to caldera collapse (e.g. Bishop Tuff, USA, Chamberlain *et al.,* 2015; Minoan, Santorini, Simmons *et al.,* 2016; Oruanui supereruption, Taupō, New Zealand, Allan *et al.,* 2017; Campanian Ignimbrite, Silleni *et al.,* 2020) but ignimbrites lacking this early Plinian phase are less common. When recognised, these eruptions have occurred predominantly in extensional tectonic environments (Bachmann *et al.*, 2002; Maughan *et al.*, 2002a; Folkes *et al.*, 2011; Willcock *et al.*, 2013; Yamamoto, 2021) and are generally interpreted to represent eruptions that initiate with sustained pyroclastic density currents along bounding ring faults following catastrophic decompression during regional extension events (cf. Gottsmann *et al.*, 2009; Gregg *et al.,* 2015). The resulting deposits are typified by voluminous and thick ignimbrite sheets with vesicle-poor juvenile clasts, low lithic content, syn-eruption of co-magmatic plutonic lithics and a high proportion of crystal fragments due to explosive expansion of phenocryst-hosted melt inclusions.

Based on the textural features in the Waitearikí Ignimbrite, the lack of lateral and vertical compositional variations and the newly revised geological setting of the Tauranga region, we infer that the Waitearikí supereruption most likely consisted of a multi-vent fissure style eruption. Active crustal rifting led to a deep-seated failure of the magma reservoir causing rapid decompression and large-scale evacuation of the Omanawa Caldera magmatic system (cf. Gottsmann *et al.,* 2009). The diverse range of phenocryst compositions reported here is consistent with the simultaneous extraction and eruption of magma covering a large depth range followed by southward propagation and syn-eruptive mixing of Type B magma after the initiation of eruption.

3.11 The Waitearikí Ignimbrite: a monotonous intermediate at the dawn of the TVZ

The Waitearikí Ignimbrite is characterised by high-crystallinity (25–51%, ave. 37%), consistent mineral assemblage and homogenous bulk-rock geochemistry and therefore does not conform with typical TVZ ignimbrite endmembers of crystal-poor or crystal-rich rhyolite. Instead, the Waitearikí ignimbrite is more consistent with the archetypal large-volume ignimbrite eruptions produced by monotonous dacitic systems of the Great Basin/Colorado Plateau, USA (Bachmann *et al.*, 2002; Maughan *et al.*, 2002) and the Antiplano-Puna Plateau (Kay *et al.*, 2010). The Waitearikí Ignimbrite is identified here as the first example of a monotonous intermediate ignimbrite in the New Zealand volcanic record.

Silicic volcanism associated with the TgaVC was more frequent and voluminous than previously recognised (**Chapter 2**, Prentice *et al.*, 2022) and there is a clear overlap between volcanism of the TgaVC (c. 3–1.9 Ma; Pittari *et al.,* 2021; **Chapter 2**, Prentice *et al.,* 2022), waning silicic volcanism of the CVZ (Briggs *et al.*, 2005), and its onset within the TVZ (c. 2–1.8 Ma, Wilson & Rowland, 2016; Chambefort *et al.*, 2014; Milicich *et al.*, 2020). While rhyolitic volcanism has been continuous over this time (Carter *et al.*, 2003), there appears to be a stark contrast between the scale of volcanism of two volcanic zones, with the CVZ generally characterised by small caldera sizes and associated eruptive volumes (< 30 km^3 for CVZ, Briggs *et al.,* 2005; 30–1500 km^3 for TVZ, Wilson *et al.,* 2009). Wilson and Rowland (2016) defines the TVZ as the region enveloping all inferred or known volcanic vents active within the last c. 2 Ma occurring within the structural boundaries of the Taupō Rift. It has been subdivided into three temporal evolutionary stages: Old TVZ (> 350 ka), Young TVZ (350–61 ka), and Modern TVZ (< 61 ka) that largely coincides with those proposed for the Taupō Rift (Villamor *et al.*, 2017). The western structural boundary of the Old Taupō Rift has been inferred from gravity data to lie just to the west of Tauranga city (Villamor *et al.*, 2017; Stagpoole *et al.*, 2021) and may coincide

with the Wairoa/Opuiaki River fault identified here. As such, volcanism associated with the Omanawa Caldera and broader TgaVC occurred within the defined structural boundaries of the Taupō Rift and therefore represents the first silicic system of the TVZ (**Fig. 3.24**). Therefore, the change from the CVZ to the TVZ was established by c. 2.5 Ma with the initiation of continental back-arc rifting within onshore parts of the North Island of Aotearoa New Zealand within the regions now referred to as the Old TVZ. The silicic lavas and ignimbrites of the Waihi Caldera (Vincent, 2012; Julian, 2016) and predominately intermediate pyroclastic deposits of the Aongatete formation (Briggs *et al.*, 2005) then represent the final stages of CVZ volcanism which occurred between 3.9 and 3.5 Ma.

The question then arises as to what led to the eruption of a monotonous rhyodacite magma during the early stages of the TVZ where high-silica, crystal-poor rhyolite magmas dominate? Numerous studies have demonstrated a complex magmatic-tectonic relationship between regional rifting and

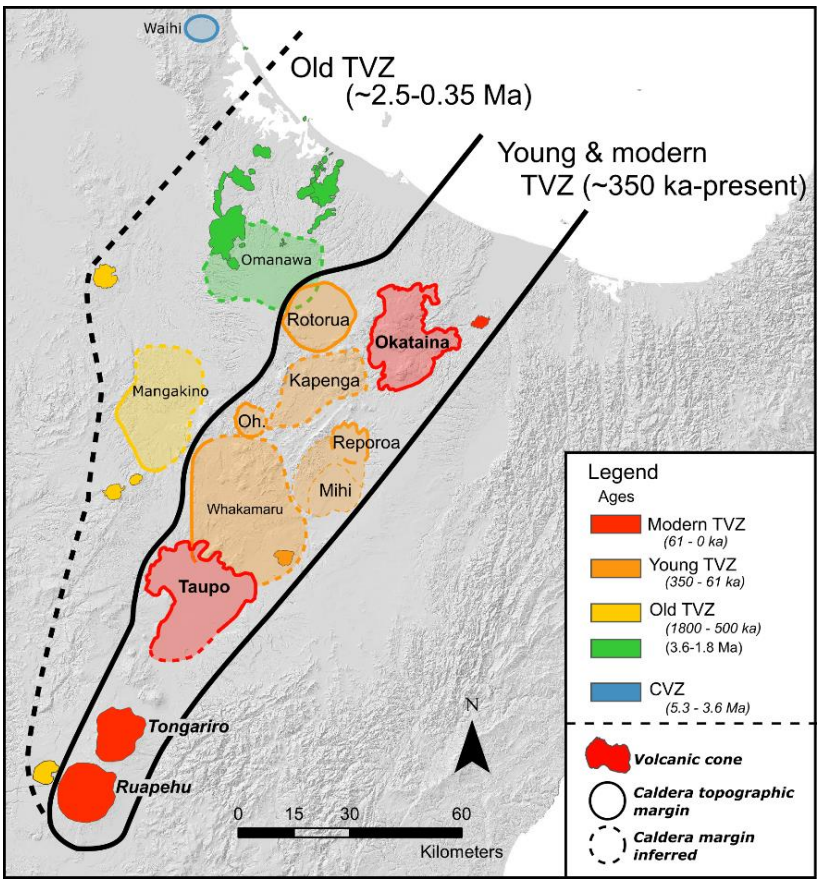

Figure 3.24. Map illustrating the distribution and ages of calderas and prominent lava domes and stratovolcanoes in central regions of Te Ika-a-Māui/North Island throughout the history of the Taupō Volcanic Zone (TVZ). Note the general southward-younging of centres of the old TVZ and the prominent eastward shift of centres of the young and modern TVZ.

volcanism (Charlier *et al.*, 2003; Gravley *et al.*, 2007; Barker *et al.*, 2021; Muirhead *et al.,* 2022; Villamor *et al.*, 2022) referred to as magma-assisted rifting (Rowland *et al.*, 2010). Extension has thinned the crust underlying the TVZ to c. 20 km, allowing the extraction of high-SiO_2 interstitial melt from evolving mush systems in the central TVZ to move into increasingly shallower portions of the crust (e.g. Bégué *et al.,* 2014; Cooper *et al.,* 2014; Gualda *et al.*, 2018), from where they are subsequently erupted. As volcanism of the TgaVC occurred relatively early in the history of the Taupō Rift, one could expect crustal thicknesses to have been greater than under the modern TVZ and possibly more comparable to those found immediately east of the TVZ (~ 35 km; Reyners *et al.,* 2006) within the normal range for continental arcs (e.g. 30– > 40 km; Hughes & Mahood, 2011). Volcanism in the region rapidly evolved from the eruption of intermediate magmas at a single edifice (Otawa Volcano) to diffuse rhyolitic events represented by the numerous lava domes throughout the TgaVC, coeval with the onset of rifting (see previous section; **Fig. 3.22**). This demonstrates that external tectonic forces have played an important role in the eruption of the TgaVC magmas. The rarity of crystal-rich ignimbrites within the TVZ implies that a specific mechanism is required for them to erupt. We suggest that the Waitearikí, Ongatiti and Whakamaru supereruptions (Cooper *et al.,* 2014; Brown *et al.,* 1998a; this study) and the volumetrically smaller, but still significant, Rotoiti Ignimbrite (Burt *et al.*, 1998) represent periods of accelerated rifting in the TVZ, where regional faults have intersected the underlying magma body, leading to the eruption of pockets of high-silica crystal poor rhyolite with varying degrees of increased evacuation of the underlying low-silica mush zones. This is consistent with the above model of a two-stage extraction process where high silica rhyolite melts are stored in the upper crust after extraction from an underlying low silica rhyolite mush zone (Bachmann *et al.*, 2002; Cashman & Giordano, 2014).

Although the total erupted volume of the TgaVC is dominated by the crystal-rich monotonous rhyodacite magma of the Waitearikí Ignimbrite, a diverse range of lithologies from basaltic andesite to rhyolite (61–78% SiO_2) also exists (Briggs *et al.*, 1996). These minor lithologies reflect the processes involved during magma petrogenesis throughout the history of the TgaVC, and a detailed study of these minor lithologies (**Chapter 4**) will elucidate the origin of geochemical heterogeneity and its implications for the construction and evolution of the Omanawa magma system and the greater TgaVC.

3.12 Conclusions

The Waitearikí Ignimbrite of the TgaVC represents a M8 eruption of 1470–1506 km^3 (870 ± 87 km^3 DRE) crystal-rich rhyodacite magma which was erupted from the newly defined Omanawa Caldera. The Omanawa Caldera is identified on the basis of ignimbrite thickness variations, textural features

and the presence of numerous silicic lava domes in association with a prominent negative gravity anomaly situated at the southern end of an asymmetrical rifted graben underlying the northern Mamaku Plateau. Topographical evidence for the caldera remains mostly ambiguous due to subsequent burial by younger, widespread ignimbrites originating from the young TVZ. As volcanism associated with the Omanawa Caldera and the broader TgaVC occurred within the defined structural boundaries of the Taupo Rift, we regard volcanism of the TgaVC to represent the first silicic system of the TVZ.

The Waitearikí Ignimbrite is a monotonous intermediate deposit, which are relatively common globally but unique within the history of the TVZ that is dominated by high-silica, crystal-poor rhyolitic magmas. The composition of the Waitearikí Ignimbrite is homogenous, with a consistent mineralogical assemblage and restricted ranges in whole-rock and matrix glass compositions that lack compositional gradients. Phenocrysts, however, record a complex evolutionary history, providing evidence for a highly heterogeneous mush-source zone that was erupted when active crustal rifting led to a deep-seated failure of the magma reservoir. This likely caused rapid decompression and large-scale evacuation of the Omanawa magmatic system.

CHAPTER 4:

4 Geochemical, isotopic and magma storage constraints on the evolution of silicic volcanism at the commencement of the Taupō Volcanic Zone: Tauranga Volcanic Centre, Aotearoa New Zealand

4.1 Introduction

The Taupō Volcanic Zone (TVZ) is the southernmost ~300 km continental extension of the ~2800 km long Tonga-Kermadec arc which results from oblique, westward subduction of the Pacific Plate beneath the Australian Plate (Wilson & Rowland, 2016). Consisting of a rifting arc, rather than a conventional arc-back arc system (Wilson & Rowland, 2016; Villamor *et al.*, 2017), long-lived and voluminous silicic centres are a prominent feature of the TVZ which has become infamous for its high caldera density and eruptive volumes (Hughes & Mahood, 2011). The Tauranga Volcanic Centre (TgaVC) located in the western Bay of Plenty of the North Island, New Zealand is the first silicic centre associated with the opening of the Taupō rift, and therefore represents the earliest known volcanic activity of the globally renown TVZ (cf. **Chapter 3**).

The deposits of the TgaVC include intermediate to silicic lavas (Otawa Formation, Minden Rhyolite Subgroup) which were erupted as clusters of spatially discrete domes or dome complexes and at least seven ignimbrites within the Pāpāmoa and Waitеariki formations. Silicic activity was mostly episodic yet frequent, with at least eight eruptions occurring within the TgaVC between 2.4 and 2 Ma, culminating with the eruption of the very large-volume, crystal-rich (37 %) rhyodacite Waitеariki Ignimbrite (**Chapter 3**; Pittari *et al.*, 2021; **Chapter 2**, Prentice *et al.*, 2022). The eruption of voluminous crystal-rich, mostly rhyodacite magmas is typical throughout the history of the TgaVC, but is rare within the broader TVZ where the erupted volumes are dominated by crystal-poor (< c. 10%) rhyolites. Thus, the TgaVC provides an excellent opportunity to examine the repeated eruption of rare crystal-rich magmas over a protracted time period (c. 1 Myr) providing important insights into voluminous silicic activity occurring at the dawn of the TVZ. We use the detailed whole-rock geochemical and mineralogical data available for the Waitеariki Ignimbrite (**Chapter 3**) and new major and trace element data of TgaVC lavas and juvenile clasts of the Welcome Bay Ignimbrite to investigate compositional and mineralogical variations and gain insight into the evolution and petrogenetic relationships of volcanic units that have previously been inferred to be broadly synchronously derived (Briggs *et al.*, 2005; Prentice *et al.*, 2022). We explore the nature of upper crustal differentiation

processes by investigating the relative proportions of fractional crystallisation relative to crustal assimilates of key compositional groups through geochemical modelling and radiogenic (Sr and Nd) and stable (quartz and plagioclase $\delta^{18}O$) isotopes. Pre-eruptive magma residence depths and temperatures of generation are inferred through single-crystal geothermobarometry. I then compare my results to the established geochemical and geophysical framework of the broader TVZ to elucidate temporal or spatial variations in magma generation and storage conditions of rhyolitic magma bodies throughout the history of the TVZ.

4.2 Geological background

4.2.1 Tauranga Volcanic Centre

The silicic TgaVC is located in the western Bay of Plenty region of Te Ika-a-Māui/North Island, New Zealand (**Fig. 4.1**) and was active from 2.95 to 1.90 Ma. The centre comprises an eroded andesitic stratovolcano (Otawa Formation), a solitary exposure of basalt (Matakana Basalt), several dacite-rhyolite lava domes or dome complexes (Minden Rhyolite Subgroup), and the ~30 x 25 km Omanawa caldera (cf. **Chapter 3**) with two associated and distinct pyroclastic successions comprised of multiple ignimbrites and related fall deposits (Pāpāmoa Formation) and the climactic eruption of the dacitic Waitеariki Ignimbrite. Volcanic activity within the centre evolved in a similar fashion to that of the Mangakino and Taupō volcanic centres (cf. Krippner *et al.,* 1998; Barker *et al.,* 2021) where volcanism evolved rapidly from initial andesitic activity (Otawa Formation) to coevel minor silicic activity (Minden Rhyolite Subgroup), followed by frequent eruptions of pyroclastic density currents (Pāpāmoa Formation), numerous rhyolitic lava dome extrusions (Minden Rhyolite Subgroup), and the emplacement of the voluminous Waitеariki Ignimbrite (**Chapter 3**; Pittari *et al.*, 2021; **Chapter 2**, Prentice *et al.*, 2022). The volcanic stratigraphy is summarised in **Figure 4.1 c**. The eruption of lavas is linked to regional extensional faulting, resulting in the prominent northeast alignment of dome structures (cf. **Section 3.9**).

4.2.2 General characteristics of TgaVC lavas and ignimbrites

Magmas erupted from the TgaVC are typically crystal-rich (30-50% phenocrysts) with a consistent mineral assemblage of plagioclase > hornblende ≥ orthopyroxene ± quartz ± biotite with accessary Fe-Ti oxides, zircon and apatite (Briggs *et al.*, 1996). Olivine and sanidine are present only in the Matakana Basalt and Bowentown Rhyolite respectively with clinopyroxene limited to subordinate amounts within some Otawa Formation lavas (Briggs *et al.,* 1996) and xenocrysts within the Waitеariki

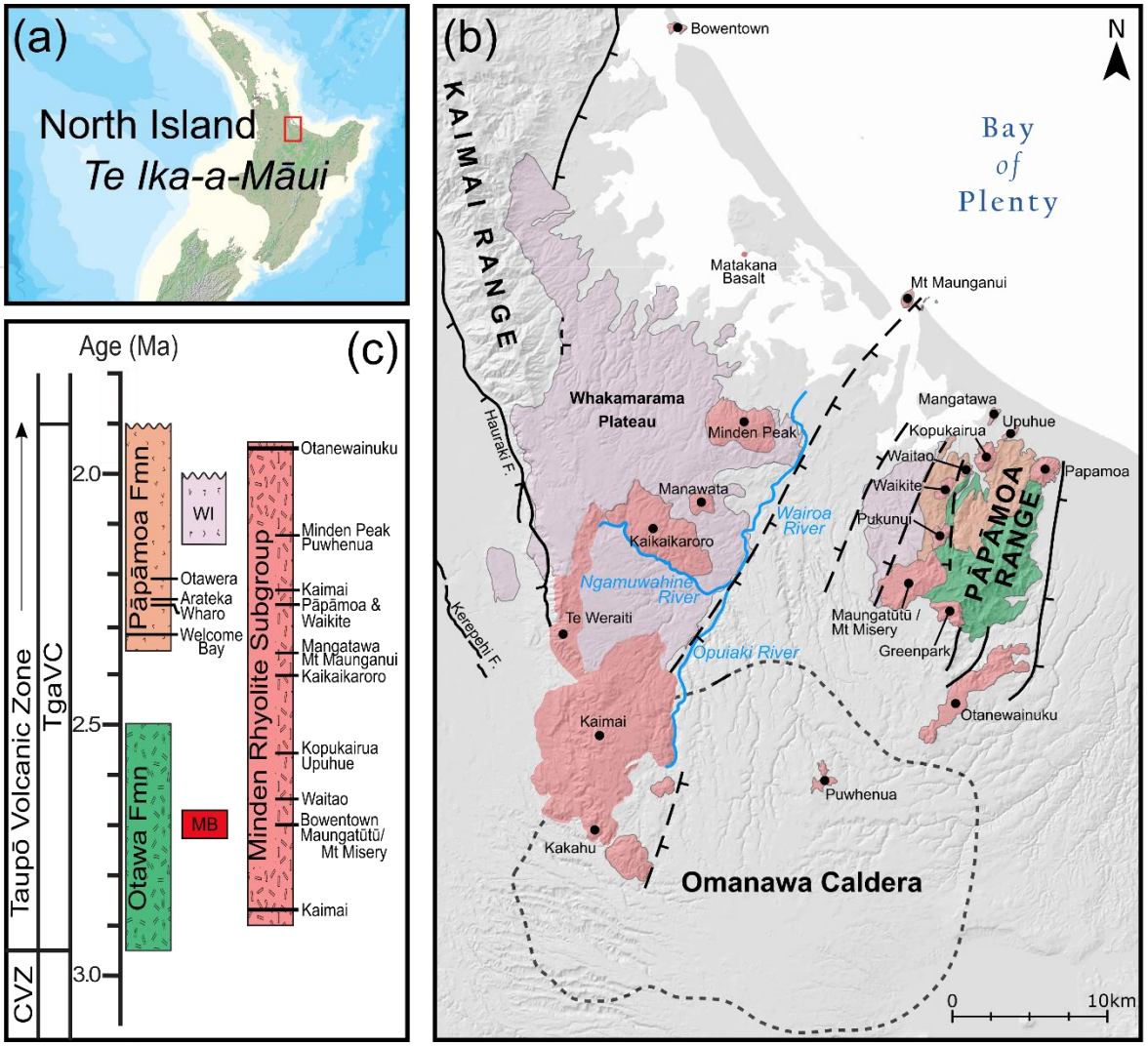

Figure 4.1. Overview and simplified geological map highlighting the distribution and stratigraphy of volcanic landforms and structures associated with the Tauranga Volcanic Centre (TgaVC). **(a)** Te Ika-a-Māui/North Island of New Zealand. Red box highlights western Bay of Plenty study area. **(b)** Simplified geological map of the TgaVC with key physiographic features labelled. Extensional faults associated with the TgaVC (this study) are shown as dashed lines, with previously identified non-active faults from Leonard *et al.* (2010) shown as solid lines. Omanawa Caldera is defined on the basis of ignimbrite thickness variations, textural features and the presence of numerous silicic lava domes in association with a prominent negative gravity anomaly situated at the southern end of an asymmetrical rifted graben (cf. **Section 3.8**). **(c)** Volcanic stratigraphy of the TgaVC. Stratigraphic formation age ranges are shown as coloured bars with dated individual volcanic centres (Minden Rhyolite Subgroup) or defined ignimbrites (Pāpāmoa Formation). Ages taken from: Otawa Fmn, Stipp (1968); Pāpāmoa Fmn, Prentice *et al.* (2022); Minden Rhyolite Subgroup, Pittari *et al.* (2021). Fmn, Formation; WI, Waiteariki Ignimbrite; MB, Matakana Basalt Formation.

Ignimbrite (cf. **section 3.10**). Crystal-poor magmas are rare and restricted to Mt Maunganui, Waikite and Bowentown lava domes, erupted in the northern parts of the centre. All lavas are pervasively devitrified.

Whole-rock compositions span the calc-alkaline compositional range from the Matakana Basalt to andesite and dacite lavas of the Otawa Formation and the dacites and rhyolites of the Minden Rhyolite Subgroup (Hughes, 1993; Hall, 1994; Whitbread-Edwards, 1994; Hollis, 1995; Julian, 2016). Briggs *et al.* (2005) divided the silicic domes of the Minden Rhyolite Subgroup into four groups based on their spatial, mineralogical and geochemical characteristics. The Minden Peak group incorporate the lava domes of Minden Peak, Manawata, and Kaikaikaroro which lie to the northwest of the Wairoa River (**Fig. 4.1 b**). At the northern end of this lineament lie the crystal-poor Mt Maunganui group lavas which have the most evolved compositions found throughout the TgaVC (SiO_2 > 76 wt. %, Zr < 110 ppm; Briggs *et al.,* 2005). The domes of the Mangatawa group are found exclusively in the east of the centre and include all domes disseminated along the western and northern margins of the Pāpāmoa Range and the domes of Otanewainuku and Puwhenua located to the south (**Fig. 4.1 b**). The Maungatūtū/Mt Misery group includes the large dome of Maungatūtū/Mt Misery and the adjacent Pukanui and Greenpark domes located at the southern end of the Pāpāmoa Range. Despite the geographical association of the Maungatūtū/Mt Misery domes with those of the Mangatawa group, Briggs *et al.* (2005) differentiated these domes due to their anomalously high Zr contents (> 200 ppm). Bowentown dome has textural, mineralogical and geochemical affinities to Mt Maunganui group lavas but, like the Matakana Basalt, is spatially removed from all other volcanic vents of the TgaVC (Pittari *et al.*, 2021). The large dome complex of Kaimai-Kakahu-Te Weraiti of the former Kaimai Volcanic Centre, has been incorporated into the TgaVC due to its spatial and temporal association and mineralogical affinities (Pittari *et al.*, 2021). Little geochemical data is available for Kaimai-Kakahu-Te Weraiti dome complex (hereafter referred to simply as the Kaimai dome), but nevertheless, it represents a substantial volume of rhyolitic, biotite-bearing lavas which are situated at the southern end of the Minden Peak group lineament on the northwest margin of the Omanawa Caldera (**Fig. 4.1**).

Voluminous pyroclastic activity is represented by the Waitearikiand Welcome Bay ignimbrites. The Welcome Bay Ignimbrite is the oldest differentiated pyroclastic unit of the Pāpāmoa Formation and crops out extensively in the northern Pāpāmoa Range. Juvenile clasts are distinctive in hand specimen and comprised of two distinct whole-rock compositions (Namaliu, 2021). The dominant clast type is a white-coloured rhyodacite (~67 wt. % SiO_2) with a mineral assemblage comprising plagioclase, hornblende, and pyroxene. Subordinate clasts of dark-grey coloured andesite (~61 wt. % SiO_2) are less common and contain plagioclase and pyroxene but lack hornblende. Magma mingling between these two end-members is evident in flow-banded clasts of dacitic compositions. The Waitearikiignimbrite represents the eruption of ~900 km^3 (DRE) of crystal-rich (37 %) rhyodacite (ave. 70.7 wt. % SiO_2) magma from the newly defined Omanawa Caldera (cf. **Chapter 3**) and the climatic and final stages of volcanic activity within the TgaVC. The composition of the Waitearikiignimbrite is homogenous, with

a consistent mineralogical assemblage and restricted ranges in whole-rock and matrix glass compositions that lack compositional gradients. Phenocrysts, however, record a complex evolutionary history, providing evidence for a highly heterogeneous mush-source zone that was erupted when active crustal rifting led to a deep-seated failure of the magma reservoir.

4.3 Methods

Whole-rock major and trace-element analysis of lavas throughout the TgaVC were undertaken at the School of Science, University of Waikato (New Zealand). Thirty-four samples were lightly crushed and fresh rock chips were handpicked and powdered in a tungsten-carbide mill. Loss-on-ignition (LOI) was measured by the weight loss of ~2 g of sample after heating for an hour at 1100 °C. Homogeneous glass disks were made using 0.8 g of dried sample powder mixed with 8 g of Li-metaborate 12-22 flux and fusing at 1050 °C for 20 minutes in a platinum crucible. Analysis was conducted using a Bruker S8 Tiger X-ray fluorescence (XRF) spectrometer. LOI values for all lavas were < 2.5% with three Welcome Bay Ignimbrite pumice samples returning LOI values between 2.97-3.45%. Major element abundances cited in the text and shown on diagrams were recalculated to total 100 wt. % on an anhydrous basis. Analytical precision was assessed using repeat analyses of the international standards AGV-2 and RGM-2. Mean values are within 2.5% of the recommended values with the exception of TiO_2 and MnO for RGM-2 which demonstrated 6.8% and 5.9% offset respectively and analytical precision (2σ) was better than 0.6 wt% for all elements. Trace elements were determined by laser ablation inductively coupled plasma mass spectrometry (LA-ICP-MS) of fused glass disks following XRF analysis as described in **Section 3.3** with the full dataset presented in **supplementary data table SM3.5.** Samples were analysed during the same analytical run as samples from the Waitеariki Ignimbrite with details of accuracy and precision outlined in **section 3.3** with details presented in **supplementary data table SM3.4**. Sample localities, the full dataset and whole-rock standard data for this chapter is presented in **Supplementary data tables SM4.1, SM4.2** and **SM4.3**.

Thirty samples were analysed for Sr and Nd isotopes at Victoria University of Wellington, New Zealand following the concomitant isolation procedure of Pin et al. (2014). The Sr and Nd fractions were analysed for isotopic ratios using a ThermoFinnigan Triton thermal ionization mass spectrometer (TIMS). Total procedural blanks were less than 100 pg for both Sr and Nd. For Sr, samples were loaded on previously outgassed single Re filaments in 1 µL 9 M HNO_3 with 0.7 µL Ta_2F_5 activator and measured using a static collection routine for 240 ratios using 16 s. integrations. The NBS 987 solution standard (500 ng) gave an average of $^{87}Sr/^{86}Sr$ = 0.710249 ± 0.000009 (2SE; n=9) (**supplementary data table SM4.4**). These values are identical to the long-term instrument average $^{87}Sr/^{86}Sr$ = 0.710256 ± 0.000006. For Nd, samples were dissolved in 1 µL 2.5 M HCl, then loaded on one side of a double Re

filament assembly along with 1 µL 0.25 M H_3PO_4 emitter solution. Ratios were measured using a static collection routine and 270 ratios with 8.389 s. integrations. Replicate analyses of the JNdi-1 solution standard gave = 0.512101 ± 0.000009 (2SD; n=4). Mass fractionation was corrected by normalising to $^{86}Sr/^{88}Sr$ = 0.1194 and $^{146}Nd/^{144}Nd$ = 0.7219 using the exponential law.

Five additional samples were analysed for Sr-Nd isotopes at Analabs, Western Australia in 1994 (R.M. Briggs, unpublished data). Sr samples were loaded in 1 µl 1 M H_3PO_4 onto single Ta filaments; stable ion beams of 2–4x10^{-11}A ^{88}Sr were obtained at filament temperatures of 1300–1450°C. Mass fractionation was corrected by normalizing to $^{86}Sr/^{88}Sr$ = 0.1194. Typically, 5–7 blocks of 10x8 sec integrations produced in-run precisions (2SE) of +0.003%. $^{87}Sr/^{86}Sr$ (±2SD) for SRM987 (n=100) is 0.71023 ± 7 (0.01%), BCR1 (n=6) is 0.70500 ± 4, BHVO-1 (n=19) is 0.70348 ± 6. Nd was loaded in H_3PO_4-doped 1M HNO_3 onto the Ta side of a Ta-Re double filament assembly; stable ion beams of 1-3x10^{-11} A ^{144}Nd were obtained at Re filament temperatures of around 1700°C. Mass fractionation was corrected by normalizing to $^{146}Nd/^{144}Nd$ = 0.7219. Typically, 5–7 blocks of 10x8 sec integrations produced in-run precisions (2SE) of ± 0.0025%. $^{143}Nd/^{144}Nd$ (±2SD) for La Jolla (n=100) is 0.511860 ± 16, BCR-1 (n=7) is 0.512634 ± 18, BHVO1 (n=5) is 0.512989 ± 13. To enable comparison of Sr and Nd isotopic values with the main dataset, $^{87}Sr/^{86}Sr$ data was normalised to NBS987 = 0.710250 (Thirlwall, 1991) and $^{143}Nd/^{144}Nd$ data to La Jolla = 0.511858 (Lugmair & Carlson, 1978).

Stable O isotopes for quartz and plagioclase crystals were analysed at the GNS Science National Isotope Centre (Lower Hutt, New Zealand) on a subset of samples previously analysed for Sr and Nd isotopes. In most cases, individual grains (~1–1.5mg) were analysed, otherwise aggregates of several grains were used. Samples and standards were heated overnight to 200 °C before loading into the vacuum extraction line. Prior to extraction of oxygen from samples, blank BrF_5 runs were done until the yield was < 0.2 µmoles oxygen. Oxygen was extracted from samples by heating with a CO_2-laser in BrF_5 vapour (Sharp, 1990) and converted to CO_2 in a graphite furnace before isotopic analysis on a GVI IsoPrime mass spectrometer. Results are reported in the standard delta permil notation (δ) relative to Vienna Standard Mean Ocean Water (VSMOW), where $\delta^{18}O = ((^{18}O/^{16}O_{sample} - ^{18}O/^{16}O_{VSMOW})/^{18}O/^{16}O_{VSMOW}) \times 1000$. Measured $^{18}O/^{16}O$ isotope ratios of samples were normalised to the international NBS-28 quartz standard using a $\delta^{18}O$ value of +9.58 ‰ (Gonfiantini *et al.*, 1995). Estimates of 2 SD external precision based on four replicate analyses of NBS-28 for each analytical session were usually better than ± 0.2 ‰ (average = ± 0.16 ‰, N=16). A laboratory internal standard (twice per session) with value of +11.4 ‰ was also run in each session and some samples were analysed in duplicate as an additional check. Feldspar samples MRhy32 and MRhy34 had very high $\delta^{18}O$ values so were re-run and calibrated against NBS-28 and SKFS, a chert, with a published value of

+33.93 ‰ (Miller *et al.*, 2020). Replicate analyses conducted on the same sample overlap within error and have been averaged to provide a single value for each geological unit.

$\delta^{18}O_{melt}$ values were estimated using determined $\delta^{18}O_{qtz}$ and $\delta^{18}O_{plag}$ values and $\Delta^{18}O_{qtz\text{-}melt}$ and $\Delta^{18}O_{plag\text{-}melt}$ fractionations calculated using the rhyolite model of Zhao and Zheng (2003) in conjunction with average temperature estimates for each lava and ignimbrite determined in this study (**cf. section 4.6.2 supplementary data table SM4.5**). Median anorthite contents (X_{An}) used in these calculations were obtained from either plagioclase compositions determined in this study (**supplementary data table SM3.7**) or from student theses (Hughes, 1993; Hall, 1994; Whitbread-Edwards, 1994; Hollis, 1995; Cook, 2016) (**supplementary data table SM4.6**). Uncertainties on $\delta^{18}O_{melt}$ estimates were estimated by propagating the 2 SD estimates on mean $\delta^{18}O_{qtz}$ and $\delta^{18}O_{plag}$ values and assuming nominal temperature and X_{An} uncertainties of ± 41°C and ± 10 mol %, respectively.

Mineral compositional data for plagioclase, orthopyroxene and clinopyroxene crystals from the Waitеariki Ignimbrite were obtained using a scanning electron microscope coupled with energy dispersive spectroscopy (SEM-EDS) at the Otago Micro and Nanoscale Imaging Centre at the University of Otago, Dunedin as outlined in **section 3.3** (**supplementary data tables SM3.7** and **SM3.8)**. Hornblende crystal compositional data was obtained over two separate analytical sessions at Victoria University of Wellington and the University of Auckland (**supplementary data table SM3.9)**. Additional compositional data for crystal rim-glass pairs in plagioclase and orthopyroxene used for geothermobarometers was obtained using a JEOL 8530F field emission electron probe microanalyser at the University of Auckland equipped with a time-dependant intensity correction (TDI) system. Accelerating voltage was 15 kV with a beam current and diameter of 20 nA and 1 µm respectively. Analysis totals range from 96.5–100 % with H_20 calculated by difference. Calibration standards include plagioclase (USNM11590), clinopyroxene and VGA-568 (rhyolite glass) and mineral data are presented in **supplementary data table SM4.5**.

4.4 Geochemical characteristics of the TgaVC magmatic system

4.4.1 Major and trace elements

TgaVC lava and pumice whole-rock compositions from the Welcome Bay Ignimbrite are augmented with data from Waitеariki Ignimbrite fiamme (cf. **Section 3.7**, **supplementary data table SM3.6**. Magmas erupted throughout the TgaVC span a broad and almost continuous range from medium-K basaltic andesite to rhyolite and high-K rhyolite (53.76–76.69 wt. % SiO_2; 0.87–4.55 wt. % K_2O; **Fig. 4.2**; Le Maitre, 2002).

In bivariate diagrams, magmas of the TgaVC produce a strong linear trend, with systematic increases of silica and alkali contents (Na_2O and K_2O) with concurrent decreases of compatible elements (Al_2O_3, TiO, Fe_2O_3, MgO, MnO (not shown) and CaO) from mafic to intermediate and felsic lavas and juvenile clasts (**Fig. 4.3**). Major element compositions from individual formations, however, define discrete compositional fields. Lavas from the Otawa Formation are medium-K andesites-dacites (58.38–65.40 wt. % SiO_2) which approach the composition of low-SiO_2 dacitic magmas of the Minden Rhyolite group and the dark coloured pumice of the Welcome Bay Ignimbrite. Minden Rhyolite magmas (MRhy) range from 66.90 wt. % SiO_2 (MRhy57-Kopukairua dacite) to med- to high-K high-SiO_2 rhyolites with the dacites overlapping the compositional range of Waitearikiki (69.79–71.13, average (n=7): 70.48 wt. % SiO_2) and Welcome Bay (69.58–69.62 wt. % SiO_2) ignimbrite rhyodacite magmas (**Fig. 4.3**). The most evolved magmas are found at Mt Maunganui and Waikite which consist of high-K rhyolites (76.33–76.69 wt. % SiO_2; 4.02–4.55 K_2O) with the lowest abundances of Al_2O_3, TiO, Fe_2O_3 and CaO. Key characteristics for each of the volcanic units are summarised in **Table 4.1**.

Trends in trace element compositions mimic those seen in the major elements where relatively strong liquid lines of descent are evident for compatible (e.g. Sr, V) and incompatible (e.g. Rb, Ba, Nb-not shown) elements (**Fig. 4.4**). The prominent linear trends in the classification diagrams are

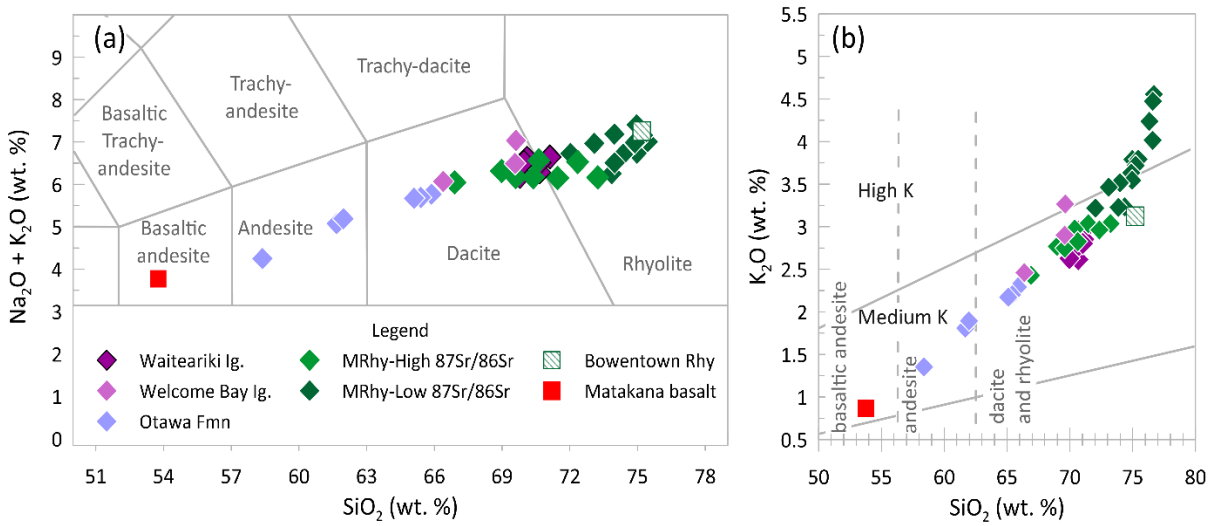

Figure 4.2. Classification diagrams for magmas erupted at domes throughout the Tauranga Volcanic Centre (TgaVC) and the Welcome Bay and Waitearikiki ignimbrites. **(a)** Total alkali verses silica (TAS) diagram and **(b)** subdivision of calc-alkaline rocks using K_2O verses SiO_2 after Le Maitre *et al.* (2002). Dacites and rhyolites of the Minden Rhyolite Formation (MRhy) have been subdivided into "high" and "low" radiogenic Sr. Refer to text for descriptions and discussion. 2σ analytical error calculated from repeat analyses of AGV-2 and RGM-2 standards is smaller than symbol size.

Table 4.1. Summary of the main characteristics of the volcanic units erupted from the Tauranga Volcanic Centre (TgaVC).

Volcanic unit	Description	Composition	Petrography	Age (Ma)
Waiteariki Ignimbrite	Fiamme: pyroclastic deposit	rhyodacite, 69.79–71.13 wt. % SiO_2	Crystal-rich: plag + opx + hbl + qtz	2.18 ± 0.031-2.09 ± 0.029 [1]
Welcome Bay Ignimbrite	Fiamme: pyroclastic deposit	rhyodacite-dacite, 66.38–69.62 wt. % SiO_2	Crystal-rich: plag + opx ± hbl ± qtz	2.31 ± 0.046[1]
Matakana Basalt	Basalt lavas offshore of Matakana Island, Tauranga harbour	basaltic andesite, 53.37 wt. % SiO_2	plag + ol + opx	2.7 ± 0.1[2]
Otawa Formation	Stratovolcano lavas	andesite-dacite, 58.38–65.87 wt. % SiO_2	Crytal-rich: plag + opx + hbl ± cpx	2.95 ± 0.3 – 2.54 ± 0.05[3]
Minden Rhyolite – Low $^{87}Sr/^{86}Sr$	Rhyolitic lavas from western domes: Minden Peak, Manawata, Kaikaikaroro, Kaimai, Mt Maunganui	rhyolite, 72.03–76.69 wt. % SiO_2. $^{87}Sr/^{86}Sr < 0.7058$	Typically, crystal-rich: plag + hbl ± opx ± bt Mt Manganui: crystal-poor	2.87 – 2.16[4]
Minden Rhyolite – high $^{87}Sr/^{86}Sr$	Dacitic-rhyolitic lavas from eastern domes: Mangatawa, Upuhue, Papamoa, Kopukairua, Waitao, Pukanui, Maungatūtū/Mt Misery, Greenpark, Otanewainuku	dacite-rhyolite, 66.90–73.24 wt. % SiO_2. $^{87}Sr/^{86}Sr > 0.7059$	Crystal-rich: plag + hbl + opx ± qtz ± bt	2.69-1.95[4]
Bowentown Rhyolite	Rhyolite lava dome, northern Tauranga harbour	rhyolite, 75.18 wt. % SiO_2.	Crystal-poor: plag + qtz +sa + opx + bt	2.83 ± 0.16[5]

[1] This study
[2] Hollis (1995)
[3] Stipp (1968)
[4] Briggs *et al.* (2005)
[5] Pittari *et al.* (2021)
Mineral abbreviations as follows: plag, plagioclase; hbl, hornblende; opx, orthopyroxene; qtz, quartz; bt, biotite; sa, sanidine.

interjected by strong inflection points in Al_2O_3, MgO, Zr and to a lesser degree Fe_2O_3, V and Ba and reflect changes within the crystallizing assemblage (**Fig. 4.4 b**). Lavas from Pukanui and Greenpark have high concentrations of Zr (226.3 ppm and 225.8 ppm respectively) and relative to all other units within the TgaVC.

Primitive mantle normalised REE and multi-element plots for all TgaVC eruptives are presented in **Figure 4.5**. All samples show near identical REE patterns that demonstrate LREE enrichment with moderately steep LREE-MREE and flat MREE-HREE trends and subdued to moderately negative Eu anomalies (Eu/Eu* ($Eu_N/(Sm_N x Gd_N)^{0.5}$) = 0.47–0.99). Prominent, yet variable negative Ce anomalies (Ce/Ce* ($Ce_N/(La_N x Pr_N)^{0.5}$) = 0.25–0.87) and MREE-HREE enrichment are observed in a number of Minden Rhyolite analyses with a range which exceeds that of the ignimbrites and Otawa Formation.

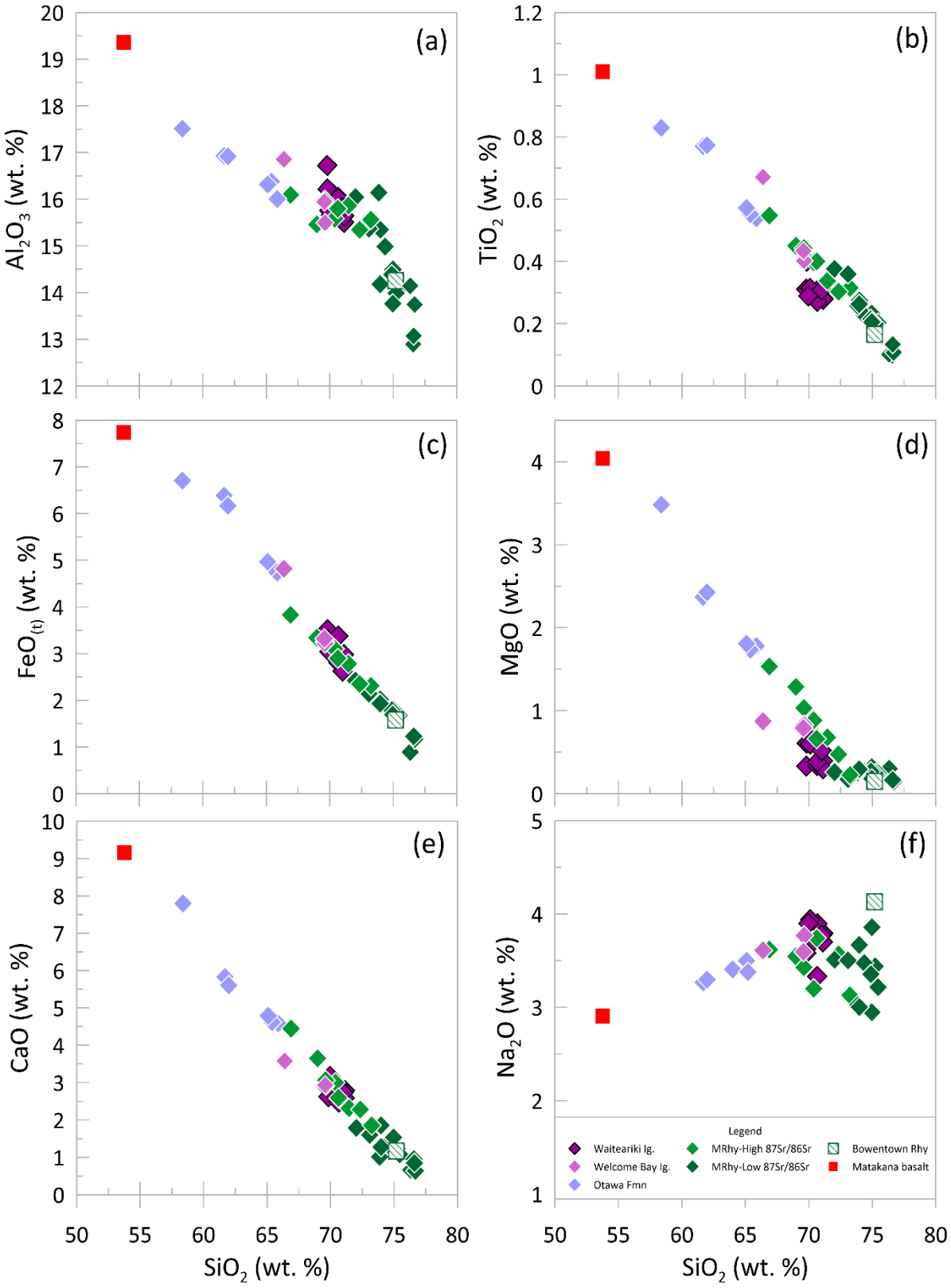

Figure 4.3. Bivariate plots of major element compositions (normalised to 100% volatile free, total iron as Fe_2O_3) verses SiO_2 for the Tauranga Volcanic Centre (TgaVC) lavas and the juvenile clasts from the Welcome Bay and Waitea riki ignimbrites. Analytical error (2σ) calculated from repeat analyses of AGV-2 and RGM-2 standards and is smaller than symbol size.

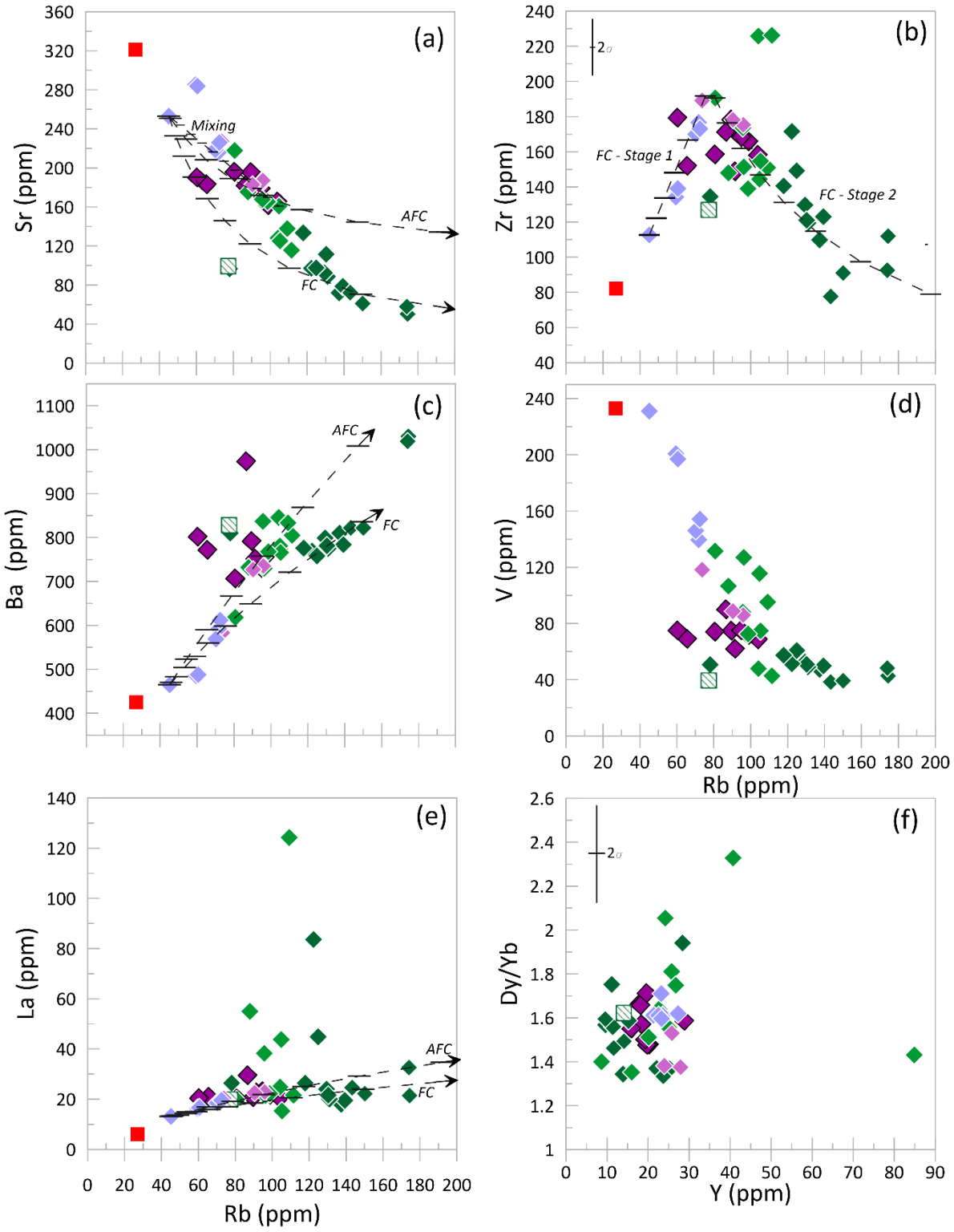

Figure 4.4. Selected bivariate plots of trace element compositions against Rb **(a-e)** and Y **(f)** for Tauranga Volcanic Centre (TgaVC) lavas and the juvenile clasts from the Welcome Bay and Waiteariki ignimbrites. Symbology is as per **Figure 4.3**. Analytical error (2σ) calculated from repeat analyses of AGV-2 and RGM-2 standards and is smaller than symbol size unless shown. Black vectors in **(a), (c)** and **(e)** show fractional crystallisation (FC), assimilation combined with FC (AFC) and mixing models calculated following DePaolo (1981) using Otawa33 and MRhy41 as the mafic and silicic endmember respectively. Tick marks represent 10% crystallisation increments. See text for full details.

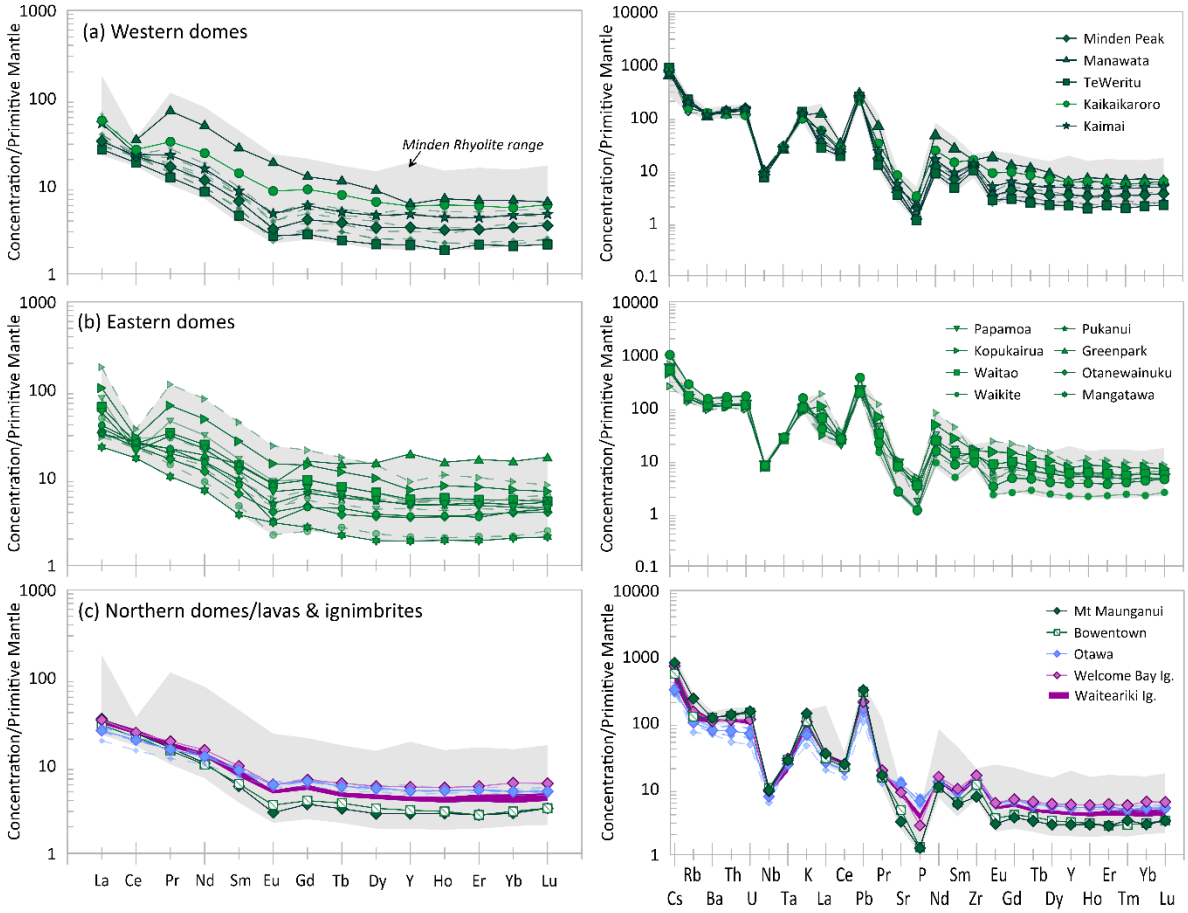

Figure 4.5. Average primitive mantle normalised rare earth element (REE) and multi-element plots for the Tauranga Volcanic Centre (normalising values from Sun & McDonough (1989)). **(a)** Minden Rhyolite eruptives from lava domes west of the Waihou River (cf. **Fig. 4.1**); **(b)** Minden Rhyolite eruptives from eastern lava domes along the Papamoa Range; and **(c)** Otawa Formation, northern domes and ignimbrite juvenile clasts. Grey fields define the total compositional variation for all Minden Rhyolite Subgroup rocks.

These samples represent individual analyses from several separate eruptive centres distributed throughout the TgaVC with low to moderate LOI values (e.g. LOI = 2.45–0.82 %) that are inconsistent with extensive post-depositional weathering. Multi-element diagrams show enrichment in large ion lithophile elements (LILEs) consistent with subduction-related arc magmas and flat high-field strength elements (HFSEs) tends with strong depletions in Nb, Ta, Sr, and P and enrichments of Pb and uniformly strong enrichments of Pb, U, and Th **(Fig. 4.5)**. Multi-element trends are almost identical between the individual formations; however, Otawa Formation lavas show lower normalised abundances of relatively incompatible large iron lithophile (LIL) elements and less pronounced Sr and P anomalies (**Fig. 4.5c**).

4.4.2 Sr, Nd and O isotopic composition of TgaVC magmas

The Sr-Nd and O isotopic compositions of magmas from the TgaVC are summarised in **Figure 4.6** with the data presented in **Table 4.2** (see **supplementary data table SM4.4 and SM4.5** for further details).

4.4.2.1 Sr and Nd isotopes

Radiogenic isotopic ratios show limited compositional diversity with $^{87}Sr/^{86}Sr$ values between 0.706450–0.705373 and $^{143}Nd/^{144}Nd$ from 0.512815 to 0.512544 and forms a coherent inverse correlation that extends from Kermadec and TVZ basalts and overlaps with the isotopic range of silicic

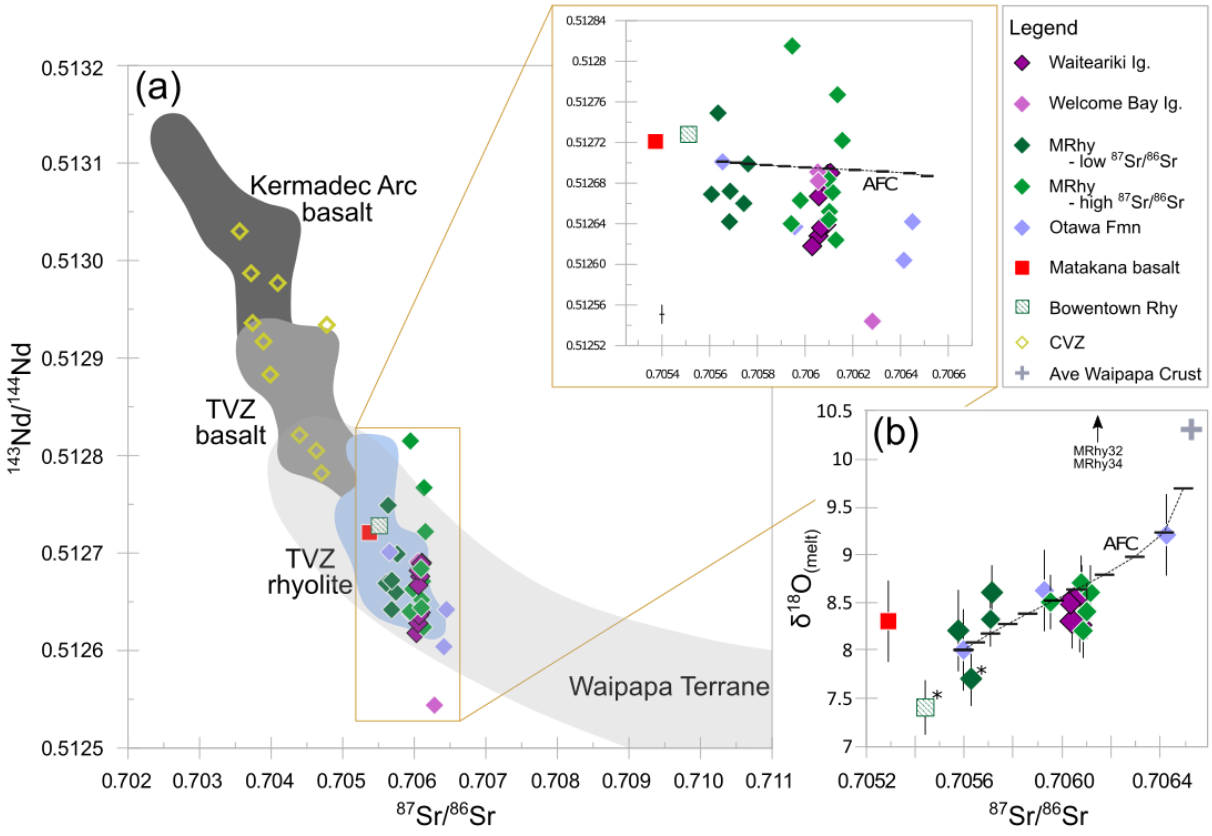

Figure 4.6. Isotope systematics of the Tauranga Volcanic Centre compared to data from Kermadec Arc basalts and TVZ basalts (Gamble *et al.*, 1993; McCulloch *et al.*, 1994) and rhyolites (Briggs *et al.*, 1993; Sutton *et al.*, 1995; Sutton *et al.*, 2000; Bowyer, 2001; Schmitz & Smith, 2004; Wilson *et al.*, 2006; Deering *et al.*, 2008), lavas of the Coromandel Volcanic Zone (Lindsay *et al.*, 1999; Huang *et al.*, 2000) and Waipapa Terrane (Blattner & Bunting, 1980; Blattner & Reid, 1982; McCulloch *et al.*, 1994; Woldemichael, 1998; Price *et al.*, 2015). **(a)** Sr-Nd isotopic array. All data normalised to $^{87}Sr/^{86}Sr = 0.710250$ (NBS987 standard) and $^{143}Nd/^{144}Nd = 0.511858$. **(b)** Oxygen isotope variation of TgaVC magmas in relation to $^{87}Sr/^{86}Sr$. Data points marked with an * are not in isotopic equilibrium and do not provide reliable proxies for melt values. Black vectors show assimilation combined with FC (AFC) models calculated following DePaolo (1981) using Otawa33 and the average Waipapa Terrane values as the mafic and crustal endmembers respectively. Tick marks represent 10% crystallisation increments. See text for full details.

Table 4.2. Sr, Nd and O isotope compositions for Tauranga Volcanic Centre (TgaVC) magmas.

Sample #	Formation	$^{87}Sr/^{86}Sr$	$^{143}Nd/^{144}Nd$	$\delta^{18}O_{(Plag)}$ (‰)	*n*	$\delta^{18}O_{(Qtz)}$ (‰)	*n*	$\delta^{18}O_{(Sa)}$ (‰)	$\delta^{18}O_{(glass)}$ (‰)	$\delta^{18}O_{(melt)}$ (‰)	2σ
WAI16	Waiteariki Ignimbrite	0.706083	0.512676								
WAI22	Waiteariki Ignimbrite	0.706089	0.512639	8.05	*2*	8.84				8.3	0.2
WAI22p	Waiteariki Ignimbrite	0.706106	0.512690								
WAI29	Waiteariki Ignimbrite	0.706060	0.512682	8.4		9.0				8.3	0.2
WAI55	Waiteariki Ignimbrite	0.706056	0.512628	8.3		9.2				8.5	0.2
ES112-165p	Waiteariki Ignimbrite	0.706030	0.512618								
ES112-243p	Waiteariki Ignimbrite	0.706067	0.512636								
ES112-411p	Waiteariki Ignimbrite	0.706058	0.512667								
ES112-501	Waiteariki Ignimbrite	0.706096	0.512689	8.5		9.1			8.7	8.6	0.2
Otawa33	Otawa Formation	0.705654	0.512701	7.5						8.0	0.3
Otawa36	Otawa Formation	0.705957	0.512637	8.1						8.6	0.3
Otawa38	Otawa Formation	0.706414	0.512604	8.7	*2*					9.2	0.3
Otawa39	Otawa Formation	0.706450	0.512642								
MRhy30a	Minden Rhyolite- Maungatūtū/Mt Misery			8.1		9.2				8.5	0.3
MRhy30b	Minden Rhyolite- Maungatūtū/Mt Misery			8.1		8.5				8.5	0.3
MRhy32	Minden Rhyolite- Greenpark	0.706136	0.512767	21.4	*2*						
MRhy34	Minden Rhyolite- Pukanui	0.706156	0.512722	21.9	*2*						
MRhy40	Minden Rhyolite- Kopukairua	0.706115	0.512671	8.3	*2*	9.2				8.7	0.2
MRhy41	Minden Rhyolite- Waitao	0.706095	0.512684	7.9	*2*	8.6	*2*			8.2	0.2
MRhy42	Minden Rhyolite- Mangatawa	0.706102	0.512652	8.1		9.3	*2*			8.6	0.2
MRhy45	Minden Rhyolite- Papamoa	0.706129	0.512624	8.2		9.0				8.5	0.2
MRhy51	Minden Rhyolite- Minden Peak	0.705635	0.512749	7.9		8.7				8.2	0.3
MRhy52	Minden Rhyolite- Kaikaikaroro	0.705946	0.512815								
MRhy53	Minden Rhyolite- Manawata	0.705743	0.512660								
MRhy56	Minden Rhyolite- Otanewainuku	0.705980	0.512663	8.0		9.1				8.4	0.2

Table 4.2. Continued

Sample #	Formation	$^{87}Sr/^{86}Sr$	$^{143}Nd/^{144}Nd$	$\delta^{18}O_{(Plag)}$ (‰)	*n*	$\delta^{18}O_{(Qtz)}$ (‰)	*n*	$\delta^{18}O_{(Sa)}$ (‰)	$\delta^{18}O_{(glass)}$ (‰)	$\delta^{18}O_{(melt)}$ (‰)	2σ
MRhy61	Minden Rhyolite- Mt Maunganui	0.705755	0.512666	8.2		8.8				8.4	0.2
MRhy63	Minden Rhyolite- Kaimai	0.705761	0.512699	8.3		9.1				8.6	0.2
MRhy64	Minden Rhyolite- Kaimai	0.705683	0.512642	7.8		8.0				7.7	0.2
MRhy65	Minden Rhyolite- Bowentown	0.705512	0.512728	7.8		7.3		13.7		7.4	0.2
MB66/H41*	Matakana Basalt	0.705373	0.512721	7.8						8.3	0.3
H41*	Minden Rhyolite-Kopukairua	0.705942	0.512640								
H8*	Minden Rhyolite-Mangatawa	0.706100	0.512644								
M36*	Minden Rhyolite-Minden Peak	0.705608	0.512669								
H37*	Minden Rhyolite-Mt Maunganui	0.705686	0.512672								
L2WP-1	Welcome Bay Ignimbrite	0.706053	0.512691								
L2BP-1	Welcome Bay Ignimbrite	0.706282	0.512544								
L2BP	Welcome Bay Ignimbrite	0.706055	0.512682								

*normalised to $^{87}Sr/^{86}Sr$ NBS987 0.710248 (Thirlwall, 1991) and $^{143}Nd/^{144}Nd$ La Jolla 0.511858 equivalent to JNDi-1 0.512115 (Lugmair and Carlson, 1978)

Plag, plagioclase; *Qtz,* quartz; *Sa,* Sanidine; *n,* number of analyses contributing to average

O isotopes are reported relative to Vienna standard mean ocean water (VSMOW)

rocks erupted from the TVZ and crustal rocks from the Waipapa Terrane (**Fig. 4.6a**). There is no systematic variation of Sr-Nd isotopic ratios with rock-type (following TAS classification), except for the Matakana Basalt which has moderately-high $^{143}Nd/^{144}Nd$ (0.512644) and low $^{87}Sr/^{86}Sr$ (0.705373) relative to other TgaVC magmas. Minden Rhyolite dacites and rhyolites can be subdivided into those which erupted in the eastern half of the centre, that are enriched in radiogenic Sr (e.g. $^{87}Sr/^{86}Sr$ > 0.7059) relative to those erupted in the west ($^{87}Sr/^{86}Sr$ < 0.7058) of the centre. The high-$^{87}Sr/^{86}Sr$ isotopic group mostly overlap with isotopic ratios obtained for rhyodacite juvenile clasts from the Waitearikiand Welcome Bay ignimbrites, but three samples (MRhy32-Greenpark, MRhy34-Pukanui and MRhy52-Kaikaikaroro) have statistically higher $^{143}Nd/^{144}Nd$ values of 0.512767, 0.512722, and 0.512815 respectively (**Fig.4.6 a, Table 4.2**). Sr-Nd isotopic compositions of Otawa Formation andesites and dacites span a more diverse range, particularly for $^{87}Sr/^{86}Sr$ ratios. Andesite and dacite lavas from the western side of the Pāpāmoa Range have Sr-Nd ratios which overlap with those of the low- and high-$^{87}Sr/^{86}Sr$ Minden Rhyolites (Otawa33 – 0.705654; Otawa36 – 0.705957). In contrast, the andesites from the north-east have significantly higher values of 0.706414 (Otawa38) and 0.706450 (Otawa39) which are the highest $^{87}Sr/^{86}Sr$ ratios obtained as part of this study. Other samples that have distinct isotopic compositions include the dark-coloured, dacitic pumice in the Welcome Bay Ignimbrite which has high $^{87}Sr/^{86}Sr$ and low $^{143}Nd/^{144}Nd$ ratios of 0.706282 and 0.512544 respectively, and the Matakana Basalt and Bowentown Rhyolite which have low $^{87}Sr/^{86}Sr$ (0.705373–0.705512) and relatively high $^{143}Nd/^{144}Nd$ (0.512644–0.512728).

4.4.2.2 O isotopes

The O isotope ratios of plagioclase and quartz crystals together with calculated melt compositions are presented in **Table 4.2** and summarised in **Figure 4.7**.

Oxygen isotope values derived from plagioclase crystals range from +7.5– +21.9 ‰ with the majority of samples falling within a 1 ‰ range between +7.8– +8.7 ‰. Highly elevated $\delta^{18}O$ values of +21.4 and +21.9 ‰ were obtained for lavas from Greenpark and Pukanui domes respectively. Additionally, sanidine crystals from Bowentown Rhyolite gave anomalously high values of +13.7 ‰. Quartz crystals from Minden Rhyolite dacites and rhyolites and the Waitearikiignimbrite give $\delta^{18}O$ values that range from +7.3– +9.3 ‰. The lower limits of this range are extended by two relatively low- $\delta^{18}O$ values of +7.3 and +8.0 ‰ obtained for lavas from Bowentown (MRhy65) and Kaimai (MRhy64) domes, respectively.

Where $\delta^{18}O$ values were obtained for both plagioclase and quartz, the isotopic equilibrium of the mineral phases was assessed by comparing the oxygen isotope fractionation factors between quartz

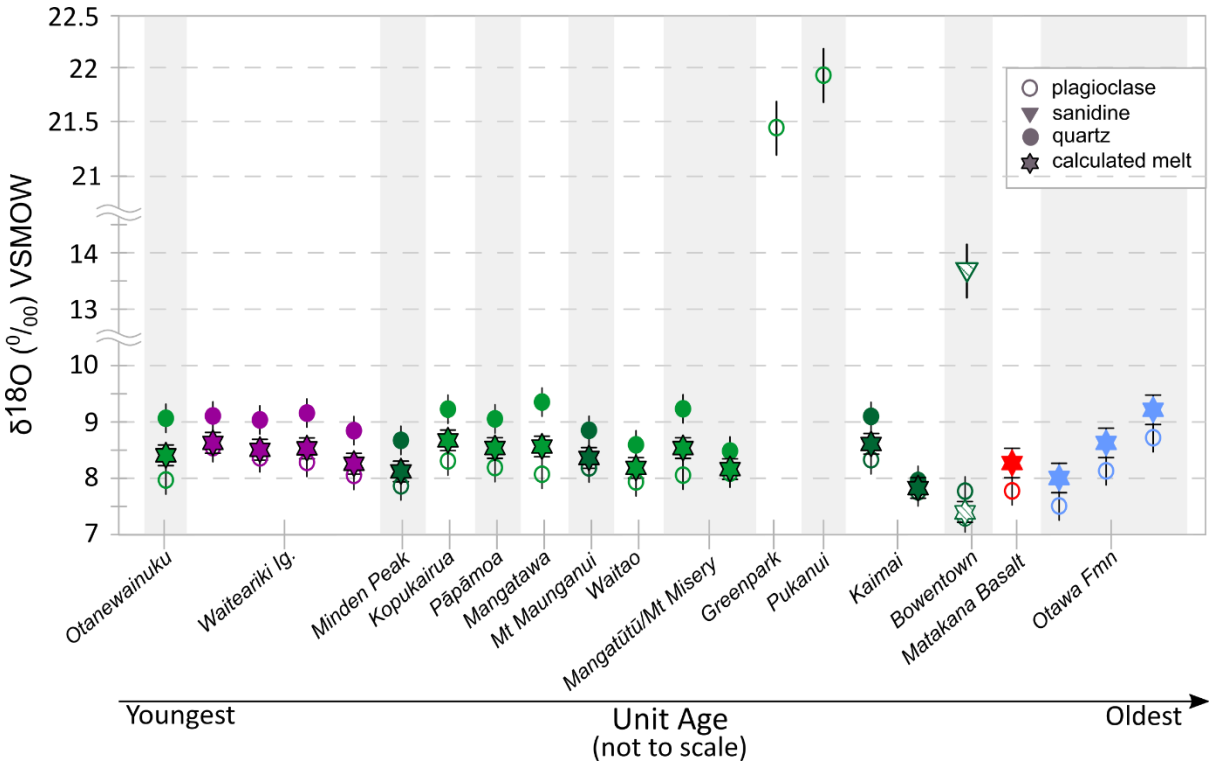

Figure 4.7. Oxygen isotope compositions of phenocrysts from Tauranga Volcanic Centre (TgaVC) lavas and the Waitea riki ignimbrite, and calculated melt compositions. Samples are arranged in order of age with no implied scale. Unit colours as per **Figure 4.6**. Full details are provided in **supplementary data table SM4.5**.

and feldspar ($\Delta_{qtz\text{-}plag}$) calculated in this study (**supplementary data table SM4.5**) to expected values of sodic feldspars ($An_{30–40}$) between 750 and 950 °C (0.88–0.11 ‰; Vho *et al.,* 2019). Generally, the calculated $\Delta_{qtz\text{-}plag}$ fractionation values are within error to that expected for andesine plagioclase crystals and therefore consistent with isotopic equilibrium. Exceptions include the Bowentown Rhyolite (MRhy65) and a second lava analysed from the Kaimai lava dome (MRhy64) which have $\Delta_{qtz\text{-}plag}$ values of -0.5 ± 0.4 ‰ and +0.2 ± 0.4 ‰ respectively. Additionally, for the Bowentown Rhyolite, $\Delta_{qtz\text{-}sa}$ = -6.4 ‰ which is well outside the deviation expected due to isotopic fractionation ($\Delta_{qtz\text{-}sa}$ = +1.02 – 1.25 ‰ between 750 and 950 °C; Vho *et al.,* 2019) and likely a result of post-depositional alteration, consistent with observations during crystal picking.

Calculated $\delta^{18}O_{(melt)}$ values from plagioclase and quartz crystals typically overlapped within error and a weighted average of the values have been used to provide a single representative melt value. Melt values calculated for Bowentown Rhyolite (MRhy65) and a second lava analysed from the Kaimai lava dome (MRhy64) do not provide a reliable proxy for magmatic values as quartz and plagioclase are not in isotopic equilibrium. Calculated equilibrium $\delta^{18}O_{(melt)}$ values for TgaVC lavas fall in a narrowly restricted range of +8.0 to +9.3 ‰ and are high compared to average MORB values (+5.4– +5.9 ‰; Eiler, 2001). There is no correlation with age (**Fig. 4.7**), however, **Figure 4.6 b** demonstrates a

systematic variation where $\delta^{18}O_{(melt)}$ values for the Minden Rhyolites, Waitearikiri Ignimbrite and Otawa Formation are generally positively correlated with $^{87}Sr/^{86}Sr$. The Matakana Basalt is decoupled from this trend and has $\delta^{18}O_{(melt)}$ values comparable to the high-Sr Minden Rhyolite isotopic group yet has the lowest $^{87}Sr/^{86}Sr$ ratio. Two of the low-Sr Minden Rhyolites (Mt Maunganui-MRhy61 and Kaimai-MRhy63) also have high $\delta^{18}O_{(melt)}$ values for their respective $^{87}Sr/^{86}Sr$ ratios.

4.5 Magma differentiation and petrogenetic modelling

Whole-rock major and trace element compositions of TgaVC lavas demonstrate a strong linear correlation with increasing SiO_2 and/or Rb. This linearity may result from mixing of mafic and silicic endmembers, in which the composition of the resulting hybrid magma is related to the proportions of the two endmember magmas:

$$C_{(mix)} = C_aX_a+C_bX_b \quad \text{(Eq. 1)}$$

Where $C_{(mix)}$ is the composition of the hybrid melt, C_a and C_b are the respective mafic and silicic endmembers, and X_a and X_b is the mass fraction of the least and most-evolved endmembers. However, strong inflection points or slightly curved trends and in conjunction with systematic variation in Sr and O isotope compositions, indicates that magmatic differentiation may be dominated by either fractional crystallisation (FC) or assimilation fractional (AFC), or a combination of all the above processes. Below, I present FC and AFC models to assess the relative importance of these processes and the evaluate the amount of crust assimilated by mantle-derived magmas.

4.5.1 Endmember composition

The endmember compositions used in FC, AFC and mixing models are shown in **Table 4.3**. Typically, primitive basalts are preferably chosen as the mafic endmembers for model calculations, however, in continental arcs, truly primitive magmas are rare and most basalts are likely to have had at least some interaction with crustal material (Gamble *et al.*, 1993). Within the TgaVC, basaltic material is sparse, with only a single exposure of basaltic-andesite found in the vicinity of Matakana Island, colloquially referred to as the Matakana Basalt (MB66). The Matakana Basalt, however, is not primitive ($Mg\#_{48}$; $Mg\#= Mg/(Mg+Fe_{(t)})x100$) and is considered a poor choice for petrogenetic modelling as it has a distinct isotopic composition and does not always fit the geochemical trends defined by the other magmas of the TgaVC. We acknowledge the likelihood of a range of possible mantle source compositions for the TgaVC and with this limitation in mind, we have used the least evolved Otawa Formation andesite – MRhy33 ($Mg\#_{48}$) as our starting composition for FC, AFC and mixing models.

Table 4.3. Representative whole-rock major (wt. %), trace element (ppm) compositions and Sr, Nd and O isotopic ratios of endmember magmas used in FC, AFC and mixing models.

	Model end-member data			
	Least-evolved end-member[1]	*Intermediate endmember*[2]	*Crustal end-member*[3]	*Mixing*[1,4]
Major elements (wt. %)				
SiO_2	58.38	66.90	64.17	70.38
TiO_2	0.83	0.55	0.88	0.40
Al_2O_3	17.51	16.09	17.36	15.59
Fe_2O_3	7.45	4.25	6.49	3.45
MnO	0.16	0.08	0.14	0.06
MgO	3.48	1.53	2.10	0.88
CaO	7.80	4.45	1.99	3.00
Na_2O	2.90	3.62	3.85	3.20
K_2O	2.35	2.43	2.82	2.97
P_2O_5	0.14	0.10	0.21	0.07
Mg#	48	42		34
Trace elements (ppm)				
Rb	45.10	80.74	88.50	104.80
Ba	464.70	618.10	708.00	780.80
Sr	253.10	217.80	329.00	160.70
Zr	112.60	190.60	192.00	144.40
La	13.16	19.77	20.95	43.78
Eu	0.95	0.97	1.19	1.41
$^{87}Sr/^{86}Sr$	0.705654		0.706507	0.706095
$^{143}Nd/^{144}Nd$	0.512701		0.512685	0.512684
$\delta^{18}O$	8.0		10.3	8.2

[1] Otawa33 (this study)
[2] MRhy57 (this study). FC models only
[3] Major and trace-element data after Price et al., (2015). Sr and Nd isotope data from Price *et al.*, (2015) and McCulloch *et al.*, (1994). O isotope data from McCulloch *et al.*, (1994), Woldemichael (1998), Blattner & Reid (1982) and Blattner & Bunting (1980)
[4]MRhy41 (this study)

Using an intermediate magma as our starting composition excludes modelling of petrogenetic processes occurring in the lower crust, but is necessary due to the lack of constraints for the composition of mantle source compositions and the degree of partial melting.

With respect to the assimilated crustal endmember, we have adopted a nominal composition for calculation purposes as TgaVC lavas do not typically contain large crustal xenoliths and basement rocks do not crop out within the Tauranga basin. However, surficial Mesozoic greywackes of the Waipapa Composite Terrane are located both to the east and west of the region and are inferred to underlie the volcanogenic sequence at depth (Milicich *et al.*, 2021). Therefore, the composition for the crustal endmember used in our models is an average of the geochemical and isotopic data reported in McCulloch *et al.* (1994) and Price *et al.* (2015).

4.5.2 Role of fractional crystallisation (FC), assimilation-FC (AFC) and mixing

To model FC and AFC processes using trace elements and Sr and O isotopes, I used the classical approaches of Rayleigh crystal fractionation (Shaw, 1970) and mass balance AFC (DePaolo, 1981). This approach was chosen over the energy- and mass-constrained Magma Chamber Simulator (MCS) as the limitations for the MCS include those inherent to rhyolite-MELTS which include the stabilisation of water- bearing minerals (e.g. hornblende) which are important mineral phases in TgaVC lavas and the user input data which covers the initial magma and wall rock compositions, including their water contents which are not yet well constrained for the greater TgaVC. Bulk distribution coefficients (D) were determined based on average modal mineralogy of TgaVC lavas (i.e., 58 % plagioclase, 17 % hornblende, 11 % orthopyroxene, 7 % oxides (magnetite + ilmenite)), and mineral partition coefficients obtained from the Geochemical Earth Reference Model (GERM) database (**supplementary data table SM4.6**). Quartz and biotite only occur as minor components except for the more evolved rhyolitic units and thus are not included here as they appear too late in the crystallisation sequence to significantly influence the overall compositional trends.

The trace element composition of the melt produced from fractional crystallisation (C_l^{FC}) of a more primitive melt is calculated using:

$$C_l^{FC} = C_o F^{D-1} \quad \text{(Eq. 2)}$$

where C_0 is the initial trace element composition of the source rock or melt, D is the bulk partition coefficient and F is defined as the fraction (%) of the initial magma remaining after fractional crystallisation.

For assimilation-fractional crystallisation models, C_l^{AFC} is calculated using:

$$C_l^{AFC} = C_o\left(F^{-z} + \left(\frac{r}{r+D-1}\right)\frac{C_a}{Co}\ (1 - \ F^{-z})\right) \quad \text{(Eq. 3)}$$

where

$$z = \frac{r+D-1}{r-1} \quad \text{(Eq. 4)}$$

and C_a is the concentration of the trace element in the assimilating material. The ratio of assimilated material to crystallized material (r) was varied from 0.2–0.4 until the best fit for the natural dataset was found.

Closed system differentiation processes (e.g. FC) does not change radiogenic isotope ratios of the initial magma, however, open system processes such as assimilation does. Radiogenic isotopic ratios of the differentiated melt can be calculated using:

$$IC_l^{AFC} = \frac{\left(\frac{r}{r-1}\right)\left(\frac{Ca}{z}\right)(1-F^{-z})\,IC_a + C_o F^{-z} IC_o)}{\left(\frac{r}{r-1}\right)\left(\frac{Ca}{z}\right)(1-F^{-z})\,IC_a + C_o F^{-z}} \quad \text{(Eq. 5)}$$

For light stable isotopes such as oxygen ($\delta^{18}O$) of the assimilation-fractional crystallisation δC_l^{AFC} is calculated using:

$$\delta C_l^{AFC} = (\delta C_a - \delta C_o - \frac{\Delta}{r})(1 - F^{-z}) + \delta C_o \quad \text{(Eq. 6)}$$

where it is assumed the D = 1 for $\delta^{18}O$ and δC_o and δC_a is the stable isotope concentration of starting material and assimilated material respectively. The mineral-melt fractionation factor (Δ) is determined by:

$$\Delta = \delta^{18}O_{crystals} - \delta^{18}O_{melt} \quad \text{(Eq. 7)}$$

where $\delta^{18}O_{crystals}$ is determined by the weighted sum fraction that each mineral contributes to the overall normative mineral assemblage (Bindeman, 2008). This study uses an Δ value of 0.1 which is estimated using a weighted average of quartz and plagioclase for $\delta^{18}O_{crystals}$ which are the two most abundant phases for the normative mineral assemblage of the Waiteariki Ignimbrite and lavas of the Minden Rhyolite subgroup.

FC modelling shows that the low-$^{87}Sr/^{86}Sr$ Minden Rhyolites can be produced by 70–80 % crystallisation of an andesitic melt with the composition of Otawa33 (**Fig. 4.4 a,c,e**). This scenario is consistent for all trace elements, except those which partition into zircon (i.e. Zr, U, Th, Dy), which requires a 2-stage model (**Fig. 4.4 b**). During stage 1, Zr is acting as an incompatible element as the zircon is not part of the fractionating mineral assemblage. Zircon saturation is evidenced by the strong inflection point in the Zr versus Rb bivariate plot at ~74 ppm Rb after approximately 48 % crystallisation from the original composition. Sample MRh57 (Kopukairua) was selected to be used as the starting composition for stage 2 as it fell along the FC trend of stage 1 and is one of the least evolved Minden Rhyolites. The model composition matches that of the natural samples after a further 40–50 % crystallisation of the remaining melt (**Fig. 4.4 b**), which equates to ~ 75 % crystallisation of the original melt, consistent with models for elements incompatible with zircon.

The AFC petrological model requires moderate crustal assimilation (r = 0.3) in conjunction with ~ 50 % FC and runs from the composition of the less-evolved intermediate magma (Otawa33) toward more differentiated compositions of the high-$^{87}Sr/^{86}Sr$ Minden Rhyolites, passing through the intermediate compositions of juvenile clasts in the Waiteariki and Welcome Bay ignimbrites (**Fig. 4.4**). This scenario also reproduces the isotopic compositions for these units well (**Fig. 4.6**) and overall, the models reasonably reproduce the analysed dataset. However, the crystal-poor lavas from Mt Maunganui and Waikite do not consistently fit with either model, nor does the rhyolite from Bowentown (**Fig. 4.4 a–**

c,e). Mixing between the starting composition and a magma of the composition of MRhy41 provides a reasonable fit for dacitic Otawa Formation lavas that are adjacent to and underlie Pukanui Dome. The andesites found near Papamoa dome in the northeast have Sr and O isotopic values which are predicted well by the AFC model, however it fails to predict $^{143}Nd/^{144}Nd$ (**Fig. 4.6**).

4.6 Magma storage conditions

To better constrain the relationships between erupted lavas and ignimbrite forming magmas plagioclase-liquid, orthopyroxene-liquid, clinopyroxene and Al-in-hornblende were used to determine pre-eruptive magmatic temperatures and estimates of crystallisation pressures in conjunction with the Waters and Lange (2015) hygrometer and MagmaSat (Ghiorso & Gualda, 2015) to gain an insight into the broad range of magmatic conditions throughout the history of the TgaVC and evolution of the Omanawa caldera. These models were chosen as they cover all dominant mineral phases present in TgaVC lavas and provide multiple independent determinations of the various intensive variables which can be compared.

To assess the crystallisation conditions of the Waiteariki Ignimbrite, a mixture of mineral rim-glass, mineral core-melt inclusion and mineral core and whole-rock compositions were used (**supplementary data files SM3.6–SM3.9**, and **SM4.7**). Mineral data for all other TgaVC lavas were sourced from student theses (Hughes, 1993; Hall, 1994; Whitbread-Edwards, 1994; Hollis, 1995; Cook, 2016) and paired with whole-rock compositions obtained as part of this study. However, it was not always clear in the theses whether the analyses represented mineral cores or rims. For the purposes of this study, it has been assumed that they represent the former, although it is acknowledged that this assumption may not be always correct. As many crystals display disequilibrium textures, the first step is to test for equilibrium between crystals and their carrier melt (for rims) or a hypothetical melt which is assumed to be equivalent in composition to the whole-rock composition of the host magma (Putirka, 2008).

4.6.1 Equilibrium tests

Commonly used tests for mineral-melt equilibrium include the Fe-Mg exchange coefficient ($K_D(Fe\text{-}Mg)_{opx\text{-}liq}$ = 0.29 ± 0.06) for pyroxenes and the Ab-An exchange ($K_D(Ab\text{-}An)_{plag\text{-}liq}$ = 0.1 ± 0.05) for feldspars (Putirka, 2008). It is important to note, however, that the exchange coefficients are highly sensitive to temperature, melt composition and dissolved water content. Thus, I tested for equilibrium of orthopyroxene using K_D = 0.21 ± 0.09 and clinopyroxene using K_D = 0.17 ± 0.09, which have been determined by Rooyakkers *et al.* (2021) using orthopyroxene-liquid and clinopyroxene-

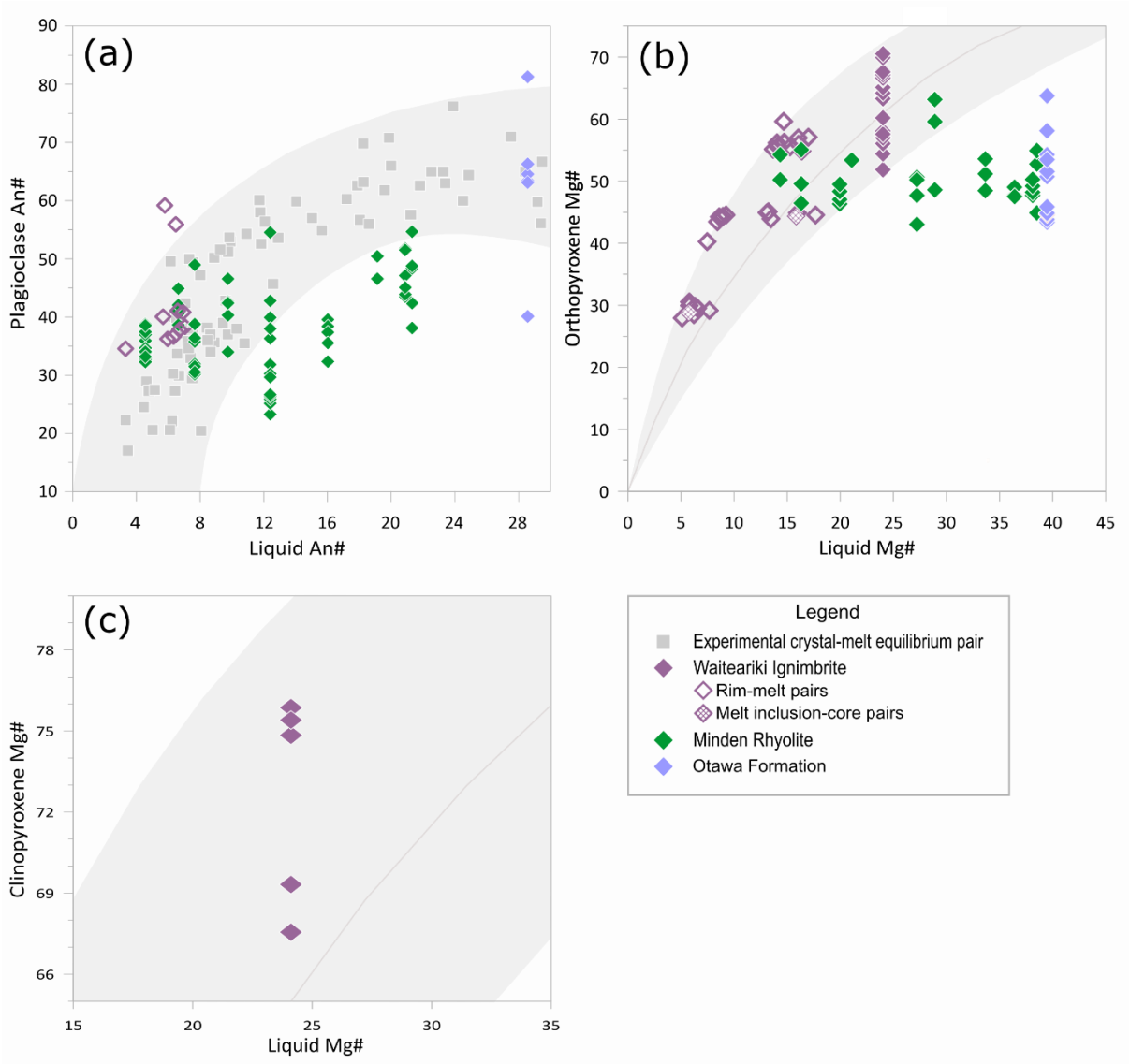

Figure 4.8. Equilibrium tests for **(a)** plagioclase, **(b)** orthopyroxene and **(c)** clinopyroxene phenocrysts within TgaVC lavas and the Waiteariki Ignimbrite. Cores were paired with average whole-rock compositions for their respective unit (TgaVC and Waiteariki Ignimbrite). Additionally, for the Waiteariki Ignimbrite, mineral rims were matched with matrix glass and mineral cores with melt inclusions. Equilibrium plagioclase crystal-melt pairs from phase equilibria experiments on rhyolitic compositions are shown as grey dots. Grey shaded envelopes represent equilibrium ranges of pyroxene compositions for a given melt Mg# assuming $K_D(Fe\text{-}Mg)^{opx\text{-}liq}$ = 0.21 ± 0.09 and $K_D(Fe\text{-}Mg)^{cpx\text{-}liq}$ = 0.17 ± 0.09. For plagioclase the grey envelope encloses all experimental plagioclase-liquid equilibrium pairs (grey squares) used to calibrate the **Waters & Lange (2015)** plagioclase-melt hygrometer.

liquid pairs in phase equilibria experiments of rhyolites with Mg# <20, and are therefore more consistent with matrix glasses and whole-rock compositions analysed in this study **(Fig. 4.8)**. Based on the tests described above, almost all Waiteariki Ignimbrite orthopyroxene core and rim compositions are in equilibrium with average whole-rock and melt compositions (**Fig. 4.8 b**) with ~50 % of crystals for other TgaVC units. The remainder are close to and/or have compositions which are consistent with silicic melts and may represent incorrectly paired rim-whole-rock compositions.

Clinopyroxene crystals have only been identified in the Waitearikí Ignimbrite and are not in textural equilibrium and are thereby considered xenocrystic (cf. **Section 3.6.2**). Notwithstanding, the composition of clinopyroxene cores are appropriate for equilibrium with a melt of equivalent composition to Waitearikí whole-rock samples (**Fig. 4.8 c**).

Due to the high sensitivity of plagioclase to temperature and dissolved water content within a magma, there is a wide range of plagioclase compositions which can crystallise under equilibrium conditions (Waters & Lange, 2015). Thus, plagioclase crystals were tested for equilibrium by comparing the observed compositions to those of plagioclase-melt equilibrium pairs used to calibrate the Waters and Lange (2015) hygrometer (**Fig. 4.8 a**). Matrix glass compositions for lavas of the TgaVC are not available due to pervasive devitrification, so plagioclase compositions have been paired with whole-rock compositions and several crystal compositions are appropriate for a melt of that composition. Similarly to orthopyroxene crystals, an equal amount lie outside the equilibrium range with plagioclase compositions that are too evolved for the hypothetical carrier melt and like non-equilibrium orthopyroxene crystals are likely incorrectly paired rim-whole-rock compositions.

4.6.2 Estimates of temperature and pressure conditions

4.6.2.1 Mineral-based geothermobarometers

The pre-eruptive temperature (T) and pressure conditions (P) for magmas of the TgaVC have been estimated using several geothermobarometers from Putirka (2008): orthopyroxene-liquid (T = Eq. 28a, ± 39 °C; P = Felsic liquid model, ± 1.2 kbar), clinopyroxene-only (T = Eq. 32d, ± 87 °C; P = Eq. 32a, ± 3.1 kbar) and plagioclase-liquid (T = Eq. 24a, ± 36 °C), and the Al-in-amphibole model, Amp-TB2, of Ridolfi (2021). Results of individual geothermometric calculations are presented in **supplementary data table SM4.8** with the results summarised in **Table 4.4**. For each model, a combination of mineral rims-glass, melt inclusion-adjacent crystal (for the Waitearikí Ignimbrite) and mineral core-whole-rock compositions (all units) were paired to give temperature and pressure estimates for all available TgaVC units.

Orthopyroxene phenocrysts in the Waitearikí Ignimbrite record temperatures which fall into two distinct bands that range from ~740–870 °C (opx rim-liquid pairs and opx-melt inclusion pairs) and ~900–990 °C (opx core and whole-rock pairs) (**Fig. 4.9**). Clinopyroxene crystals record much hotter temperatures of 1130–1160 °C. The temperature range for equilibrium orthopyroxene crystals from

Table 4.4. Summary of temperature, pressure, H_2O estimates from mineral geothermobarometers and probable CO_2 range consistent with these estimates determined using Magmasat (Ghiorso & Gualda, 2015).

Volcanic Unit	Temperature (°C)	Pressure (MPa)*	Model	Host mineral	CO_2 ** (ppm)	H_2O (wt. %)
Waitepuna Ignimbrite	740-870	20 ± 120	1	Opx	250-400	2.5-3***
	900-990	130 ± 120	2	Opx	100-400	5.4
	1130-1160	678 ± 310	3	Cpx		
	759-848		4	Plag		
	739-921	95-373	6	Hbl		
Minden Rhyolite Formation lavas						
Minden Peak	838-857	46 ± 120	2	Opx	250-500	
	902-924		5	Plag		3.1
	769-802	116-142	6	Hbl		
Kopukairua	1009-1017		5	Plag		2.6
	768-772	112-118	6	Hbl		
Papamoa	1012		5	Plag		2.5
	755-796	108-140	6	Hbl		
Mangatawa	859-885	53 ± 120	2	Opx	200-350	
	921-941		5	Plag		3.7
	784-801	115-135	6	Hbl		
Mt Maunganui	869-874		5	Plag		3.0
	827	116	6	Hbl		
Kaimai	889	135 ± 120	2	Opx	300-600	
	911-924		5	Plag		3.2
	781	118	6	Hbl		
Kaikaikaroro	1086	494 ± 210	2+	Opx		
	826-879	156-250	6	Hbl		
Upuhue	1050-1051		5	Plag		2.3
	737-786	94-111	6	Hbl		
Waitao	790-794	125-129	6	Hbl		
Bowentown	851-866	38 ± 120	2	Opx	300-500	2.8
	914-922		5	Plag		
Otawa Formation lavas	1054-1058		5	Plag		2.3

* Average of individual determinations and associated model error for models 1-3.
**Estimate from MagmaSat (Ghiorso & Gualda, 2015) which equates to pressure and temperature range of model 1 and 2.
*** H2O estimate from MagmaSat (Ghiorso & Gualda, 2015) which equates to pressure and temperature range of models.
1. Orthopyroxene rim-matrix glass pairs; orthopyroxene-liquid model (T = Eq. 28a, ± 39 °C; P = Felsic liquid model, ± 1.2 kbar), Putirka (2008).
2. Orthopyroxene core-whole-rock pairs; orthopyroxene-liquid model (T = Eq. 28a, ± 39 °C; P = Felsic liquid model, ± 1.2 kbar), Putirka (2008).
2+. Orthopyroxene core-whole-rock pairs; orthopyroxene-liquid model (T = Eq. 28a, ± 39 °C; P = Eq. 29a, ± 2.1 kbar), Putirka (2008).
3. Clinopyroxene core-whole-rock pairs; clinopyroxene-only model (T = Eq. 32d, ± 87 °C; P = Eq. 32a, ± 3.1 kbar), Putirka (2008).
4. Plagioclase rim-matrix glass pairs; plagioclase-liquid model (T = Eq. 24a, ± 36 °C), Putirka (2008).
5. Plagioclase core-whole-rock pairs; plagioclase-liquid model (T = Eq. 24a, ± 36 °C), Putirka (2008).
6. Amp-TB2, Ridolfi (2021). Model errors are: T = 22 °C, P = 18 and 16 MPa for TgaVC lavas and Waitepuna Ignimbrite respectively.

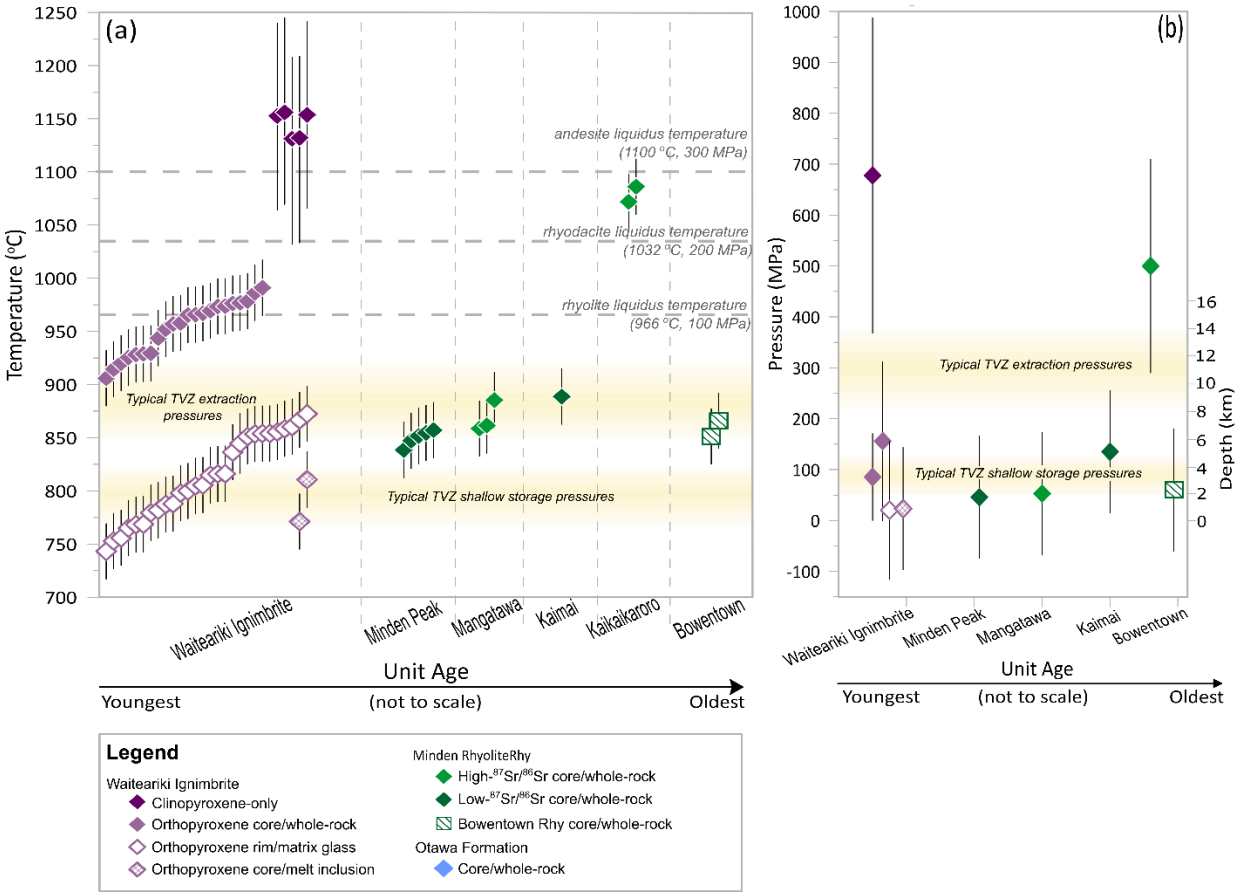

Figure 4.9. Temperature and pressure estimates obtained from orthopyroxene (opx) and clinopyroxene (cpx) phenocrysts from TgaVC lavas and the Waiteariki Ignimbrite using the geothermobarometer of Putirka (2008). Eruptive units are ordered in increasing age (left to right) with individual data points shown in ascending order for ease of visualisation. **(a)** Crystallisation temperature estimates. Error bars represent the quoted standard error of the estimate (SEE) at ± 39 and 58 °C for orthopyroxene-liquid (Eq.28a; **Putirka, 2008**) and clinopyroxene-only (Eq.32d; **Putirka, 2008**) models respectively. Yellow bands represent typical pre-eruptive crystallisation temperatures for TVZ rhyolites from Shane and Smith (2013) and Bégué *et al.* (2014). **(b)** Average crystallisation pressure estimates from pyroxenes using the cpx-only (Eq. 32a) and opx-liquid (felsic) geobarometers with given errors of 310 and 120 MPa for cpx and opx respectively. Liquidus temperatures calculated using rhyolite-MELTS, v1.1 (Gualda *et al.*, 2012). Typical shallow storage and extraction crystallisation pressures for TVZ rhyolites from Gualda *et al.* (2018) are shown for comparison.

Minden Rhyolite lavas span < 100 °C from 840–900 °C and overlaps with and between the two temperature bands determined for Waiteariki crystals. Two equilibrium mineral/whole-rock pairs from Kaikaikaroro gave significantly higher temperature estimates of 1070 °C and 1086 °C.

Individual pressure estimates using the clino- and orthopyroxene barometers have large associated uncertainties (310 and 120 MPa respectively; Putirka 2008) and have been averaged to give a general indication of crystallising pressures. Calculated pressures for the Waiteariki and Minden Rhyolite lavas fall between 50 and 160 MPa, except for the high-temperature crystals from Kaikaikaroro and

clinopyroxene xenocrysts in the Waiteariki Ignimbrite which produced significantly higher pressure estimates of ~500 and 675 MPa (**Fig. 4.9**).

For the plagioclase thermometer, analysis of Waiteariki Ignimbrite plagioclase crystals is restricted to rim-matrix glass pairs and crystal-whole-rock pairs for TgaVC lava. Due to the large range in individual pressure estimates from orthopyroxene crystals (-30–270 MPa) a nominal pressure of equilibration of 1 atm was used, which yields a lower limit for plagioclase-liquid temperatures (Putirka, 2008). Temperature estimates for the Waiteariki Ignimbrite range from 759–848 °C with the majority of individual estimates of ~ 800 °C (**Fig. 4.10**). This is highly comparable with those determined from orthopyroxene rim-matrix glass pairs. Plagioclase crystal-whole-rock pairs for TgaVC lavas span a wider and higher temperature range (869–1045 °C) compared to those determined from orthopyroxene (840–900 °C; **Fig. 4.9**). Generally, western eruptive centres produced slightly lower temperature estimates between 870 and 925 °C, with those in the east returning higher temperature estimates between 920 and 1050 °C which overlap within error of the high-temperature estimates of orthopyroxene from Kaikaikaroro.

Estimates of temperature and pressure were obtained from amphibole crystals using the Al-in-amphibole geothermobarometer model, Amp-TB2 of Ridolfi (2021). Amphibole cores from the Waiteariki Ignimbrite show a mostly continuous range in temperatures and pressures from 737–872 °C and 94–209 MPa (**Fig.4.11 a**; **supplementary data table SM4.8**) with a few sporadic cores extending the range up to a maximum of 920 °C and 372 MPa. Amphibole rims show a similar range in temperature and pressure with the majority of determinations falling between 750–800 °C and 100–150 MPa extending to higher temperatures and pressures that overlap with core determinations. Estimates from Minden Rhyolite amphibole crystals show a similar pre-eruptive temperature and pressure range to the Waiteariki Ignimbrite with higher estimates from crystals in Kaikaikaroro lavas (**Fig. 4.11 b**). Average pre-eruptive temperature and pressure estimates from amphibole crystals are within uncertainty of the those estimated from orthopyroxene and plagioclase.

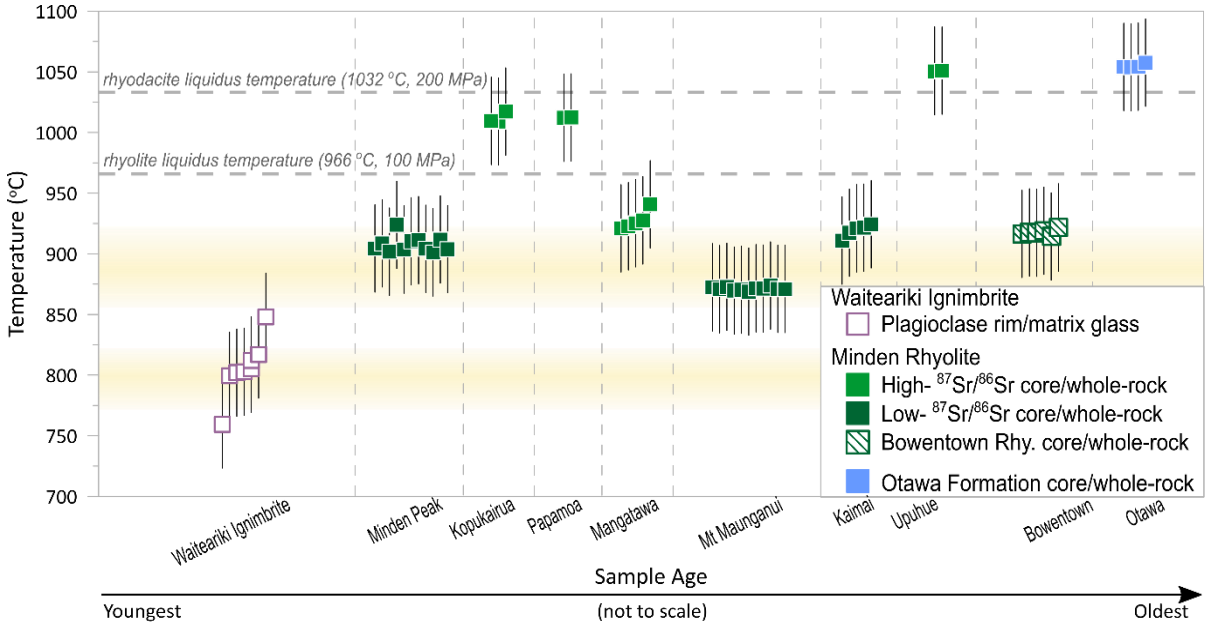

Figure 4.10. Temperature estimates obtained from plagioclase phenocrysts from Tauranga Volcanic Centre (TgaVC) lavas and the Waiteariki Ignimbrite using the geothermobarometer of Putirka (2008). Eruptive units are ordered according in increasing age (left to right). SEE bars are ± 39 °C (Eq. 24a; Putirka, 2008). Liquidus temperatures for plagioclase are calculated using rhyolite-MELTS, v1.1 (Gualda *et al.*, 2012). Yellow bands represent typical pre-eruptive crystallisation temperatures for TVZ rhyolites from Shane and Smith (2013) and Bégué *et al.* (2014).

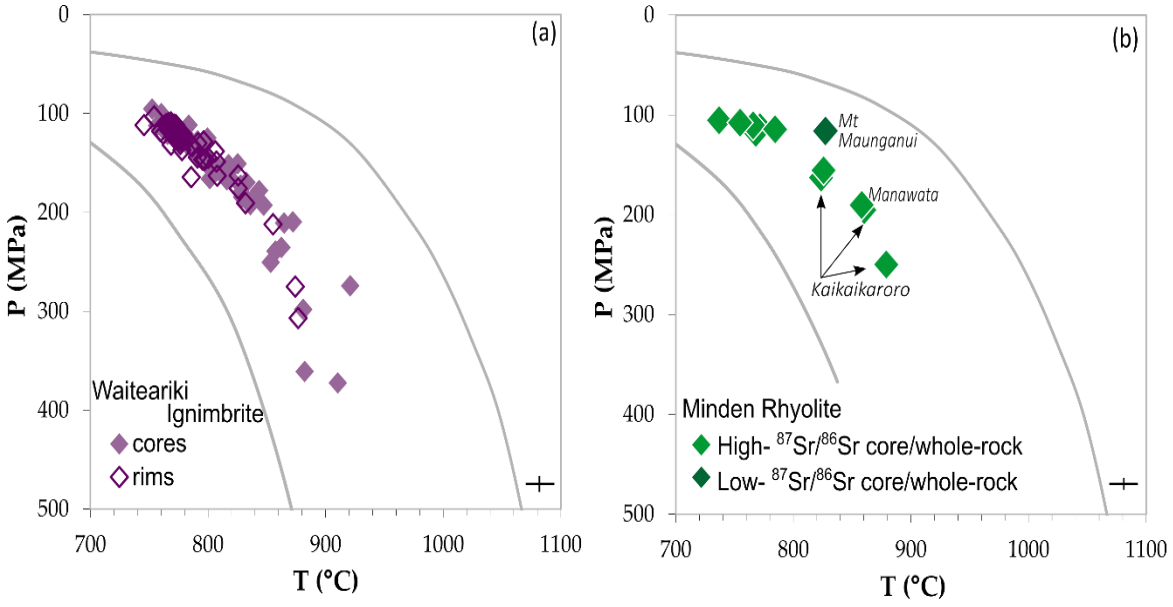

Figure 4.11. Temperature and pressure estimates of amphibole crystals from the Waiteariki Ignimbrite **(a)** and Tauranga Volcanic Centre (TgaVC) lavas **(b)** using the Al-in-amphibole geothermobarometer of Ridolfi (2021). Error bars represent average model errors of 22 °C and 18 and 16 MPa for TgaVC lavas and Waiteariki Ignimbrite, respectively. Individual model estimates and errors are available in **Supplementary data table SM4.8**.

4.6.2.2 Haplogranitic ternary diagram

Projecting glass compositions onto the haplogranitic (quartz-albite-orthoclase) ternary using the projection scheme of Blundy and Cashman (2001) provides crystallisation pressure estimates independent from mineral-based geobarometers (**Fig. 4.12**). Waitearikiri matrix glasses form a tight cluster, particularly so for the high Ba/Sr matrix glass inferred to represent biotite-rich magmas from northern and eastern Minden Rhyolite domes (cf. **Chapter 3**). Projected glass compositions are distributed between pressures of < 50–200 MPa quartz-feldspar cotectic, suggesting crystallisation within that range. The error associated with these pressure estimates is unknown, nonetheless, the distribution of glass compositions in the ternary indicates similar ranges of crystallisation pressures as suggested by the orthopyroxene and amphibole barometers above.

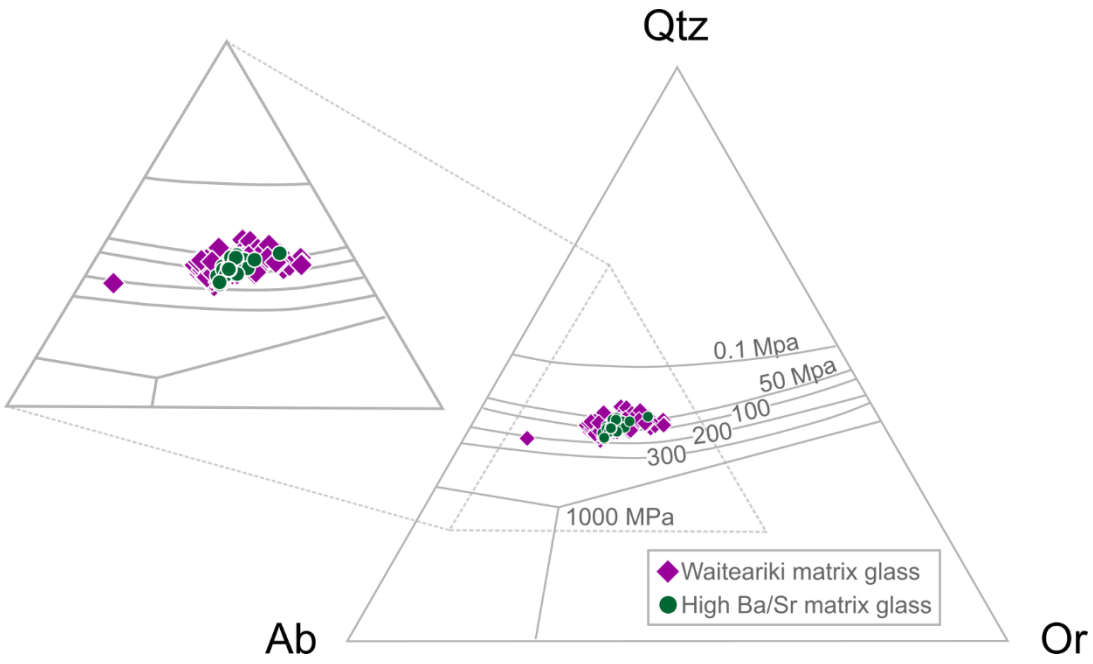

Figure 4.12. Projection of Waitearikiri matrix glass compositions onto the haplogranitic ternary diagram following Blundy and Cashman (2001). Crystallisation pressures of between < 50 and 200 MPa are indicated, consistent with estimates from the mineral-based geobarometers.

4.6.2.3 Rhyolite-MELTS

To further assess magma evolution of the Waitearikiri Ignimbrite, we also conducted crystallisation models in rhyolite-MELTS (v1.1). Models were run from above its liquidus temperature of 1050 °C (liquidus = 1032 °C) to 750 °C, the lowest temperature recorded by our mineral-melt thermometry, with a pressure range of 300 MPa down to 75 MPa with redox constrained by the NNO buffer. In this study we use rhyolite-MELTS in a qualitative capacity, as I acknowledge that the application to hydrous intermediate magma compositions, such as the Waitearikiri Ignimbrite, is limited due to the lack of

appropriate thermodynamic models for hydrous mafic silicates such as amphibole and biotite (Gualda *et al.* 2012). Due to unequivocal evidence of plagioclase-quartz disequilibrium, magma evolution paths were explored using whole-rock compositions rather than matrix glass.

The resulting model indicates plagioclase as the liquidus phase which begins to crystallize at ~1025 °C, followed by orthopyroxene and quartz from 950 °C and 900 °C, respectively (**Fig. 4.13**). Sanidine is not present in the Waiteariki Ignimbrite, but rhyolite-Melts predicts crystallisation to occur from 750 °C, which is below our minimum modelled temperatures and the point of solidus, inferred here to represent > 85 % crystallisation. The simulated evolutionary paths accurately predict the more

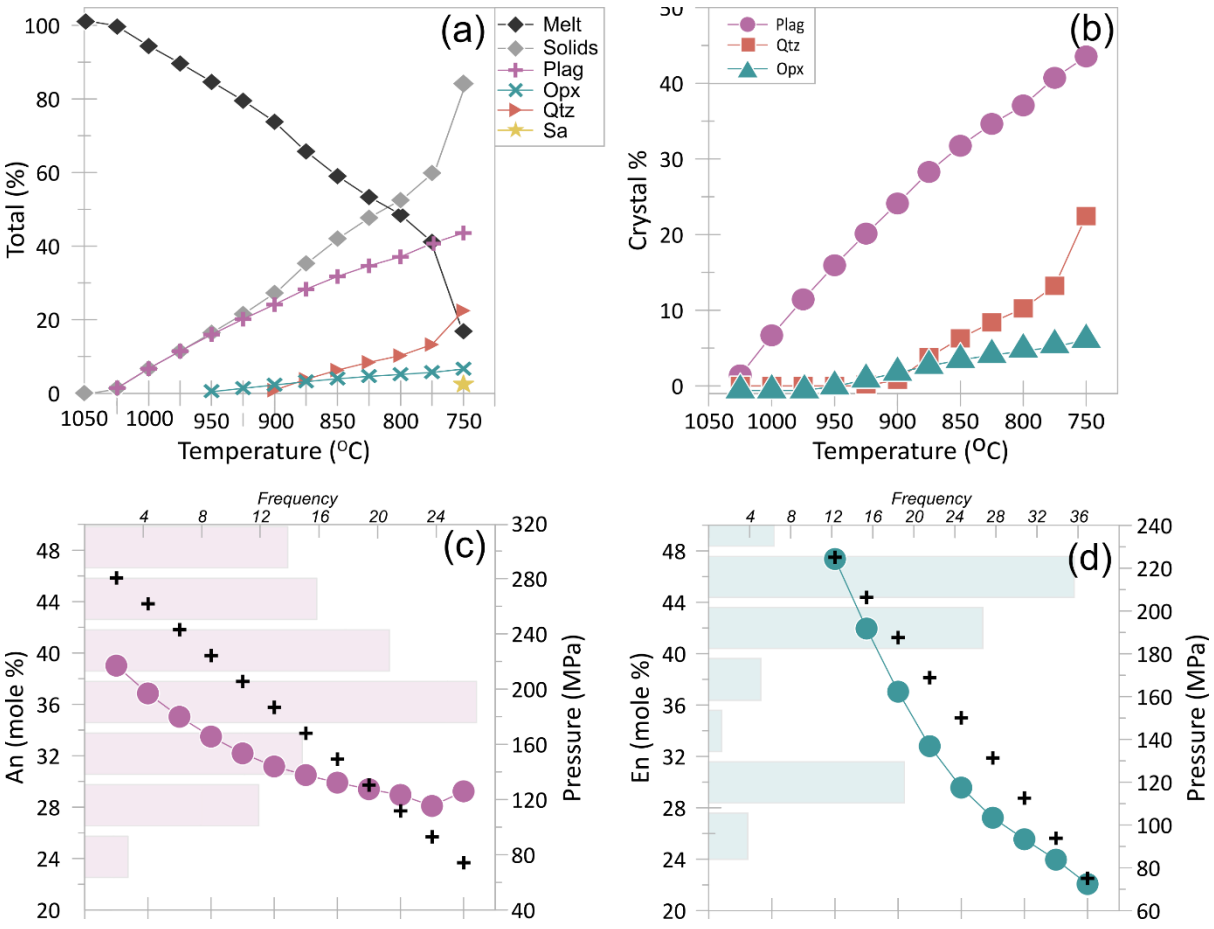

Figure 4.13. Model outputs for a magma with a starting composition equal to average Waiteariki Ignimbrite whole-rock fiamme using rhyolite-MELTS (v1.1) (Gualda *et al.*, 2012). Model temperature ranges were 1050–750 °C and 300–75 MPa, with redox constrained to the NNO buffer. **(a)** Total solids, remaining melt and crystallising phases over the modelled temperature range. **(b)** Phenocrysts phases as a proportion of total solids. **(c)** Predicted plagioclase (An mole %; coloured circles) and **(d)** orthopyroxene (En mole %) compositions for modelled temperature and pressure (black crosses) range. Coloured bars represent compositional histograms for ante- and autocrysts of Waiteariki Ignimbrite (data from Chapter 3; **Supplementary data table SM3.7 and SM3.8**).

evolved range of plagioclase and orthopyroxene compositions found in the natural samples (**Fig. 4.13 c,d**). Plagioclase crystals crystallising from the liquidus to 975 °C have anorthite contents between An_{40} and An_{35} which continue to become more sodic as crystallisation temperature and pressure of the system decreases (**Fig. 4.13 c**). Predicted orthopyroxene crystallising from 950–925 °C have compositions between En_{48} and En_{42} which overlap with a strong peak within the histogram of natural sample compositions. A second peak occurs between En_{32} and En_{28} and the rhyolite-MELTS model suggests that these compositions crystallised between 875 and 825 °C with pressures of 130–100 MPa. The outlined ranges overlap with low- and mid-An plagioclase (**Fig. 3.7**) and orthopyroxene (**Fig. 3.9**) compositions inferred to represent auto- and antecrysts respectively, representing late-stage crystallisation of the Omanawa magmatic system. These temperature and pressure estimates are consistent with mineral-based geothermobarometers and phase-equilibria estimates.

4.6.3 Estimates of H_2O and CO_2

The H_2O content of magmas erupted throughout the TgaVC have not been measured directly and instead have been estimated from thermodynamic calculations. The plagioclase-melt equilibria temperature from Putirka (2008) is pressure sensitive and a nominal values of 1 atm was used for temperature calculations, however, Kilgour *et al.* (2021) demonstrated that pressure has a negligible impact on the hygrometer results. As a comparison, we also employed the plagioclase hygrometer of Waters and Lange (2015). Estimated H_2O contents for the Waitearikí Ignimbrite and lavas of the TgaVC are presented in **Table 4.4** and **Figure 4.14** with the full dataset is available in **supplementary data table SM4.8**.

Using the plagioclase-melt equilibria model of Putirka (2008; Eq. 25b), H_2O contents are estimated to range from 4.0–6.1 wt. % (ave = 4.9 wt. %) for the Waitearikí Ignimbrite, and between 2.1 and 4.0 wt. % (ave = 3.0 wt. %) and 2.5–2.6 wt. % for Minden Rhyolite and Otawa Formation lavas respectively. Estimates using the Waters and Lange (2015) hygrometer are comparable, with formation averages for the Waitearikí Ignimbrite of 5.8 wt. %, Minden Rhyolite lavas of 3.1 wt. %, and 2.0 wt. % for lavas of the Otawa Formation. Generally, the calculated averages of the two models overlap within error, so for our purposes, we conservatively use the average of the two models as our estimated dissolved H_2O estimates.

CO_2 has been estimated using MagmaSat (Ghiorso & Gualda, 2015) with bulk magma compositions taken from the average XRF whole-rock compositions for each volcanic unit (**supplementary data tables**, **SM 3.6** and **SM4.3**), combined with temperature and estimated dissolved H_2O determined by

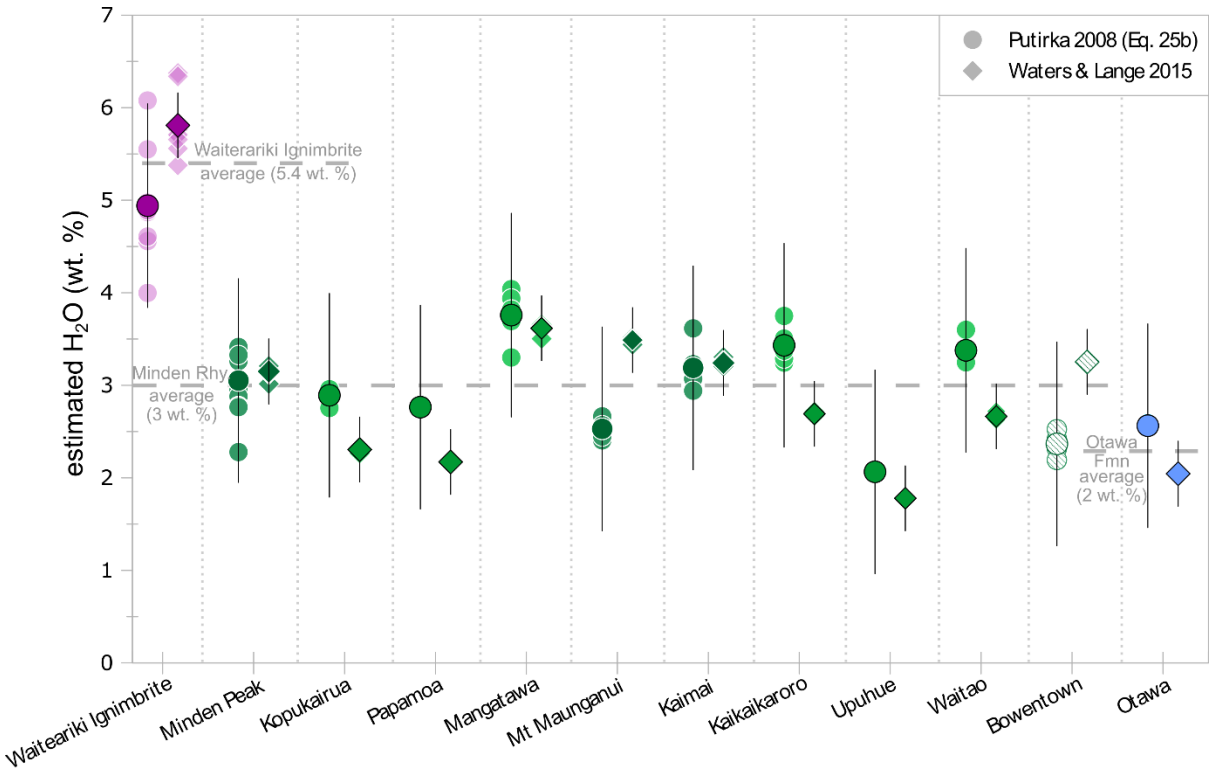

Figure 4.14. Estimates of dissolved H_2O for magmas of the TgaVC and Waitearikl ignimbrite obtained using the plagioclase-melt equilibria temperature model of Putirka (2008) and Waters and Lange (2015) hygrometer. Both models produce average estimates which generally overlap within error. Eruptive unit colours follow classification scheme outlined in **Figs. 4.2-4.6**.

the mineral thermobarometers. CO_2 contents were varied in increments of 50 ppm until estimated pressures were within error bounds of the mineral geobarometers. Model calculations reveal estimated CO_2 contents to range between 100–800 ppm for lavas of the TgaVC with most estimates between 300 and 600 ppm (**Table 4.4**). Due to higher estimated dissolved H_2O contents for the Waitearikl Ignimbrite, CO_2 estimates were expectedly lower which results from the preferential partitioning of CO_2 into a fluid phase, extracting it from the melt (Ghiorso & Gualda, 2015). However, the model suggests that to obtain pressures ~100 MPa consistent with low-pressure estimates obtained from orthopyroxene-rim and matrix glass pairs and Al-in-amphibole geobarometers, H_2O is required to be between 2.5 and 3 wt. %.

4.7 Discussion

4.7.1 Spatial, mineralogical and geochemical relations of silicic dome lavas and voluminous ignimbrites of the TgaVC

Whole-rock major and trace element concentrations of TgaVC lavas and juvenile products from the Waiteariki and Welcome Bay ignimbrites correlate strongly and linearly with each other, yet form discrete yet overlapping compositional groupings between individual formations and Minden Rhyolite subgroups. The most-evolved lavas are those of the Mt Maunganui group (SiO_2 >76 wt. %, Rb > 140 ppm, K_2O >3 wt. %), but also lavas from Waikite of the Mangatawa group. These biotite-bearing lavas have geochemical and mineralogical affinities with the Minden Peak group along with the currently ungrouped Kaimai dome, and with the exception of Waikite, form the prominent northeast lineament north of the Wairoa River (**Fig. 4.1**). All other lavas of the Mangatawa and Maungatūtū/Mt Misery group form a relatively restricted compositional group which overlaps with juvenile products of the Waiteariki and Welcome Bay ignimbrites (**Figs 4.2–4.4**). The high Zr contents of the Maungatūtū/Mt Misery lavas (i.e. Zr >220 ppm; **Fig. 4.4 b**) reflects delayed onset of zircon crystallisation, but otherwise the Maungatūtū/Mt Misery are lavas geochemically and mineralogically similar to other domes located in eastern parts of the TgaVC.

The Sr-Nd array (**Fig. 4.6**) demonstrates that magmas of the TgaVC have an isotopic composition consisting of low $^{143}Nd/^{144}Nd$ (< 0.512820) and high $^{87}Sr/^{86}Sr$ (> 0.705400) consistent with an evolved mantle source or significant crustal contribution to their petrogenesis. TgaVC magmas erupted west and east of the Wairoa River (**Fig. 4.1 b**) and inferred Wairoa/Opuiaki river fault (cf. **section 3.8**), have low- and high-$^{87}Sr/^{86}Sr$ ratios respectively and provides evidence that the petrogenesis and differentiation histories for individual lavas erupted throughout the centre are varied and spatially controlled. Thus, we simplify the Minden Rhyolite classification scheme of Briggs *et al.,* 2005 from the four geochemical groupings of Minden Peak, Mt Maunganui, Mangatawa and Maungatūtū/Mt Misery, to just two, either low- or high-$^{87}Sr/^{86}Sr$ (**Table 4.1**). Low-$^{87}Sr/^{86}Sr$ are defined as lavas with $^{87}Sr/^{86}Sr$ < 0.705800 and include the domes of Mt Maunganui, Minden Peak, Manawata, Kaikaikaroro and Kaimai (i.e. western domes). The high-$^{87}Sr/^{86}Sr$ group includes the domes of Mangatawa, Upuhue, Pāpāmoa, Kopukairua, Waitao, Pukanui, Maungatūtū/Mt Misery, Greenpark and Otanewainuku where $^{87}Sr/^{86}Sr$ ratios are > 0.705900 and are exclusively found east of the Wairoa River. Juvenile products of the Waiteariki Ignimbrite and the white-coloured dacitic pumice of the Welcome Bay ignimbrite, are mineralogically, geochemically and isotopically consistent with the high-$^{87}Sr/^{86}Sr$ Minden Rhyolites, which connects these domes and ignimbrites to the magmatic system underlying the Omanawa Caldera.

Individual lavas of the Otawa Formation demonstrate isotopic and geochemical affinities with the low- or high-$^{87}Sr/^{86}Sr$ Minden Rhyolites (Otawa33 and Otawa36 respectively), indicative of a common petrogenic source and evolution. However, those from the northeast of the Pāpāmoa Range (Otawa38, Otawa39; **Fig. 4.1**) have the highest Sr isotope rations (> 0.706400) and with the dark dacitic juvenile clasts of the Welcome Bay Ignimbrite, represent either crustal melts or higher amounts of crustal assimilation (Winter, 2013). The low $^{143}Nd/^{144}Nd$ ratio of dark dacitic juvenile clasts of the Welcome Bay Ignimbrite (0.512544, ε_{ND} = -1.68; CHUR, 0.512630; Bouvier *et al.,* 2008) is consistent with partial melting of relatively young crustal material, while those of the Otawa Formation have $^{143}Nd/^{144}Nd$ ratios (ε_{ND} = +0.23, Otawa39; ε_{ND} = -0.51, Otawa38), typical of TgaVC magmas and suggestive of crustal assimilation (Winter, 2013) and we explore this further in the following section. Lavas with relatively high $^{143}Nd/^{144}Nd$ (e.g. Kaikaikaroro, 0.512815 and Greenpark, 0.512767) occur sporadically throughout the TgaVC. The Matakana Basalt and Bowentown Rhyolite are generally poorly correlated with the geochemical and isotopic trends defined by the other magmas of the TgaVC and represent discrete melt batches which have evolved independently.

4.7.2 Petrogenesis of TgaVC magmas

The positive correlation between $\delta^{18}O_{(melt)}$ and $^{87}Sr/^{86}Sr$ values (**Fig. 4.6 b**) provides strong evidence of significant crustal contribution of $\delta^{18}O$ enriched Waipapa Terrane crust in conjunction with AFC or FC during upper crustal differentiation of TgaVC intermediate magmas. I reiterate that the petrogenetic modelling of trace elements and isotopes in this study, examines the dominant processes associated with the differentiation of isotopically evolved andesite, and not any potential primitive melts.

For low-$^{87}Sr/^{86}Sr$ Minden Rhyolite magmas erupted west of the Wairoa River, modelling suggests the general geochemical and isotopic composition of these lavas can be produced by 70–80 % crystallisation of an andesitic melt with the composition equal to that of Otawa33. Near-parallel REE patterns (**Fig. 4.5)** and relatively uniform Sr and Nd isotopic compositions are all consistent with protracted fractional crystallisation (Teixeira *et al.*, 2021; Rooyakkers *et al.*, 2022). For Minden Rhyolite lavas in the east of the centre, models suggest moderate crustal assimilation (r = 0.3) in conjunction with ~ 50 % FC is required (**Fig. 4.4**). Consistent with this AFC scenario, Prentice *et al.*, 2022 (**Chapter 2**) identified greywacke-derived zircon xenocrysts (94–300 Ma) within pyroclastic units of the Pāpāmoa Formation and Waiteariki Ignimbrite that attest to significant degrees of melting and disaggregation of the metasedimentary basement.

While the AFC model passes through the compositions of the less-evolved intermediate magma (Otawa33) and the intermediate compositions of juvenile clasts in the Waiteariki and Welcome Bay ignimbrites, simple mixing models between our mafic (Otawa33) and silicic (MRhy41) endmembers

may provide a more geologically plausible explanation for some eruptive units. The Waiteariki Ignimbrite is younger than almost all of the Minden Rhyolite domes and the composition of this magma can be explained by 50–70 % of mixing with a silicic magma with a composition equivalent to MRhy41 (**Fig. 4.4 a**). In contrast, some Otawa Formation dacite lavas only require ~40% mixing between endmembers, however with only a formation-level age constraint, it is uncertain if these magmas are the product of mixing or AFC processes. However, the stratigraphic position of Otawa andesite samples Otawa 35 and 36 suggest that they are older than Pukanui rhyolite lavas and thus AFC as the dominant process is the more realistic.

In reality, the processes that ultimately have given rise to the magmas erupted throughout the TgaVC is undoubtedly more complex than the end-member processes that have been modelled here. The high $^{87}Sr/^{86}Sr$ isotope values and low Mg# of our mafic endmember attests to prior differentiation which cannot be investigated here due to the complete absence of primitive melts erupted within the TgaVC. The modelling process also requires significant assumptions with inherent limitations and thus it is unsurprising that the models do not capture all of the compositional variety observed from the TgaVC (e.g. the most evolved magmas from Mt Manganui and Waikite do not consistently fit either of the models). While the Matakana Basalt and Bowentown Rhyolite magmas have a similar petrogenesis and occur spatially and temporally within the confines of the broader TgaVC, we regard them as discrete batches of melt which have evolved separately, yet their petrogenic relationship to each other remains to be tested. The dark pumice from the Welcome Bay Ignimbrite may represent an isolated crustal melt, but the sparsity of geochemical and isotopic data has precluded modelling at this time. Despite the above limitations, the models provide a simple and realistic explanation for the majority of the observed major, trace element and isotopic compositions within the TgaVC.

4.7.3 Petrological model of a vertically and laterally extensive magma system

Models of volcanic systems that integrate geophysical, geochemical, and petrological information have concluded that magma differentiation beneath arc-related volcanoes likely takes place throughout the crust in transcrustal magma systems (Annen *et al.*, 2006; Cashman *et al.*, 2017; Kennedy *et al.*, 2018; Marxer *et al.*, 2022). Within the TgaVC, there are multiple lines of evidence that suggest this is also the case. The majority of temperature and pressures estimates calculated from geothermobarometry are in the shallow crust (750–900 °C, 0–150 MPa; < 6 km, based on an average crust density of 2700 kg/m^3), but all models indicated that some crystals originated from deeper parts of the magmatic system where pre-eruptive temperatures were up to 1160 °C (**Figs. 4.9**, **4.10**, **4.11**). Calculated pressures from clinopyroxene, orthopyroxene and amphiboles extend to and possibly exceed 500 MPa (**Figs. 4.9**, **4.11**, **4.12**) which likely reflect changes in pressure and associated

crystallisation, recording snapshots of the crystal-rich magma reservoir at depth. The compositional and textural variety observed within erupted crystal cargoes (cf. **Chapter 3**), combined with geochemical evidence for mixing of discrete magma and melt bodies, suggest that broader TgaVC's magmatic system comprises of a crystal-rich mush zone, referred to here as the Omanawa magma body, and multiple additional, variably evolved reservoirs distributed throughout the crust.

A conceptual model illustrating the various processes of magma differentiation for the Omanawa magma body and greater TgaVC is shown in **Fig. 4.15**. In this model, rising hydrous mantle-derived parental basalts stall in the lower crust, undergoing differentiation. Differentiated melts of intermediate composition (plag + opx ± hbl ± cpx) then rise and erupt on the surface forming an andesitic stratovolcano (2.95–2.54 Ma, Stipp, 1968; Otawa Formation). Some magmas are stored in an upper-level magma chamber which assimilates crustal material and undergoes extensive fractional

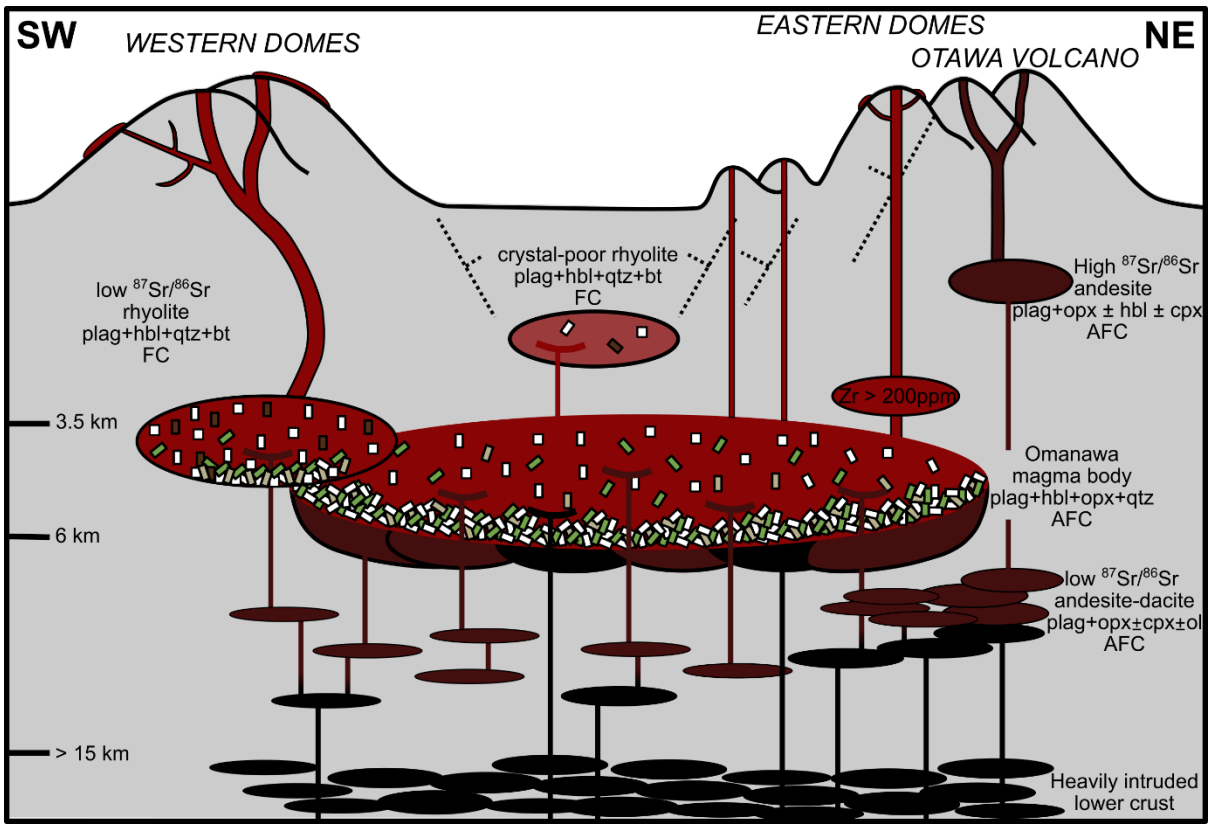

Figure 4.15. Schematic sketch illustrating a general model for magma differentiation within the Tauranga Volcanic Centre proposed in this study. Mantle-derived melts stall in the lower crust with differentiated melts erupting at a long-lived stratovolcano (Otawa Formation). The Omanawa magma body is dominated by crystal mush within the upper crust (3.5-6 km), assimilating greywacke basement material and undergoing fractional crystallisation, and is the main magma source feeding the high-$^{87}Sr/^{86}Sr$ eastern domes. Highly evolved magmas feeding the western and northern domes are are dominated by fractional crystallisation, mostly segregated from the Omanawa magma body. Regional extensional faults act as a pathway for vertical and lateral movement of magmas througout the system and during large eruption events. Plag, plagioclase; hbl, hornblende; opx, orthopyroxene; cpx, clinopyroxene; qtz, quartz; bt, biotite; ol, olivine.

crystallisation to produce the high-$^{87}Sr/^{86}Sr$ andesites erupted in the northeast Pāpāmoa Range. Meanwile, the Omanawa magma body is developing (mineral assembledge: plag + opx + hbl + qtz), differentiating by assimilating the underlying greywacke basement and fractional crystalisation, at depths of ~3.5–6 km. The crystal mush mostly acts as a barrier to more primitive melts which either stall in the roots of the system or mixes with the main magma body during recharge events. Extensive crystalisation generates cumulate residues which are disaggregated and erupted as microcrystalline clots during large eruptions (cf. **Chapter 3**). The magmatic system feeding the western domes was highly evolved (mineral assembledge: plag + hbl + bt + qtz) yet segregated from the main magma body of the Omanawa Caldera and did not incorporate significant proportions of the crust during late-stage differentiation. Limited variation in $^{143}Nd/^{144}Nd$ isotope values across the centre suggests magmas may have been derived from a common source region. Regional extensional faults enabled segregated rhyolitic melt or crystal-rich dacitic-rhyolitic magma from the mush zone to either erupt explosively as caldera-forming pyroclastic density currents from an unknown vent source(s), or travel laterally, degassing on ascent to erupt at the surface producing lava domes. Mixing and/or mingling of these compositionally similar magmas occurred within the conduit during the Waitearikі supereruption, which also drew magma from deeper storage zones (cf. **Section 3.10**).

4.7.4 Comparison to TVZ magmas

4.7.4.1 Radiogenic and stable isotope composition

The Sr-Nd isotopic ratio of rhyolites erupted throughout the TVZ show limited compositional diversity with $^{87}Sr/^{86}Sr$ values between 0.7050 and 0.7063 and $^{143}Nd/^{144}Nd$ from 0.5128–0.5126 (**Fig. 4.6 a**, normalised to NBS987 = 0.710250, $^{87}Sr/^{86}Sr$; Thirlwall, 1991 and La Jolla = 0.511858, $^{143}Nd/^{144}Nd$; Lugmair & Carlson, 1978). The isotopic composition of magmas from the TgaVC overlap with this range, and the high $^{87}Sr/^{86}Sr$ values of the Waitearikі Ignimbrite, Otawa andesites and high-$^{87}Sr/^{86}Sr$ Minden Rhyolites are equivalent to the highest obtained for TVZ rhyolites.

Calculated $\delta^{18}O_{melt}$ values for the TgaVC range from +8.0– +9.3 ‰. Arc-related silicic magmas with $\delta^{18}O_{melt}$ values higher than c. +7 ‰ cannot be derived from closed-system fractional crystallisation of typical mantle-derived melts and require a mass contribution through the assimilation of high-$\delta^{18}O$ crustal sources (Bindeman, 2008). Thus, magmas with $\delta^{18}O_{(melt)}$ values higher than c. +7 ‰, like those of the TgaVC, are typically referred to as "high-$\delta^{18}O$ magmas". High-$\delta^{18}O$ magmas predominate throughout the greater TVZ where calculated $\delta^{18}O_{(melt)}$ values derived from phenocrysts typically range from ~+7.3– +8.0 ‰ with occasional higher-and lower-$\delta^{18}O$ values reflecting additions of either high- (greywacke-derived) or low-$\delta^{18}O$ value (hydrothermally altered) material (Blattner *et al.*, 1996; Rooyakkers *et al.*, 2022). The postive correlation of $\delta^{18}O_{(melt)}$ magmas with $^{87}Sr/^{86}Sr$ (**Fig. 4.6 b**) indicate limited interaction of the underlying magma body with hydrothermally altered chamber roof rocks

within the TgaVC as volcanic activity occurred during the early stages of Taupō rift development (Villamor *et al.*, 2017).

Subtle temporal trends of decreasing $\delta^{18}O$ values over successive eruption events at both Ōkataina and Taupō reflect repeated tapping of magmas from a common upper crustal mush body (Rooyakkers *et al.*, 2022). Temporal variations of this kind are not imediately evident in magmas from the TgaVC (**Fig. 4.7**) and are difficult to test as the high temporal resolution and complementary isotopic data required are not currently available. However, over the entire lifespan of the TVZ, there is a gradual decrease in $\delta^{18}O_{(melt)}$ values through time (**Fig. 4.16 a**) from +9.3– +8.0 ‰ in the TgaVC to +8.4– +7.5 ‰ across young TVZ centres (e.g. Kapenga, Reporoa and Whakamaru; Blattner *et al.,* 1996) to +8.0 to +7.3 ‰ within modern TVZ centres (Rooyakkers *et al.*, 2022). The limited $\delta^{18}O$ data available on lavas from the Coromandel Volcanic Zone (CVZ; Blattner *et al.*, 1996) have a broad range (+7.1– +8.6 ‰) which spans that of the entire TVZ (**Fig. 4.16 b**). Samples are concentrated around Whitianga on the northeastern coast of the Coromandel Peninsula (**Fig. 4.16 c**) and while they cover a wide age range (~7–10 Mya), most have $\delta^{18}O_{(melt)}$ values between +8.1 and +8.6 ‰ and it has been suggested that magmas erupted in the CVZ generally had high-$\delta^{18}O$ values that may have decreased with time (Blattner *et al.,* 1996). However, the scarcity of isotopic data for CVZ magmas prevents any meaningful interpretation of temporal and spatial trends. Duplicate analyses of the Wharepapa and Pumpkin Rock ignimbrites from separate localities (**Fig. 4.16 b, c**) suggest that some relatively low $\delta^{18}O$ values (+7.6 ‰ versus +8.1 ‰, Wharepapa Ignimbrite; +7.1 ‰ versus and +8.3 ‰, Pumpkin Rock Ignimbrite) may represent localised post-depositional isotopic exchange with meteoric water (Berg *et al.*, 2018), rather than primary magmatic values as quartz-plagioclase fractionation is larger than expected ($\Delta_{Qtz\text{-}plag}$ = 1.94; Blattner *et al.,* 1996).

High $\delta^{18}O$ plagioclase crystals

Extraordinarily high (> +20 ‰) $\delta^{18}O$ values were obtained from plagioclase crystals within Pukanui and Greenpark lavas which differ greatly for the regional sample suite and from the TVZ rhyolites in general (**Fig. 4.7**). These dome lavas contain thin (1–2 mm) to coarse (> 10 cm) thick bands which vary in origin from flow-derived concentration of devitrified groundmass, to veins consisting of recrystallised polymorphs of quartz (typically cristobalite) and alkali feldspars (sanidine) (Kinley, 2022). Phenocrysts include plagioclase ± hornblende ± orthopyroxene, but the absence of phenocrystic quartz in lavas that are geochemically classified as rhyolites is unusual. Thus, $\delta^{18}O$ values could only be obtained from plagioclase and while individual crystals were observed as milky during picking, no obvious signs of weathering/alteration were noted (K. Faure, personal communication, 2022).

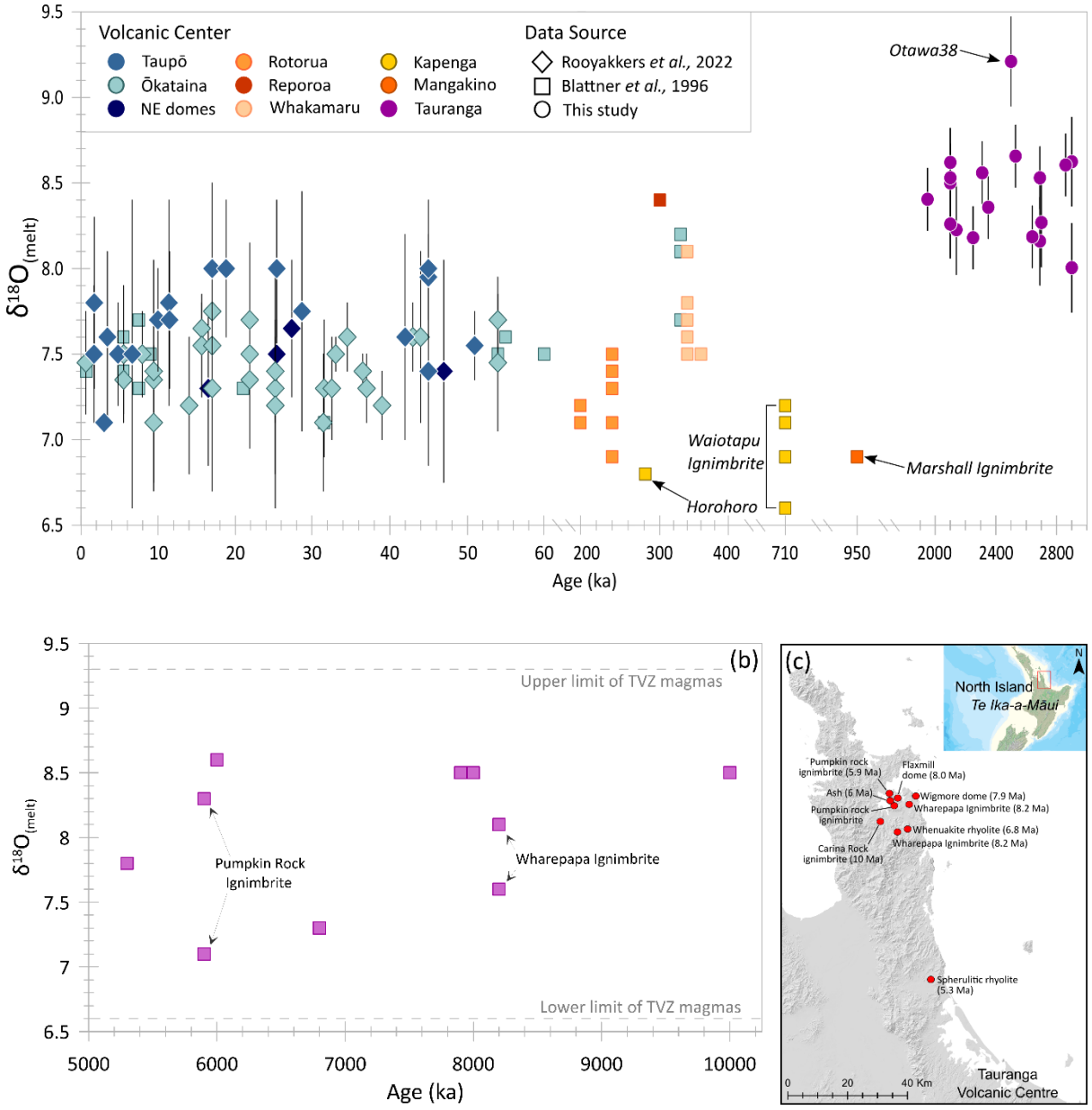

Figure 4.16. Calculated melt $\delta^{18}O$ values versus eruption age for volcanic centres of the **(a)** Taupō Volcanic Zone (TVZ) and **(b)** Coromandel Volcanic Zone (CVZ). Oxygen isotope values and ages taken from Rooyakkers *et al.* (2022), Blattner *et al.* (1996) and this study. Within the TVZ, $\delta^{18}O_{(melt)}$ values generally decrease through time from +9.3– +8.0 ‰ (TgaVC), +8.4– +7.5 ‰ (young TVZ centres) to +8.0– +7.3 ‰ (modern TVZ centres). Higher- and lower-$\delta^{18}O$ values reflect assimilation of either high-(greywacke-derived) or low-$\delta_{18}O$ value (hydrothermally altered) material and are labelled with individual eruptive units for reference. This systematic temporal variation is not evident in $\delta^{18}O$ values derived from phenocrysts in CVZ lava which span the whole range observed throughout the TVZ (+7.1– +8.6 ‰; Blattner *et al.,* 1996). **(c)** Spatial distribution and ages of CVZ samples relative to the TgaVC. Refer to text for discussion.

Mean plagioclase $\delta^{18}O$ values for Pukanui and Greenpark were +21.9 ‰ and +21.4 ‰ respectively. These values are three times higher than typical magmatic $\delta^{18}O_{(plag)}$ values for TVZ eruptives (+6.7 to +7.8 ‰; Rooyakkers *et al.,* 2022) and double that of plagioclase grains that could feasibly be derived

from melting Waipapa basement greywackes (+10.3 ‰, Waipapa Terrane average; Blattner & Bunting, 1980; McCulloch *et al.,* 1994; Woldemichael, 1998). The measured $\delta^{18}O_{(plag)}$ values are remarkably similar and the exceptionally high values exclude a magmatic origin (i.e., crustal melts, xenocrystic grains). Therefore the $\delta^{18}O$ value of these crystals must have been elevated via fluid interactions which have preferentially removed lighter ^{16}O isotopes at both spatially separate (c. 5 km) domes (**Fig. 4.1 b**). Such high $\delta^{18}O$ values are rarely recorded in volcanic rocks, but have been documented in Iceland (Berg *et al.*, 2018). Berg *et al.* (2018) attributed the elevated $\delta^{18}O$ values (+15.5 and +17.6 ‰) to pervasive isotopic exchange with ^{18}O-enriched fluids within a near-surface hot spring enviroment at the distal end of an intra-caldera hydrothermal system, or alternatively, those produced during evaporation and boiling of standing water in caldera lakes.

Extensive quarrying at both domes has altered the original morphology and topography, yet both are inferred to represent vent sites where compositionally similar magma was erupted (Kinley, 2022). The degree of anthropogenic modification makes it difficult to unambiguously attribute the origin of the high- $\delta^{18}O_{(plag)}$ to either of the above processes, as both are plausible with the current data, but we prefer the former. One major deviation from the Iceland lavas, is the Maungatūtū/Mt Misery domes are not intra-caldera domes, but instead segregated melts from the Omanawa magma body (cf. **Section 4.7.1**) that were erupted through and onto the remains of the Otawa stratovolcano, located just northwest of the inferred margin of the Omanawa Caldera (**Fig. 4.1 b**). The presence of accretionary lapilli in the Otawera pyroclastic sequence inferred to be derived from the Pukanui vent (Kinley, 2022), indicates water-magma interaction either through a hot dome-crater lake, or more likely, a shallow hydrothermal system. Maungatūtū/Mt Misery is a substantial sized lava dome (4.8 x 2.5 km; 478 masl) and Pukanui and Greenpark are located on the periphery along an inferred fault which may have acted as a pathway for the same magma to be erupted simultaneously at separate vent sites or deposits may have been displaced by strike-slip fault movements. It is likely that such a substatial dome complex had an active hydrothermal system, and therefore secondary silicification as a result of percolating low-temperature hydrothermal fluids leading to progressive wall-rock isotopic exchange is the most plausible explaination for increasing the $\delta^{18}O$ value of plagioclase crystals.

4.7.4.2 Magma residence depths

The TVZ is world-renown for its exceptional productivity of silicic magmas and caldera densities and is defined as the region enveloping all inferred or known volcanic vents active within the structural boundaries of the Taupo Rift (Wilson & Rowland, 2016). Significant work has been undertaken in recent years to determine the pressure and temperatures under which silicic magma bodies reside in the crust throughout the TVZ (Deering *et al.*, 2011a; Shane & Smith, 2013; Bégué *et al.*, 2014; Cooper & Wilson, 2014; Gualda *et al.*, 2018; Pamukçu *et al.*, 2020). Eruptive deposits of the TVZ typically

record shallow storage depths which range in pressure from ~50–250 MPa, corresponding to an apparent ~2–10 km depth (assuming a crustal density of 2700 kg/km^3). The vast majority fall between 100–150 MPa or ~4–6 km, but some studies demonstrate higher pressures of up to 300 MPa (amphibole geobarometry; Deering *et al.,* 2011a; Shane & Smith, 2013) or 400 MPa (Fe-Ti oxide barometry; Ghiorso & Sack, 1991). Pre-eruptive temperature ranges are typically between 700–900 °C where documented, with most estimates clustering around 775–800 °C, consistent with shallow magma storage in the upper to mid crust. However, subtle yet systematic differences occur among individual volcanoes and even between specific eruptions at some volcanic centres imply that the majority of rhyolitic magma systems in the TVZ have large vertical extents (Gualda *et al.*, 2018; Pamukçu *et al.*, 2020). The H_2O and CO_2 content of rhyolitic TVZ magmas range from 3.0–5.5 wt % and < 300 ppm respectively (Deering *et al.*, 2011b; Bégué *et al.*, 2015; Hughes *et al.*, 2021), with more mafic magmas having much higher CO_2 levels (up to 1000 ppm; Hughes *et al.,* 2021; Kilgour *et al.,* 2021).

Magmas of the TgaVC have intensive parameters that are consistent with that of the broader TVZ. Pressure and temperature estimates of between 50–160 MPa and 740–900 °C indicate magma residence depths around 3.5 to 6 km depth, although higher and lower values in conjunction with mineralogical observations attest to individual magma batches within a vertically extensive magma system. Estimated H_2O and CO_2 contents are also consistent with those of the 'wet' R1 rhyolites of the TVZ, with H_2O contents ranging 1.8–6.6 wt. % and CO_2 between 100 and 600 ppm (Deering *et al.*, 2011b; Bégué *et al.*, 2015).

Thus, residence depths for rhyolitic magmas across the TVZ are remarkably consistent and are some of the shallowest on Earth, believed to be a consequence of the unique rifted arc setting which enhances the accommodation of magmas within the upper crust (Bégué *et al.*, 2014; Wilson & Rowland, 2016). The TgaVC, however, is unique within the TVZ as voluminous silicic volcanism is dominated by crystal-rich rhyodacite magmas (e.g. Waiteariki and Welcome Bay ignimbrites), rather than crystal-poor rhyolitic melts. The low- and high-$^{87}Sr/^{86}Sr$ groups of Minden Rhyolite lavas and ignimbrite juvenile products are relatively geochemically homogenous over a period of several hundred thousand years, and geothermobarometry results indicate there is no discernible difference between the residence depths for the two groups, or that of the wider TVZ. Such monotonous systems consisting of magmas with crystal contents of 55–65 % (which is close to the maximum phenocryst content in Waiteariki Ignimbrite fiamme of up to 50 %) undergo continuous replenishment by magma inputs of a broadly similar composition, and settle into a 'petrological trap' where they change little in physical and chemical properties over time (Caricchi & Blundy, 2015). The thicker, less-rifted crust, has suppressed the segregation of crystal-poor melts with the TgaVC and erupted magmas have been

derived directly from the main mush body assisted by regional structural faults associated with the fledgling Taupō rift. Rare crystal-rich Ongatiti, Whakamaru (Brown *et al.*, 1998a; Cooper & Wilson, 2014) and Rotoiti (Burt *et al.*, 1998) ignimbrites, plutonic xenoliths (Brown *et al.*, 1998b) and crystal inheritance (Cooper *et al.*, 2016; Barker *et al.*, 2021) attest to the presence and regeneration of such crystal mush zones in subsequent TVZ volcanic centres and while, undoubtably, shallow crustal differentiation and storage of magmas across the TVZ are unique to each individual centres, magmas have broadly resided under near-identical conditions over the lifespan of the TVZ (~2.4 Ma).

4.8 Summary and Conclusions

The Tauranga Volcanic Centre (TgaVC) located in the western Bay of Plenty of the North Island, New Zealand is the first silicic centre associated with the opening of the Taupō rift, and as such represents early TVZ volcanism. The TgaVC provides an excellent opportunity to examine the repeated eruption of rare TVZ crystal-rich magmas over a protracted time period (c. 1 Myr) which has provided important insights into early voluminous silicic activity occurring from 2.4–2 Ma at the dawn of the TVZ.

It has been demonstrated that magmas erupted across the TgaVC are relatively homogenous with a consistent mineral assemblage of plagioclase ± hornblende ± orthopyroxene, quartz ± biotite. Individual lavas of the Minden Rhyolite Subgroup can be grouped into either low- or high-$^{87}Sr/^{86}Sr$ magmas, with the low-$^{87}Sr/^{86}Sr$ defined as lavas with $^{87}Sr/^{86}Sr < 0.705800$ and include the domes of Mt Maunganui, Minden Peak, Manawata, Kaikaikaroro and Kaimai (i.e. western domes). The high-$^{87}Sr/^{86}Sr$ group includes the domes of Mangatawa, Upuhue, Pāpāmoa, Kopukairua, Waitao, Pukanui, Maungatūtū/Mt Misery, Greenpark and Otanewainuku where $^{87}Sr/^{86}Sr$ ratios are > 0.705900 and were exclusively erupted east of the Wairoa River. Juvenile products of the Waitetariki Ignimbrite and the white-coloured dacitic pumice of the Welcome Bay ignimbrite, are mineralogically, geochemically and isotopically consistent with the high-$^{87}Sr/^{86}Sr$ Minden Rhyolites and connects these domes to the magmatic system underlying the Omanawa Caldera. Nd and Sr isotopic values across the TgaVC are comparable to those of the broader TVZ with relatively low $^{143}Nd/^{144}Nd$ (0.512815–0.512544) and high $^{87}Sr/^{86}Sr$ (0.706450–0.705373).

Calculated $\delta^{18}O_{melt}$ values for the TgaVC range from +8.0– +9.3 ‰ and while there is limited variability and no evident temporal variations throughout the TgaVC, there is a subtle temporal trend of decreasing $\delta^{18}O$ values through time in the TVZ as a whole. CVZ magmas appear to have $\delta^{18}O$ values similar to those observed at the TgaVC, but temporal trends cannot be ascertained with the available data. The exceptionally high $\delta^{18}O$ plagioclase values at Pukanui and Greenpark may be the result of

secondary silicification due to perculating low-temperature hydrothermal fluids and progressive wall-rock isotopic exchange.

Geochemical modelling and geothermobarometry of crystals in TgaVC magmas indicate crystallisation and storage within the mid- to shallow crust (c. 3.5–6 km depth) between 50–160 MPa and 740–900 °C, forming part of a vertically and laterally extensive magma system. The Omanawa magma body consisted of a geochemically and isotopically well-mixed mush that was fed by mafic inputs from a common source region. Subsequent differentiation was either dominated by FC (i.e western domes) or AFC followed by mixing of magmas (eastern domes). Limited segregated melts have unique late-stage differentiation histories. Comparison to the broader TVZ demonstrates magmas have broadly resided under near-identical, shallow conditions over the lifespan of the TVZ (~2.4 Ma).

CHAPTER 5:

5 Synthesis and Conclusions

5.1 Key findings

The research has documented many previously unknown aspects in regards to the temporal and magmatic evolution and scale of volcanism of Tauranga Volcanic Centre (TgaVC). **Chapter 2** used major and trace element geochemistry of glass in conjunction with U-Pb dating of zircons to confirm previously postulated links between proximal ignimbrites of the TgaVC and age-equivalent tephra deposits in northern Hawke's Bay. The Esk Mst-T1 (correlative to Arateka ignimbrite) and Esk Mst-T2 tephra provide the first radiometric age constraints (2.2 Ma) for the lower Esk Mudstone Formation, and a robust isochron for the wider region. The correlation between the Hikuroa Pumice Member and the Waitearikí Ignimbrite indicate that silicic volcanism of the TgaVC was more extensive than previously recognised. This research has made significant advances towards establishing an eruptive stratigraphy for ignimbrite units of the TgaVC and highlights that rhyolitic activity was frequent with at least eight eruptions occurring between 2.4 and 2 Ma, culminating with the eruption of the very large-volume Waitearikí Ignimbrite. This record provides a maximum mean repose period for the TgaVC of ca. 50 kyrs.

The confirmation of distal Waitearikí Ignimbrite deposits 150–170 km southeast from the southern-most proximal exposures, confirmed previous inferences that the eruption of the Waitearikí Ignimbrite was a significant large-scale silicic event. This was explored further in **Chapter 3** where the eruptive volume of the Waitearikí Ignimbrite was calculated to be c. 1500 km^3, equivalent to 870 ± 87 km^3 of erupted magma. This magnitude 8 (M8; Crosweller *et al.,* 2012) eruption is classified as a super caldera-forming ignimbrite (Giordano & Cas, 2021), more commonly referred to as a supereruption. The ignimbrite is inferred to have erupted from a diffuse source within the newly defined Omanawa Caldera situated at the southern end of an asymmetrical rifted graben underlying the northern Mamaku Plateau. As volcanism associated with the Omanawa Caldera and the broader TgaVC occurred within the defined structural boundaries of the Taupō Rift, volcanism of the TgaVC is regarded here to represent the first silicic system of the Taupō Volcanic Zone (TVZ).

The composition of the Waitearikí Ignimbrite is homogenous, with a consistent mineralogical assemblage and restricted ranges in whole-rock and matrix glass compositions that lack compositional gradients. Such "monotonous intermediate" ignimbrites are relatively common globally but unique within the history of the TVZ that is dominated by high-silica, crystal-poor rhyolitic magmas. It is inferred here, that crustal rifting led to a deep-seated failure of the underlying magma reservoir causing rapid decompression and large-scale evacuation of the Omanawa magmatic system and I

propose a similar mechanism to explain the rare occurrence of other crystal-rich ignimbrites of the TVZ.

Chapter 4, shifts the focus from the Waiteariki Ignimbrite to the wider TgaVC and the numerous and varied lavas erupted over time. The whole-rock major and trace element and mineral geochemical dataset of **Chapter 3** is augmented with analyses of lavas from TgaVC lavas and Sr, Nd and O isotopes. In this chapter I investigate the spatial, geochemical and petrogenetic relationships of the TgaVC magmas and their pre-eruptive storage conditions.

Individual lavas of the Minden Rhyolite Subgroup of the TgaVC can be grouped into either low- and high-$^{87}Sr/^{86}Sr$ magmas exclusively erupted in the west and east, respectively. Juvenile products within the Waiteariki and Welcome Bay ignimbrites are mineralogically, geochemically, and isotopically consistent with the high-$^{87}Sr/^{86}Sr$ Minden Rhyolites, which connects these domes to the magmatic system underlying the Omanawa Caldera (the Omanawa magma body). Nd and Sr isotopic values across the TgaVC are comparable to those of the broader TVZ. Calculated $\delta^{18}O_{melt}$ values for the TgaVC magmas indicate a temporal trend of decreasing $\delta^{18}O$ values in the TVZ through time. CVZ magmas appear to have $\delta^{18}O$ values similar to those observed at the TgaVC, but temporal trends cannot be ascertained with the data presently available.

Geothermobarometry indicate crystallisation and storage occurred within the mid- to shallow crust (c. 3.5–6 km depth) between 50–160 MPa and 740–900 °C. Upper crustal differentiation was dominated by FC (i.e western domes) or AFC followed by mixing of magmas (Omanawa magma body and eastern domes). Segregated melts (e.g. Bowentown, Mt Maunganui, Maungatūtū/Mt Misery) have unique late-stage differentiation histories. Comparison to the broader TVZ demonstrates magmas have broadly resided under near-identical, shallow conditions over the lifespan of the TVZ (~2.4 Ma).

Below, I revisit the key research questions raised in the introduction chapter (**Section 1.2**) and outline how this research has answered them and advanced the understanding of silicic volcanism in Aotearoa New Zealand at the transition between CVZ and TVZ volcanism.

5.1.1 Frequency and distribution of silicic volcanism within the Tauranga Volcanic Centre

This study demonstrates the importance of combining proximal and distal records in reconstructing the early eruptive histories of active volcanic regions. However, reconstructing the eruptive histories of individual volcanoes or volcanic centres such as the TgaVC is challenging as proximal records are often incomplete due to burial or destruction by subsequent volcanic activity and/or tectonism and

by the preferential erosion of unconsolidated pyroclastic deposits over resistant welded ignimbrites and lavas. Medial to distal tephra archives can help to fill key gaps, but it can be difficult to make robust correlations. The approach used in this study was multi-faceted and incorporated tephrostratigraphy with radiometric dating (U-Pb zircon ages) in conjunction with major and trace element geochemistry (**Chapter 2**). The newly-established correlation between the Hikuroa Pumice Member and Waiteariki Ignimbrite provided, for the first time, evidence that silicic volcanism within the TgaVC was much more voluminous and extensive than previously recognised, and may rival that of the super-volcanic systems of the TVZ (e.g. Taupō, Whakamaru, Mangakino). Volcanism was also frequent, with at least eight eruptions occurring within TgaVC between 2.4 and 2 Ma, culminating with the Waiteariki super-eruption. At least four ignimbrite eruptions (Welcome Bay, Wharo, Otawera, and Arateka ignimbrites) occurred within c. 90 kyrs between 2.3 and 2.2 Ma (**Fig. 2.8**), and this period may represent an early ignimbrite flare-up event, similar to those described for the TVZ (Gravley *et al.*, 2016). This study acts as a case study on how combined proximal and distal volcanic records allow advances in the understanding of eruptive histories for long-lived silicic systems. While common within young volcanic systems, detailed eruptive histories of older systems are rare, and this study makes significant advances towards a comprehensive stratigraphic record for the TgaVC. These findings also allow the transition of volcanic activity from the previously active CVZ to the TVZ to be reassessed and have implications for our understanding of the onset of large-volume rhyolitic activity during the Early Quaternary at the dawn of the TVZ, some of which are addressed within this thesis.

5.1.2 Waiteariki Ignimbrite: eruptive volume, source, and physical and chemical characteristics

The eruptive volume of the Waiteariki Ignimbrite is calculated to be c. 1500 km^3, equivalent to 870 ± 87 km^3 of erupted magma which is inferred to have erupted from the Omanawa Caldera (**Chapter 3**). The Omanawa Caldera is identified on the basis of ignimbrite thickness variations, textural features and the presence of silicic lava domes in association with a prominent negative gravity anomaly underlying the northern Mamaku Plateau. Topographic evidence for the caldera is ambiguous due to subsequent burial by younger, widespread ignimbrites originating from the young TVZ, but faults displacing the Waiteariki Ignimbrite within the upper reaches of the Opuiaki and Mangapapa rivers (cf. **Fig. 3.2**) may represent northern ring faults that were reactivated sometime after ignimbrite emplacement.

The Waiteariki Ignimbrite is the only known example of a monotonous intermediate type ignimbrite within Aotearoa New Zealand. This crystal-rich (37 %), rhyodacite (ave. 70.7 wt. % SiO_2) ignimbrite is characterised by a consistent mineralogical assemblage of plagioclase, hornblende, pyroxene, quartz ± biotite and accessory Fe-oxides, zircon and apatite; restricted ranges in whole-rock geochemistry

and matrix glass compositions; and the complete absence of compositional gradients and a precursory Plinian phase. It is subdivided into two eruptive units (Eu I and Eu II; **Fig. 3.4**), where the volumetrically minor Eu II deposits are distinguished from Eu I by the presence of large lithic clasts of recycled Waitearikí Ignimbrite and the general presence of trace amounts of biotite in juvenile clasts. Juvenile clast textures vary but are dominated by dense fiamme, however, poorly vesicular sub-rounded, fibrous and vapour phase altered pumices are present in the upper 20 m of Eu I deposits. Abundances of juvenile clasts range between 5–24 % with an average of 15 %.

In contrast to this macro-scale homogeneity, textural and chemical variations within individual crystals of plagioclase, orthopyroxene and amphibole, suggest a complex and dynamic magmatic system. Plagioclase and orthopyroxene crystals exhibit very broad compositional ranges, ($An_{22–78}$; $En_{28–79}$; **Figs. 3.7**, **3.9**) which form distinct textural and compositional populations. The diversity in composition of multiple phenocryst phases and incorporation of co-magmatic cumulates indicate complex and contrasting early growth histories along with open-system processes within a trans-crustal magmatic reservoir. Many crystals were then mixed or assimilated into a final common mush-zone (Omanawa magma body) where they experienced further rim growth prior to eruption. The partial resorption of quartz, xenocrystic clinopyroxene, and high-temperature amphibole crystal populations document heating and partial melting of the upper mush zone during recharge events. The periodic injection of the biotite-bearing magma and high Ba/Sr matrix-glass subgroup attest to the syn-eruptive mixing with a volumetrically minor second magma within the conduit.

5.1.3 What are the magmatic processes and eruption mechanisms associated with the eruption of crystal-rich magmas of the TgaVC?

The crystal-rich magmas erupted across the TgaVC share mineralogically, geochemically and isotopically affinities with that erupted during the Waitearikí super-eruption (**Chapter 4**). However, individual formations define discrete and relatively homogenous compositional fields (**Figs. 4.2–4.4**). This study focuses on the magmas of the Minden Rhyolite Subgroup and the petrogenetic relationships between them and the Waitearikí Ignimbrite with those of the more intermediate Otawa Formation. I have simplified the compositional groupings of the Minden Rhyolites into either low- and high-$^{87}Sr/^{86}Sr$ magmas. Low-$^{87}Sr/^{86}Sr$ magmas are defined as lavas with $^{87}Sr/^{86}Sr < 0.705800$ and include the domes of Mt Maunganui, Minden Peak, Manawata, Kaikaikaroro and Kaimai (i.e. western domes). The high-$^{87}Sr/^{86}Sr$ group includes the domes of Mangatawa, Upuhue, Pāpāmoa, Kopukairua, Waitao, Pukanui, Maungatūtū/Mt Misery, Greenpark and Otanewainuku where $^{87}Sr/^{86}Sr$ ratios are > 0.705900 and were exclusively erupted east of the Wairoa River. Juvenile products of the Waitearikí Ignimbrite and the white-coloured dacitic pumice of the Welcome Bay Ignimbrite, are mineralogically, geochemically and isotopically consistent with the high-$^{87}Sr/^{86}Sr$ Minden Rhyolites, which connects

these domes to the magmatic system underlying the Omanawa Caldera. Geothermobarometry indicate the Omanawa magma body and magmas associated with the broader TgaVC were situated within the mid- to shallow crust (c. 3.5 to 6 km depth) between 50–160 MPa and 740–900 °C (**Figs. 4.9-4.12**). Upper crustal differentiation was dominated by assimilation (r = 0.3) combined with c. 50 % fractional crystallisation (AFC) followed by mixing of magmas within the Omanawa magma body, while the western domes were dominated by extensive fractional crystallisation (FC) of a magma with a composition equivalent to Otawa33, the least-evolved magma currently recognised within the TgaVC. The AFC model is supported by greywacke-derived zircon xenocrysts (94–300 Ma) identified within pyroclastic units of the Pāpāmoa Formation and Waitearikі Ignimbrite during U-Pb dating (cf. **Chapter 2**) and the positive correlation between $\delta^{18}O_{(melt)}$ and $^{87}Sr/^{86}Sr$ values attest to significant degrees of melting, disaggregation and significant crustal contribution by the $\delta^{18}O$-enriched Waipapa Terrane crust.

The strong spatial association between the newly recognised faults, silicic domes and the Omanawa caldera structure (**Section 3.8**) suggests that TgaVC magmas erupted throughout the region is likely to have occurred in close association with external tectonic forces which have played an important role in determining eruption locations and volume of erupted deposits. Numerous studies within the TVZ have also demonstrated this complex magmatic-tectonic relationship, but the exact timing of volcanism relative to faulting in the TgaVC remains to be determined.

5.1.4 Is there a geochemical signature for silicic volcanism of the Tauranga Volcanic centre?

The magmas of the TgaVC have typical calc-alkaline compositions and mineral assemblages reflective of their continental-ocean subduction origin. Whole-rock pumice and matrix glass compositions of the Minden Rhyolites and ignimbrite units span from dacite to high-SiO_2 rhyolite which overlap between each other and the broader TVZ, yet distinct compositional fields are evident at the formation level (e.g high- versus low-$^{87}Sr/^{86}Sr$ Minden Rhyolites). Ignimbrite matrix glass values for SiO_2/K_2O and Na_2O+K_2O ratios are between 14.4–25.2 and 6.8–8.2, respectively, which appears to be characteristic of magmas erupted from pre- and early TVZ sources (Hopkins *et al.*, 2021b). **Chapter 2** demonstrated that many of the ignimbrites of the Pāpāmoa Formation contained physical and chemical evidence for magma mixing between a single mafic and silicic endmember, yet glass analyses of Otawera Ignimbrite were distinct (lower Al_2O_3, CaO, and Sr; high abundances of Na_2O, K_2O, Rb, Ba, Y and higher Ba/Sr and Rb/Sr trace-element ratios; **Fig. 2.9**) and this particular ignimbrite has subsequently been inferred to represent the deposits of a pyroclastic flow generated by an eruption from Pukanui Dome, rather than a source within the Omanawa Caldera (Kinley, 2022). Additionally, the high Ba/Sr subgroup within Waitearikі Ignimbrite matrix glass may be a characteristic of the

magma feeding the low-$^{87}Sr/^{86}Sr$ Minden Rhyolites (i.e. western domes), however pervasive devitrification prevents the characterisation of glass for lavas of the Minden Rhyolite Subgroup.

Radiogenic isotopic ratios show limited compositional diversity with $^{87}Sr/^{86}Sr$ values between 0.706450–0.705373 and $^{143}Nd/^{144}Nd$ from 0.512815–0.512544, and calculated $\delta^{18}O_{melt}$ values range from +8.0– +9.3 ‰ (**Fig. 4.6**). High-$\delta^{18}O$ magmas predominate throughout the greater TVZ, but there appears to be a gradual decrease in $\delta^{18}O_{(melt)}$ values over the lifespan of the TVZ from values typical of those in the TgaVC, down to +8.0– +7.3 ‰ within modern TVZ centres (Rooyakkers *et al.*, 2022).

While the above geochemical traits are generally characteristic of TgaVC magmas, they are not completely unambiguous. The TgaVC was active for around one million years, and during this time, crystal-rich rhyodacite to rhyolite magmas of near-identical mineral and isotopic compositions were continually erupted. Such chemical homogeneity has been linked to long-lived lower crustal mush bodies which act as a buffer between the addition of mafic melts and the upper crustal reservoirs (Folkes *et al.*, 2011) but this contrasts the behaviour observed in other well-studied TVZ silicic centres (i.e. Whakamaru, Taupō), which demonstrate the complete regeneration of the underlying magmatic system, rather than the simple reheating and recycling of residual mush, following large eruptive events (Gravley *et al.*, 2016; Barker *et al.*, 2021). This may, in part, simply reflect the timing of large events within the individual centres, as the Whakamaru and Oruanui supereruptions which occurred during the early stages of their respective caldera histories, whereas the eruption of the Waitetariki Ignimbrite occurred in the final stages of TgaVC volcanism. Further geochemical investigations of the ignimbrites of the Pāpāmoa Formation will shed light on how the Omanawa magma body recovered following consecutive voluminous pyroclastic eruptive events.

5.1.5 How does volcanism of the Tauranga region sit within the broader context of a migrating continental-arc?

Traditionally, volcanism of the TgaVC has been viewed to represent the final stages of volcanic activity of the CVZ, primarily due to the close proximity of volcanic deposits in the Tauranga region to those of the CVZ in the southern Coromandel Peninsula (Carter *et al.*, 2004; Briggs *et al.*, 2005; Booden *et al.*, 2012). However, while it is impossible to fully understand eruptive volumes of caldera-forming ignimbrites of the CVZ due to the high degree of erosion and the likelihood of extensive offshore deposition, documented calderas are relatively small (c. 8 km diameter) compared to those in the TVZ (≥ 20 km; *Briggs et al.,* 2005). The Omanawa caldera measures ~30 x 25 km and is situated at the southern end of an asymmetrical rifted graben which consists of a series of down-faulted blocks along the western flanks of the Pāpāmoa Range and the Wairoa/Opuiaki river fault (**Fig. 3.2**). The western structural boundary of the Old Taupō Rift has been inferred from gravity data to lie just to the west of

Tauranga city (Villamor *et al.*, 2017; Stagpoole *et al.*, 2021), and is inferred here to be represented by the major Wairoa/Opuiaki River fault. As volcanism associated with the Omanawa Caldera and broader TgaVC occurred within the defined structural boundaries of the Taupō Rift, it therefore represents the first silicic system of the TVZ. This implies that the change from the CVZ to the TVZ was established by c. 2.5 Ma (500 ka earlier than previously thought), evidenced by overlapping arc-volcanism and continental rifting within the TgaVC throughout onshore parts of the western Bay of Plenty. The silicic lavas and ignimbrites of the Waihi Caldera (Vincent, 2012; Julian, 2016) and predominately intermediate pyroclastic deposits of the Aongatete formation (Briggs *et al.*, 2005) therefore represent the final stages of CVZ volcanism which occurred between 3.9 and 3.5 Ma.

5.2 Limitations of this research

Throughout this thesis research there have been multiple challenges that have affected the collection of data to be used in models that form the basis of major interpretations and for comparative purposes with other literature sources. In this section, I address some of these limitations encountered during this research project.

5.2.5 Glass and mineral geochemical data acquisition

Electron probe microanalysis (EPMA) is widely used for determining the major- and minor-element composition of volcanic glass either as individual shards, pumice fragments, melt inclusions, and loose phenocrysts or crystal fragments (e.g. Lowe *et al.,* 2017). Many of the key findings of this study have been based on results obtained from the geochemical analysis of rhyolitic silicate glass acquired through EPMA in conjunction with laser ablation inductively coupled plasma-mass spectrometry (LA-ICP-MS), and mineral phases using either EPMA or a scanning electron microscope coupled with energy dispersive spectroscopy (SEM-EDS).

In **Chapter 2** I analysed individual glass shards obtained from distal tephras and matrix glass from proximal ignimbrites using EPMA followed by LA-ICP-MS to obtain geochemical data that could be used for correlation purposes. I acknowledge and agree with the general practice of separating and lightly crushing pumice clasts to obtain glass shards for analysis as these clasts provide direct sampling of the melt fraction of the erupted magma. However, due to the degree of welding of proximal deposits in ignimbrite units of the TgaVC and the limited size of juvenile clasts (typically ash to fine lapilli) of distal deposits, it was often simply not possible to extract them for analysis. Therefore, matrix glass was analysed to enable consistent comparison between both proximal and distal deposits, to avoid systematic differences and/or differences in the degree of apparent heterogeneity in the composition between the tephra and proximal deposits (Tomlinson *et al.*, 2015).

Glass within the Waitеariki Ignimbrite is also highly devitrified, which makes it unsuitable for geochemical analysis. The only exception was in the lower 10 m of the core ES112 where light-brown perlitic glass was observed. This brown-coloured glass in the lower Waitеariki Ignimbrite was examined using a SEM prior to analysis which demonstrated that microlite development from devitrification is not widespread at this stratigraphic level although a degree of post-depositional hydration is a certainty due to the formation of perilitic cracking within the fiamme (Denton *et al.*, 2009). However, the relatively high analytical totals (ave = 97.08 %) and consistent geochemical composition (**Supplementary data table SM2.5, Fig. 2.10**) obtained in this study indicate that the brown Waitеariki glass remains a fair approximation of melt composition, although there appears to be a systematic variation in the abundances of FeO and CaO (**Fig. 2.10**) and outliers of anomalously low or high concentrations of Na_2O and K_2O are evident relative to rapidly quenched distal matrix glasses (**Figs. 3.18 b, 3.19 f**).

While EPMA remains the primary choice for geochemical analysis of silicate glass and minerals (Lowe *et al.*, 2017) there has been a considerable increase in the number of quantitative determinations using SEM-EDS in recent years (Graeter *et al.*, 2015; Willcock *et al.*, 2015; Yousefi *et al.*, 2017; Srivastava *et al.*, 2020). This increase is due to the widespread prevalence and application of the microscopes, the appearance of a new generation detector which allows for high counting rates, and progress in the development of corresponding software (Lavrent'ev *et al.*, 2015). My intention was to analyse the silicate glass and all mineral phases via EPMA at Victoria University of Wellington over two analytical sessions. The first session conducted in 2019 went ahead as planned, and included matrix glass analyses used in **Chapter 2** and randomly selected amphibole crystals from matrix and fiamme within polished thin-sections of the Waitеariki Ignimbrite. The second analytical session was abandoned due to ongoing delays relating to COVID-19 lockdown protocols and unexpected machine maintenance. Due to the increasing prevalence of SEM-EDS in petrological studies and that EDS and wavelength-dispersive spectrometers have been demonstrated to have similar accuracies for the major and minor (> 1 wt. %) components of rock-forming minerals (Lavrent'ev *et al.*, 2015). General mineral characterisation of the major mineral phases within the Waitеariki Ignimbrite (**Chapter 3**) was undertaken using SEM-EDS at the Otago Micro and Nanoscale Imaging Centre at the University of Otago, Dunedin. For consistency of amphibole analyses, these crystals were analysed using a JEOL 8530F field emission electron probe microanalyser at the University of Auckland along with additional compositional data for plagioclase and orthopyroxene crystal rim-glass pairs used for geothermobarometry (**Chapter 4**).

These crystals were handpicked from distal Waitеariki Ignimbrite samples (i.e. Hikuroa Pumice Member deposits) under a binocular microscope embedded in epoxy blocks and polished. Inspection

of the mineral grain mounts using SEM indicated that some grains (particularly plagioclase and orthopyroxene) had small amounts (typically c. 5–10 µm) of adhering glass and these were targeted for EPMA analysis at the University of Auckland. Backscatter imaging during analysis also highlighted the presence of microlites within some of the glass, so analysis was conducted using a narrow 1 µm beam size. The typical range used for geochemical analysis of rhyolitic glass is usually within 5–20 µm, but analysis of cryptotephras has documented beam sizes as small as 3 µm (Pearce *et al.*, 2014; Lowe *et al.*, 2017). The main concern when using such a small beam size during analysis of rhyolitic glass is the well-documented effect of alkali element migration which involves the physical migration of Na atoms (and to a lesser extent K) out of the excitation volume, or the portion of the sample that is penetrated by the electron beam during analysis (Walker & Howitt, 1989; Kuehn *et al.*, 2011) and leads to increasingly lower Na, and higher Si and Al counts which affect analytical accuracy. This is typically accounted for during data acquisition using lower beam currents and larger, defocused beams (Pearce *et al.*, 2014) and this method was used for data collected by EPMA at Victoria University of Wellington. The field emission EPMA at the University of Auckland is equipped with a time-dependant intensity correction (TDI) system which reads the incoming counts in dedicated time intervals over the whole count time of the selected elements which capture any time-dependent decay in the count-rate of the target element. Plotting this decay then allows the user to back calculate to the correct intensity value for T_0 (Walshaw, 2018).

5.2.2 Challenges with estimating intensive parameters

The relatively restricted mineral assemblage in the Waitеariki Ignimbrite and lavas of the TgaVC, and the pervasive devitrification of glass means that only certain techniques could be used to estimate values of and variations in intensive parameters such as temperature and pressure. In this study I concentrated on orthopyroxene and plagioclase core and whole-rock or rim and glass equilibrium pairs (Putirka, 2008) and the Al-in-hornblende (Ridolfi, 2021) geothermobarometers. Overall, there was good agreement in the estimated temperatures and pressures between the models (see **Figs 4.9–4.11**), which was corroborated using independent methods (e.g. haplogranitic ternary projection, **Fig. 4.12**). Although widely used, the potential of Al-in-hornblende geobarometers has always been debated (cf. Erdmann *et al.,* 2014), particularly in regards to volcanic systems where there is a high thermodynamic variance (i.e. saturated in only a few phases), although there is more confidence when amphibole barometers are applied to the restricted conditions of granitic systems (T< 800 °C and $Fe\#_{Amp} = Fe_{Amp}/(Fe_{Amp}+Mg_{Amp}) < 0.65$; Putirka, 2016). While the Waitеariki Ignimbrite is clearly volcanic, microcrystalline clots (see **Section 3.6**) and low pre-eruptive temperatures (e.g. **Fig. 4.9**) attest to plutonic tendencies of the Omanawa magma body and the applicability of the application of the Al-in-hornblende barometer.

The temperature and pressure estimates obtained for the Waitearikí Ignimbrite are consistent with those determined for the wider TVZ (<50–150 MPa), but are notably lower than those obtained from experiments of the Fish Canyon Tuff, which is the archetypal monotonous intermediate (200 MPa; Caricchi & Blundy, 2015). This is likely a result of active thinning of the crust underlying the TVZ due to continental rifting, however, experimental work would be extremely valuable for confirming the estimated conditions of crystallisation from petrological techniques, and further constraining the depths at which important magmatic processes occur both in the TgaVC and the broader TVZ.

Application of these models to lavas of the wider TgaVC, however, is more tentative. Mineral data for TgaVC lavas was sourced from student theses (Hughes, 1993; Hall, 1994; Whitbread-Edwards, 1994; Hollis, 1995; Cook, 2016) and paired with average whole-rock compositions obtained as part of this study for each dome. A major assumption used here is that the data represents mineral core analyses, however, this was not directly stipulated and this assumption may at times be incorrect, as demonstrated by disequilibrium between crystal-melt pair compositions (**Fig. 4.8**). Many of these compositions are too evolved for the hypothetical carrier melt, and are likely incorrectly paired rim-whole-rock compositions and therefore do not provide meaningful temperature or pressure estimates. However, limited data obtained for equilibrium pairs for lavas of the TgaVC, demonstrate broad similarity with those of the Waitearikí Ignimbrite. It is important to note that core and whole-rock pairs are reflective of earlier crystallisation stages, and this may be reflected in the generally higher temperature estimates for the Minden Rhyolite lavas compared to the Waitearikí Ignimbrite. The subtle variations in magma storage which occurs through time and between formations has not been explored here due to the limited data available for lavas of the TgaVC.

5.2.3 Geochemical modelling

Modelling of FC and AFC processes using geochemical data generally requires significant assumptions with inherent limitations. While these are clearly outlined within **Chapter 4** (see **Sections 4.5** and **4.7.2**), I would like to reiterate some of those which have the most effect on the modelling process and outcomes.

Firstly, using an intermediate magma composition (Otawa33, $Mg\#_{48}$) as a starting composition excludes modelling of petrogenetic processes occurring in the lower crust. I reiterate that the petrogenetic modelling carried out in this study only examines the dominant processes associated with the differentiation of isotopically evolved andesite in the upper crust, and not any potential primitive melts. The modal mineralogy used to determine bulk distribution coefficients (i.e., 58% plagioclase, 17% hornblende, 11% orthopyroxene, 7% oxides (magnetite + ilmenite)), reflect average modal abundances, normalised to remove mineral phases not considered in the models (e.g. quartz,

biotite). This modal mineral assemblage is most reflective of the high-$^{87}Sr/^{86}Sr$ Minden Rhyolites and the rhyodacite magmas of the Waitеariki and Welcome Bay ignimbrites, which were the main compositional groups targeted by the AFC models. The mineral-melt fractionation factor (Δ) used for AFC modelling of oxygen isotopes is open to refinement. Oxygen isotopes were only analysed on plagioclase and quartz mineral phases and therefore the Δ value of 0.1 used here is only an estimate whereas the accurate determination of a mineral-melt fractionation factor requires the determination of $\delta^{18}O$ for all major mineral phases. Mineral-melt fractionation factors for TVZ rhyolites are as low as -0.8 (S. Rooyakkers, personal communication, 2022), however, at this value, the model failed to recreate TgaVC compositions. For ratios of assimilated material to crystallized material (r) between 0.3 and 0.4, that are indicated by trace-element modelling, a mineral-melt fractionation factor of between 0.1 to 0.5 was required which is consistent with that determined from plagioclase and quartz.

5.3 Future directions and suggestions for further research

In drawing this thesis to a conclusion, I bring to attention some potential areas for future research within the TgaVC and for the general theme of magma genesis and eruption in large silicic magma systems:

1. *Higher resolution of geochemical and temporal data for individual lava domes.*

   This study has provided a broad overview of the mineralogical and geochemical characteristics of almost all of the lava domes associated with the TgaVC. However, some domes are less represented than others. Particular domes of interest include the large Kaimai-Kakahu-Te Wheraiti dome complex overlying the north-west edge of the Omanawa Caldera. Radiometric age dating suggests this dome re-activated during the later stages of TgaVC or was active throughout. Western portions of the dome have been downfaulted along the Hauraki fault and may provide a unique window into the history of one of the largest domes in the centre. Additionally, the intra-caldera dome of Puwhenua has never been sampled and Otanewainuku is believed to have erupted after the Waitеariki Ignimbrite and could provide insights into the state of the magmatic system following the catastrophic super-eruption and the waning stages of volcanism in the TgaVC.

2. *Determination of magmatic volatiles within TgaVC magmas.*

   The presence of water and other volatiles in magma prior to eruption affects crystallisation during ascent and eruption explosivity. In this study, H_2O and CO_2 contents were not

measured directly and instead estimated using thermodynamic calculations. Such parameters could be measured directly using mineral-hosted melt inclusions which are relatively common within the Waitearikí Ignimbrite. Melt-inclusions in proximal deposits however are typically affected by post-entrapment crystallisation and many crystals have fractured around melt-inclusions as a result of rapid decompression during eruption. In contrast to proximal deposits, distal deposits are not affected by devitrification, and the rapid quenching of glass during eruption and pyroclastic flow transportation may provide many crystals (particularly quartz) with melt inclusions suitable for analysis.

3. *Determining the origins and rates of interaction between mafic magmas and silicic magmas in the TgaVC.*

   The complete absence of mafic magmas within the TgaVC is perplexing. Despite this, there are many lines of evidence which indicate that the silicic magmas of the TgaVC had a close relationship with mafic melts. These include the presence of mafic xenocrysts, resorption and reverse zonation of phenocrysts and physical evidence of magma mixing recorded in juvenile clasts of the Welcome Bay Ignimbrite. Several major questions remain and include what are the composition and origins of the mafic magmas feeding the TgaVC? Do these originate directly from the mantle or from regions underlying the main mush body within the crust? At what depth do the mafic magmas stall and what is the main process involved with their differentiation?

4. *How did the Omanawa magma body evolve and/or reset following sequential large pyroclastic eruptions from the Omanawa Caldera?*

   The Waitearikí super-eruption has provided a detailed view of the dynamic state of the magmatic system of the Omanawa Caldera at the later stages of volcanism associated with the TgaVC. It has been demonstrated that the magmatic systems associated with the Whakamaru and Taupō calderas underwent rapid and complete regeneration of the underlying magmatic system after following large eruptive events (Gravley *et al.*, 2016; Barker *et al.*, 2021). This could be investigated by geochemical analysis of the Welcome Bay, Wharo and Arateka ignimbrites of the Pāpāmoa Formation, which are inferred here to have erupted from the Omanawa Caldera and would provide snapshots into the development of the magmatic system though time. Additionally, changes in crystallisation depths may show gradual conditioning of the crust like that observed during the 350-280 ka ignimbrite flare-up event (Gualda *et al.*, 2018).

5. *Potential seismic hazard risk with the western Bay of Plenty.*

   Within New Zealand, the identification and mapping of active fault traces have formed major components of defining the earthquake risk of a region (Seebeck *et al.*, 2022) and the unexpected rupture of unknown faults can have disastrous consequences to human life and infrastructure (Davey, 2011). This study identifies several faults buried under volcanogenic sediments and pyroclastic deposits within central regions of the Tauranga Basin. These faults are extensional faults associated with the early development of the Taupō Rift and are not considered active. The c. 90 m offset along the Wairoa/Opuiaki River fault indicates that significant movement occurred following the deposition of the Waitekariki Ignimbrite (i.e up to 2 Ma) but no further constraints on the timing of fault ruptures are available at this time. Geophysical studies to further investigate the paleo seismic history of the Tauranga region and the extent of regional faulting and its relationship with the timing of volcanism would be prudent as there is the potential for further faults within the Tauranga region.

This is the first study to examine in detail the eruptive products originating from the TgaVC and has made significant advances in our knowledge of the volcanic stratigraphy and in the understanding of the magmatic processes behind arc-related silicic volcanism in Aotearoa New Zealand between 3-2 Ma. The TgaVC provides a window in time allowing us to observe and document the initiation of rifted continental arcs followed by the subsequent maturation of the crust, the onset of regional hydrothermal circulation and how volcanism responds to fundamental changes at convergent plate boundaries.

References

Adams, C. J., Graham, I. J., Seward, D., Skinner, D. N. B., Adams, C. J., Skinner, D. N. B., & Moore, P. R. (1994). Geochronological and geochemical evolution of late cenozoic volcanism in the Coromandel Peninsula, New Zealand. *New Zealand Journal of Geology and Geophysics, 37*(3), 359-379.

Allan, A., Barker, S. J., Millet, M.-A., Morgan, D. J., Rooyakkers, S. M., Schipper, C. I., & Wilson, C. J. (2017). A cascade of magmatic events during the assembly and eruption of a super-sized magma body. *Contributions to Mineralogy and Petrology, 172*(7), 1-34.

Alloway, B., Westgate, J., Pillans, B., Pearce, N., Newnham, R., Byrami, M., & Aarburg, S. (2004). Stratigraphy, age and correlation of middle Pleistocene silicic tephras in the Auckland region, New Zealand: a prolific distal record of Taupo Volcanic Zone volcanism. *New Zealand Journal of Geology and Geophysics, 47*(3), 447-479.

Amma-Miyasaka, M., Miura, D., Nakagawa, M., Uesawa, S., & Furukawa, R. (2020). Stratigraphy and chronology of silicic tephras in the Shikotsu-Toya volcanic field, Japan: Evidence of a Late Pleistocene ignimbrite flare-up in southwestern Hokkaido. *Quaternary International, 562*, 58-75.

Anderson AT, Swilhart GH, Artioli G, Geiger CA (1984) Segregation vesicles, gas filter-pressing, and igneous differentiation. J Geol 92:55–72.

Annen, C., Blundy, J., & Sparks, R. (2006). The genesis of intermediate and silicic magmas in deep crustal hot zones. *Journal of Petrology, 47*(3), 505-539.

Ashwell, P., Kennedy, B., Gravley, D., von Aulock, F., & Cole, J. (2013). Insights into caldera and regional structures and magma body distribution from lava domes at Rotorua Caldera, New Zealand. *Journal of Volcanology and Geothermal Research, 258*, 187-202.

Bachmann, O., & Bergantz, G. W. (2003). Rejuvenation of the Fish Canyon magma body: A window into the evolution of large-volume silicic magma systems. *Geology, 31*(9), 789-792.

Bachmann, O., & Bergantz, G. W. (2004). On the origin of crystal-poor rhyolites: extracted from batholithic crystal mushes. *Journal of Petrology*, *45*(8), 1565-1582.

Bachmann, O., & Bergantz, G. W. (2008). Rhyolites and their source mushes across tectonic settings. *Journal of Petrology, 49*(12), 2277-2285.

Bachmann, O., Dungan, M. A., & Lipman, P. W. (2002). The Fish Canyon Magma Body, San Juan Volcanic Field, Colorado: Rejuvenation and Eruption of an Upper-Crustal Batholith. *Journal of Petrology, 43*(8), 1469-1503.

Bachmann, O., & Huber, C. (2016). Silicic magma reservoirs in the Earth's crust. *American Mineralogist, 101*(11), 2377-2404.

Barker, S. J., Wilson, C. J., Illsley-Kemp, F., Leonard, G. S., Mestel, E. R., Mauriohooho, K., & Charlier, B. L. (2021). Taupō: an overview of New Zealand's youngest supervolcano. *New Zealand Journal of Geology and Geophysics, 64*(2-3), 320-346.

Bégué, F., Gravley, D. M., Chambefort, I., Deering, C. D., & Kennedy, B. M. (2015). Magmatic volatile distribution as recorded by rhyolitic melt inclusions in the Taupo Volcanic Zone, New Zealand. *Geological Society, London, Special Publications, 410*(1), 71-94.

Bégué, F., Gualda, G. A., Ghiorso, M. S., Pamukcu, A. S., Kennedy, B. M., Gravley, D. M., Deering, C. D., & Chambefort, I. (2014). Phase-equilibrium geobarometers for silicic rocks based on rhyolite-MELTS. Part 2: application to Taupo Volcanic Zone rhyolites. *Contributions to Mineralogy and Petrology, 168*(5), 1-16.

Berg, S. E., Troll, V. R., Harris, C., Deegan, F. M., Riishuus, M. S., Burchardt, S., & Krumbholz, M. (2018). Exceptionally high whole-rock δ18O values in intra-caldera rhyolites from Northeast Iceland. *Mineralogical Magazine, 82*(5), 1147-1168.

Bergantz GW, Schleicher JM, Burgisser A (2015) Oepn-system dynamics and mixing in magma mushes. Nat Geosci 8:793–797

Bindeman, I. (2008). Oxygen isotopes in mantle and crustal magmas as revealed by single crystal analysis. *Reviews in Mineralogy and Geochemistry, 69*(1), 445-478.

Bland, K. J., Kamp, P. J., & Nelson, C. S. (2007). *Systematic lithostratigraphy of the Neogene succession exposed in central parts of Hawke's Bay Basin, eastern North Island, New Zealand*. Hamilton, New Zealand: The University of Waikato.

Blattner, P., & Bunting, D. (1980). Stable Isotopes of Minerals and Rocks of The Ngawha Geothermal Field, Northland and Magmatic Water Revisited. *Unpublished DSIR Geothermal Circular PB/DGB-102*.

Blattner, P., & Reid, F. (1982). The origin of lavas and ignimbrites of the Taupo Volcanic Zone, New Zealand, in the light of oxygen isotope data. *Geochimica et Cosmochimica Acta, 46*(8), 1417-1429.

Blattner, P., Rui-Zhong, H., Graham, I. J., & Houston-Eleftheriadis, C. (1996). Temperatures and isotopic evolution of silicic magmas, Taupo Volcanic Zone and Coromandel, New Zealand. *New Zealand Journal of Geology and Geophysics, 39*(3), 353-362.

Blundy, J., & Cashman, K. (2001). Ascent-driven crystallisation of dacite magmas at Mount St Helens, 1980–1986. *Contributions to Mineralogy and Petrology, 140*(6), 631-650.

Booden, M. A., Smith, I. E. M., Mauk, J. L., & Black, P. M. (2012). Geochemical and isotopic development of the Coromandel Volcanic Zone, northern New Zealand, since 18 Ma. *Journal of Volcanology and Geothermal Research, 219–220*, 15-32.

Bouvier, A., Vervoort, J. D., & Patchett, P. J. (2008). The Lu–Hf and Sm–Nd isotopic composition of CHUR: constraints from unequilibrated chondrites and implications for the bulk composition of terrestrial planets. *Earth and Planetary Science Letters, 273*(1-2), 48-57.

Bowyer, D. A. (2001). *Petrologic, geochemical and isotopic evolution of rhyolite lavas from the Okataina, Rotorua and Kapenga volcanic centres, Taupo Volcanic Zone, New Zealand.* PhD thesis, The University of Waikato, Hamilton, New Zealand.

Brathwaite, R. L., & Christie, A. B. (1996). *Geology of the Waihi area: part sheets T13 and U13, scale 1: 50 000*. Institute of Geological & Nuclear Sciences Limited.

Briggs, R., Gifford, M., Moyle, A., Taylor, S., Norman, M., Houghton, B., & Wilson, C. (1993). Geochemical zoning and eruptive mixing in ignimbrites from Mangakino volcano, Taupo Volcanic Zone, New Zealand. *Journal of volcanology and geothermal research, 56*(3), 175-203.

Briggs, R., Houghton, B., McWilliams, M., & Wilson, C. (2005). 40Ar/39Ar ages of silicic volcanic rocks in the Tauranga-Kaimai area, New Zealand: Dating the transition between volcanism in the Coromandel Arc and the Taupo Volcanic Zone. *New Zealand Journal of Geology and Geophysics, 48*(3), 459-469.

Briggs, R. M., Hall, G. J., Harmsworth, G. R., Hollis, A. G., Houghton, B. F., Hughes, G. R., Morgan, M. D., & Whitbread-Edwards, A. R. (1996). *Geology of the Tauranga area: sheet U14 1:50 000*. Hamilton, N.Z.: Hamilton, N.Z. : Dept. of Earth Sciences, University of Waikato.

Brown, S., Burt, R., Cole, J., Krippner, S., Price, R., & Cartwright, I. (1998b). Plutonic lithics in ignimbrites of Taupo Volcanic Zone, New Zealand; sources and conditions of crystallisation. *Chemical Geology, 148*(1-2), 21-41.

Brown, S. K., Crosweller, H. S., Sparks, R. S. J., Cottrell, E., Deligne, N. I., Guerrero, N. O., ... & Takarada, S. (2014). Characterisation of the Quaternary eruption record: analysis of the Large Magnitude Explosive Volcanic Eruptions (LaMEVE) database. *Journal of Applied Volcanology*, *3*, 1-22.

Brown, S. J. A., Wilson, C. J. N., Cole, J. W., & Wooden, J. (1998a). The Whakamaru group ignimbrites, Taupo Volcanic Zone, New Zealand: evidence for reverse tapping of a zoned silicic magmatic system. *Journal of Volcanology and Geothermal Research, 84*(1), 1-37.

Bryant, C., Arculus, R., & Eggins, S. (2003). The geochemical evolution of the Izu-Bonin arc system: A perspective from tephras recovered by deep-sea drilling. *Geochemistry, Geophysics, Geosystems, 4*(11). https://doi.org/10.1029/2002GC000427

Burt, R., Brown, S., Cole, J., Shelley, D., & Waight, T. (1998). Glass-bearing plutonic fragments from ignimbrites of the Okataina caldera complex, Taupo Volcanic Zone, New Zealand: remnants of a partially molten intrusion associated with preceding eruptions. *Journal of Volcanology and Geothermal Research, 84*(3-4), 209-237.

Caratori Tontini, F., Bassett, D., de Ronde, C. E., Timm, C., & Wysoczanski, R. (2019). Early evolution of a young back-arc basin in the Havre Trough. *Nature Geoscience, 12*(10), 856-862.

Caricchi, L., Annen, C., Blundy, J., Simpson, G., & Pinel, V. (2014). Frequency and magnitude of volcanic eruptions controlled by magma injection and buoyancy. *Nature Geoscience, 7*(2), 126-130.

Caricchi, L., & Blundy, J. (2015). Experimental petrology of monotonous intermediate magmas. *Geological Society, London, Special Publications, 422*(1), 105-130.

Carter, L., Alloway, B., Shane, P., & Westgate, J. (2004). Deep-ocean record of major late Cenozoic rhyolitic eruptions from New Zealand. *New Zealand Journal of Geology and Geophysics, 47*(3), 481-500.

Carter, L., Shane, P., Alloway, B., Hall, I. R., Harris, S. E., & Westgate, J. A. (2003). Demise of one volcanic zone and birth of another—a 12 my marine record of major rhyolitic eruptions from New Zealand. *Geology, 31*(6), 493-496.

Cashman, K. V., & Giordano, G. (2014). Calderas and magma reservoirs. *Journal of Volcanology and Geothermal Research, 288*, 28-45.

Cashman, K. V., Sparks, R. S. J., & Blundy, J. D. (2017). Vertically extensive and unstable magmatic systems: a unified view of igneous processes. *Science, 355*(6331), eaag3055.

Chambefort, I., Lewis, B., Wilson, C., Rae, A., Coutts, C., Bignall, G., & Ireland, T. (2014). Stratigraphy and structure of the Ngatamariki geothermal system from new zircon U–Pb geochronology: Implications for Taupo Volcanic Zone evolution. *Journal of Volcanology and Geothermal Research, 274*, 51-70.

Chamberlain, K. J., Wilson, C. J., Wallace, P. J., & Millet, M.-A. (2015). Micro-analytical perspectives on the Bishop Tuff and its magma chamber. *Journal of Petrology, 56*(3), 605-640.

Charlier, B. L. A., Peate, D. W., Wilson, C. J. N., Lowenstern, J. B., Storey, M., & Brown, S. J. A. (2003). Crystallisation ages in coeval silicic magma bodies: 238U–230Th disequilibrium evidence from the Rotoiti and Earthquake Flat eruption deposits, Taupo Volcanic Zone, New Zealand. *Earth and Planetary Science Letters, 206*(3), 441-457.

Cheng, H., Edwards, R. L., Shen, C.-C., Polyak, V. J., Asmerom, Y., Woodhead, J., Hellstrom, J., Wang, Y., Kong, X., & Spötl, C. (2013). Improvements in 230Th dating, 230Th and 234U half-life values, and U–Th isotopic measurements by multi-collector inductively coupled plasma mass spectrometry. *Earth and Planetary Science Letters, 371*, 82-91.

Christiansen, E. H. (2005). Contrasting processes in silicic magma chambers: evidence from very large volume ignimbrites. *Geological Magazine*, *142*(6), 669-681.

Cole, J., Deering, C., Burt, R., Sewell, S., Shane, P., & Matthews, N. (2014). Okataina Volcanic Centre, Taupo Volcanic Zone, New Zealand: A review of volcanism and synchronous pluton development in an active, dominantly silicic caldera system. *Earth-Science Reviews, 128*, 1-17.

Cook, E. T. (2016). *Felsic volcanism in the eastern Waihi area; process origins of the Corbett and Ratarua ignimbrites and the Hikurangi Rhyolite.* MSc thesis, University of Waikato, Hamilton, New Zealand.

Cook, G. W., Wolff, J. A., & Self, S. (2016). Estimating the eruptive volume of a large pyroclastic body: the Otowi Member of the Bandelier Tuff, Valles caldera, New Mexico. *Bulletin of Volcanology, 78*(2), 1-11.

Cooper, G. F., Blundy, J. D., Macpherson, C. G., Humphreys, M., & Davidson, J. P. (2019). Evidence from plutonic xenoliths for magma differentiation, mixing and storage in a volatile-rich crystal mush beneath St. Eustatius, Lesser Antilles. *Contributions to Mineralogy and Petrology, 174*(5), 1-24.

Cooper, G. F., Morgan, D. J., & Wilson, C. J. (2017). Rapid assembly and rejuvenation of a large silicic magmatic system: Insights from mineral diffusive profiles in the Kidnappers and Rocky Hill deposits, New Zealand. *Earth and Planetary Science Letters, 473*, 1-13.

Cooper, G. F., & Wilson, C. J. (2014). Development, mobilisation and eruption of a large crystal-rich rhyolite: the Ongatiti ignimbrite, New Zealand. *Lithos, 198*, 38-57.

Cooper, G. F., Wilson, C. J., Millet, M.-A., & Baker, J. A. (2016). Generation and rejuvenation of a supervolcanic magmatic system: a case study from Mangakino volcanic centre, New Zealand. *Journal of Petrology, 57*(6), 1135-1170.

Cooper, G. F., Wilson, C. J., Millet, M.-A., Baker, J. A., & Smith, E. G. (2012). Systematic tapping of independent magma chambers during the 1 Ma Kidnappers supereruption. *Earth and Planetary Science Letters, 313*, 23-33.

Coote, A. C., & Shane, P. (2016). Crystal origins and magmatic system beneath Ngauruhoe volcano (New Zealand) revealed by plagioclase textures and compositions. *Lithos, 260*, 107-119.

Crosweller, H. S., Arora, B., Brown, S. K., Cottrell, E., Deligne, N. I., Guerrero, N. O., Hobbs, L., Kiyosugi, K., Loughlin, S. C., & Lowndes, J. (2012). Global database on large magnitude explosive volcanic eruptions (LaMEVE). *Journal of Applied Volcanology, 1*(1), 4.

Cunningham, M. J., Lowe, D. J., Wyatt, J. B., Moon, V. G., & Churchman, G. J. (2016). Discovery of halloysite books in altered silicic Quaternary tephras, northern New Zealand. *Clay Minerals, 51*(3), 351-372.

Davey, F. (Compiler) (2011). *Natural hazards—the Christchurch earthquakes*: Taylor & Francis.

Davidge, S. C. (1982). *A geophysical study of the south Hauraki lowlands (MSc thesis)*. New Zealand: University of Auckland.

de Silva, S., & Self, S. (2022). Capturing the Extreme in Volcanology: The Case for the Term "Supervolcano". *Frontiers in Earth Science, 10*, 859237.

de Silva, S., Zandt, G., Trumbull, R., & Viramonte, J. (2006). Large-scale silicic volcanism—The result of thermal maturation of the crust. *Advances in Geosciences: Volume 1: Solid Earth (SE)*, 215-230.

Deering, C., Bachmann, O., Dufek, J., & Gravley, D. (2011b). Rift-related transition from andesite to rhyolite volcanism in the Taupo Volcanic Zone (New Zealand) controlled by crystal–melt dynamics in mush zones with variable mineral assemblages. *Journal of Petrology, 52*(11), 2243-2263.

Deering, C., Cole, J., & Vogel, T. (2008). A rhyolite compositional continuum governed by lower crustal source conditions in the Taupo Volcanic Zone, New Zealand. *Journal of Petrology, 49*(12), 2245-2276.

Deering, C., Cole, J., & Vogel, T. (2011a). Extraction of crystal-poor rhyolite from a hornblende-bearing intermediate mush: a case study of the caldera-forming Matahina eruption, Okataina volcanic complex. *Contributions to Mineralogy and Petrology, 161*(1), 129-151.

Denton, J. S., Tuffen, H., Gilbert, J. S., & Odling, N. (2009). The hydration and alteration of perlite and rhyolite. *Journal of the Geological Society, 166*(5), 895-904.

DePaolo, D. J. (1981). Trace element and isotopic effects of combined wallrock assimilation and fractional crystallisation. *Earth and Planetary Science Letters, 53*(2), 189-202.

Downs, D., Rowland, J., Wilson, C., Rosenberg, M., Leonard, G., & Calvert, A. (2014). Evolution of the intra-arc Taupo-Reporoa Basin within the Taupo Volcanic Zone of New Zealand. *Geosphere, 10*(1), 185-206.

Edbrooke, S. W. (2001). *Geology of the Auckland area. 1:250,000 Geological Map, 3.* Lower Hutt, New Zealand: Institute of Geological and Nucear Sciences.

Eggins, S. M. (2003). Laser ablation ICPMS analysis of geological materials prepared as lithium borate glasses. *Geostandards and Geoanalytical Research, 27*(2), 147-162.

Engwell, S., Aspinall, W., & Sparks, R. (2015). An objective method for the production of isopach maps and implications for the estimation of tephra deposit volumes and their uncertainties. *Bulletin of Volcanology, 77*(7), 1-18.

Erdmann, S., Martel, C., Pichavant, M., & Kushnir, A. (2014). Amphibole as an archivist of magmatic crystallisation conditions: problems, potential, and implications for inferring magma storage prior to the paroxysmal 2010 eruption of Mount Merapi, Indonesia. *Contributions to Mineralogy and Petrology, 167*(6), 1-23.

Folkes, C. B., de Silva, S. L., Wright, H. M., & Cas, R. A. (2011). Geochemical homogeneity of a long-lived, large silicic system; evidence from the Cerro Galán caldera, NW Argentina. *Bulletin of Volcanology, 73*(10), 1455-1486.

Gamble, J., Smith, I., McCulloch, M., Graham, I., & Kokelaar, B. (1993). The geochemistry and petrogenesis of basalts from the Taupo Volcanic Zone and Kermadec Island Arc, SW Pacific. *Journal of Volcanology and Geothermal Research, 54*(3-4), 265-290.

Ghiorso, M. S., & Gualda, G. A. (2015). An H2O–CO2 mixed fluid saturation model compatible with rhyolite-MELTS. *Contributions to Mineralogy and Petrology, 169*(6), 1-30.

Ghiorso, M. S., & Sack, O. (1991). Fe-Ti oxide geothermometry: thermodynamic formulation and the estimation of intensive variables in silicic magmas. *Contributions to Mineralogy and Petrology, 108*(4), 485-510.

Giordano, G., & Cas, R. A. (2021). Classification of ignimbrites and their eruptions. *Earth-Science Reviews, 220*, 103697.

Gonfiantini, R., Stichler, W., & Rozanski, K. (1995). *Standards and intercomparison materials distributed by the International Atomic Energy Agency for stable isotope measurements.* (No. IAEA-TECDOC--825).

Gottsmann, J., Lavallée, Y., Martí, J., & Aguirre-Díaz, G. (2009). Magma–tectonic interaction and the eruption of silicic batholiths. *Earth and Planetary Science Letters, 284*(3-4), 426-434.

Graeter, K. A., Beane, R. J., Deering, C. D., Gravley, D., & Bachmann, O. (2015). Formation of rhyolite at the Okataina Volcanic Complex, New Zealand: New insights from analysis of quartz clusters in plutonic lithics. *American Mineralogist, 100*(8-9), 1778-1789.

Gravley, D., Deering, C., Leonard, G., & Rowland, J. (2016). Ignimbrite flare-ups and their drivers: A New Zealand perspective. *Earth-Science Reviews, 162*, 65-82.

Gravley, D. M., Wilson, C. J. N., Leonard, G. S., & Cole, J. W. (2007). Double trouble: Paired ignimbrite eruptions and collateral subsidence in the Taupo Volcanic Zone, New Zealand. *GSA Bulletin, 119*(1-2), 18-30.

Gregg, P. M., Grosfils, E. B., & de Silva, S. L. (2015). Catastrophic caldera-forming eruptions II: The subordinate role of magma buoyancy as an eruption trigger. *Journal of Volcanology and Geothermal Research*, *305*, 100-113.

Grocke, S., de Silva, S., Iriarte, R., Lindsay, J., & Cottrell, E. (2017). Catastrophic caldera-forming (CCF) monotonous silicic magma reservoirs: Geochemical and petrological constraints on heterogeneity, magma dynamics, and eruption dynamics of the 3· 49 Ma Tara Supereruption, Guacha II Caldera, SW Bolivia. *Journal of Petrology, 58*(2), 227-260.

Grove, T. L., & Brown, S. M. (2018). Magmatic processes leading to compositional diversity in igneous rocks: Bowen (1928) revisited. *American Journal of Science, 318*(1), 1-28.

Gualda, G. A., Ghiorso, M. S., Lemons, R. V., & Carley, T. L. (2012). Rhyolite-MELTS: a modified calibration of MELTS optimized for silica-rich, fluid-bearing magmatic systems. *Journal of Petrology, 53*(5), 875-890.

Gualda, G. A., Gravley, D. M., Connor, M., Hollmann, B., Pamukcu, A. S., Bégué, F., Ghiorso, M. S., & Deering, C. D. (2018). Climbing the crustal ladder: Magma storage-depth evolution during a volcanic flare-up. *Science Advances, 4*(10), eaap7567.

Hall, G. J. (1994). *Volcanic Geology of the Southeastern Tauranga Basin* MSc thesis, University of Waikato, Hamilton, New Zealand.

Harmsworth, G. R. (1983). *Quaternary stratigraphy of the Tauranga basin (MSc thesis)*. Hamilton, New Zealand: University of Waikato.

Hawthorne, F. C., Oberti, R., Harlow, G. E., Maresch, W. V., Martin, R. F., Schumacher, J. C., & Welch, M. D. (2012). Nomenclature of the amphibole supergroup. *American Mineralogist, 97*(11-12), 2031-2048.

Haywick, D. W., Lowe, D. A., Beu, A. G., Henderson, R. A., & Carter, R. M. (1991). Pliocene-Pleistocene (Nukumaruan) lithostratigraphy of the Tangoio block, and origin of sedimentary cyclicity, central Hawke's Bay, New Zealand. *New Zealand Journal of Geology and Geophysics, 34*(2), 213-225.

Healy, J. (1967). Geological report on proposed tunnel line, Kaimai Railway Deviation. *NZ Geological Survey, DSIR, unpublished report file T14/90-99: 68p*.

Healy, J., Schofield, J., & Thompson, B. (Cartographer). (1964). Sheet 5 Rotorua. Geological Map of New Zealand 1:250 000.

Hegan, B. D. (1972). *Kaimai railway deviation. Kaimai Tunnel, eastern side geological investigations.* NZ Geological Survey, DSIR, unpublished report file EG 129: 3p.

Hegan, B. D. (1973). *Eastern side geological investigations, Kaimai tunnel. Kaimai Railway Deviation.* Unpublished report NZ Geological Survey, Turangi, New Zealand.

Heled, Y., Rowe, M. C., Chambefort, I., & Wilson, C. J. (2022). Significance of tridymite distribution during cooling and vapor-phase alteration of ignimbrites. *American Mineralogist: Journal of Earth and Planetary Materials, 107*(3), 460-475.

Hildreth, W. (1981). Gradients in silicic magma chambers: implications for lithospheric magmatism. *Journal of Geophysical Research: Solid Earth, 86*(B11), 10153-10192.

Hildreth, W. (2004). Volcanological perspectives on Long Valley, Mammoth Mountain, and Mono Craters: several contiguous but discrete systems. *Journal of Volcanology and Geothermal Research*, *136*(3-4), 169-198.

Hollis, A. G. (1995). *Volcanic geology of the central Tauranga Basin, New Zealand.* MSc thesis, University of Waikato, Hamilton, New Zealand.

Holness, M. B. (2018). Melt segregation from silicic crystal mushes: a critical appraisal of possible mechanisms and their microstructural record. *Contributions to Mineralogy and Petrology*, *173*(6), 48.

Hopkins, J. L., Bidmead, J. E., Lowe, D. J., Wysoczanski, R. J., Pillans, B. J., Ashworth, L., Rees, A. B., & Tuckett, F. (2021b). TephraNZ: a major- and trace-element reference dataset for glass-shard analyses from prominent Quaternary rhyolitic tephras in New Zealand and implications for correlation. *Geochronology, 3(2)*, 465-504.

Hopkins, J. L., Lowe, D. J., & Horrocks, J. L. (2021a). Tephrochronology in Aotearoa New Zealand. *New Zealand Journal of Geology and Geophysics, 64(1-2)*, 153-200.

Hopkins, J. L., & Seward, D. (2019). Towards robust tephra correlations in early and pre-Quaternary sediments: A case study from North Island, New Zealand. *Quaternary Geochronology, 50*, 91-108.

Houghton, B. F., & Cuthbertson, A. S. (1989). *Kaimai sheet T14 BD*. Lower Hutt, Wellington, N.Z.: New Zealand Geological Survey, Department of Scientific and Industrial Research.

Huang, Y., Hawkesworth, C., Smith, I., van Calsteren, P., & Black, P. (2000). Geochemistry of late cenozoic basaltic volcanism in Northland and Coromandel, New Zealand: implications for mantle enrichment processes. *Chemical Geology, 164*(3), 219-238.

Huber, C., Bachmann, O., & Dufek, J. (2012). Crystal-poor versus crystal-rich ignimbrites: A competition between stirring and reactivation. *Geology, 40*(2), 115-118.

Hughes, E. C., Law, S., Kilgour, G., Blundy, J., & Mader, H. (2021). Storage, evolution, and mixing in basaltic eruptions from and around the Okataina Volcanic Centre, Taupō Volcanic Zone, Aotearoa New Zealand. *Journal of Volcanology and Geothermal Research*, 434, 107715.

Hughes, G. R. (1993). *Volcanic geology of the eastern Tauranga Basin and Papamoa Range.* MSc thesis, University of Waikato, Hamilton, New Zealand.

Hughes, G. R., & Mahood, G. A. (2011). Silicic calderas in arc settings: Characteristics, distribution, and tectonic controls. *GSA Bulletin, 123*(7-8), 1577-1595.

Jackson, M., Blundy, J., & Sparks, R. (2018). Chemical differentiation, cold storage and remobilization of magma in the Earth's crust. *Nature, 564*(7736), 405-409.

Julian, H. A. (2016). *Volcanology of the Owharoa and Waikino ignimbrites, Waihi, Coromandel Volcanic Zone.* MSc thesis, University of Waikato, Hamilton, New Zealand.

Karhunen, R. (1993). *The Pokai and Chimp ignimbrites of NW Taupo Volcanic Zone. .* PhD thesis, University of Canterbury, Christchurch, New Zealand.

Kay, S. M., Coira, B., Wörner, G., Kay, R. W., & Singer, B. S. (2011). Geochemical, isotopic and single crystal 40 Ar/39 Ar age constraints on the evolution of the Cerro Galán ignimbrites. *Bulletin of Volcanology, 73*(10), 1487-1511.

Kay, S. M., Coira, B. L., Caffe, P. J., & Chen, C.-H. (2010). Regional chemical diversity, crustal and mantle sources and evolution of central Andean Puna plateau ignimbrites. *Journal of Volcanology and Geothermal Research, 198*(1-2), 81-111.

Kennedy, B. M., Holohan, E. P., Stix, J., Gravley, D. M., Davidson, J. R. J., & Cole, J. W. (2018). Magma plumbing beneath collapse caldera volcanic systems. *Earth-Science Reviews, 177*, 404-424.

Kilgour, G., Moune, S., Christenson, B., & Pasqua, F. D. (2021). Insights into the 1976–2000 eruption episode of Whakaari/White Island, New Zealand: an eruption fuelled by repeated mafic recharge. *Bulletin of Volcanology, 83*(6), 1-21.

Kilgour,G.N., & Smith, R.T. (2008). Stratigraphy, dynamics and eruption impacts of the dual magma Rotorua eruptive episode, Okataina Volcanic Centre, New Zealand. *New Zealand Journal of Geology and Geophysics, 51(4), 367-378*.

Kinley, T. (2022). *Volcanic history of the Mount Misery rhyolite domes, Tauranga Volcanic Centre* MSc thesis, University of Waikato, Hamilton, New Zealand.

Krippner, S. J. (2000). *Volcanic geology, geochemistry and geochronology of the Kapowai caldera complex, Coromandel volcanic zone, New Zealand.* PhD thesis, The University of Waikato, Hamilton, New Zealand.

Krippner, S. J. P., Briggs, R. M., Wilson, C. J. N., & Cole, J. W. (1998). Petrography and geochemistry of lithic fragments in ignimbrites from the Mangakino Volcanic Centre: Implications for the composition of the subvolcanic crust in western Taupo Volcanic Zone, New Zealand. *New Zealand Journal of Geology and Geophysics, 41*(2), 187-199.

Kuehn, S. C., Froese, D. G., Shane, P. A., & Participants, I. I. (2011). The INTAV intercomparison of electron-beam microanalysis of glass by tephrochronology laboratories: results and recommendations. *Quaternary International, 246*(1-2), 19-47.

Kutterolf, S., Schindlbeck, J. C., Anselmetti, F. S., Ariztegui, D., Brenner, M., Curtis, J., Schmid, D., Hodell, D., Mueller, A., & Perez, L. (2016). A 400-ka tephrochronological framework for Central America from Lake Petén Itzá (Guatemala) sediments. *Quaternary Science Reviews, 150*, 200-220.

Lavrent'ev, Y. G., Karmanov, N., & Usova, L. (2015). Electron probe microanalysis of minerals: Microanalyzer or scanning electron microscope? *Russian Geology and Geophysics, 56*(8), 1154-1161.

Le Maitre, R. W., Streckeisen, A., Zanettin, B., Le Bas, M., Bonin, B., & Bateman, P. (2002). *Igneous rocks: a classification and glossary of terms: recommendations of the International Union of Geological Sciences Subcommission on the Systematics of Igneous Rocks*. Cambridge University Press.

Leake, B. E., Woolley, A. R., Arps, C. E., Birch, W. D., Gilbert, M. C., Grice, J. D., Hawthorne, F. C., Kato, A., Kisch, H. J., & Krivovichev, V. G. (1997). Report. Nomenclature of amphiboles: report of the subcommittee on amphiboles of the international mineralogical association commission on new minerals and mineral names. *Mineralogical Magazine, 61*(2), 295-321.

Lee, J., Bland, K., Townsend, D., & Kamp, P. (2011). Geology of the Hawkes Bay Area, QMAP 1: 250,000 Geological Map. *GNS Sciences, Lower Hutt, New Zealand, 97*.

Leonard, G. S., Begg, J. G., & Wilson, C. J. N. (2010). *Geology of the Rotorua area. Institute of Geological & Nuclear Sciences 1:250 000 geological map5*. 1 sheet + 102p. Lower Hutt, New Zealand. GNS Science.

Lindsay, J. M., Schmitt, A. K., Trumbull, R. B., De Silva, S. L., Siebel, W., & Emmermann, R. (2001). Magmatic evolution of the La Pacana caldera system, Central Andes, Chile: Compositional variation of two cogenetic, large-volume felsic ignimbrites. *Journal of Petrology*, *42*(3), 459-486.

Lindsay, J., Worthington, T., Smith, I. M., & Black, P. (1999). Geology, petrology, and petrogenesis of Little Barrier Island, Hauraki Gulf, New Zealand. *New Zealand Journal of Geology and Geophysics, 42*(2), 155-168.

Lloyd, E. (1965). Geological report on the proposed Omanawa Mangapapa Opuiaki hydro-electric scheme. *Unpublished Report. New Zealand Geological Survey, Rotorua*.

Locock, A. J. (2014). An Excel spreadsheet to classify chemical analyses of amphiboles following the IMA 2012 recommendations. *Computers & Geosciences, 62*, 1-11.

Lowe, D. J. (2011). Tephrochronology and its application: A review. *Quaternary Geochronology, 6*(2), 107-153.

Lowe, D. J., Pearce, N. J., Jorgensen, M. A., Kuehn, S. C., Tryon, C. A., & Hayward, C. L. (2017). Correlating tephras and cryptotephras using glass compositional analyses and numerical and statistical methods: Review and evaluation. *Quaternary Science Reviews, 175*, 1-44.

Lugmair, G., & Carlson, R. (1978). The Sm-Nd history of KREEP. In *Lunar and Planetary Science Conference Proceedings* (Vol. 9, pp. 689-704).

Lukács, R., Harangi, S., Guillong, M., Bachmann, O., Fodor, L., Buret, Y., Dunkl, I., Sliwinski, J., von Quadt, A., & Peytcheva, I. (2018). Early to Mid-Miocene syn-extensional massive silicic volcanism in the Pannonian Basin (East-Central Europe): Eruption chronology, correlation potential and geodynamic implications. *Earth-science reviews, 179*, 1-19.

Malengreau, B., Skinner, D., Bromley, C., & Black, P. (2000). Geophysical characterisation of large silicic volcanic structures in the Coromandel Peninsula, New Zealand. *New Zealand Journal of Geology and Geophysics, 43*(2), 171-186.

Marxer, F., Ulmer, P., & Müntener, O. (2022). Polybaric fractional crystallisation of arc magmas: an experimental study simulating trans-crustal magmatic systems. *Contributions to Mineralogy and Petrology, 177*(1), 1-36.

Mason, B. G., Pyle, D. M., & Oppenheimer, C. (2004). The size and frequency of the largest explosive eruptions on Earth. *Bulletin of Volcanology, 66*(8), 735-748.

Maughan, L. L., Christiansen, E. H., Best, M. G., Gromme, C. S., Deino, A. L., & Tingey, D. G. (2002). The Oligocene Lund Tuff, Great Basin, USA: a very large volume monotonous intermediate. *Journal of Volcanology and Geothermal Research, 113*(1-2), 129-157.

McCulloch, M., Kyser, T., Woodhead, J., & Kinsley, L. (1994). Pb− Sr− Nd− O isotopic constraints on the origin of rhyolites from the Taupo Volcanic Zone of New Zealand: evidence for assimilation followed by fractionation from basalt. *Contributions to Mineralogy and Petrology, 115*(3), 303-312.

Milicich, S., Chambefort, I., Wilson, C., Alcaraz, S., Ireland, T., Bardsley, C., & Simpson, M. (2020). A zircon U-Pb geochronology for the Rotokawa geothermal system, New Zealand, with implications for Taupō Volcanic Zone evolution. *Journal of Volcanology and Geothermal Research, 389*, 106729.

Milicich, S. D., Mortimer, N., Villamor, P., Wilson, C. J., Chambefort, I., Sagar, M. W., & Ireland, T. R. (2021). The Mesozoic terrane boundary beneath the Taupo Volcanic Zone, New Zealand, and potential controls on geothermal system characteristics. *New Zealand Journal of Geology and Geophysics, 64*(4), 518-529.

Milicich, S. D., Wilson, C. J. N., Bignall, G., Pezaro, B., & Bardsley, C. (2013b). Reconstructing the geological and structural history of an active geothermal field: A case study from New Zealand. *Journal of Volcanology and Geothermal Research, 262*, 7-24.

Milicich, S. D., Wilson, C. J. N., Bignall, G., Pezaro, B., Charlier, B. L. A., Wooden, J. L., & Ireland, T. R. (2013a). U–Pb dating of zircon in hydrothermally altered rocks of the Kawerau Geothermal Field, Taupo Volcanic Zone, New Zealand. *Journal of Volcanology and Geothermal Research, 253*, 97-113.

Miller, M. F., Pack, A., Bindeman, I. N., & Greenwood, R. C. (2020). Standardizing the reporting of Δ'17O data from high precision oxygen triple-isotope ratio measurements of silicate rocks and minerals. *Chemical Geology, 532*, 119332.

Milner, D., Cole, J., & Wood, C. (2003). Mamaku Ignimbrite: a caldera-forming ignimbrite erupted from a compositionally zoned magma chamber in Taupo Volcanic Zone, New Zealand. *Journal of Volcanology and Geothermal Research, 122*(3-4), 243-264.

Morgan, M. D. (1986). *Geology of the northern Mamaku Plateau (MSc thesis)*. Hamilton, New Zealand: University of Waikato.

Morgan, M.D. (1998). Exploration geology of the northeast rim of the MFR eastern Kaimai Caldera, eastern Kaimai Volcanic Complex, Bay of Plenty. Unpublished report.

Muirhead, J. D., Illsley-Kemp, F., Barker, S. J., Villamor, P., Wilson, C. J., Otway, P., ... & Shalla, Y. (2022). Stretching, shaking, inflating: volcanic-tectonic interactions at a rifting silicic caldera. *Frontiers in Earth Science*, 233.

Nairn, I., Wood, C., & Bailey, R. (1994). The Reporoa caldera, Taupo volcanic zone: source of the Kaingaroa ignimbrites. *Bulletin of Volcanology, 56*(6), 529-537.

Naish, T., Kamp, P. J., Alloway, B. V., Pillans, B., Wilson, G. S., & Westgate, J. A. (1996). Integrated tephrochronology and magnetostratigraphy for cyclothemic marine strata, Wanganui Basin: implications for the Pliocene-Pleistocene boundary in New Zealand. *Quaternary International, 34*, 29-48.

Namaliu, M. (2021). *Volcanic geology of the early Pleistocene ignimbrite succession in the western Papamoa Region, Bay of Plenty (MSc thesis).* University of Waikato, Hamilton, New Zealand.

Neave, D. A., Buisman, I., & Maclennan, J. (2017). Continuous mush disaggregation during the long-lasting Laki fissure eruption, Iceland. *American Mineralogist: Journal of Earth and Planetary Materials, 102*(10), 2007-2021.

Pamukcu, A. S., Carley, T. L., Gualda, G. A., Miller, C. F., & Ferguson, C. A. (2013). The evolution of the Peach Spring giant magma body: Evidence from accessory mineral textures and compositions, bulk pumice and glass geochemistry, and rhyolite-MELTS modeling. *Journal of Petrology, 54*(6), 1109-1148.

Pamukçu, A. S., Wright, K. A., Gualda, G. A., & Gravley, D. (2020). Magma residence and eruption at the Taupo Volcanic Center (Taupo Volcanic Zone, New Zealand): insights from rhyolite-MELTS geobarometry, diffusion chronometry, and crystal textures. *Contributions to Mineralogy and Petrology, 175*(5), 1-27.

Paton, C., Hellstrom, J., Paul, B., Woodhead, J., & Hergt, J. (2011). Iolite: Freeware for the visualisation and processing of mass spectrometric data. *Journal of Analytical Atomic Spectrometry, 26*(12), 2508-2518.

Pearce, N. J., Abbott, P. M., & Martin-Jones, C. (2014). Microbeam methods for the analysis of glass in fine-grained tephra deposits: a SMART perspective on current and future trends. *Geological Society, London, Special Publications, 398*(1), 29-46.

Pearce, N. J., Westgate, J. A., Gualda, G. A., Gatti, E., & Muhammad, R. F. (2020). Tephra glass chemistry provides storage and discharge details of five magma reservoirs which fed the 75 ka Youngest Toba Tuff eruption, northern Sumatra. *Journal of Quaternary Science, 35*(1-2), 256-271.

Pearce, N. J. G., Perkins, W. T., Westgate, J. A., & Wade, S. C. (2011). Trace-element microanalysis by LA-ICP-MS: the quest for comprehensive chemical characterisation of single, sub-10 µm volcanic glass shards. *Quaternary International, 246*(1-2), 57-81.

Petrus, J. A., & Kamber, B. S. (2012). VizualAge: A novel approach to laser ablation ICP-MS U-Pb geochronology data reduction. *Geostandards and Geoanalytical Research, 36*(3), 247-270.

Pin, C., Gannoun, A., & Dupont, A. (2014). Rapid, simultaneous separation of Sr, Pb, and Nd by extraction chromatography prior to isotope ratios determination by TIMS and MC-ICP-MS. *Journal of Analytical Atomic Spectrometry, 29*(10), 1858-1870.

Pittari, A., Prentice, M. L., McLeod, O. E., Yousef Zadeh, E., Vincent, K. A., Kamp, P. J. J., & Danisik, M. (2021). Inception of the modern North Island (New Zealand) volcanic setting: Spatio-temporal patterns of volcanism between 3.0 and 0.9 Ma. *New Zealand Journal of Geology and Geophysics, 64(1-2)*, 250-272.

Ponomareva, V., Bubenshchikova, N., Portnyagin, M., Zelenin, E., Derkachev, A., Gorbarenko, S., Garbe-Schönberg, D., & Bindeman, I. (2018). Large-magnitude Pauzhetka caldera-forming eruption in Kamchatka: Astrochronologic age, composition and tephra dispersal. *Journal of Volcanology and Geothermal Research, 366*, 1-12.

Ponomareva, V., Portnyagin, M., & Davies, S. M. (2015). Tephra without borders: far-reaching clues into past explosive eruptions. *Frontiers in Earth Science, 3*, 83.

Prentice, M., Pittari, A., Lowe, D. J., Kilgour, G., Kamp, P. J., & Namaliu, M. (2022). Linking proximal ignimbrites and coeval distal tephra deposits to establish a record of voluminous Early Quaternary (2.4–1.9 Ma) volcanism of the Tauranga Volcanic Centre, New Zealand. *Journal of Volcanology and Geothermal Research, 429*, 107595.

Prentice, M. L., Pittari, A. K., P., Lowe, D. J., & Kilgour, G. (2020). The 2.1 Ma Waitearikí Ignimbrite: defining a new supereruption at the onset of TVZ volcanism. In K. N. Bassett*, et al.* (Eds.), *Geosciences 2020: Abstract Volume. Geoscience Society of New Zealand Miscellaneous Publication 157A* (pp. 227). Wellington: Geoscience Society of New Zealand.

Price, R., Mortimer, N., Smith, I., & Maas, R. (2015). Whole-rock geochemical reference data for Torlesse and Waipapa terranes, North Island, New Zealand. *New Zealand Journal of Geology and Geophysics, 58*(3), 213-228.

Putirka, K. (2016). Amphibole thermometers and barometers for igneous systems and some implications for eruption mechanisms of felsic magmas at arc volcanoes. *American Mineralogist, 101*(4), 841-858.

Putirka, K. D. (2008). Thermometers and barometers for volcanic systems. *Reviews in Mineralogy and Geochemistry, 69*(1), 61-120.

Reyners, M., Eberhart-Phillips, D., Stuart, G., & Nishimura, Y. (2006). Imaging subduction from the trench to 300 km depth beneath the central North Island, New Zealand, with Vp and Vp/Vs. *Geophysical Journal International*, *165*(2), 565-583.

Ridolfi, F. (2021). Amp-TB2: an updated model for calcic amphibole thermobarometry. *Minerals, 11*(3), 324.

Rooyakkers, S. M., Faure, K., Chambefort, I., Barker, S. J., Elms, H. C., Wilson, C. J., & Charlier, B. L. (2022). Tracking magma-crust-fluid interactions at high temporal resolution: Oxygen isotopes in young silicic magmas of the Taupō Volcanic Zone. *Geochemistry, Geophysics, Geosystems*, e2022GC010694.

Rooyakkers, S. M., Stix, J., Berlo, K., Petrelli, M., Hampton, R. L., Barker, S. J., & Morgavi, D. (2021). The origin of rhyolitic magmas at Krafla Central Volcano (Iceland). *Journal of Petrology, 62*(8), egab064.

Rosenberg, M. (2017). *Volcanic and tectonic perspectives on the age and evolution of the Wairakei-Tauhara geothermal system.* PhD thesis, Te Herenga Waka-Victoria University of Wellington, Wellington, New Zealand.

Rowland, J. V., Wilson, C. J., & Gravley, D. M. (2010). Spatial and temporal variations in magma-assisted rifting, Taupo Volcanic Zone, New Zealand. *Journal of Volcanology and Geothermal Research, 190*(1-2), 89-108.

Sagar, M. W., Browne, G. H., Arnot, M. J., Seward, D., & Strogen, D. P. (2019). New U–Pb zircon ages and a revised integrated age model for the late Miocene northern Taranaki coastal section, New Zealand. *New Zealand Journal of Geology and Geophysics, 62*(3), 357-370.

Schaen, AJ, Cottle JM, Singer BS, Keller CB, Garibaldi N, Schoene B (2017) Complementary crystal accumulation and rhyolite melt segregation in a late Miocene Andean pluton. Geology 45:835–838.

Schärer, U. (1984). The effect of initial230Th disequilibrium on young UPb ages: the Makalu case, Himalaya. *Earth and Planetary Science Letters, 67*(2), 191-204.

Schmitz, M. D., & Smith, I. E. (2004). The petrology of the Rotoiti eruption sequence, Taupo Volcanic Zone: an example of fractionation and mixing in a rhyolitic system. *Journal of Petrology, 45*(10), 2045-2066.

Schneider, J. L., Le Ruyet, A., Chanier, F., Buret, C., Ferrière, J., Proust, J. N., & Rosseel, J. B. (2001). Primary or secondary distal volcaniclastic turbidites: how to make the distinction? An example from the Miocene of New Zealand (Mahia Peninsula, North Island). *Sedimentary Geology*, *145*(1-2), 1-22.

Seebeck, H., Nicol, A., Villamor, P., Ristau, J., & Pettinga, J. (2014). Structure and kinematics of the Taupo Rift, New Zealand. *Tectonics, 33*(6), 1178-1199.

Seebeck, H., Van Dissen, R., Litchfield, N., Barnes, P., Nicol, A., Langridge, R., Barrell, D., Villamor, P., Ellis, S., & Rattenbury, M. (2022). New Zealand Community Fault Model–version 1.0.

Shane, P., & Smith, V. C. (2013). Using amphibole crystals to reconstruct magma storage temperatures and pressures for the post-caldera collapse volcanism at Okataina volcano. *Lithos, 156*, 159-170.

Sharp, Z. D. (1990). A laser-based microanalytical method for the in situ determination of oxygen isotope ratios of silicates and oxides. *Geochimica et Cosmochimica Acta, 54*(5), 1353-1357.

Shaw, D. M. (1970). Trace element fractionation during anatexis. *Geochimica et Cosmochimica Acta, 34*(2), 237-243.

Silleni, A., Giordano, G., Isaia, R., & Ort, M. H. (2020). The Magnitude of the 39.8 ka Campanian Ignimbrite Eruption, Italy: Method, Uncertainties and Errors. *Field Data, Models and Uncertainty in Hazard Assessment of Pyroclastic Density Currents and Lahars: Global Perspectives*.

Simmons, J. M., Cas, R., Druitt, T., & Folkes, C. (2016). Complex variations during a caldera-forming Plinian eruption, including precursor deposits, thick pumice fallout, co-ignimbrite breccias and climactic lag breccias: The 184 ka Lower Pumice 1 eruption sequence, Santorini, Greece. *Journal of Volcanology and Geothermal Research, 324*, 200-219.

Sisson TW, Bacon CR (1999) Gas-driven filter pressing in magmas. Geology 27:613–616.

Sliwinski JT, Bachmann O, Dungan MA, Huber C, Deering CD, Lipman PW, Martin LHJ, Liebske C (2017) Rapid pre-eruptive thermal rejuvenation in a large silicic magma body: the case of the Masonic Park Tuff, Southern Rocky Mountain volcanic field, CO, USA. Contrib Mineral Petrol 172:30.

Smith, N., Cassidy, J., Locke, C., Mauk, J., & Christie, A. (2006). The role of regional-scale faults in controlling a trapdoor caldera, Coromandel Peninsula, New Zealand. *Journal of Volcanology and Geothermal Research, 149*(3-4), 312-328.

Spencer, C. J., Kirkland, C. L., & Taylor, R. J. (2016). Strategies towards statistically robust interpretations of in situ U–Pb zircon geochronology. *Geoscience Frontiers, 7*(4), 581-589.

Srivastava, P., Krishna, A., Jawed, S., & Sarkhel, P. (2020). Quantitative minerological analysis of some granite rocks of deoghar jharkhand. *Earth Sci. Res, 9*, 30.

Stacey, J. S., & Kramers, J. D. (1975). Approximation of terrestrial lead isotope evolution by a two-stage model. *Earth and Planetary Science Letters, 26*(2), 207-221.

Stagpoole, V., Miller, C., Caratori Tontini, F., Brakenrig, T., & Macdonald, N. (2021). A two million-year history of rifting and caldera volcanism imprinted in new gravity anomaly compilation of the Taupō Volcanic Zone, New Zealand. *New Zealand Journal of Geology and Geophysics, 64*(2-3), 358-371.

Steiger, R. H., & Jäger, E. (1977). Subcommission on geochronology: convention on the use of decay constants in geo-and cosmochronology. *Earth and Planetary Science Letters, 36*(3), 359-362.

Stevens, M. T. (2010). Miocene and Pliocene Silicic Coromandel Volcanic Zone Tephras from ODP Site 1124-C: Petrogenetic Applications and Temporal Evolution (MSc thesis). Victoria University of Wellington, New Zealand.

Stipp, J. J. (1968). *The geochronology and petrogenesis of the Cenozoic volcanics of North Island, New Zealand.* PhD thesis, Australian National University, Canberra, Australia.

Straub, S. M., Woodhead, J. D., & Arculus, R. J. (2015). Temporal evolution of the Mariana Arc: Mantle wedge and subducted slab controls revealed with a tephra perspective. *Journal of Petrology, 56*(2), 409-439.

Sun, S., & McDonough, W. (1989). Chemical and isotopic systematics of oceanic basalts: implications for mantle composition and processes. *Geological Society, London, Special Publications, 42*(1), 313-345.

Sutton, A. N., Blake, S., & Wilson, C. J. (1995). An outline geochemistry of rhyolite eruptives from Taupo volcanic centre, New Zealand. *Journal of Volcanology and Geothermal Research, 68*(1-3), 153-175.

Sutton, A. N., Blake, S., Wilson, C. J., & Charlier, B. L. (2000). Late Quaternary evolution of a hyperactive rhyolite magmatic system: Taupo volcanic centre, New Zealand. *Journal of the Geological Society, 157*(3), 537-552.

Takagi, M. (1995). *Miocene-Pliocene arc volcanism of the Hauraki region in North Island, New Zealand (MSc thesis)*. Okayama, Japan: Hiruzen Research Institute.

Teixeira, R., Neiva, A. M., Gomes, M., Corfu, F., Cuesta, A., & Croudace, I. (2021). The importance of sequential partial melting and fractional crystallisation in the generation of syn-D3 Variscan two-mica granites from the Carrazeda de Ansiães area, northern Portugal. *Journal of Iberian Geology, 47*(1), 281-305.

Thirlwall, M. (1991). Long-term reproducibility of multicollector Sr and Nd isotope ratio analysis. *Chemical Geology: Isotope Geoscience section, 94*(2), 85-104.

Tomlinson, E. L., Smith, V. C., Albert, P. G., Aydar, E., Civetta, L., Cioni, R., Çubukçu, E., Gertisser, R., Isaia, R., & Menzies, M. A. (2015). The major and trace element glass compositions of the productive Mediterranean volcanic sources: tools for correlating distal tephra layers in and around Europe. *Quaternary Science Reviews, 118*, 48-66.

Vermeesch, P. (2018). IsoplotR: A free and open toolbox for geochronology. *Geoscience Frontiers, 9*(5), 1479-1493.

Vho, A., Lanari, P., & Rubatto, D. (2019). An internally-consistent database for oxygen isotope fractionation between minerals. *Journal of Petrology, 60*(11), 2101-2129.

Villamor, P., & Berryman, K. (2001). A late Quaternary extension rate in the Taupo Volcanic Zone, New Zealand, derived from fault slip data. *New Zealand Journal of Geology and Geophysics, 44*(2), 243-269.

Villamor, P., Berryman, K., Ellis, S., Schreurs, G., Wallace, L., Leonard, G., Langridge, R., & Ries, W. (2017). Rapid evolution of subduction-related continental intraarc rifts: The Taupo Rift, New Zealand. *Tectonics, 36*(10), 2250-2272.

Villamor, P., Litchfield, N. J., Gómez-Ortiz, D., Martin-González, F., Alloway, B. V., Berryman, K. R., Clark, K. J., Ries, W. F., Howell, A., & Ansell, I. A. (2022). Fault ruptures triggered by large rhyolitic eruptions at the boundary between tectonic and magmatic rift segments: The Manawahe Fault, Taupō Rift, New Zealand. *Journal of Volcanology and Geothermal Research, 427*, 107478.

Vincent, K. A. (2012). *U-Pb Dating of Silicic Volcanic Rocks of the Eastern Coromandel Peninsula.* MSc thesis, University of Waikato, Hamilton, New Zealand.

Walker, T., & Howitt, D. G. (1989). Field-induced migration of sodium in soda silicate glasses during scanning electron microscopy. *Scanning, 11*(1), 5-11.

Walshaw, R. (2018). Electron probe microanalysis (EMPA) in the Earth Sciences. In *Book of Turorials and Abstracts. 13th Regional workshop on "Microbeam Analysis in the Earth Sciences", 04-07 Sep 2018* (pp. 77-92). University of Bristol: European Microbeam Analysis Society.

Waters, L. E., & Lange, R. A. (2015). An updated calibration of the plagioclase-liquid hygrometer-thermometer applicable to basalts through rhyolites. *American Mineralogist, 100*(10), 2172-2184.

Whitbread-Edwards, A. N. (1994). *Volcanic Geology of the Western Tauranga Basin.* MSc thesis, University of Waikato, Hamilton, New Zealand.

White, J., & Houghton, B. (2006). Primary volcaniclastic rocks. *Geology, 34*(8), 677-680.

Willcock, M., Bargossi, G., Weinberg, R., Gasparotto, G., Cas, R., Giordano, G., & Marocchi, M. (2015). A complex magma reservoir system for a large volume intra-to extra-caldera ignimbrite:

Mineralogical and chemical architecture of the VEI8, Permian Ora ignimbrite (Italy). *Journal of Volcanology and Geothermal Research, 306*, 17-40.

Willcock, M., Cas, R. A. F., Giordano, G., & Morelli, C. (2013). The eruption, pyroclastic flow behaviour, and caldera in-filling processes of the extremely large volume (> 1290 km3), intra-to extra-caldera, Permian Ora (Ignimbrite) Formation, Southern Alps, Italy. *Journal of Volcanology and Geothermal Research, 265*, 102-126.

Williams, I. S. (1998). U-Th-Pb geochronology by ion microprobe. *Reviews in Economic Geology, 7*, 1-35.

Wilson, C., Gravley, D., Leonard, G., & Rowland, J. (2009). Volcanism in the central Taupo Volcanic Zone, New Zealand: tempo, styles and controls. *Studies in Volcanology: the legacy of George Walker. Special Publications of IAVCEI, 2*, 225-247.

Wilson, C., Houghton, B., Kampt, P., & McWilliamst, M. (1995b). An exceptionally widespread ignimbrite with implications for pyroclastic flow emplacement. *Nature, 378*(6557), 605-607.

Wilson, C. J., Blake, S., Charlier, B., & Sutton, A. (2006). The 26· 5 ka Oruanui eruption, Taupo volcano, New Zealand: development, characteristics and evacuation of a large rhyolitic magma body. *Journal of Petrology, 47*(1), 35-69.

Wilson, C. J., Cooper, G. F., Chamberlain, K. J., Barker, S. J., Myers, M. L., Illsley-Kemp, F., & Farrell, J. (2021). No single model for supersized eruptions and their magma bodies. *Nature Reviews Earth & Environment, 2*(9), 610-627.

Wilson, C. J. N. (1986). Reconnaissance stratigraphy and volcanology of ignimbrites from Mangakino volcano. In I. E. M. Smith (Ed.), *Late cenozoic volcanism in New Zealand* (pp. 179-193). Wellington, New Zealand: The Royal Society of New Zealand Bulletin 23.

Wilson, C. J. N., Houghton, B. F., McWilliams, M. O., Lanphere, M. A., Weaver, S. D., & Briggs, R. M. (1995a). Volcanic and structural evolution of Taupo Volcanic Zone, New Zealand: a review. *Journal of Volcanology and Geothermal Research, 68*(1), 1-28.

Wilson, C. J. N., & Rowland, J. V. (2016). The volcanic, magmatic and tectonic setting of the Taupo Volcanic Zone, New Zealand, reviewed from a geothermal perspective. *Geothermics, 59, Part B*, 168-187.

Winter, J. D. (2013). *Principles of Igneous and Metamorphic petrology*. (2nd ed.). Harlow, UK: Pearson Education.

Woldemichael, S. (1998). *Low grade metamorphism and hydrothermal alteration in the basement greywacke terranes of the northern and central North Island, New Zealand: reconnaissance study.* PhD thesis, University of Auckland, Auckland, New Zealand.

Yamamoto, T. (2021). Geochemistry of caldera-forming and resurgent magmas in the Pliocene Hiwada caldera, northeast Japan: An example of a monotonous intermediate system. *Island Arc, 30*(1), e12415.

Yousef Zadeh, E. (2020). *Eruption and emplacement of the 1.3-Ma Ongatiti Ignimbrite, New Zealand: Regional pathways, particle processes, and pumice evolution associated with a large-volume pyroclastic flow deposit.* PhD thesis, The University of Waikato, Hamilton, New Zealand.

Yousefi, F., Sadeghian, M., Wanhainen, C., Ghasemi, H., Lambrini, P., Bark, G., Rezaei-Kahkhaei, M., & Koroneos, A. (2017). Mineral chemistry and PT conditions of the adakitic rocks from Torud–Ahmad Abad magmatic belt, S-SE Shahrood, NE Iran. *Journal of Geochemical Exploration, 182*, 110-120.

Zellmer, G. F. (2021). Gaining acuity on crystal terminology in volcanic rocks. *Bulletin of Volcanology, 83*(11), 1-8.

Zhao, Z.-F., & Zheng, Y.-F. (2003). Calculation of oxygen isotope fractionation in magmatic rocks. *Chemical Geology, 193*(1-2), 59-80.

Appendix A:

Sample Catalogue

Sample ID	Waikato ID #	Site description	Easting (NZTM)	Northing (NZTM)	Elevation (m)	Rock type	Geological Unit
TePu	W18 0001	Te Puna Station Road	1872497	5823877	6	Ignimbrite	Pakaumanu Group
WAI#2	W18 0002	McLaren Falls	1868122	5811428	82	Ignimbrite	Waiteariki Formation
HP1	W18 0003	Darkys Spur Road	1929975	5649026	412	Ignimbrite	Hikuroa Pumice Member
HP2	W18 0004	Darkys Spur Road	1929975	5649026	414	Ignimbrite	Hikuroa Pumice Member
HP3	W18 0005	Darkys Spur Road	1929975	5649026	414	Ignimbrite	Hikuroa Pumice Member
HP4	W18 0006	Darkys Spur Road	1929975	5649026	414	Ignimbrite	Hikuroa Pumice Member
L12	W18 0007	Private land, Reid Road	1888249	5819579	30	Otawera Ignimbrite	Papamoa Formation
Esk Mst-T1	W18 0008	Waikoau River	1933272	5650502	137	Coarse tuff	Esk Mudstone Fmn
Esk Mst-T2	W18 0009	Waikoau River	1933274	5650509	129	Coarse tuff	Esk Mudstone Fmn
Pap4/L11	W18 0010	Top of bluffs, Waitoa Road	1884539	5817005	110	Arateka Ignimbrite	Papamoa Formation
Pap1	W18 0011	Road cutting Road	1886604	5820334	61	Wharo Ignimbrite	Papamoa Formation
L5	W18 0012	Welcome Bay Road	1887590	5819156	105	Wharo Ignimbrite	Papamoa Formation
Pap2	W18 0013	Rocky Cutting Road	1885981	5817180	120	Welcome Bay Ignimbrite	Papamoa Formation
L2WP	W18 0014	Rocky Cutting Road	1885981	5817180	120	Welcome Bay ignimbrite (white pumice)	Papamoa Formation
L2BP	W18 0015	Rocky Cutting Road	1885981	5817180	120	Welcome Bay ignimbrite (dark-grey pumice)	Papamoa Formation
L4	W18 0016	Private land, Welcome Bay Rd	1887378	5819275	112	Welcome Bay Ignimbrite	Papamoa Formation
L7	W18 0017	Private land, Welcome Bay Rd	1886829	5819376	60	Welcome Bay Ignimbrite	Papamoa Formation
WAI3	W18 0018	Top of Wairere Falls	1853795	5819773	406	Ignimbrite	Waiteariki Formation
WAI4	W18 0019	Wairere Falls. Fallen block	1853478	5819659	305	Ignimbrite	Waiteariki Formation
WAI6	W18 0020	McLaren Falls – lower falls	1868122	5811428	82	Ignimbrite	Waiteariki Formation
WAI11	W18 0021	lower Aongatete River	1856538	5826490	163	Ignimbrite	Waiteariki Formation
WAI12	W18 0022	Mangaputa Stream	1862502	5812254	205	Ignimbrite	Waiteariki Formation
MRhy15	W18 0023	Upper Ngamuwahine River	1860336	5815034	360	Rhyolite	Minden Rhyolite-TeWheritu
WAI16	W10 0024	Waterfall on Rataroa Stream	1860160	5807868	394	Ignimbrite	Waiteariki Formation
WAI22	W18 0025	Upper Aongatete River	1855485	5825788	280	Basal ignimbrite	Waiteariki Formation
WAI23	W18 0026	Aongatete Loop track river crossing	1856780	5825826	253	Ignimbrite	Waiteariki Formation
WAI25	W18 0027	Aongatete River	1856608	5826461	178	Ignimbrite	Waiteariki Formation
WAI28	W18 0028	Aongatete River	1856651	5826397	218	Ignimbrite	Waiteariki Formation
WAI29	W18 0029	Ohauiti Road	1879745	5813844	143	Ignimbrite	Waiteariki Formation
MRhy30	W18 0030	Farm track; Maungatūtū/Mt Misery	1880335	5810259	380	Weathered rhyolite	Minden Rhyolite-Manungatūtū/Mt Misery
MRhy32	W18 0031	Oropi Quarry, McPhail Road	1881711	5808984	288	Flow banded rhyolite	Minden Rhyolite-Greenpark
Otawa33	W18 0032	Jswap Tauranga Quarry, Kaitemako Rd. Base, Top Quarry	1882842	5814073	119	Andesite	Otawa Formation
MRhy34	W18 0033	Jswap Tauranga Quarry, Kaitemako Rd. Top, Top Quarry	1882785	5814368	242	Rhyolite	Minden Rhyolite-Pukunui

Sample ID	Waikato ID #	Site description	Easting (NZTM)	Northing (NZTM)	Elevation (m)	Rock type	Geological Unit
Otawa35	W18 0034	Jswap Tauranga Quarry, Kaitemako Rd. Pit - Base Old Quarry	1882901	5815006	64	Dacite	Otawa Formation
Otawa36	W18 0035	Jswap Tauranga Quarry, Kaitemako Rd. Mid level - Old Quarry	1883095	5815049	127	Dacite	Otawa Formation
Otawa37	W18 0036	Jswap Tauranga Quarry, Kaitemako Road. Top level - Old Quarry	1883311	5815007	236	Dacite	Otawa Formation
Otawa38	W18 0037	Poplar Lane Quarry	1889043	5817865	80	Andesite	Otawa Formation
Otawa39	W18 0038	Poplar Lane Quarry	1889276	5817756	80	Andesite	Otawa Formation
MRhy40	W18 0039	Kopukairua Dome	1885009	5818435	20	Dacite	Minden Rhyolite-Kopukairua
MRhy41	W18 0040	Waitao Dome	1884461	5818601	20	Dacite	Minden Rhyolite-Waitao
MRhy42	W18 0041	Mangatawa	1885770	5822694	22	Rhyolite	Minden Rhyolite-Mangatawa
MRhy45	W18 0042	Papamoa Dome	1889979	5819202	80	Dacite	Minden Rhyolite-Papamoa
MRhy46	W18 0043	Waikite	1883778	5817668	200	Rhyolite	Minden Rhyolite-Waikite
MRhy47	W18 0044	Crawford Road; A. Whitbread-Edwards (W94322)	1870471	5820284	130	Rhyolite	Minden Rhyolite-Minden Peak
MRhy48	W18 0045	Crawford Road; A. Whitbread-Edwards (W94323)	1870477	5819997	120	Rhyolite	Minden Rhyolite-Minden Peak
MRhy49	W18 0046	Te Puna Quarry; A. Whitbread-Edwards (W94338)	1868578	5822495	120	Rhyolite	Minden Rhyolite-Minden Peak
MRhy50	W18 0047	Te Puna Quarry; A. Whitbread-Edwards (W94340)	1868578	5822495	120	Rhyolite	Minden Rhyolite-Minden Peak
MRhy51	W18 0048	Te Puna Quarry; A. Whitbread-Edwards (W94341)	1868578	5822495	120	Rhyolite	Minden Rhyolite-Minden Peak
MRhy52	W18 0049	Kaikaikaroro, Sth of track from end Kumikumi Rd; A. Whitbread-Edwards (W94327)	1863992	5813919	380	Rhyolite	Minden Rhyolite-Kaikaikaroro
MRhy53	W18 0050	Sth slope; A. Whitbread-Edwards (W94329)	1865970	5816479	305	Rhyolite	Minden Rhyolite-Manawata
Wai55	W18 0051	McLaren Falls; A.Whitbread-Edwards (W94350)	1868098	5811375	100	Ignimbrite	Waiteariki Formation
MRhy56	W18 0052	Mangatoi & Mountain Rds intersection; G. Hughes (W9316)	1865970	5816479	305	Rhyolite	Minden Rhyolite-Otanewainuku
MRhy57	W18 0053	SE slope, Kopukairua; G. Hughes (W9317)	1884798	5818892	60	Dacite	Minden Rhyolite-Kopukairua
MRhy58	W18 0054	Waikite peak; G. Hughes (W9332)	1882492	5817591	180	Rhyolite	Minden Rhyolite-Waikite
MRhy60	W18 0055	Northern slope; G. Hughes (W9352)	1889979	5819202	80	Dacite	Minden Rhyolite-Papamoa Dome
MRhy61	W18 0056	Western slope, base track; G. Hall (W95976)	1879531	5830696	20	Rhyolite	Minden Rhyolite-Mt Maunganui
MRhy62	W18 0057	Moturiki Island; G. Hall (W95978)	1881058	5830312	10	Rhyolite	Minden Rhyolite-Moturiki Island
MRhy63	W18 0058	Kaimai Dome, rocky knoll leady to cell tower	1858431	5804386	551	Rhyolite	Minden Rhyolite-Kaimai Dome
MRhy64	W18 0059	Kaimai Swap Farm, rocky ridge E of farm buildings	1857093	5803363	411	Rhyolite	Minden Rhyolite-Kaimai Dome
MRhy65	W18 0060	Bowentown Heads rock outcrop; E. Cook (W150325)	1864235	5849082	30	Rhyolite	Minden Rhyolite-Bowentown
MB66	W18 0061	Rocky outcrop offshore Matakana Island; A. Hollis (W95214)	1868404	5833950	5	Basaltic andesite	Matakana Basalt
ES112-138	W18 0062	Core - ES112. Top of ridge by Aongatete Lodge	1856969	5826951	222	Ignimbrite	Waiteariki Formation
ES112-165	W18 0063	Core - ES112. Top of ridge by Aongatete Lodge	1856969	5826951	222	Ignimbrite	Waiteariki Formation
ES112-243	W18 0064	Core - ES112. Top of ridge by Aongatete Lodge	1856969	5826951	222	Ignimbrite	Waiteariki Formation

Sample ID	Waikato ID #	Site description	Easting (NZTM)	Northing (NZTM)	Elevation (m)	Rock type	Geological Unit
ES112-288	W18 0065	Core - ES112. Top of ridge by Aongatete Lodge	1856969	5826951	222	Ignimbrite	Waiteariki Formation
ES112-309	W18 0066	Core - ES112. Top of ridge by Aongatete Lodge	1856969	5826951	222	Ignimbrite	Waiteariki Formation
ES112-330	W18 0067	Core - ES112. Top of ridge by Aongatete Lodge	1856969	5826951	222	Ignimbrite	Waiteariki Formation
ES112-351	W18 0068	Core - ES112. Top of ridge by Aongatete Lodge	1856969	5826951	222	Ignimbrite	Waiteariki Formation
ES112-366	W18 0069	Core - ES112. Top of ridge by Aongatete Lodge	1856969	5826951	222	Ignimbrite	Waiteariki Formation
ES112-393	W18 0070	Core - ES112. Top of ridge by Aongatete Lodge	1856969	5826951	222	Ignimbrite	Waiteariki Formation
ES112-411	W18 0071	Core - ES112. Top of ridge by Aongatete Lodge	1856969	5826951	222	Ignimbrite	Waiteariki Formation
ES112-432	W18 0072	Core - ES112. Top of ridge by Aongatete Lodge	1856969	5826951	222	Ignimbrite	Waiteariki Formation
ES112-462	W18 0073	Core - ES112. Top of ridge by Aongatete Lodge	1856969	5826951	222	Ignimbrite	Waiteariki Formation
ES112-483	W18 0074	Core - ES112. Top of ridge by Aongatete Lodge	1856969	5826951	222	Ignimbrite	Waiteariki Formation
ES112-489	W18 0075	Core - ES112. Top of ridge by Aongatete Lodge	1856969	5826951	222	Ignimbrite	Waiteariki Formation
ES112-501	W18 0076	Core - ES112. Top of ridge by Aongatete Lodge	1856969	5826951	222	Ignimbrite	Waiteariki Formation

Appendix B:

Co-Authorship Form

THE UNIVERSITY OF WAIKATO

Co-Authorship Form

Postgraduate Studies Office
Student and Academic Services Division
Waharoa Ratonga Matauranga Akonga
The University of Waikato
Private Bag 3105
Hamilton 3240, New Zealand
Phone +64 7 838 4439
Website: http://www.waikato.ac.nz/sasd/postgraduate/

This form is to accompany the submission of any PhD that contains research reported in published or unpublished co-authored work. **Please include one copy of this form for each co-authored work.** Completed forms should be included in your appendices for all the copies of your thesis submitted for examination and library deposit (including digital deposit).

Please indicate the chapter/section/pages of this thesis that are extracted from a co-authored work and give the title and publication details or details of submission of the co-authored work.

Chapter 2 - Linking Proximal ignimbrites & coeval distal tephra deposits to establish a record of voluminous Early Quaternary (2.4-1.9 Ma) volcanism of the Taupo Volcanic Centre - Journal of Volcanology & Geothermal research (2022) 429, 107512

Nature of contribution by PhD candidate	Conceptualization, Investigation, Analysis & validation. Writing & editing. & Revisions.
Extent of contribution by PhD candidate (%)	90

CO-AUTHORS

Name	Nature of Contribution	
Adrian Pittari	Supervision, Review & editing	2%
David Lowe	Supervision, Review	2%
Geoff Kilgour	Supervision, Review	2%
Peter Kamp	Advisor, field work assistance	1%
Miriam Nahalia	Field work assistance, analysis & provided some preliminary data on the Papapoa Formation	3%

Certification by Co-Authors

The undersigned hereby certify that:

- the above statement correctly reflects the nature and extent of the PhD candidate's contribution to this work, and the nature of the contribution of each of the co-authors; and

Name	Signature	Date
Geoff Kilgour		23/01/2023
Adrian Pittari	Adrian Pittari	25/01/2023
David Lowe	D Lowe	25/01/2023
Peter Kamp	P.J. Kamp.	26/1/2023
MIRIAM NAHALIA		18/01/2023

July 2015

Appendix C: Conference Abstracts arising from thesis

The 2.1 Ma Waitearikí Ignimbrite: Product of a large explosive silicic eruption during the Coromandel-Taupō transition

M. Prentice[1], M.D Rosenberg[2], A. Pittari[1], D.J. Lowe[1] & G. Kilgour[2]

[1] School of Science, University of Waikato, Private Bag 3105, Hamilton, New Zealand

[2]GNS Science, Private Bag 2000, Taupo, New Zealand

prenticelm@gmail.com

Subduction-related volcanism within the North Island, New Zealand has migrated southeast since the Late Miocene. The resulting volcanic deposits and landforms are classified as two broad volcanic zones – the currently active Taupo Volcanic Zone (TVZ) and the older Coromandel Volcanic Zone (CVZ). The transition from the CVZ to the TVZ occurred ~ 2.9-1.9 Ma, and is represented by the Tauranga and Kaimai Volcanic Centres. Outcrops of eruptives associated with this transitional interval are exposed in the eastern Tauranga Basin and adjacent Kaimai Range. Despite its significance, our understanding of volcanism during this period remains limited. The focus on this eruptive period and locality forms the basis of a PhD programme that aims to reconstruct the proximal record, ages and scale of volcanism of the Tauranga and Kaimai volcanic centres with a major focus on large-scale explosive events.

The voluminous and crystal-rich c. 2.1 Ma Waitearikí Ignimbrite, forms the gently sloping upper surface of the Whakamarama Plateau that dips eastward beneath younger sediments of the Tauranga Basin forming the regional basement. Preliminary analysis of ~170 m of continuous core through the Waitearikí Ignimbrite reveals that the ignimbrite is extensively devitrified and welded and is composed of a least two cooling units and a basal sequence of pumiceous breccias and ash. We present initial petrological descriptions detailing crystallinity, mineral phases and variations in pumice and lithic size along with whole-rock XRF analyses of juvenile clasts. The physical characterisation of the Waitearikí Ignimbrite is the first step to unravelling the extent of explosive volcanism during the initiation of the TVZ with future work focusing on mineral phases and mineral-hosted melt inclusions, which will provide insights into the magmatic system fuelling volcanism of the Tauranga and Kaimai Volcanic Centres.

The 2.1 Ma Waitearikí Ignimbrite: Super-eruption at the dawn of the TVZ

M. Prentice[1], P. Kamp[1], A. Pittari[1], D.J. Lowe[1], G. Kilgour[2]

[1] School of Science, University of Waikato, Private Bag 3105, Hamilton

[2]GNS Science, Private Bag 2000, Taupo

prenticelm@gmail.com

The crystal-rich c. 2.1 Ma Waitearikí Ignimbrite is the most voluminous and prominent volcanic deposit of the Tauranga and Kaimai volcanic centres which were active ~ 2.9–1.9 Ma. During this time, subduction-related volcanic activity transitioned from the older Coromandel Volcanic Zone (CVZ) to the currently active Taupo Volcanic Zone (TVZ). Despite its significance, our understanding of volcanism during this period remains limited.

Major and trace element analysis of glass and new LA-ICP-MS U-Pb zircon ages have confirmed a distal ignimbrite (Hikuroa Pumice Member) found within Mangaheia Group rocks of Nukumaruan age in the Lake Tutira region of Hawkes Bay, to be the distal deposits of the Waitearikí Ignimbrite. Based on this newly-defined distribution, we calculate a minimum eruptive volume estimate of 540 Km^3 DRE, that it is almost certainly the product of a caldera forming super-eruption. We suggest the presence of the Omanawa caldera structure buried below younger deposits of the northern Mamaku Plateau, situated at the southern end of an asymmetrical rifted graben, which lies between the Kaimai and Papamoa Ranges. Faulting has been episodic, and associated with periods of dome growth throughout the region. The western fault occurs along the Wairoa River, which has channelized young pyroclastic density currents entering the Tauranga Region from the modern TVZ. Thus, we propose the definition of the early TVZ be extended to include the super-eruption of the Waitearikí Ignimbrite. The Tauranga and Kaimai volcanic centres have been redefined as the Tauranga volcanic centre, which includes all volcanic deposits within the region aged between 3–1.9 Ma. Going forward, research will be focused on the geochemical analysis of the Waitearikí Ignimbrite, to chemically characterise and determine the pre-eruptive conditions of the underlying magmatic system, which fuelled the eruption of New Zealand's earliest identified supereruption.

Advances towards a comprehensive ignimbrite stratigraphy of the Tauranga Volcanic Centre, North Island, New Zealand

Marlena Prentice[1], Miriam Namaliu[1], Adrian Pittari[1], David J. Lowe[1], Peter Kamp[1] and Geoff Kilgour[2]

[1] *School of Science/Te Aka Mātuatua, University of Waikato, Hamilton, New Zealand*

[2] *GNS Science, Taupo, New Zealand*

prenticelm@gmail.com

The Tauranga Volcanic Centre (TgaVC), in western Bay of Plenty, was active from 2.95 to 1.90 Ma. Volcanic products of TgaVC comprise an eroded andesitic stratovolcano (Otawa Formation), numerous rhyolite-dacite lava dome/dome complexes (Minden Rhyolite Subgroup), minor exposures of basalt near Matakana Island within Tauranga Harbour, and a pyroclastic succession comprising multiple ignimbrites that was conventionally split into a package of multiple, related ignimbrite and fall deposits of the older Papamoa Formation and the climactic ignimbrite of the Waitekariki Formation.

We have revised the stratigraphy of the pyroclastic succession of the Papamoa Formation which is confined to the northern and western foothills of the Papamoa Range, overlying the Otawa Formation. Five ignimbrites have been identified and four locally widespread units are named as follows: non-welded Welcome Bay and welded Wharo ignimbrites (together formerly Lower Papamoa Ignimbrite); non-welded Otawera Ignimbrite; and non-welded Arateka Ignimbrite (formerly Upper Papamoa Ignimbrite). These ignimbrites can be distinguished on the basis of proportion of pumice types, textural properties, and geochemical composition. Radiometric dating indicates they were erupted between ~2.4 and ~2.2 Ma. The ~2.1 Ma voluminous, welded, crystal-rich Waitekariki Ignimbrite is proximally-exposed over a wide area west of the Papamoa Range.

By combining this revised proximal stratigraphy of the TgaVC and distal tephra records identified in contemporaneous sediments of northern Hawke's Bay, we identify eight explosive rhyolitic eruptions that took place between ~2.4 and 2.0 Ma, giving an average repose period between explosive eruptions for the TgaVC of ~50 kyrs. This is a maximum value as local dome eruptions have been excluded due to uncertain links between them and known tephra-fall deposits. The eruption tempo indicates that the period 2.4–2.0 Ma was a time of frequent rhyolitic activity centered within the TgaVC throughout the contiguous Tauranga and Kaimai regions which culminated with the eruption of the Waitekariki Ignimbrite.

Silicic volcanism at the dawn of the TVZ: Trends in geochemistry, mineralogy and magma storage, of the Tauranga Volcanic Centre, NZ

Marlena Prentice[1], Adrian Pittari[1], Geoff Kilgour[2] and David Lowe[1]

[1] School of Science/Te Aka Mātuatua, University of Waikato, Hamilton, New Zealand

[2] GNS Science, Taupō, New Zealand.

prenticelm@gmail.com

The Tauranga Volcanic Centre (TgaVC), in western Bay of Plenty, was active from ~2.95 to 1.90 Ma, around the time of Taupō Volcanic Zone initiation. Volcanic products of TgaVC include minor exposures of basalt (Matakana Basalt), an eroded andesitic stratovolcano (Otawa Formation), several dacite-rhyolite- lava dome/dome complexes (Minden Rhyolite Subgroup), and a pyroclastic succession comprising multiple ignimbrites and related fall deposits (Papamoa Formation) followed by the climactic eruption of the rhyodacite Waiteariki Ignimbrite. Silicic volcanism throughout the region was frequent yet episodic, with two key periods of activity occurring between ~2.5–2.3 and ~2.2–2.1 Ma. The NE alignment of domes is linked to regional extensional faulting where the western boundary coincides with that of the old Taupō Rift.

Magmas erupted from the TgaVC are typically crystal-rich (up to 40–50% phenocrysts) with a consistent mineral assemblage of plagioclase > hornblende ≥ orthopyroxene ± quartz ± biotite with olivine and sanidine present only in the Matakana basalt and Bowentown Rhyolite, respectively. Whole-rock compositions span a continuous range between basalt (53.8 wt. % SiO_2, 4.0 wt. % MgO; Mg# 48) to rhyolite (76.7 wt. % SiO_2) which in conjunction with trace element and isotopic compositions suggest a genesis involving fractionation, partial melting and assimilation of the surrounding crust and interaction with more primitive melts. Estimates of magmatic conditions for the Waiteariki Ignimbrite are modelled using multiple independent crystal-melt (plag-liq, opx-liq) or crystal-only (cpx; Al-in-hornblende) geothermobarometers to give pre-eruptive temperature ranges between 740–840°C and 900–990°C (ave. 790°C, and 950 °C, respectively) with a broader range observed for TgaVC lavas. Pressure estimates for all units range from < 50–150 MPa and indicative of multiple extraction zones and shallow, upper-crustal storage similar to models for rhyolites of the TVZ.

Eruption of a large-volume, monotonous intermediate ignimbrite at the dawn of Taupō Volcanic Zone activity, New Zealand

Marlena Prentice[1], Adrian Pittari[1], Geoff Kilgour[2] and David J. Lowe[1]

[1] *School of Science/Te Aka Mātuatua, University of Waikato, Hamilton, New Zealand*

[2] *GNS Science, Taupō, New Zealand*

prenticelm@gmail.com

Voluminous (> 100 km^3) silicic volcanism within New Zealand has been a prominent feature during the > 2 Ma history of the Taupō Volcanic Zone (TVZ). During this time, there have been numerous eruptions of crystal-poor (< c. 10 vol. %) rhyolites that are compositionally variable, but often not systematically zoned, whereas the eruption of voluminous crystal-rich (> c. 20 vol. %) ignimbrites has been rare (e.g., Ongatiti, Whakamaru and Rotoiti ignimbrites). The Waiteariki Ignimbrite, erupted from the Omanawa caldera in the Tauranga Volcanic Centre (TgaVC) c. 2 Ma, does not conform with these typical endmember ignimbrites. This large-volume (870 ± 44 km^3 DRE; magnitude, *M*, 8.3), dacitic (67.27–71.13 wt. % SiO_2) ignimbrite is crystal-rich (c. 30–50 vol.%, ave. 41 vol.%), and has a consistent mineral assemblage of plagioclase, hornblende, orthopyroxene, quartz, with accessory Fe-Ti oxides, zircon and apatite. Additionally, whole-rock and glass major and trace element compositions vary minimally within a narrow range throughout the < 150 m vertical thickness, analogous to typical monotonous intermediate-type ignimbrites (cf. Fish Canyon Tuff). Despite this apparent homogeneity, the Waiteariki Ignimbrite is highly heterogenous at the microscopic level and demonstrates textural evidence of the syn-eruption of coexisting magma bodies and subsequent mixing of magmas. Plagioclase crystals span a broad compositional range ($An_{22–78}$) with both normal and reverse zoning juxtaposed, and many crystals display complex textural features. Similar compositional and textural variations are observed in orthopyroxene ($En_{28–79}$, $Wo_{1–4}$) and hornblende ($Al_{(t)}$=1.15–2.11 apfu), all reflective of remobilisation of the underlying mush zone with a complex evolutionary history. Estimates of magmatic conditions are modelled using multiple independent crystal-melt (plag-liq, opx-liq) or crystal-only (cpx; Al-in-hornblende) thermo-geobarometers to give pre-eruptive temperature ranges between 740–840°C and 900–990 °C (ave. 790°C and 950 °C, respectively) and pressures between < 50–150 MPa that are indicative of multiple extraction zones with shallow, upper-crustal storage.